Hydrodynamically Modulated Voltammetry in Microreactors

Luwen Meng

Department of Chemical Engineering and Biotechnology

University of Cambridge

This dissertation is submitted for the degree of

Doctor of Philosophy

Abstract

Hydrodynamically modulated voltammetry in microreactors

Luwen Meng

This thesis describes modulated methods using both voltammetric and microfluidic perturbations to study mechanisms of electrolysis reactions.

The initial chapters provide an overview of applications and research development in the fields of micro-engineering and electrochemistry, including microfabrication methodology, electrochemical detection techniques and analysis methods. Some typical electrochemical reactions have been studied for different kinds of industrial applications. Also hydrodynamic modulation methods have been investigated.

The result chapters begin in Chapter 3 with detailed investigation of various electrochemical reactions by using cyclic voltammetry (CV) and large amplitude Fourier transformed alternating current voltammetry (FTACV) under microfluidic conditions. Single electron transfer reactions with different kinetics were studied first by using potassium ferrocyanide and ferrocenecarboxylic acid (FCA). Dual electron transfer reactions with different pathways were investigated by using 2,5-dihydroxybenzoic acid for one step oxidation and N,N,N',N'-tetramethyl-*para*-phenylene-diamine (TMPD) for two consecutive one-electron step oxidation. An irreversible reaction was explored by using borohydride solution. Examples of homogeneous reaction mechanisms were studied by using the combinations of $Fe(CN)_6^{4-}$/L-cysteine or TMPD/ascorbic acid. The current response of all the electrolysis reactions except single electron transfer reactions was first reported under microfluidic conditions with FTACV, which has shown sensitive with the change of volume flow rates and the substrate concentrations when homogeneous reactions are involved. The linear relationships between peak current and volume flow rates or substrate concentrations can be obtained in every harmonic component.

In chapter 4, the modulated technique was applied to microfluidic hydrodynamic systems. A range of electrolysis mechanisms including single electron transfer reactions, dual electron transfer reactions, irreversible reaction and homogeneous reactions were studied under hydrodynamic modulated conditions. The system showed rapid response with the change of

volume flow rates during one measurement. The linear relationships between peak current and flow rates, as well as substrate concentrations, can be obtained simultaneously in one scan, which reveals a promising approach to get more information in a short-time measurement.

Chapter 5 demonstrated a new protocol by forcing an oscillation of the electrochemical active solution flowing. Analysis of transition time and its effect on limiting current are presented to begin exploration of this new tool for supporting researchers on understanding redox mechanisms. A short simulated study was carried out to help better understand the mechanism under different hydrodynamic conditions.

For my family,

Past, present and future

Declaration

I hereby declare that except where specific reference is made to the work of others, the contents of this dissertation are original and have not been submitted in whole or in part for consideration for any other degree or qualification in this, or any other University. This dissertation is the result of my own work and includes nothing which is the outcome of work done in collaboration, except where specifically indicated in the text. This dissertation contains less than 65,000 words including appendices, bibliography, footnotes, tables and equations and has less than 150 figures.

Luwen Meng

September 2018

Acknowledgements

First and foremost, I would like to express my gratitude to my supervisor Dr Adrian Fisher, who offered me the opportunity to undertake my PhD study in the group and paid his unbelievable patience to me. I am grateful to my advisor, Dr Kamran Yunus, for his help and guidance. My appreciation sends to Dr Peng Song as well. Thank you for your advice in both research and life in Cambridge even if you are not around.

A big thank you to all of my colleagues in CREST group: Dr Chencheng Dai, Dr Hongkai Ma, Dr Arely Gonzalez, Dr. Viet Nguyen, Dr. Xiangming Gao, Aazraa Pankan, Yian Wang for all the discussion and help in the last four years and especially Feng Zheng, who wrote me a MATLAB script to minimize my pain of analysing AC data. Special thanks to Dr Ashoke Raman for the discussion about the simulation work. Also, I'd like to express my appreciation to Ziyan Zhao, Yao Du and Andi Tao for accompanying for these years in the department. Special thanks extend to all other supporting staff in our department, Chris, Peter and other people in technician team, electronic team and domestic department.

I am grateful for all friends based in Cambridge and UK. Thank you so much for being with me and making my life so colourful these four years, especially Molly, Hanae and Susan who are always my dinner and wine buddies to help me get through the tough time. Special thanks to Rui Li and Anastasiya Sybirna for being my case practice partners and all the support they gave me. Also, I can't finish this PhD with all my friends back to China, Fangyuan Chen and Chengyan Zhan who always gave me mental support since we have known each other and Zhao Zeng who can always answer my video call whenever and wherever it is.

Special thanks to Wayne (JJ) Lin, who inspired me through these 15 years with his music. Thank you for being such a great model to gain me courage and belief, which always push me forward to pursue my dreams.

Last but not least, I would like to express my sincerest gratitude to my parents and all my family. Thank you for bringing me to this world and offering all the support through my whole life. I hope I didn't let you down. And I love you to the moon and back.

Contents

List of Figures

List of Tables

Abbreviations

Abbreviation	Meaning
AC	Alternating current
ADC	Analog-to-digital converter
CE	Counter electrode
CV	Cyclic voltammetry
DAC	Digital-to-analog converter
DC	Direct current
DHB	2,5-dihydroxybenzoic acid
DSP	Digital signal process
EC	Heterogeneous electron transfer followed by homogeneous chemical reaction
ECE	Heterogeneous electron transfer, homogeneous chemical reaction and heterogeneous electron transfer in sequence
EC'	Catalytic regeneration of the electroactive species in a following homogeneous reaction
EE	Two electron transfer reaction
FCA	Ferrocenecarboxylic acid
FFT	Fast Fourier transformed
FT	Fourier transform
FTACV	Fourier transformed alternating current voltammetry
HMV	Hydrodynamic modulation voltammetry
LIGA	German acronym for Lithographie, Galvanoformung, Abformnung

LSV	Linear sweep voltammetry
MALDI	Matrix-assisted laser desorption/ionization
Micro-EDM	Micro-electrical discharge machining
Micro-ECM	Micro-electrochemical machining
MOFs	Metal organic frameworks
MST	Micro-system technology
OHP	Outer Helmholtz plane
PEMFCs	Proton exchange membrane fuel cells
PDMS	Poly(dimethylsiloxane)
RDE	Rotating disc electrode
RE	Reference electrode
SWV	Square wave voltammetry
TMPD	N,N,N',N'-tetramethyl-*para*-phenylene-diamine
UMEs	ultramicroelectrodes
UV	Ultraviolet
WE	Working electrode
μTAS	Miniaturized total analysis systems

Common Symbols

Symbol	Definition	Unit
A	Electrode area	cm^2
C_{dl}	Double layer capacitance	F
c	Concentration of species	mol L^{-1}
c_0	Bulk concentration	mol L^{-1}
c_{R0}	Initial concentration of reductant	mol L^{-1}
C_{O0}	Initial concentration of oxidant	mol L^{-1}
D	Diffusion coefficient	cm^2 s^{-1}
d	Cell width	cm
D_R	Diffusion coefficient for reductant	m^2/s
D_O	Diffusion coefficient for oxidant	m^2/s
E	Electrode potential	V
E^0	Standard electrode potential	V vs SHE
$E_{1/2}$	Half peak potential	V
E_{app}	Applied potential	V
E_{dc}	Potential of DC signal	V
E_p	Peak potential	V
E_t	Real-time potential	V
ΔE	Amplitude of AC component	V
ΔE_p	Pulse height	V
ΔE_s	Potential step	V

F	Faraday constant	C mol^{-1}
f	Frequency	Hz
h	Cell half height	cm
i	Current	A
i_0	Standard exchange current	A
i_a	Anodic current	A
i_c	Cathodic current	A
i_L	Limiting current	A
i_m	Maximum current amplitude	A
i_p	Peak current	A
i_t	Real-time current	A
j	Flux of the species	mol cm^{-2} s^{-1}
j_c	Reductive flux	mol cm^{-2} s^{-1}
j_a	Oxidative flux	mol cm^{-2} s^{-1}
j_m	Migratory flux	mol cm^{-2} s^{-1}
k	Rate constant	cm s^{-1}
k_c	Heterogeneous rate constant for reduction	depends on order
k_a	Heterogeneous rate constant for oxidation	depends on order
k_{EC}	Rate constant of EC reaction	depends on order
k_{ECE}	Rate constant of ECE reaction	depends on order
$k_{EC'}$	Second-order rate constant of the catalytic step	cm s^{-1}
k^0	Standard heterogeneous rate constant	cm s^{-1}
L_e	Electrode length	mm
L_c	Channel length	mm
n	Number of moles of electrons transferred	mol mol^{-1}

p	Pressure	Pa
q^m	Excess charge on metal	C
q^s	Excess charge on solution	C
R	Universal gas constant	$J\ K^{-1}\ mol^{-1}$
R_{ct}	Charge transfer resistance	Ω
R_s	Series resistance in an equivalent circuit	Ω
R_u	Uncompensated resistance	Ω
r	Rate of homogeneous production	
s	Stoichiometric coefficient	
T	Temperature	K
t	Time	s
t_p	Pulse width	s
t_s	Time when flow rate changed	s
u	Ionic mobility	$cm^2\ s^{-1}\ V^{-1}$
u_i	Velocity vector	
V_f	Volume flow rate	$mL\ min^{-1}$
v	Viscosity of the solution	$kg\ m^{-1}\ s^{-1}$
v_s	Scan rate	$V\ s^{-1}$
v_x	Velocity of the solution on x firection	$cm\ s^{-1}$
w	Electrode width	cm
x_e	Electrode length	cm
$x,\ y,\ z$	one-dimensional Cartesian coordinate	cm
z_i	Charge number	
Z	Impedance	Ω
α	Charge transfer coefficient	
θ	Phase difference	
φ	Electrostatic potential	V

η	Overpotential	V
ω	Angular frequency	rad s^{-1}
ρ	Density	kg m^{-3}

Chapter 1   Introduction of Electrochemical Fundamentals

1.1   Introduction

Electrochemistry plays a critical role in synthesis, sensing and analytical (bio)chemistry. In recent years, these developments have accelerated due to the establishment of miniaturized engineering approaches. This has led to advanced high through put electrochemical analysis techniques. In this thesis, the development of high sensitivity and selectivity measurements are explored, including both modulated hydrodynamic and voltammetric sensing. This chapter aims to provide an overview of the research development in the fields of electrochemistry and micro-engineering. Some typical electrochemical reactions including pure electron transfer reactions and homogeneous reactions have been studied for different kinds of industrial applications. Also, hydrodynamic modulation methods have been investigated for the further research purpose.

1.2   Introduction of electrochemical applications

Electrochemical techniques explore the interplay between electricity and chemistry, namely, the measurements of electrical quantities, such as current, potential, or charge and their relationship to chemical parameters [1].

The application of electrochemical measurements is vast, including environmental monitoring [2], industrial quality control [3] and biomedical analysis [4–6]. Especially in sensing area, the combination of micromachined units and electrochemical analysis techniques shows promise for specific chemical detections. This section will introduce a few typical applications of electrochemistry.

1.2.1 Synthesis

The concept of green sustainable chemistry has become increasingly important in the past decades, which allows the design of the reaction path to prevent waste, have lower energy consumption and encourage the utilization of catalysis process. Organic or inorganic electrosynthesis has attracted growing attention as it is a more environmentally-friendly process [13].

Electrosynthesis refers to the synthesis of chemical compounds in an electrochemical cell. In comparison to the ordinary redox reaction, the advantage of electrosynthesis is that it eludes the potentially wasteful side reactions and can reduce unnecessary energy consumption by precisely tuning the required power input in the chemical reactions.

This Figure is not shown due to copyright issues

Fig 1.1 Comparison between a conventional chemical process (A) and electrochemical process (B) [14]

The field of inorganic electrosynthesis is well established and has a high profile. Over 4000 tons per hour of chlorine is produced by the chlor-alkali industry, in conjunction with sodium hydroxide and hydrogen. This high tonnage bulk chemical operation has changed radically over past decades. It has also accelerates the development of new cell design, electrodes and materials. Furthermore, one major aspect of the metal extraction and production industry is the employment of molten salt electrolysis in the production of metals, such as aluminium [15]. Electrosynthesis on a nano-scale has also been well-developed. Researchers have managed to produce gold nanorods [16] and silver nanoparticles [17]. The electrochemical synthesis process is relatively simpler and cheaper compared with other alternatives. In addition, the shape and the size of the particles can be easily controlled by changing electrolytic conditions [18].

2

As for organic electrosynthesis, it has come to be recognized as one of the methodologies that can meet the criteria for developing more environmentally sustainable processes. Electrosynthesis can replace the toxic or dangerous oxidizing or reducing regents in conventional synthesis method, as well as the in-situ production of unstable and hazardous regents.

There are various ways to conduct organic electrosynthesis, including pairing electrochemical reactions, electrocatalytic reactions and the electrochemical reactions involving ionic liquids, electrogenerated reactants, micro- and nano-emulsions or renewable starting materials, for example, biomass [14].

Electrosynthesis has been applied to produce different organic substances. Researchers have managed to synthesize different kinds of conducting polymers. According to Iroh *et al.* [19], the composite coatings on steel occurred in three stages. The first step is the electroadsorption of monomer and electrolyte and the initiation of formation of the passive film. Then the growth and impingement of the passive film and the decomposition of the latter took place. The final step is the formation of composite coatings. The product has shown improved processibility, reduced porosity and improved corrosion performance.

Another typical example of organic electrosynthesis is metal organic frameworks (MOFs). Several MOFs that are based on copper, aluminum, or zinc and linkers with different coordinating moieties and connectivities can be synthesized via anodic dissolution by Martinez and the co-workers [20]. This technique can provide a faster synthesis process at lower temperatures than the conventional method and the metal salts are no longer needed, which means prior to solvent recycle the separation of anions from the synthesis solution is not necessary.

Besides providing the driving force of synthesis, electrochemical methods are also utilized as process control techniques for accurate synthesis. The size of particles was successfully controlled by the electrochemical preparation method [21].

This Figure is not shown due to copyright issues

Fig 1.2 Schematic view of an electrochemical synthesis cell [20]

To achieve better green synthesis goal by utilizing more catalytic process, the appropriate electrochemical cell design as well as the reaction control process should be considered carefully. Therefore, the full and detailed understanding of reaction mechanisms is required. The traditional electrochemical detection techniques are usually can meet the criteria while sometimes fail to do so. To solve this problem, researchers proposed some advanced electrochemical techniques or modulated methods could be developed.

1.2.2 Sensing

Electrochemical sensors are widely used in many branches of industry, including environmental and biomedical monitoring. They are well-established and powerful tools to obtain real-time information for process control by *in situ* measurements of chemical composition without sampling. The sensors can be applied ranging from -30 °C up to 1600 °C depending on the type of electrolyte. In low-temperature environments, electrochemical sensors are mainly used to measure pH values, electrical conductivity and concentrations of specific ions with conventional liquid electrolyte. For the exhaust gases and molten metal with high temperatures, sensors are equipped with solid electrolyte for applications in the steel, cement and glass making industry [22].

Compared to spectrometric, mass spectrometric and chromatographic techniques, the electrochemical sensors are often simple to setup procedures and also require less equipment operation and data acquisition. Using electrochemical sensors, for instance, requires less maintenance and calibration care. Consequently electrochemical sensors are often preferred tools for screening purposes. Nonetheless, in terms of precision and detection limit,

electrochemical sensors cannot always replace the aforementioned standard methods in the laboratory use.

1.2.2.1 Electrochemical sensors used in aqueous phases

In recent years, miniaturized electrochemical sensors have been developed and applied to many applications. Rod-shaped sensors have been utilized for biological processes. In (bio-)electrochemical sensing, the reaction under investigation would either generate a measurable current, a measurable potential or charge accumulation or measurably alter the conductive properties of a medium between electrodes [23]. A lot of substances can affect the sensitivity and selectivity of the sensors. The emphasis of applying miniaturized devices to shrink the dimensions of the electrochemical sensor elements can increase the signal-to-noise ratio.

This Figure is not shown due to copyright issues

Fig 1.3 Diagrammatic representation of the architecture of a second-generation amperometric biosensor [24]

Lab-on-chip is an integrated structure which was microengineered electrochemical sensors. This technology typically combines fluidic. Micro-techniques with electrodes, which are allocated on the chip based on specific design. There are many advantages of this kind of sensors, including portability and good signal to noise. It is also relatively safer as these

sensors contain very small quantities of chemicals. Moreover, the sensors are cheap and easy to be replicated.

1.2.2.2   Electrochemical sensors used in gas phase

Based on the sensing principles, gas sensors can be classified into three categories, solid electrolyte gas sensors, catalytic combustion gas sensors and semiconductor gas sensors [25]. The advantage of applying solid electrolyte in sensors is higher selectivity for certain components in a broader matrix of other gases can be obtained. For long-term use, the stability is superior to those in liquid phase and less maintenance is required. Also, they not only respond faster, but also have a high-temperature tolerance, which is necessary for the combustion process or self-cleaning behaviour [22].

An oxygen sensor works based on the principle of oxygen ion conduction. The conductor acts as the solid electrolyte and as a separator for the two compartments with gaseous mixtures having different oxygen potentials or partial pressures. They are widely used for combustion control in heat-treatment furnaces, glass tank furnaces and other applications.

Amperometric techniques are mainly used to construct O_2 and NO gas sensors. Previous research has shown that, the silicon micromachining technology is also applied to fabricate gas sensors which can provide a fast response. In order to design an electrochemical gas sensor with fast response time, it is useful to analyze the time constants associated with the individual steps occurring in the gas phase. The first step is to analyze the transport or permeation of the gas to the surface of the gas-permeable membrane. Next the diffusion of the gas through the membrane should be taken into consideration. Then the dissolution of the gas into the internal electrolyte, further reaction or dissociation of the gas in the electrolyte would take place in sequence. The last steps would be the diffusion of the gas to the sensing electrode and sensing at the electrode [7]. Fig 1.4 is a typical gas sensor cell.
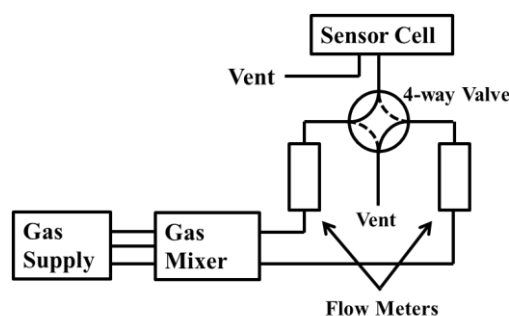
Fig 1.4 Schematic of the gas delivery system and sensor testing cell

6

Potentiometric sensors have also been developed to detect CO_2 by Maruyama, *et al.* [26]. The sensor operated at temperatures between 600 and 1000 K, and the experimental results have indicated that the response of the sensor is considerably rapid and stable in the high-temperature environment.

Besides aforementioned applications, electrochemistry is employed in chloride removal [27], protein [28], pharmaceutical and biochemical analysis [29]. In every field, electrochemical alternative has shown fast response, efficiency as well as low-cost characteristics.

In this thesis, novel electrochemical detection strategies have been used for detection and analysis purposes. Experiments are reported to correlate precise signal analysis in conjunction with control of liquid flow through the microreactors. The following sections discuss the background information and combination of electrochemistry with miniaturized technologies.

1.3   Introduction of micro-engineering

The use of micro-products and micro-components has increased significantly over the past decade. The most important applications of these microsystems include the production of IT components (ink jet printers, reading caps for hard disks *etc.*), medical and biomedical products (pacemakers, analysis equipment, sensors *etc.*), as well as motion sensors for the automotive industry.

However, it is relatively difficult to define microengineering precisely. The definition of microengineering should contain both the philosophy and the characteristics of a micro-product. According to Alting [30], the definition of microengineering is:

"Micro-engineering deals with development and manufacture of products, whose functional features or at least one dimension are in the order of μm. The products are usually characterized by a high degree of integration of functionalities and components."
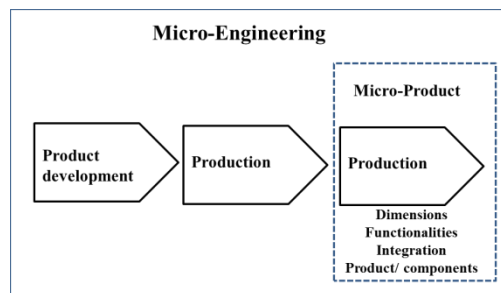
Fig 1.5 Definition of micro-engineering concept

As for the design of micro-products, micromachining is one of the key technologies that can enable the realization of such products and fields with such requirements are rapidly expanding [31].

Micromachining includes several techniques such as micro-EDM (micro-Electrical Discharge Machining) [32], microcutting [33], LIGA [30], micromolding [34], micro-ECM (micro-Electrochemical Machining) [35]. Many potential applications can be identified based on these methods. Among them, micro-holes and micro-pins are the most well-known examples [31]. More recently, 3D products have attracted increasing attention. The sizes of these products are small and there are fewer errors in the manufacturing process. Consequently, they are now widely used in manufacturing industry.

1.3.1 Microreactors

In the recent years, the miniaturization of chemical processing has greatly advanced the chemical industry that have been constantly searching for controllable, information rich, high throughput, environmentally friendly methods of producing products with a high degree of chemical selectivity [36].

Microreactors are miniaturized reaction systems fabricated, at least partly, by microtechnology and precision engineering. The characteristic dimensions of the internal structures of microreactors such as fluid channels, typically ranging from the sub-micrometer to the sub-millimeter regime [37].

In comparison with macro reaction systems, the potential advantages of microreactors include:

- Enhanced heat transfer

Large contact areas and temperature gradients are required to effectively transfer heat from one flowing fluid across a solid boundary to another flowing fluid. Another important criterion is the ratio of heat transfer to pressure loss. In the microreactors, reducing the dimensions of the fluid flow increases the temperature gradients and the exchange surface to volume ratio, that is, miniaturization leads to a better heat exchange. The reduced flow dimensions will inevitably result in an increase in viscous losses, but the overall heat transfer to pressure loss ratio is improved [38–40], Compared with the conventional heat exchanger, the heat transfer coefficients are enhanced by at least one order of magnitude [41]. Moreover, the heat exchanger is often integrated within the reactor allowing efficient control of the

highly exothermic or endothermic reactions. In the case of multiphase systems, the specific interface is also drastically increased in comparison with traditional reactors. [42]

- Enhanced mass transport

Similarly with heat transfer, the mass transport in the microreactors will be enhanced due to high surface-to-volume ratios, short diffusion and conduction paths, high interfacial areas, and strictly controlled flow conditions [43]. The high heat and mass transfer rates in the microfluidic systems allow reactions to be carried out under more aggressive conditions leading to higher yields that normally cannot be achieved by using conventional reactors [44]. According to Losey's work [42], for heterogeneous reactions, for example gas-liquid absorption, it has been measured that the overall mass transfer coefficients were nearly two orders of magnitude larger than the of standard laboratory-scale reactors. Similar results can be obtained from liquid-liquid phase absorption [45,46].

- Production flexibility

As most of the conventional reactors are initially designed for laboratory use, it is crucial to scale them up in order to realise their full potential. In the fine chemical or pharmaceutical industry, due to the large amount of reactions that have been studied and limited resources, it is impossible to develop a specific reactor for only one reaction. A toolbox concept is therefore necessary [47]. Although it is impractical to alter the size of the reactors, in terms of micromachining, it is not difficult to increase or reduce micro-units to satisfy the different requirements of the reaction systems. This is mainly because microreactors need less space than the macroscopic counterpart.

- Lower cost

Miniaturization allows measurements to be performed within a device that often has a shorter response time and requires less space, materials and energy. It also reduces the input and waste and ascertains the potential for catalyst recycling and the opportunity for low-volume optimization [48,49]. Miniaturized devices can be produced in parallel by batch processing at low cost. It is also a well-known fact that in microelectronics a dramatic improvement of performance can be achieved by integration of a multitude of miniaturized functional elements [40]. Microreaction technology is regarded as a key strategy for economic growth, because it is timesaving and costs less, and for sustainable development and saving natural resources.

- Safety characteristics

For those reactions or processes that involve dangerous chemicals, the use of microreactors certainly increases safety because they require smaller amount of hazardous materials to be used [50]. Even if a microreactor failed, the small quantity of chemicals released could be easily contained. Moreover, the presence of integrated sensor and control units could allow the failed reactor to be isolated and replaced while other parallel units continue production [44,51–53]. These inherent safety characteristics suggest that production-scale systems of multiple microreactors should enable distributed point-of-use synthesis of chemicals with storage and shipping limitations, such as highly reactive and toxic intermediates (e.g., cyanides, peroxides, azides).

In addition, because of the size of microreactors, the reaction volume in the microreactors is small, which means it is much easier to control the parameters such as temperature, pressure, residence time, and the flow rate. When some explosive or extremely exothermic reactions are involved, the potential hazard can also be reduced significantly [54].

Microreactors, however, have their own problems. For example, with chemical reaction, the microchannels might clog. During scaling up, the high area to volume ratio and uniform residence time cannot be easily maintained. These problems should be considered when searching for a successful manufacturing process.

1.3.1.1   Potential applications

Gas-phase microreactors have a long history but those involving liquids started to appear in the late 1990s [55]. One of the first microreactors with embedded high performance heat exchangers was made by using mechanical micromachining techniques that were a spin-off from the manufacture of separation nozzles for uranium enrichment in the early 1990s by the Central Experimentation Department (Hauptabteilung Versuchstechnik, HVT) of Forschungszentrum Karlsruhe [56] in Germany. As a result of these microfabrication processes, microminiaturization is no longer exclusive to microelectronics. Mechanical, optical, thermal, and fluid microdevices became a part of daily life including laser heads for CD players, read/write heads for hard disks, microsensors in automobiles, ink jet printer heads and minimum invasion surgical instruments [57]. Recently, microdevices have also become of interests for chemical, pharmaceutical, and biotechnical applications [58].

- NMR

Bart and his colleagues [59] have succeeded in demonstrating an integrated microfluidic NMR flow probe for the study of reaction kinetics. Furthermore, the possibility of using the stripline design for screening of mass-limited biological samples has been demonstrated. With the currently available microfabrication toolbox, a completely integrated platform in one chip that can handle and detect raw samples without preparative laboratory work is within reach.

- Synthesis

Scaling-up the laboratory reactions in order to achieve optimal mass transport presents a problem in conventional process technology. Microreactors have been widely used for chemical synthesis, especially organic synthesis [60–64]. According to Yoshida *et al.* [65], Flow microreactors can contribute to green and sustainable chemical synthesis by several ways, including improving product selectivity to give less waste, avoiding energy-consuming cryogenic cooling setups, and protecting-group-free synthesis to improve atom and step economy.

The channel networks which connect the reservoirs with chemical reagents inside construct the "lab on a chip" devices. The dimensions of these kinds of devices are around a few centimeters, as shown in Fig 1.6. This device allows the reagents to flow into the cell where reactions take place in a specific order, then mix and react for a specific time by using the electrokinetic or hydrodynamic pumping to control the channel networks [66]. Because of this character, microreactors are widely used in the pharmaceutical industry.

This Figure is not shown due to copyright issues

Fig 1.6 Reaction in process within a microreactor under Electroosmotic Flow control [66]

Meanwhile, microreactors are widely used in the field of enzyme-catalyzed polymer synthesis. Enzymes immobilized on solid supports are increasingly used for greener, more sustainable chemical transformation processes. Microreactors are used to study enzyme-

catalyzed ring-opening polymerization of ε-caprolactone to polycaprolactone. A novel microreactor design has been developed by Bhangale *et al.* [67] which was able to perform heterogeneous reactions in continuous mode, in organic media and at elevated temperatures.

- Detection and analysis

Miniaturization of chemical analytical devices started with a microfabricated gas chromatograph in the late 1970s [68]. Interest was revived in 1989 when Manz and co-workers at Ciba Geigy proposed μTAS (miniaturised total analysis systems) as an alternative to chemical sensors [69]. μTAS are currently considered as a mean for information generation for applications including DNA sequencing, high throughput drug screening and point of care chemical analysis, etc [70].
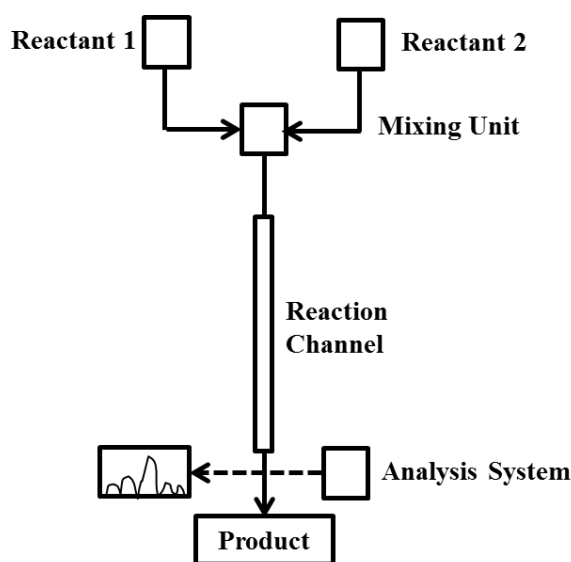
Fig 1.7 Continuous-flow reactions in microchannels

Fig 1.7 shows the principle processing steps of a continuous flow microreactor. The reactants are first mixed in the mixing unit. Then the mixture flows into the microchannel followed by the analytical unit. This design allows the individual unit to be optimized separately each time to make the system suitable to various situations.

It has been reported that microfluidic technology has been applied in many of medical analytical areas including cellular analysis, biomimetic systems, clinical diagnosis and immunoassays [71]. Zhou *et al.* [72] has already proved that the combination of microfluidic and electrochemistry is able to potentially provide an alternative to protein detection in clinical laboratory. This is not the only case in which microfluidic technology has been

applied to electrochemical detection. According to Vilkner's work [73], several optimized microfluidic reactors have been utilized for electrochemical detection. The detective results benefit from the high surface-to-volume ratio whether in terms of the precision or the saving of time and raw materials. The surface modification method is important for the different kinds of electrochemical detections, because it attempts to improve the limits of detection or selectivity or the contamination will affect the detector response [74].

Furthermore, miniaturizing the synthesis apparatus by employing microreactors is a way to greatly reduce the potential hazard of highly exothermic nitrations [75]. This makes the whole reaction system much safer than the macroscopic reactors which are utilized in nitrations for analysis.

This Figure is not shown due to copyright issues

Fig 1.8 Scheme of a microreaction process coupled with High Performance Liquid Chromatography analysis for the nitration of toluene using fuming HNO_3 [75]

- Fuel cells

A fuel cell is a device in which the chemical energy is converted to electrical energy. This concept was firstly demonstrated over 170 years ago [76]. Among all of the applications of fuel cells, the Proton Exchange Membrane Fuel Cells (PEMFCs) are the most popular ones. They are widely used in portable devices such as the batteries in cellphones or laptops due to their high power density, relatively quick start-up, rapid response to varying loads and low operating temperatures [77].

In recent times, researchers have been able to combine the microreactors and micro-fuel cells to be an alternative to conventional portable electrical sources. Pattekar and his co-workers [78] have developed and tested a silicon chip based microreactor for in-situ and on-demand production of hydrogen. They successfully implemented the concepts of macro scale into the

micro-scale to create a prototype chemical plant-on-a-chip. In the device, all the microengineered techniques were used to minimize the size of the whole device as well as to accurately monitor and control the operation. The results showed that this device sufficiently supplied enough hydrogen and the conversion of the hydrogen was high.

This Figure is not shown due to copyright issues

Fig 1.9 The final microreactor for hydrogen production in micro-fuel cell [78]

Different microreactor systems have already been developed for chemistry and have been successfully employed in the conduction of electrochemical reactors without any added electrolyte [79]. Researchers have already managed to apply micro-engineering technology to fabricate electrochemical reactors for organic synthesis or precise analysis [80–83]. It is reported that the technically important oxidation reaction of 4-methoxytoluene to 4-methoxybenzaldehyde was achieved with better selectivity compared with where in conventional processes [84]. Also, researchers have successfully applied a mass spectrometer to a ceramic electrochemical microstructures reactor, which allowed mechanistic studies of electrochemical reactions and identification of unstable intermediate steps [85]. The kinetic study has been developed in a fixed-bed reactor. According to the experimental results, a detailed kinetic scheme was proposed [86].

To conclude, the development of miniaturized technology enhanced the detection accuracy and shortened detection time. Also, the micro-electrochemical reactors are relatively more sensitive to the signal since the electrode area is smaller than the conventional ones. In that case, the current signal can be better integrated to test the system response. In this thesis, the

microreactors are mainly used as electrochemical cell to conduct measurements with various parameters.

1.4   Introduction to electrochemistry

1.4.1 Electron transfer on the electrode

Electron transfer is a process by which an electron moves from one atom or molecule to another. It is a key concept in redox chemistry – the chemistry of reactions where one reaction partner loses electrons (oxidation) and the other gains electrons (reduction).

An electrode process often involves the transfer of charge across the interface between a metallic electrode and a solution phase species, as illustrated by the following:

$$O + ne^- \rightleftharpoons R \tag{1.1}$$

in which n electrons are transferred, O and R are the oxidized and reduced forms of electroactive species in the system, respectively. Nernst showed that the potential established at the electrode under equilibrium conditions is given by

$$E = E^0 + \frac{RT}{nF} ln \frac{[O]}{[R]} \tag{1.2}$$

where the equilibrium potential E of the electrode results from the standard electrode potential E^0 of the reaction and the concentrations of O and E at the electrode surface, which, under equilibrium conditions, are the same as their values in bulk solution. R is the universal gas constant with value 8.314 J K^{-1} mol^{-1}; T is the temperature (K).

For the case of a dynamic equilibrium, even though the reduction of O and the oxidation of R are occurring in the electrolyte, no net current flows through the cell and the overall concentration of the chemical species is not varying with time. If however a potential is applied to the system which is different to that of the equilibrium value the concentration ratio of O and R at the electrode surface will try to adjust to match the values predicted by equation (1.2). In the process, an oxidative or reductive current will flow as part of this overall reaction.

The magnitude of the current is given by

$$|i| = nAFj \tag{1.3}$$

15

where F is the Faraday constant with value 96485 C mol^{-1}, A is the electrode area (cm^2), j is the 'flux' of the spices (either O or R) reaching the electrode surface (mol cm^{-2} s^{-1}). Also, j can be thought of as the rate of the electrochemical reaction. When the reaction rate is first order, it can be predicted using

$$j_c = k_c[O]_0 \tag{1.4}$$

$$j_a = k_a[R]_0 \tag{1.5}$$

where k_c and k_a are the heterogeneous rate constant for reduction and oxidation, respectively, and $[O]_0$ and $[R]_0$ are the concentrations of the oxidative and reduction species at the electrode surface.

Usually the speed for bulk solution diffusion to the interfacial region is relatively slower than the depletion rate of corresponding reactants in the electron transfer process, the conversion between oxidative and reductive species results in the concentration differences of corresponding species on the electrode surface. Therefore the concentration terms in equation (1.4) and (1.5) have a close relationship with the concentration of species on electrode surface. Consequently, the current response can be limited either by mass transport (the transport of reactants and products to and from the electrode respectively) or electrode kinetics (k_a or k_c).

Consider the electron transfer reaction in Equation (1.1), the net current [87] could be predicted using

$$i = i_c - i_a = nFA(k_c[O]_0 - k_a[R]_0) \tag{1.6}$$

where i_c is the cathodic current, i_a is the anodic current.

Considering the special case in which the interface is at equilibrium [88], the Butler-Volmer equation can be expressed as

$$i = i_0\left(\frac{[R]_0}{[R]_{bulk}}e^{\frac{(1-\alpha)F\eta}{RT}} - \frac{[O]_0}{[O]_{bulk}}e^{\frac{-\alpha F\eta}{RT}}\right) \tag{1.7}$$

$$i_0 = FAk^0[R]_{bulk}^{\alpha}[O]_{bulk}^{1-\alpha} \tag{1.8}$$

where i_0 is the standard exchange current as Equation (1.8), α is charge transfer coefficient, η is the overpotential and k^0 is standard heterogeneous rate constant. Butler-Volmer formulation is used in the treatment of almost every problem requiring an account of heterogeneous kinetics. It predicts how the observed current varies as a function of the overpotential and transfer coefficient. If the solution under investigation is well stirred, the

surface concentrations of the reactants will be equal to their bulk values i.e. ($[R]_0=[R]_{bulk}$ and $[O]_0=[O]_{bulk}$). Under these conditions, the equation above can be simplified to

$$i = i_0(e^{\frac{(1-\alpha)F\eta}{RT}} - e^{\frac{-\alpha F\eta}{RT}}) \tag{1.9}$$

This Figure is not shown due to copyright issues

Fig 1.10 The effect of overpotential on the behaviour of current flow [88]

Based on that, the variation of i is shown in Fig 1.10. As it can be seen from the figure, the current flows readily in both anodic and cathodic directions according to the sign of the overpotential applied. If the overpotential is increased to a value of which the oxidative (anodic) process is driven, then the corresponding reductive component is vanishingly small. Equally, at overpotentials that drive the reductive (cathodic) process, negligible oxidation currents flow [87]. In the former case, the Butler-Volmer equation simplifies to

$$i = i_0 e^{\frac{(1-\alpha)F\eta}{RT}} \tag{1.10}$$

and in the latter to

$$i = i_0 e^{\frac{\alpha F\eta}{RT}} \tag{1.11}$$

From these two equations above, values α can be found experimentally from a knowledge of the current/voltage characteristics of an irreversible electrode reaction, which is known as Tafel analysis and illustrated in Fig 1.11.

17

This Figure is not shown due to copyright issues

Fig 1.11 A typical Tafel plot for an electrode reaction [89]

1.4.2 Reversibility

The concept of equilibrium involves the idea that a process can move in either of two opposite directions from the equilibrium position. Thus, it comes to the concept of reversibility. According to electrochemical literature, this takes several different but related meanings and it needs to be distinguished here.

1.4.2.1   Electrochemical reversibility

Bard [88] had concluded the electrochemical reversibility as: the current flow through the cell will reverse when opposing the cell voltage with the output of a battery or other direct current source. Reversing the cell current merely reverses the cell reaction.

On the other hand, one has different electrode reactions as well as a different net process upon current reversal, hence the cell is called to be chemically irreversible. Whether or not a half-reaction exhibits electrochemical reversibility depends upon solution conditions and the time scale of the experiment.

1.4.2.2   Practical reversibility

All actual processes occur at finite rates, so they cannot proceed with strict electrochemical reversibility. However, a process may in practice be carried out when thermodynamic equations apply to a desired accuracy. Under these circumstances, one might be treated as

reversible process. Practical reversibility includes certain attitudes and expectation an observer has toward the process.

The process reversibility depends on the ability to detect the signs of the disequilibrium. In turn, that ability depends on the time domain of the possible measurements, the rate of change of the force driving the observed process, and the speed with which the system can re-establish equilibrium. Either the perturbation applied to the system is small enough, or if the system can attain equilibrium rapidly enough compared to the measuring time, thermodynamic relations will apply. A given system may not behave same reversibility in different experiments even of same genre but wide latitude experimental conditions [88].

1.4.3 Mass transport

Besides the rate of electron transfer, there are some other physical processes may contribute to the overall kinetics of a particular reaction. As the overall reaction rate will be determined by the slowest step, in this section, the effect of transportation rate of the materials flux to (or from) the electrode surface is introduced.

According to experimental conditions, there are three main transport processes:

- Diffusion

Diffusion is the movement of a species under the influence of a gradient of chemical potential, for example, a concentration gradient. Fick's first law described diffusion mathematically by considering the simple case of linear diffusion to a planar surface. The diffusional flux, j, for a species is

$$j = -D\frac{\partial c}{\partial x} \tag{1.12}$$

where c is the concentration of the species (mol cm^{-3}), D is the diffusion coefficient (cm^2 s^{-1}), which is a characteristic of the diffusing species and x represents the one-dimensional Cartesian coordinate (cm).

This Figure is not shown due to copyright issues

Fig 1.12 Diffusion to a large planar surface [87]

19

Practically, the concentration of reactant varies as a function of time. This can be established by considering variation in concentration of species within the region during a time interval. Then it can be expressed by

$$\frac{\partial c}{\partial t} = D\frac{\partial^2 c}{\partial x^2} + D\frac{\partial^2 c}{\partial y^2} + D\frac{\partial^2 c}{\partial z^2} \tag{1.13}$$

This is Fick's second law, which demonstrates how the difference of the species concentration changes with time in three dimensions.

- Convection

Movement due to convection occurs when a mechanical force acts on a solution. There are two types of conventions are mainly concerted. The first one is natural convection, which is the result of thermal gradients and/or density difference within the solution. Natural convection is a typical perturbation in electrolysis by using of conventional electrode with size of mm or above on the time-scale of 10-20 s and longer. It is generally undesirable and difficult to predict.

The other type of movement is forced convection, which may be characterized by stagnant regions, laminar flow and turbulent flow. Sometimes, forced convection was introduced into the system deliberately by electrochemist with utilization of gas bubbling [90], pumping [91] or stirring [92]. The aim of doing this is for eliminating the effect of natural convection, so ensuring that the reproducible experiments can be achieved. Compared with natural convection, the forced component when suitably controlled can produce a well-defined hydrodynamic environment and therefore, the concentration differences along with the flow of solution can be described in one dimension by

$$\frac{\partial c}{\partial t} = -v_x\frac{\partial c}{\partial x} \tag{1.14}$$

in which the v_x is the velocity of the solution.

- Migration

The electrical potential drop between the two phases results in the external electric field $(\frac{d\emptyset}{dx})$, which leads to the movement of ions in the interfacial region to or from the electrode surface. This type of movement is called migration. The migratory flux (j_m) is proportional to the concentration of the ion, the electric field and the ionic mobility (u)

$$j_m \propto -uc\frac{\partial\emptyset}{\partial x} \tag{1.15}$$

It should be noted that the charge and magnitude of the ion as well as the solution viscosity both have an influence on the ionic mobility.

The migration can result in a complex physical transport process which is hard to control or interpret. To simplify this problem, the supporting electrolyte is introduced to most of the experiments. The electrolyte does not contain any electroactive ion so that it doesn't participate in the electron transfer reaction. But due to the high concentration, it carries most of the current in the bulk solution. Calculations have shown that approximately 100 times the concentration of background electrolyte relative to that of the reactant is required. In most of the cases, the electrolyte concentration is commonly in excess of 0.1M.

In addition to minimizing the contribution of migration, the supporting electrolyte also serves other important functions such as increasing the conductivity of the solution, reducing the distance of electric potential drop between electrode and bulk solution and effectively controlling the ionic strength of the solution constant.

1.4.4 Structure of the electrode/solution interface

In previous sections, the electron transfer and mass transport have been demonstrated while the nature of the electrode/electrolyte interface has been neglected. The forces that govern the behaviour of electrolyte in bulk solution are disrupted by the discontinuity at the interface. In addition, the electrode owns a charge which can be controlled by the applied potential to the electrode. As a result, electrostatic interactions occur between the electrode and electrolyte ions in solution.

1.4.4.1   The electrical double layer

The electrode/solution interface has been shown experimentally to behave like a capacitor, and a model of the interfacial region somewhat resembling a capacitor can be given (Fig 1.13). At a given potential, there will exist a charge on the metal electrode, q^m, which arises from an excess or deficiency of electrons at the electrode surface. In order for the interface as a whole to maintain electrical neutrality the charge on the electrode must be matched in solution by an equal but opposite charge, q^s.

$$q^m = -q^s \qquad (1.16)$$

This Figure is not shown due to copyright issues

Fig 1.13 The metal/solution interface as a capacitor with a charge on the metal, q^m, (a) negative and (b) positive [88]

The whole array of charge species and oriented dipoles existing at the metal/solution interface is called the electrical double layer. At a given potential, the electrode/solution interface is characterized by a double-layer capacitance, C_{dl}. Unlike real capacitance, whose capacitances are independent of the voltage across them, C_{dl} is often a function of potential.

Helmholtz came up with the electrical double layer model in the 1850s. In this model, it is assumed that no electron transfer reactions occur at the electrode and the solution is composed only of electrolyte. The attracted ions are assumed to approach the electrode surface and form a layer balancing the electrode charge, the distance of approach is assumed to be limited to the radius of the ion and a single sphere of solvation round each ion. The overall result is double layer charge and a potential drop which is confined to only this region (termed as the outer Helmholtz Plane, OHP) in solution. The result is analogous to an electrical capacitor above.

However, many factors such as diffusion in the solution, the possibility of absorption on the surface and the interaction between solvent dipole moments and the electrode were not considered in this model. A later model put forward by Stern began to address some of these limitations.

This Figure is not shown due to copyright issues

Fig 1.14 The Stern model of the electrical double layer [87]

In this model, the ions now are assumed to be able to move in solution and so the electrostatic interactions are in competition with Brownian motion. The result is still a region close to the electrode surface containing an excess of one type of ion but now the potential drop occurs over the region called the diffuse layer.

The double layer capacitance is dependent upon the applied potential, the electrochemical cell represents a slightly more complicated problem. In the precise analysis of redox reaction, this term is considered as non-Faradaic and needed to be eliminated during analysing process. Some advanced electrochemical detection techniques need to be utilized, which will be mentioned in the later sections.

1.4.4.2 Electrochemical cell and cell resistance

The most traditional electrochemical cell includes two electrodes, a working electrode where the reaction take places and the reference electrode, which provide a stable and fixed potential so that when a voltage applied between the two electrodes the drop in potential between the working electrode and the solution, φ_m-φ_s, is precisely defined. This difference is the driving force for the electrolysis to occur at that interface. The two electrode cell is perfect for the measurement of tiny current flow, for example, when the microelectrodes are applied. However, when larger electrode is utilized, the difficulty arises. When there is a voltage, E, is applied between the working and reference electrode, the finite current is flowing between them. Then the voltage is split into three terms as

23

$$E = (\varphi_m - \varphi_s) + iR + (\varphi_s - \varphi_{REF}) \tag{1.17}$$

The first term $(\varphi_m\text{-}\varphi_s)$ is the driving force mentioned before, the second one, iR, describes the voltage drop in solution due to passage of current between the two electrodes. R is the electrical resistance of the intervening solution. The third term, $(\varphi_s\text{-}\varphi_{REF})$ is the potential drop at the reference electrode/solution interface and is fixed by the chemical composition of the chosen reference electrode.

The aim of any voltammetry experiment is to measure current, i, as a function of changes in the quantity $(\varphi_m\text{-}\varphi_s)$. For microelectrode experiments, the term iR can be neglected and since $(\varphi_s\text{-}\varphi_{REF})$ is fixed, the equation above can be simplified as

$$E = (\varphi_m - \varphi_s) + constant \tag{1.18}$$

While in some circumstances, the iR term cannot be neglected since the current flowing through the cell will also be induced to change. Moreover, the passage of large currents through the reference electrode can change its chemical composition and so the third term, $(\varphi_s\text{-}\varphi_{REF})$ may not be constant. So in this case, the two-electrode cell is no longer suitable for the electrochemical measurement.

To circumvent this problem, in electrochemical detection, the three-electrode cell is preferable. The third electrode, which is an auxiliary or counter electrode is added to the cell. These electrodes are controlled by a potentiostat which ensures that current only flows between the working and counter electrode. The potential of the working electrode is held relative to the now stable reference electrode and the electronics ensure that no current passes through the reference arm of the circuit.

This Figure is not shown due to copyright issues

Fig 1.15 Schematic of a typical three-electrode cell [93]

The counter electrode can be any convenient one, because its electrochemical properties do not affect the behaviour of the electrode of interest. Is it usually chosen to be an electrode that does not produce substances by electrolysis that will reach the working electrode surface and cause interfering reactions there.

Three-electrode cell is mostly used in electrochemical measurements due to its stability. However, even in this arrangement, not all of the iR_s term is removed from the reading made by the potentiostat. If the reference electrode is placed anywhere but exactly at the electrode surface, some fraction of iR_s will be included in the measured potential. This fraction is called uncompensated resistance, also written as R_u. This uncompensated drop, iR_u, can sometimes be removed. Any resistance in the working electrode itself will also appear in R_u [88].
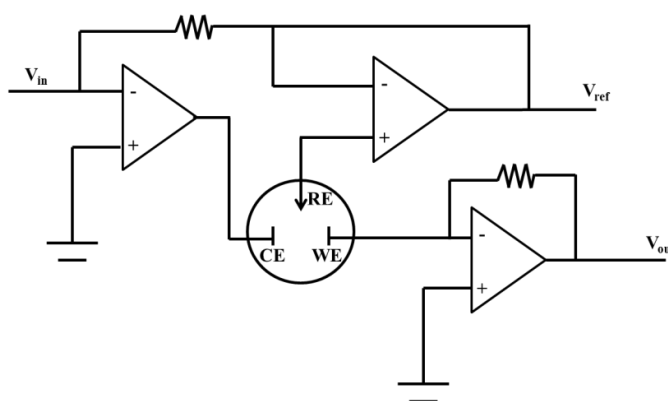
Fig 1.16 Potentiostatic three-electrode set-up

Fig 1.16 shows a control circuit of the three-electrode set-up. An external voltage V_{in} is applied between the reference (RE) and the working electrode (WE). An operational amplifier ensures that no electric current flows between working and reference electrodes. Electric current is passed from the counter electrode (CE) to the working electrode in a way that the external voltage required is achieved. This is again enabled by an operational amplifier. As there is virtually no current flowing through the reference electrode, the change in V_{in} is therefore the same as the change in the potential of the working electrode. The development of electronics has raised electrochemical analysis methods to a new level since the discovery of polarography.

1.4.5 Voltammetry techniques

The measurement of electrode current as a function of the voltage applied to the electrolysis cell can provide remarkably detailed information about the mechanism of the cell reaction. Voltammetry plays an important role in the research area of electrochemistry and has been

utilized extensively in the study of electrochemical mechanisms [94] and microreactors [95]. In this section, some voltammetric techniques applied in this thesis are illustrated.

1.4.5.1   Potential step chronoamperometry

It has been shown from previous work that potential step chronoamperometry is a useful tool in the investigation of the kinetics of electrode processes [96]. When the potential step chronoamprometry processes, the potential of the working electrode is instantaneously stepped between one value (where no electrolysis has happened) to another (where the complete conversion has been formed). The resulting current changes immediately following the step. A large current can be detected at first then it falls steadily with time, which is due to resulting current is controlled by the rate of diffusion of species from bulk solution to the electrode. Fig 1.17 shows the potential and current variation as a function of time, respectively. For an experiment at a stationary, constant-area electrode, the charging current dies away after a time equivalent to a few time constants. Therefore, for the first few seconds of the resulting current, it is the sum of the redox reaction and contribution of uncompensated resistance and double layer effect.
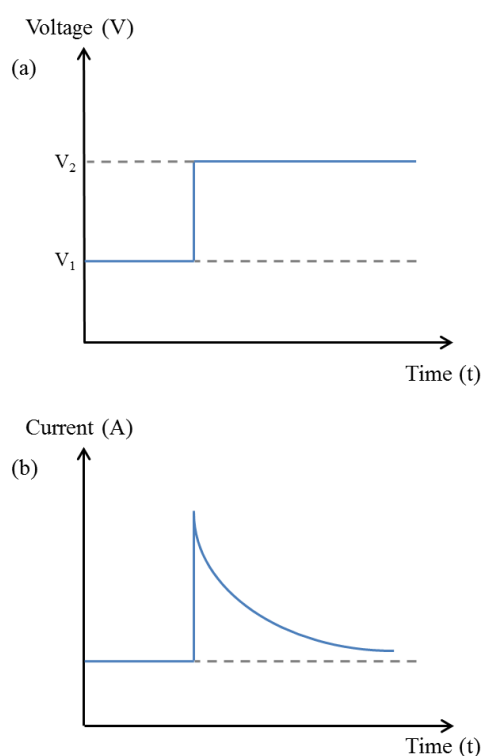
Fig 1.17 (a) The potential step jumps instantaneously from one value V_1 to another V_2;

(b) Current-time curve observed in the response of the potential step

26

The Cottrell equation describes the current response as function of time

$$|i| = nFAc_{bulk}\sqrt{\frac{D}{\pi t}} \qquad (1.19)$$

This equation suggests that potential step experiments can be used to measure diffusion coefficient.

1.4.5.2   Cyclic voltammetry

Cyclic voltammetry (CV) is arguably the most well-known electrochemical technique, because of its ease of measurement and versatility, it is widely used in many applications. When the electrochemical characteristics of an unknown compound need to be tested, CV is the most straightforward technique to perform due to its experimental simplicity and rapid response [97].
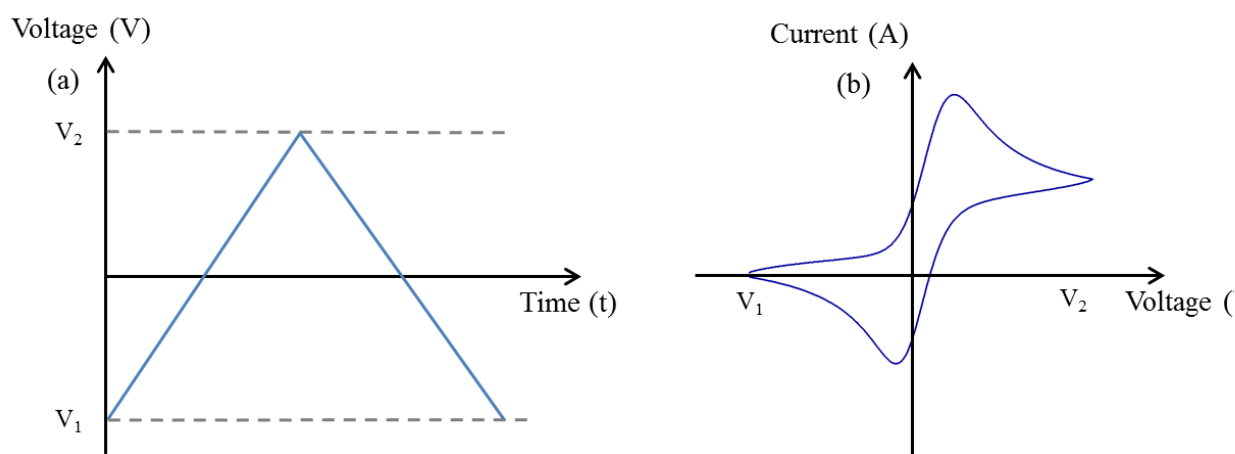
Fig 1.18 Potentials (a) and resulting current signals (b) of processing CV tests

In CV tests, the electrodes in an unstirred electrolyte will be provided with cyclic potentials. Usually the potential is varied linearly with time in a fixed potential range and once the potential reaches the end, it is reversed and swept back to the start potential, which can be seen from Fig 1.18 (a). The resulting current will be measured and a typical cyclic voltammogram for a reversible one electron transfer reaction will look like Fig 1.18 (b). The resulting current goes up with the increase of the sweep potential owing to the growing flux of the electroactive materials to the surface of the electrode. At 298K, the peak current of the reversible reaction can be calculated by

$$|i_p| = (2.69 \times 10^5)n^{\frac{3}{2}}AD^{\frac{1}{2}}v_s^{\frac{1}{2}}c_{bulk} \qquad (1.20)$$

where the i_p represents the peak current and v_s is the scan rate.

Occasionally, the potential is not swept back to the starting potential, so that the voltammogram only has the upper half. This is called linear sweep voltammetry (LSV), which is mostly utilized by some researchers when the reversed sweeping containing less information to be focused on.

Directing current cyclic voltammetry is normally used as the first alternative to electrochemical detection because it is intuitive for people to have a well guess about the electrochemical mechanisms. However, for the accurate quantitative analysis, DC cyclic voltammetry sometimes is not powerful enough to solve all the problems. In general, a potentiostat controls $E+iR_u$, rather than the true potential of the working electrode. Since the resulting current varies with time as the peak is traversed, the error in potential varies correspondingly. If i_pR_u is appreciable compared to the accuracy of measurement, the sweep will not be truly linear. The practical effect of R_u is to flatten the wave and to shift the reduction peak toward more negative potentials. Since the current increases with $v^{1/2}$, the larger the scan rate, the more peak potential (E_p) will be shifted. Uncompensated resistance can thus have the insidious effect of mimicking the response found with heterogeneous kinetic limitations. UMEs and very fast scan rates are usually used to avoid the influence caused by R_uC_{dl}, since the resulting current of UME is small and the iR_u drop does not perturb the response of the system. However, the Faradaic wave lies on top of a large capacitive current even when a UME is applied. The desired information of the total current response can be extracted via simulation method, but the practical limitation of very fast voltammetry is that the adsorption of electroactive substance onto the electrode surface or the Faradaic changes [88].

The effect of uncompensated resistance and double layer causes the inaccuracy in the redox reaction analysis, while this kind of effect cannot be eliminated once the directing current potential wave is applied during the measurement. Therefore, the development of some advanced electrochemical detection methods grew in the recent years for better understanding and analysis of electrochemistry.

1.4.5.3   Square wave voltammetry

Exceptional versatility is found in a method called square wave voltammetry (SWV), which was first invented by Barker and Jenkins [98]. In voltammetric electroanalytical methods, the minimum measurable Faradaic current is usually limited by the magnitude of the double layer charging current. The use of a discontinuous potential change, as in square wave polarography has been very successful in reducing the effect of this charging current [99]. SWV combines a square wave voltage and a rapidly changing DC ramp, which was demonstrated in Fig 1.19.

This Figure is not shown due to copyright issues

Fig 1.19 Waveform and measurement scheme for square wave voltammetry [88]

Several principle parameters including the pulse height, ΔE_p, measured with respect to the corresponding tread of the staircase, and a pulse width t_p. Alternatively, the pulse width can be expressed in terms of the square wave frequency, $f = 1/2t_p$. The staircase shifts by ΔE_s at the beginning of each cycle, which can deduce the scan rate of SWV is

$$v = \frac{\Delta E_s}{2t_p} = f\Delta E_s \qquad (1.21)$$

Consequently, t_p determines the experimental time scale and ΔE_s defines the potential step in each cyle period. Both parameters are responsible for the required scan time. In experimental practice, ΔE_s is observably smaller than ΔE_p, thus the pulse height fixes the resolution of voltammetric features in the voltammograms.

The current samples are taken twice per cycle at the end of each pulse. The forward current sample, arises from the first pulse per cycle, which is in the direction of the staircase scan. The reverse current sample, is taken at the end of the second pulse, which is in the opposite direction. A difference current is to calculate the difference between the forward and reverse current sample. The current of each pulse can be calculated by the equation below [100]

$$i = \frac{nFAD^{\frac{1}{2}}c}{\sqrt{\pi t_p}} \psi(\Delta E_s, E_{sw}) \tag{1.22}$$

where ψ is the dimensionless current function, which depends on step height, ΔE_s, and square wave amplitude, E_{sw}. When this normalized current function is plotted versus the normalized potential, $n(E-E_{1/2})$, the resulting voltammogram is independent of pulse width, concentration, or identity of reactant and so on. Thus one calculation of ψ can yield a whole family of voltammetric curves.

This Figure is not shown due to copyright issues

Fig 1.20 Dimensionless square wave voltammogram [88]

In SWV measurement, the charging current decays much more rapidly than the Faradaic current, allowing measurements to be made at a time when the charging current can be considered negligible [101].

It can be seen that square wave voltammetry offers all the advantages of square wave polarography but is accomplished at shorter analysis time. It is a rapid, sensitive, simple analytical electrochemical technique [102].

1.4.5.4   Alternating current impedance spectroscopy

Another way to study electrode reactions is to perturb the electrochemical cell with an alternating signal of small magnitude and to observe the way in which the system follows the perturbation at steady state. Many advantages accrue to these techniques. Among the most important are firstly the high-precision can be obtained. Secondly, the response can be treated theoretically linearized current-potential characteristics. Thirdly, the measurement can be conducted over a wide time range.

The experimental measurements of AC impedance are performed using an oscillating sinusoidal potential, which can be expressed as

$$E_t = \Delta E \sin(2\pi f t) \tag{1.23}$$

where E_t is the real-time potential, ΔE is the amplitude of the AC component, and f is the frequency in Hz.
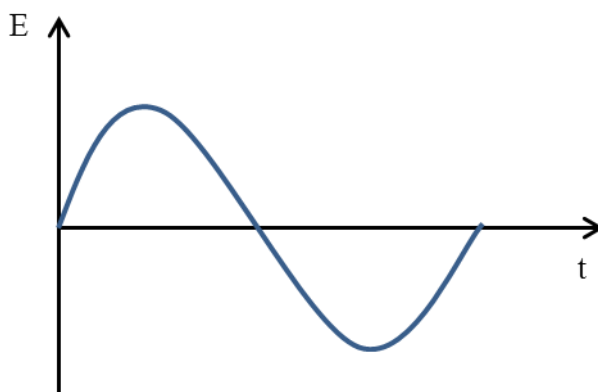
Fig 1.21 The applied potential waveform of AC impedance spectroscopy

The oscillating potential across the cell causes a current to flow given by

$$i_t = i_m \sin(2\pi f t + \theta) \tag{1.24}$$

where i_t is the real-time current, i_m is the maximum current amplitude and θ represents any phase difference between the applied voltage and detected current.

The response of electrical circuits to AC voltages is often described in terms of the impedance (*Z*) defined as

$$Z(f) = \frac{E_t}{i_t} \qquad (1.25)$$

In the real complex circuit, the phase difference between current and voltage can take on any value and according to equation (1.24), this can alter with frequency. Therefore, mathematically the impedance can be expressed by

$$Z(f) = Z' \sin(2\pi f t) - Z'' \cos(2\pi f t) \qquad (1.26)$$

Different with conventional voltammogram, the impedance measurements can be described by a plot in which the quantities Z' and $-Z''$ appear on the x- and y- axes, respectively. If the impedance, Z, at each frequency is plotted as a point with coordinate (Z', $-Z''$), the resulting vector from the origin to this point represents the impedance. It has a magnitude equal to the length of this vector and the phase difference between the current and voltage is given by θ. In impedance analysis, equivalent electrical circuits are utilized to model the electrochemical system and separate out the capacitive charging component.

The use of a three-electrode system and suitable reference electrode permits the impedance of a specific electrode/solution interface to be probed [87]. Normally the frequency range of 10^{-2} to 10^5 Hz is used. The ability of varying wide range of frequency enables the huge range of time-scales to be studied.

Fig 1.22 showed a typical impedance plot obtained under conditions when an electrolytic reaction is taking place at the electrode. For better understanding of this circumstance, the Randles circuit shown in Fig 1.23.
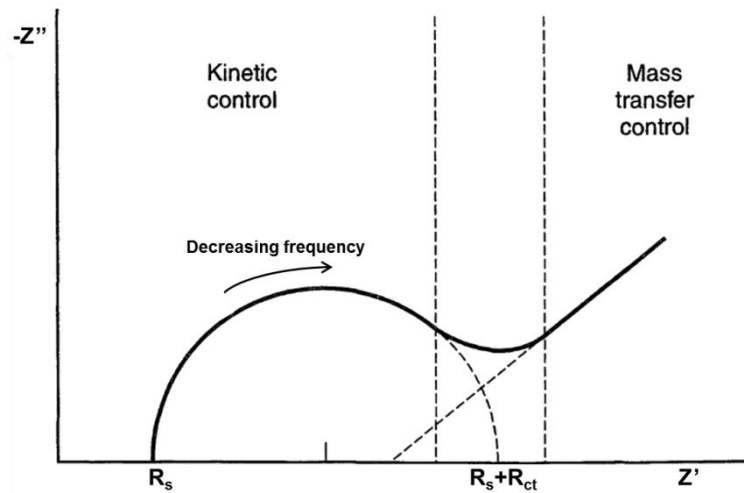
Fig 1.22 Impedance plot showing the addition of an electrolytic reaction

In comparison with the no-electrolysis case, the charge transfer resistance, R_{ct}, in parallel to the double layer capacitancity, C_{dl}, has been added to model the Faradaic charge transfer reaction. The Warburg impedance allows for the frequency dependence of diffusive transport to the electrode. At high frequency the impedance is simply that of the solution resistance, because the double layer provides a path of negligible resistance to the current. It follows that at high frequency no electrolysis takes place. When the frequency decreases, the effect of R_{ct} in parallel with the C_{dl} gives rise to the characteristic semicircular part of the plot. Finally, when the frequency enters the lowest value zone, the impedance shows a large rise, modelled by the Warburg impedance. This is the result of significant concentration changes induced by AC current which becomes increasingly difficult to replenish by diffusion as frequency decreases.
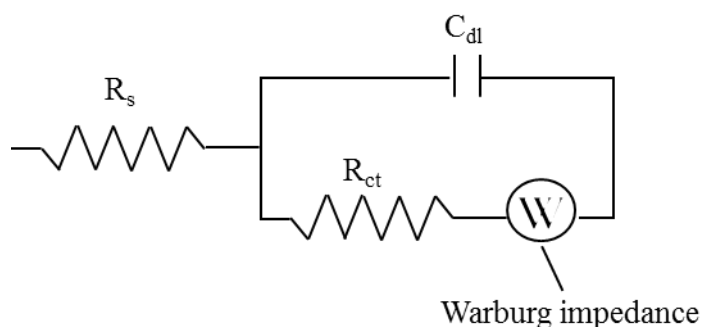
Fig 1.23 The Randles circuit

AC impedance spectroscopy is widely used in material research because it involves a relatively simple electrical measurement that can readily be automated and whose results may often be correlated with many complex materials variables, such as mass transport, chemical reaction rates, and dielectric properties [103].

The impedance technique has also been applied to channel microband electrodes [104]. With the numerical work, the equations obtained permitted the researcher to calculate impedances over the entire operating range of flow rates, cell dimensions and electrode length, etc. Furthermore, the general approach of impedance spectroscopy has also employed to study coupled homogeneous reactions and surface adsorption processes. It also contributed a lot in semiconductor electrode study and development [105].

1.4.5.5 Fourier transformed alternating current voltammetry

In the electrochemical reaction systems, the resulting current consists of two parts: a Faradaic and non-Faradaic current. The Faradaic current is only produced by the electrochemical reaction(s). The non-Faradaic current arises from the charging and discharging of the electrical double layer [106] and uncompensated resistance, etc. When the electrochemical analysis is conducted, researchers are always trying to eliminate the effect of the non-Faradaic term.

It would be of great help if the experimental technique is highly sensitive to all the unknown parameters [107]. A range of phase sensitive techniques using different waveforms overlapped with traditional DC (direct current) inputs have been developed to help distinguish between the Faradaic and non-Faradaic processes [108].

Fourier transformed alternating current voltammetry (FTACV) was proposed decades ago and developed by Bond [109], which applies a sinusoidal signal superimposed onto the linear waveform used in cyclic voltammetry which demonstrated in Fig 1.24.
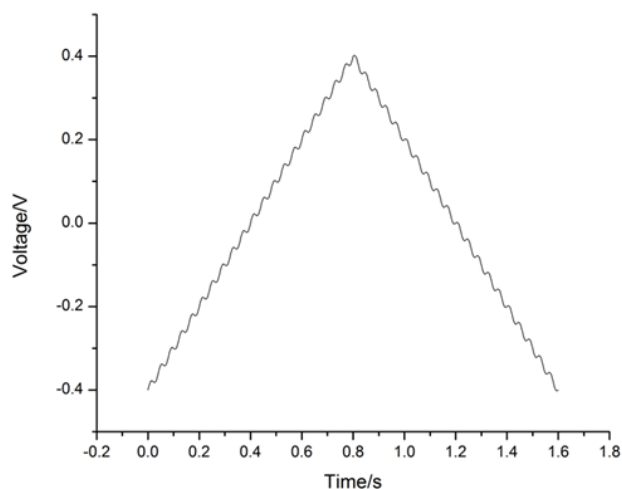
Fig 1.24 Potential waveform of Fourier transformed alternating current voltammetry

The potentials of alternating current (ac) voltammetry can be expressed by equation (1.27) as:

$$E_t = E_{dc} + \Delta E \sin(\omega t) \tag{1.27}$$

where E_{dc} is the potential of DC signal and ω is the angular frequency.

The resulting output current can be analysed by using a Fourier transform (FT) algorithm to extract both phase and magnitude information from the input signal. The kinetic parameters will be separated either from the amplitude of AC current, which is a function of E_{dc}, or from the phase angle between the AC current and AC voltage, Φ, due to the difference in time scale [110]. Different angular velocities give rise to the first to higher harmonics.

To obtain DC and harmonic components in FTACV, a certain frequency band that contains most of the energy is selected to filter the excluded portion in the power spectrum. Each component has its own frequency, which is 0 Hz for DC signal, $\frac{\omega}{2\pi}$ for the fundamental harmonic, $\frac{\omega}{\pi}$ for the second harmonic, $\frac{3\omega}{2\pi}$ for the third harmonic, and so on. The power spectrum at selected frequencies is treated by an inverse Fourier transform algorithm and the components induced by the DC and the AC signal are generated in a current-time version. The DC signal can also be obtained directly from AC voltammetry. Hence, the intuition and simplicity of the DC methodologies are recovered [111].

This Figure is not shown due to copyright issues

Fig 1.25 Schematics of data processing methodology used in FT voltammetric instrumentation [108].

In a reversible system, the rate of electron transfer is fast enough and the system is under diffusion control. A classic duck-shape curve in current-time or current-potential form can be investigated in DC component, which is identical to the result obtained directly from CV scan. As for the AC components, as it is shown in Fig 1.26, a bell-shaped curve is obtained in the fundamental harmonic. A single current peak is generated by the forward scan when $E_{dc}=E_{1/2}$, which is near the standard potential of the redox species. Ideally, the curve generated from the backward scan should retrace well with the forward one. For the second harmonic, two symmetrical peaks can be obtained from the scan in both directions. The middle point of two peaks is $E_{1/2}$. The shape and the peak height of these peaks indicate the reversibility of the reaction. In harmonic three, for the forward scan, there are three peaks with a higher middle one can be observed. The peaks of the reverse scan should be theoretically symmetrical with the forward ones. For the fourth and higher harmonic components, the behaviour of the peaks provides qualitative information while with supporting numerical models, abundant quantitative results can be obtained from the higher harmonic as well.

This Figure is not shown due to copyright issues

Fig 1.26 Fundamental to fifth Harmonics and DC component [112]

In a quasi-reversible system, in which the rate of charge transfer decreases, the behaviour of AC components varies correspondingly [113]. In conventional cyclic voltammetry, a typical quasi-reversible voltammogram showed bigger peak separation compared with reversible

reaction. In the fundamental harmonic, the two peaks generated from both directions are asymmetric due to the small kinetics. In the second harmonic, the two peaks formed in one direction scan showed different height, which is the result of competition of kinetic control and diffusion control. In third and higher harmonics, the asymmetric peaks will be obtained as well due to the quasi-reversibility of the reaction.

In the irreversible system, the situation differs due to the reaction types. As for the pure electrochemical reaction, the asymmetry of the peaks becomes more obvious due to the small kinetics. While in most of the situation, the coupled chemical reactions take place after the electron transfer, which results in the total irreversible of the system. Application of FTACV has also extended to the investigation of homogeneous reactions. Researchers have found that Fourier transformed alternating current voltammetry is able to provide mechanistic insights into couples homogeneous processes far more detailed than those that are readily accessible with DC techniques in both experimental and numerical ways [114].

In previous research, small amplitude (typically no more than 10mV) is often used in the AC impedance techniques. However, the signal-to-noise ratio may be poor and the peaks in the higher harmonics cannot be easily obtained [115]. Then the large amplitude was introduced into the AC component. Use of large-amplitude sinusoidal perturbations would amplify the nonlinearity of the electrode process and hence simplify detection of the enhanced higher harmonic component [113]. Bond and his colleagues [116–118] have presented theoretical treatments for the application of a large amplitude Fourier transformed AC voltammetry approach with ΔE ranged 50-200mV and the output signal was analysed with Fourier transform inverse Fourier transform sequence. The signal input of large amplitude Fourier transformed AC voltammetry in equation (1.27) can be presented with more detailed as the angular frequency and the amplitude, combined by harmonic sequence as

$$E_t = E_{dc} + \sum_{n=1,2,3\ldots}^{N} \Delta E \sin(\omega t) \tag{1.28}$$

The use of a Fourier series allows the periodic function to be decomposed into a linear combination of harmonic signals.

By analysing the output signal with Fourier transformation, the double layer capacitive component C_{dl} will have a different phase and magnitude relationship to the input signal. By verifying the amplitude and frequency, it is possible to discriminate the effect of solution resistance and double layer capacitance [119–121]. In addition, the second to higher

harmonics are essentially free from the effect of the double layer charging current, which means the study of coupled chemical processes can be developed based on that.

The other effect that cannot be neglected is uncompensated resistance (R_u) in the solution, which will cause potential drop with current (IR_u). Nicholson [122] has proved that uncompensated resistance and slow electrode kinetics may exhibit very similar effect on the characteristics of DC cyclic voltammograms. Especially when the system is close to reversible and IR_u provides a major influence to the voltammetric characteristics. Hence it is almost impossible to measure both the electrode kinetics and uncompensated resistance by DC cyclic voltammetry. Nevertheless, in the large amplitude Fourier transformed AC voltammetry, it was reported that the fourth and fifth harmonics characteristic are sensitive to uncompensated resistance particularly but also devoid of background current [123,124].

Also, it was confirmed that underlying electron transfer processed can be measured with higher AC harmonics even in the presence of large catalytic currents that contribute significantly in DC voltammogram [125,126]. On that basis, large amplitude FTACV analogue with traditional DC techniques performs as a truly powerful electrochemical approach.

1.4.5.6 Hydrodynamic voltammetry

Voltammetric methods involving convective mass transport of reactants and products are sometimes called hydrodynamic voltammetry. The advantage of hydrodynamic methods is that a steady state is attained rather quickly, and measurements can be made with high precision. Moreover, at steady-state, double-layer charging does not enter the measurement [88]. Also, the mass transport rates at the electrode surface under hydrodynamic conditions are typically larger than the rates of diffusion alone, so that the relative contribution of mass transport to electron-transfer kinetics is often smaller.

A hydrodynamic electrode is one in which forced convection is deliberately introduced to domain transport to the electrode. The convective way within the electrochemical cell may be induced in different ways. Commonly, the electrodes are fixed and the electrolyte solution allowed to flow across the electrode surface [127], or the electrode may move inducing convection in the solution, which was firstly proposed as rotating ring-disk electrode by Frumkin [128].

- Rotating disc electrode system

A commonly encountered hydrodynamic electrode is the rotating disc electrode (RDE) which is particularly popular because it is simple to use and easy to construct and clean after use [129]. This electrode consists of a disk of the electrode as working unit imbedded in a rod of an insulating material such as Teflon. Then the whole rod is placed into the electrochemical cell fulfilled with electrolyte solution and rotates at a constant speed. While it is working, the rotation spins the solution out from the rod surface in a radial direction and this movement results in drawing fresh solution towards the disc electrode (Fig 1.27). This sustains a steady supply of fresh electroactive material to the electrode surface [87].

This Figure is not shown due to copyright issues

Fig 1.27 The rotating disc electrode (RDE) [130]

The most intriguing aspect of the RDE is that the convective mass transport problem was solved rather rigorously by Levich via hydrodynamic and can be verified to a high degree in experimental applications [131]. The transport limiting current (i_L) as a function of the rotation speed can be calculated by

$$i_L = 0.62nFAc_{bulk}D_{bulk}^{\frac{2}{3}}v^{-\frac{1}{6}}\omega^{\frac{1}{2}} \tag{1.29}$$

in which v represents the viscosity of the solution and ω is the rotation speed. Based on equation (1.29), the linear relationship between limiting current and the rotation speed can be investigated. Fig 1.28 showed the linear sweep voltammogram of rotating disc electrode with various rotation speeds.
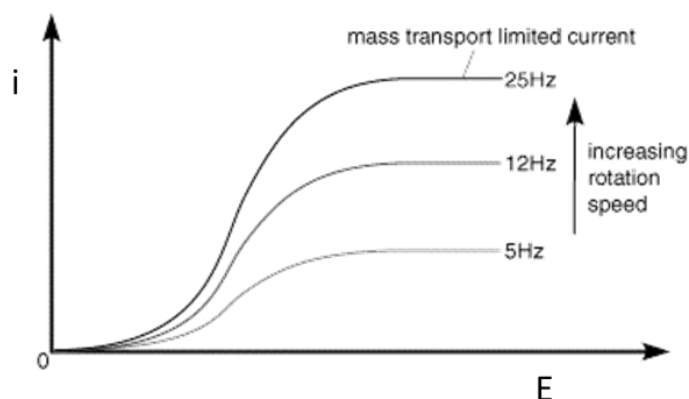
Fig 1.28 Voltammogram of RDE with increasing rotation speeds

- The channel electrode system

In a channel electrode system, the forced convection is achieved by controlling electrolyte solution flowing over a stationary electrode. It consists of an electrode embedded in the wall of a rectangular duct through which electrolyte solution is flowed as Fig 1.29. The cell design and flow rate are adjusted so that the flow pattern on the electrode is laminar and it can be described accurately for quantitative analysis. The mass transport by convection can be controlled through the channel design, the electrode size and the flow rate. Moreover, this setup enbales the incorporation of electrochemical measurements to flow systems as well as its use in spectroelectrochemistry and photoelectrochemistry.

This Figure is not shown due to copyright issues

Fig 1.29 Schematic diagram of a channel electrode [132]

As it can be seen from Fig 1.30, a steady state voltammetric response was recorded as the voltage sweep rate was sufficiently slow to allow a steady state mass transport regime to establish as the voltage was swept. As a consequence, the resulting current rises and then reaches a steady value, namely the limiting current. In addition, the values of the limiting

currents increase with the flow rates. This is because the diffusion layer is thinner when the flow rate is faster.

Unlike the RDE, convection and diffusion operate in different directions, the electrode surface is non-uniformly accessible and thus the associated mathematical problem is multidimensional. However, this can be simplified under appropriate experimental conditions. Thus, it can be assumed that the flow velocity is high enough for the transport by diffusion in the direction of the flow (x-direction) to be negligible relative to convection. Moreover, edge effects can be neglected provided that the width of the band is much smaller than that of the channel [133].
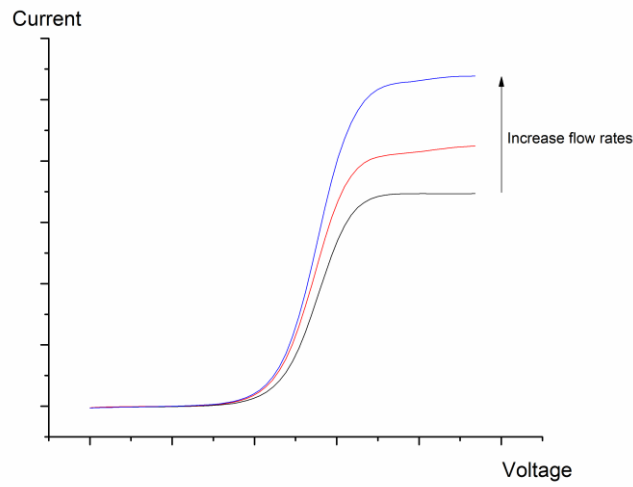
Fig 1.30 Current–voltage curves of hydrodynamic channel electrode with

increasing flow rate

For a macroscopic channel cell system, the laminar flow convective-diffusion equation describing the mass transport regime at steady-state for a large planar electrode is given by

$$\frac{\partial c}{\partial t} = D\frac{\partial^2 c}{\partial y^2} - v_x\frac{\partial c}{\partial x} = 0 \tag{1.30}$$

where x is the distance along the channel starting from the upstream edge of the electrode, y is the normal distance starting from the electrode surface alongside the height of the flow stream and v_x is the velocity of the flow in x direction.

Based on this equation, the prediction of limiting current as a function of the solution volume flow rate (V_f) by Levich equation

$$i_L = 0.925 nF c_{bulk} D^{\frac{2}{3}} V_f^{\frac{1}{3}} (h^2 d)^{-\frac{1}{3}} w x_e^{\frac{2}{3}} \tag{1.31}$$

where x_e is the electrode length, h, the cell half-height, d, the width of the cell, and w the electrode width. This equation can be applied when the flow rate is sufficiently fast that the diffusion layer thickness is much smaller than the cell height. Also, it indicates that the limiting current varies with the cube root of the volume flow rates (Fig 1.31).
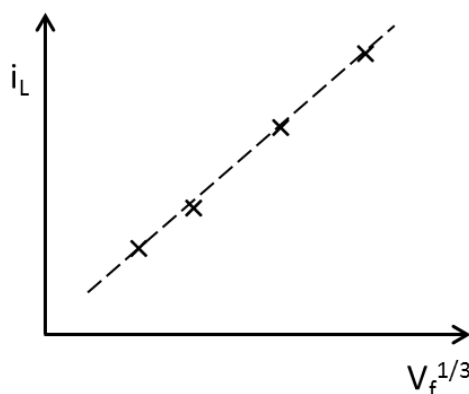
Fig 1.31 Linear relationship of limiting current and cube root of volume flow rates

The channel electrodes in hydrodynamic system offer many advantages. First, their flow-through nature facilitates continuous monitoring in analytical procedures, for example chromatographic separation. Second the rigorous mechanistic investigation of electrode processes via voltammetric methods can be achieved, which benefits from the well-defined hydrodynamics of channel electrodes. Third, the channel electrodes can be easily modified to be used for spectroelectrochemistry [134].

1.4.5.7 Hydrodynamic modulation voltammetry

In previous section, the hydrodynamic voltammetry has been discussed. The utilization of flowing solution in electrochemical analysis offer many desirable features, such as low sample consumption, the possibility of multisample analysis and on-line detection. But one of the vital drawbacks of this technique is the notorious background signal. Many electroactive species could give essentially useless signal in conventional scanning voltammetry at solid electrode. Many analytical problems which could never have been attacked by conventional voltage-scanning techniques can be handled by hydrodynamic modulation voltammetry (HMV).

According to Wang's review in 1981 [135], there are two main approaches to achieve HMV in the early years. The first one is electrode motion modulation, which has focused on rotating disc electrode switched between two different rotating speed [136–138]. The advantages of this technique is that the high sensitivity, low noise-level and precision of the response can be obtained while the shortcoming is obvious that the "relaxing" time of concentration boundary layer is quite long after the hydrodynamic step.

This Figure is not shown due to copyright issues

Fig 1.32 Current response of pulsed-rotation system [138]

The second approach is flow modulation methods, which was first proposed by Blaedel and Boyer [139]. They demonstrated that the stopped-flow technique to improve the sensitivity for tubular electrode. By controlling the solution from zero to high flow rates, the difference among the steady states current can be measured.

This Figure is not shown due to copyright issues

Fig 1.33 Definitions of currents measured by the stopped-flow technique [139]

As it can be seen from Fig 1.33, the merit of this method is the inherent sensitivity that it enables to separate Faradaic and non-Faradaic current terms. Also the simplicity of operation took a great part in it.

Since 1981, great advances have been made in HMV methodology with the advent of ultramicroelectrodes (UMEs) under convective or vibration control. Macpherson [140] concluded recent development of HMV technique, including vibrating electrode [141], channel stopped flow method, microjet electrode [142] and ultrasonic modulation [143]. By employing UMEs, these techniques would reduce the diffusional relaxation time with the aim of attaining greater detection sensitivity and reducing analysis times.

Furthermore, in 1987, Schurette and McCreery [144] introduced alternating current component into HMV. Compared to HMV, hydrodynamically modulated alternating current voltammetry technique has the advantage of a peak rather than wave response, which leads to improved detection limits and resolution. Also, the peak response resulting from the differential nature of DC polarography is more analytical useful. Schwartz [145] also presented his work in this field. He proved that Fourier transform hydrodynamic modulation voltammetry can be a powerful tool to study convective nonlinearities in mass-transfer system and the kinetic measurements can be made quickly via using this technique.

With the basis of the previous research, to apply FTACV with hydrodynamic modulation method could be an exciting way to process electrochemical analysis.

1.4.6 Electrolysis reaction mechanisms

In previous section, electron transfer reaction has shown to be stable. However, in reality most of the products of the electrochemical reaction remain highly active and are therefore capable of undergoing further reaction. In this section, some complex electrolysis mechanisms will be introduced.

1.4.6.1   Prue electron transfer reaction

As it mentioned before, the simplest electrochemical system involves only electron transfer reaction (as Equation (1.1)).   The current induces the exchange of electrons between the electrode and molecules in solution, so altering the oxidation state of the molecule, and 'electrolysis' occurs. The transfer of electrons can be in either direction; a molecule in solution may accept an electron from the electrode and become reduced [87].

A very classic cyclic voltammogram was shown below to demonstrate the pure electrochemical reaction without further reactions.
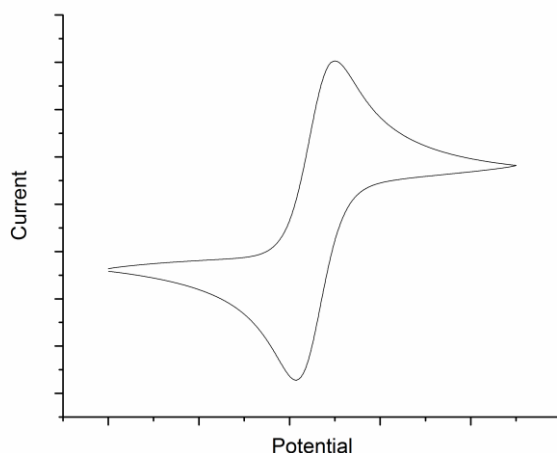
Fig 1.34 Cyclic voltammogram of pure electron transfer reaction

- Multiple electron transfer reactions

The simplest multiple electron transfer reaction is the two-electron transfer (EE) reaction. Conceptually, the EE mechanism can occur in two ways, first way is a one single step involving both electrons

$$A + 2e^- \rightleftharpoons C \tag{1.32}$$

or two consecutive one-electron steps

$$A + e^- \rightleftharpoons B \tag{1.33}$$

$$B + e^- \rightleftharpoons C \tag{1.34}$$

The later way is more commonly observed in multiple electron transfer reactions as it is easier to overcome two small activation barriers than one large one [87]. Fig 1.35 shows a typical EE reaction which undergoes two consecutive reversible electron transfer steps.

45

$$A(aq) + e^-(m) \rightleftharpoons B(aq) \quad B(aq) + e^-(m) \rightleftharpoons C(aq)$$
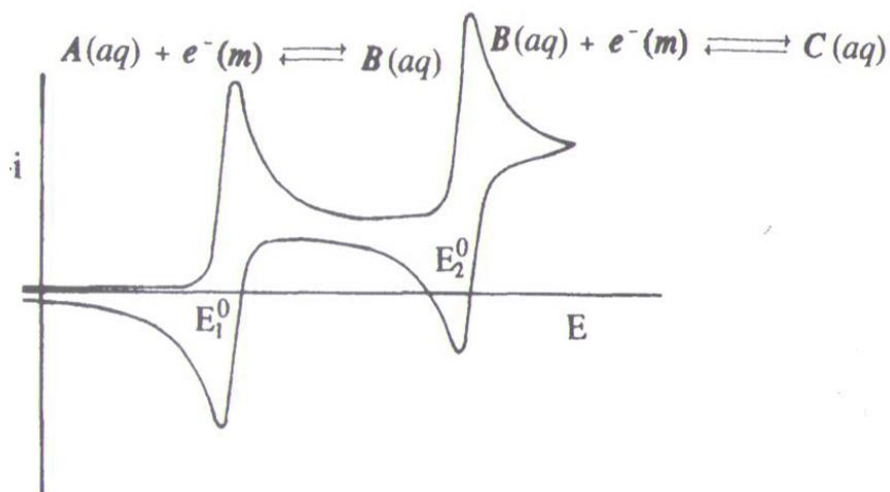
Fig 1.35 Cyclic voltammogram of two-electron transfer reaction

1.4.6.2   Coupled homogeneous reactions

Sometimes the electrochemical reaction is irreversible and quasi-irreversible due to the occurrence of the homogeneous chemical reactions. Theoretically, the electron transfer reaction at the electrode surface can be referred 'E' step as a heterogeneous reaction, then a homogeneous chemical reaction is termed as 'C' step. The following mechanisms include both of these two or more steps.

- The EC reaction

The EC reaction is considered as

$$R - e^- \rightleftharpoons O \tag{1.35}$$

$$O \xrightarrow{k_{EC}} Y \tag{1.36}$$

For the EC reaction species O, which formed at the electrode, is unstable and decays with the rate of k_{EC} to form a non-electroactive species Y. If k_{EC} is significantly fast, O will react immediately once it is formed from E step. The cyclic voltammogram will look like Fig 1.36. On the contrary, if the k_{EC} is relatively slow, then O is not depleted by the chemical reaction. The cyclic voltammogram will be similar with normal reversible reaction. Therefore, the reverse peak height becomes a useful tool to roughly estimate the value of the k_{EC}.
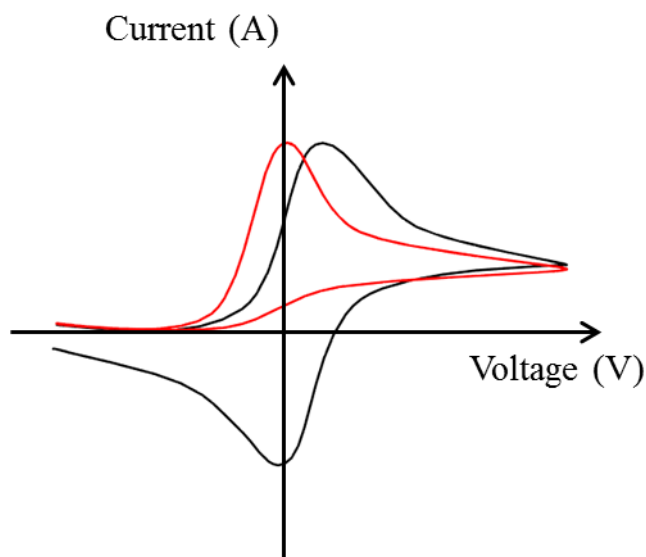
Fig 1.36 Typical cyclic voltammogram with an EC process

For the EC reaction mentioned above, when the scan rate is decreased, the residence time for the species produced at the electrode is increased, leading to a voltammetric response where there is a significantly reduced back peak due to the chemical decomposition of the species O.

In particular, the wave will shift to anodic direction if the rate constant of chemical reaction increases. This can be deduced by Nernst equation (1.2), which indicates that the ratio of equilibrium surface concentrations of R and O at a particular potential for an electrochemically reversible electrode reaction. As the homogeneous reaction consumes O at a very fast rate, which influences the equilibrium on the electrode surface. To reestablish the equilibrium concentration at the electrode surface, the reaction is driven to produce more O to replenish those reacted in the chemical step [87].

- The ECE reaction

The extension of the EC reaction is the ECE mechanism

$$R_1 - e^- \rightleftharpoons O_1 \tag{1.37}$$

$$O_1 \xrightarrow{k_{ECE}} R_2 \tag{1.38}$$

$$R_2 - e^- \rightleftharpoons O_2 \tag{1.39}$$

The product from former EC reaction now in this mechanism is electroactive, which means another electron transfer reaction follows. Normally, the second electron transfer reaction

47

takes place in a different potential as the first one. The case where R_2 is more difficult to oxidized than R_1 is described with reference to cyclic voltammetry measurements while the contrary one is described by reference to coupled convection-diffusion measurements.

When the R_1 is easier to be oxidized, there will be two separate peaks in the forward sweep of cyclic voltammogram can be found (Fig 1.37). The relative peak heights are a function of the homogeneous kinetics and potential scan rates. The magnitude of the rate constant k_{ECE} can be deduced by the analysis of peak heights.
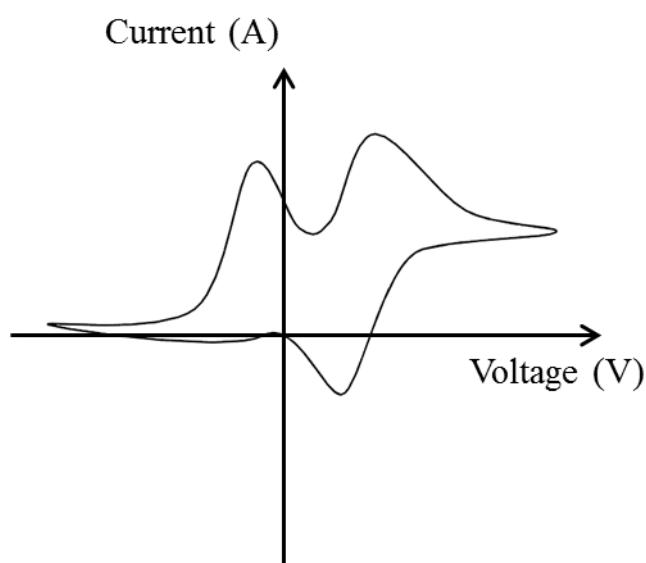
Fig 1.37 Cyclic voltammogram of ECE reaction

On the second hand, where R_2 is easier to be oxidized than R_1, further information can be obtained by using hydrodynamic voltammetry. As it can be seen from Fig 1.37, the additional current gain over one-electron is caused by the second E step.

- The EC' reaction

$$R - e^- \rightleftharpoons O \qquad (1.40)$$

$$O + Y \xrightarrow{k_{EC'}} R + product \qquad (1.41)$$

The equations above represent the EC' mechanism. The prime (') represents a catalytic process. The catalytic process occurs as the product of the electrode reaction, O, reacts with a substrate molecule Y in solution. The result of this reaction is that O is reduced back to the starting material R (the catalytic cycle) and Y is converted to products. If species Y is present in large excess compared to O, then equation (1.41) is a pseudo-first-order reaction [88].

48

Catalytic reactions are often regarded as a clean and efficient method of enhancing chemical reactivity, so they are utilized in numerous applications in industry.

Fig 1.38 shows a typical cyclic voltammogram for differing quantities of substrate Y. As the concentration of Y increases, the current gain increases compared to no substrate in the solution. When the potential is swept back, there is little O to be reduced back to R because most of O is reacted with Y in the chemical step, thus less reductive current can be detected compared to simple reversible reaction. Analogue with previous mechanisms, the catalytic current is dependent on the quantity of O and Y as well as the rate constant $k_{EC'}$ between O and Y.
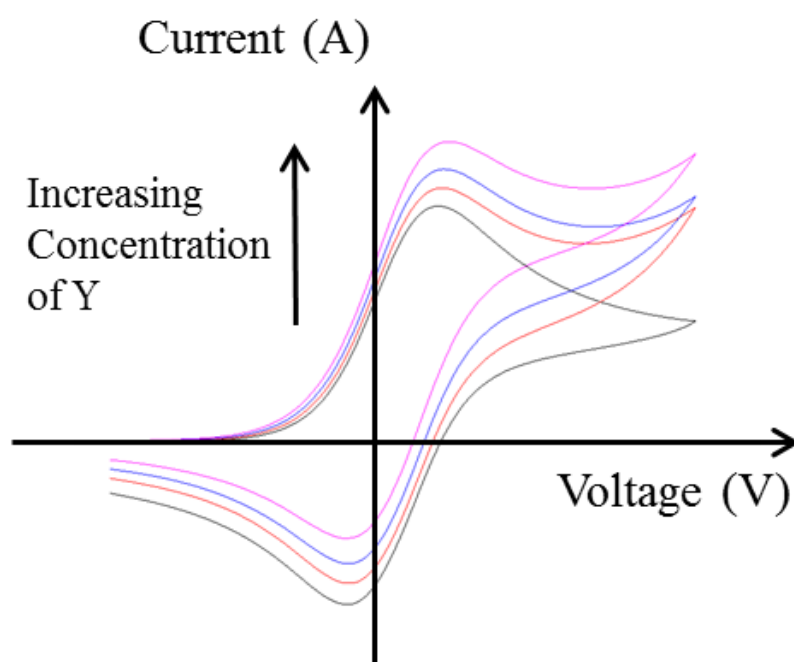
Fig 1.38 Cyclic voltammogram of the EC' reaction with various kinetics of homogeneous reaction

1.5 Research aims and thesis structure

This thesis aimed to produce self-designed microreactors and study the effect of modulated methods involved both in voltammetric and microfluidic technique. To achieve that, different kinds of electrochemical reactions including pure electron transfer reactions and homogeneous reactions have been carried out.

The remaining chapters of this thesis have the following structure:

Chapter 2 illustrates the micro-engineering area and microfabrication methodology applied to produce electrochemical microreactors. Detailed fabrication methods for producing microelectrodes and microchannels with positive and negative photoresists respectively are introduced as well as microreactor assembly.

Chapter 3 presents the details about the investigation electrolysis reaction mechanisms in electrochemical microreactors. Either stagnant or hydrodynamic system is detected by large amplitude Fourier transformed alternating current voltammetry. A range of different kinds of electrolysis reaction mechanisms involving simple electron transfer and homogeneous chemical reactions were studied.

Chapter 4 details the electrochemical behaviours under hydrodynamic modulation voltammetry. The step hydrodynamic modulation was introduced during electrochemical detection. The response from different electrolysis reactions was described.

Chapter 5 introduces a further development of hydrodynamic modulation system. The electrochemical output signal under both potential modulation voltammetric controlling and hydrodynamic modulation was recorded and analyzed. This chapter demonstrates a possible alternative for autonomous sensing.

Chapter 2   Microfabrication Technology

2.1   Introduction

In the previous chapter, the fundamental background of electrochemistry and micro-engineering was introduced. This chapter briefly reviews the basic introduction and recent developments in microfabrication methodology. Microfabrication technology will be used to fabricate the electrochemical microreactors used in this thesis. This chapter highlights the design, main procedures, instrument and materials involved to fabricate electrochemical microreactors.

2.2   Microfabrication methodology

Due to the large demands of microreactors, fabrication methodologies have been developed significantly in recent decades [146]. Microfabrication techniques and scale-up by replication have spectacular advances in the electronics industry and more recently in microanalysis chips for chemical and biological applications [147].

2.2.1 Technologies for microsystems

Micro-system technology (MST) is based both on precision engineering and semiconductor fabrication technologies, using various strategies and techniques for the production of a multitude of functional elements [148]. MST has boosted dedicated equipment development which is now entering the market [149]. They can be classified into four main types:

2.2.1.1   Photolithography based techniques

Photolithography has been the main workhorse in the semiconductor industry and for the production of integrated circuits [150]. Photolithography based techniques contain bulk micromaching using wet and dry etch techniques, surface micromaching, X-ray-LIGA and

UV-LIGA techniques. These technologies can achieve sub-µm precision, and when the high-volume batch production is needed, it is cheap to do so. Nevertheless, most of these types of productions mainly result in the fabrication of two dimensional structures [148].

Photolithography utilizes exposure of a light-sensitive polymer (photoresist) to ultraviolet (UV) light to define a desired pattern. Initially, UV light is illuminated through a photomask that consists of opaque features on a transparent substrate (e.g., quartz, glass) to make an exposure on a photoresist that is coated on a substrate [146]. In the exposed area, the polymer chains of photoresist break down resulting in more soluble in a chemical solution called developer. Subsequently, the exposed photoresist is removed in a developer to form the desired photoresist pattern.

There are three forms of photolithography: contact printing, proximity printing and projection printing as schematically illustrated in Fig 2.1. Contact and proximity printings place the photomask in contact with or in a close proximity to the photoresist. Generally, contact and proximity printings are capable of making patterns as small as a few micrometers. Therefore, they are typically used in the fabrication of moderate-resolution patterns especially in laboratories and small to medium-sized companies. It should be noted that photolithography in most of research works normally refers to contact or proximity printings. In contrast, a projection printing system applies an optical lens system to project a deep-UV pattern from an excimer laser on the photoresist enabling patter-size reduction by 2-10 times [151]. It is capable of fabricating high-resolution patterns as small as a few tens me nanometers at a high throughput [152]. However, it requires a sophisticated optical-lens system and precise control systems of temperature and position, which leads to a very expensive setup. Thus, it is employed in manufacturing of advanced integrated circuits and CPU chips. Recently, immersion lithography [153], extreme UV-lithography [154], and resolution enhancement technology [155] have been developed to improve the lithography resolution of projection printing.

This Figure is not shown due to copyright issues

Fig 2.1 Schematic illustration of three forms of photolithography [150]

2.2.1.2   Direct microfabrication

Laser microfabrication is one of the typical direct microfabrication technologies [156–158]. A laser ablation experimental scheme was illustrated as Fig 2.2. The laser beam went through the substrate and was then absorbed at the metal target surface placed behind the substrate since the fused quartz has no absorption in the UV range. Owing to the interaction of plasma generated from the target and the laser beam, significant ablation took place at the rear surface of the substrate [159].

This Figure is not shown due to copyright issues

Fig 2.2 Schematic diagram of the laser ablation setup [159]

Electron beams have also been applied directly for etching chalcogenide glasses [160] and later to build neutral cell networks by Italian researchers [161], which represents a major novelty in the use of the electron beam lithography applied to polymers.

Katoh and the co-workers [162] have managed to fabricate three dimensional products with direct writing by using synchrotron radiation etching technique. However three dimensional products can be achieved by utilizing direct microfabrication technique whilst they cannot be as precise as made by lithography based techniques.

2.2.1.3   Replication techniques

Microelectroforming [163], stamping [164], injection molding [165] and extruding [166] are recognized as replication techniques. By utilizing them, we can abundantly fabricate metallic,

plastic and ceramic copies of a very precise master. It means an expensive reproduction can be obtained cheaply but dedicated equipment which may be still under development is required.

Micro-hot-embossing comes originally from the last step of the LIGA process, which is a widely used replication technique, especially for optical application [167]. A typical micro-hot embossing process is composed of four major steps [168]:

(1) Heating the mold and substrate to molding temperature;

(2) Embossing microstructure patterns at embossing temperature;

(3) Cooling the mold and substrate to demolding temperature;

(4) Demolding the component by opening the tools.

In hot embossing, high aspect ratio structures (>10) can be replicated quite easily, as compared with injection molding. For prototyping hot embossing is much better suited than injection-molding due to the easy mounting procedure and the small numbers of parameters for the replication process to be varied. Recent progresses in machine technology, have allowed reduction in the cycle-time in hot embossing significantly for certain polymers [169]. Also, to perfect the micro-hot embossing performance, some supporting techniques were developed to enhance the process, such as ultrasonic micro-hot embossing technology [170] and gas-assisted micro-hot-embossing [171].

This Figure is not shown due to copyright issues

Fig 2.3 Schematic representation of a typical micro-hot embossing process including four major steps: heating, molding, cooling and demolding [168].

Similarly with the hot embossing method, injection molding is another important replication technique. Injection molding is a major part of the plastic industry, which accounts for more than 33% of all polymeric materials processed, and is widely used for mass producing discrete plastic parts of complex shape cost-effectively with high precision [172].

This process transfers a thermoplastic material in the form of granules from a hopper into a heated barrel so that it becomes molten and soft. Then the material is forced under pressure inside a mould cavity where it is subjected to a holding pressure for a specific time to compensate for material shrinkage. The material solidifies as the mould temperature is decreased below the glass transition temperature of the polymer. After sufficient time, the material freezes into the mould shape and gets ejected, and the cycle is repeated. A typical cycle lasts between few seconds and few minutes [173]. During the injection molding process, various polymeric material elements undergo different and complicated thermomechanical histories and experience significant change in their rheological, mechanical, and transport properties due to large pressure variations and rapid cooling. Various factors regarding the part and mold designs as well as the material selection and process setup have to be considered to ensure that the mold can be filled volumetrically [174–176].

Powder injection molding was developed as well, which combines the processability of plastics and the superior material properties of metals and ceramics to form high performance components [177].

Another replication method is replica molding. The replica molding technique involves three processing steps [178] as illustrated in Fig 2.4:

(1) Fabrication of a patterned master with desired dimensions;
(2) Generating a negative poly(dimethylsiloxane) (PDMS) replica from the original master as a mold;
(3) Casting a liquid precursor against the PDMS mold, followed by curing and peeling off to obtain the patterned polymeric structures.

This Figure is not shown due to copyright issues

Fig 2.4 Schematic illustration of the replica molding steps from a Si master to a polymer replica using a PDMS mold [178].

Replica molding is an efficient method to duplicate the pattern on rigid or elastomeric master. In order to keep as many details as the master, molding against elastomeric masters are even better to release small and fragile structures than the replication molding against rigid mold which is widely applied for mass production.

Among all these techniques, LIGA method is suitable for the laboratory-scale use. LIGA (German acronym for Lithographie, Galvanoformung, Abformnung) is based on combining synchrotron radiation lithography, galvanoforming, and plastic moulding [179]. The purpose of synchrotron radiation lithography is to generate a primary plastic template which is tiled with a metal by electrode position. This process allows three-dimensional microstructures to be fabricated from a variety of materials [180].

The LIGA process is superior compared with other techniques for fabricating mass production microstructures in complex shapes. The microproducts are significantly precise when this technique is applied. Meanwhile, the patterns of microreactors can be easily changed by replacing various masks, which means the cost will be markedly reduced compared with replication technique.

So far, there are two kinds of light resources to process LIGA method, X-ray [181] and UV light [182]. Although the X-ray LIGA method has been developed to make such deep structures for decades, the high cost and the very limited accessibility to synchrotron radiation source have greatly restricted its wide spread use. Then, the new alternative techniques such as UV photolithography combined with electroplating of metals have been developed to produce three-dimensional structures compared with those fabricated by X-ray LIGA technique but much less expensive. Furthermore the cost can be further reduced by utilizing new sacrificial layer method like photoresist.

This Figure is not shown due to copyright issues

Fig 2.5 Infrared bandpass filter made by X-ray lithography and electroforming [180]

Compared with a metal sacrificial layer, the photoresist sacrificial layer is much easier to remove, cheaper and time-saving. The light scattering occurs in the photoresist layer, especially when the photoresist layer is thick. It will result in a noticeable expansion of exposed patterns [183]. As a consequence, it is crucial to make sure the wafer loaded with photoresist is in soft contact with the mask when exposure in the UV light to diminish the effect of light scattering.

Uniform UV Exposure Illumination

Chrome on Glass Photomask

Photoresist

Substrate Wafer

Wet Chemical Development

Negative Photoresist
Photoresist is photopolymerized where exposed and rendered insoluble to the developer solution.

Positive Photoresist
Exposure decomposes a development inhibitor and developer solution only dissolves photoresist in the exposed areas.

Fig 2.6 Overview of Align/Expose/Develop Steps of UV-LIGA method

2.2.1.4   Microassembly

In most cases a monolithic integration of MST products is not possible. Therefore microassembly is an integrated key technology for the sub-μm precision assembling of μ-mechanics, μ-electronics, μ-fluidics, μ-optics in order to get high value added hybrid microsystems [148]. To achieve fluid tightness of the micro-system, a number of sealing methods between different materials have been developed.

In this thesis, the sealing method was mainly used to assemble the glass substrates with electrodes on and the PDMS microchannel parts. One technique most commonly used for getting irreversible seals is by exposing the surfaces to oxygen plasma. The changes in the surface texture and chemistry happening at such exposures have been widely studied. Most of this research indicates that PDMS material in general comprises of repeated units of $-O-Si(CH_3)_2-$, which on exposure to oxygen plasma develops silanol groups (-OH) at the expense

of methyl groups (-CH$_3$). The oxidation of the surface layer increases the concentration of hydroxyl groups and this leads to the formation of strong intermolecular bonds [184].

Another type of polymer bonding is SU-8 bonding which has been applied in the construction of many microstructured devices. SU-8 based lab-on-a-chip microsystems are often sealed by means of adhesive bonding using an intermediate layer of SU-8 photoresist. Compared with other bonding techniques *e.g.* silicon fusion bonding, low temperature direct bonding, anodic bonding, eutectic bonding and glass-frit bonding, the SU-8 bonding method requires a lower operation temperature and is less dependent on substrate material [185]. Also, as SU-8 is widely used in the construction of microstructures itself, the role of bonding can be achieved due to its high chemical and thermal stability. The method consists of three major steps. First the adhesive layer is deposited on one of the bonding surface by contact imprinting from a dummy wafer where the SU-8 photoresist was initially spun, or from a Teflon cylinder. Second, the wafers to be bonded are placed in contact and aligned. In the last step, the bonding process is performed at temperatures between 100°C and 200°C, an applied force of 1000 N in vacuum on a classical wafer bonding system. The results indicate a low stress value induced by the bonding technique [186].

2.2.2　Microfabrication materials

Due to different chemical reactions and demands for microsystems, the use of the materials differs. In this dissertation, the microelectrodes and microchannels are made by UV-LIGA based microfabrication technique. The details of the materials will be explained in later section.

2.3　Fabrication of electrochemical micro-devices

In this section, the microfabrication methods to produce electrochemical microreactors used in this thesis were detailed demonstrated. The main process includes microelectrode fabrication, microchannel fabrication and oxygen plasma assembly technique.

2.3.1　Photolithographic process

Photolithography is used to transfer the patterns from the film masks to the wafers loaded with thin photoresist layer. By alternating the different masks and the photoresists, the different shaped microelectrodes and microchannel can be obtained. In this report, the

microfabrication method is mostly based on UV-LIGA technique. Every step will be described in different situations.

- Step 1. Substrate preparation

Glass wafers were applied as the substrate both for microelectrodes and microchannels. First of all, the glass wafers without any scratch were cut into the desired sizes (mostly 6×6 cm in this dissertation). Then all wafers needed to be cleaned by soaking into the piranha solution ($V_{hydrogen\ peroxide\ (>30\%)} : V_{sulfuric\ acid\ (>95\%)} = 1:3$) for at least 20 minutes. Piranha solution has been in use for wafer cleaning for decades. This step attempts to remove the dust and other possible components will influence the photoresist coating to the substrate. The process must be carried out in the acid fume cupboard because the solution is self-heating [187]. After that, the wafers were rinsed with deionized water and dried out by nitrogen.

- Step 2. Photoresist spin coating

Photoresist is a light-sensitive material which is widely used in microstructured devices. In this research, due to the microfabrication of different kinds of microelectrodes and microchannels, two types of the photoresist were used to develop the patterns of them. The detailed information of these two is shown in Table below.

Table 2.1 Two types of photoresist

	Positive photoresist	Negative photoresist
Name	S1828	SU8-2100
Description	1-Methosy-2 propylacetate	a negative, epoxy-type, near-UV photoresist which is formulated in cyclopentanone solvent and exhibit improved coating and adhesion properties
Supplier	Shipley	MicroChem

A positive photoresist is a particular kind of polymer which when exposed to UV light becomes soluble whilst the unexposed part remains stable. In this work, as the chemical characteristic was changed by exposing it to the UV light, the photoresist layer on this part was removed by the developing solution and the rest part remained on the glass wafer. The positive photoresist was applied for the microelectrode fabrication. After the wafers coated

with the evaporating electrode material, the photoresist layer could be removed by acetone solution. Then only the patterns needed were coated with the electrode materials binding to the glass substrate permanently and would not be rinsed off by the acetone solution.

A negative photoresist behaves in reverse. After exposing it to the UV light, the patterns remained as the permanent three dimensional structures on the glass wafer but the unexposed part could be easily rinsed off by another developing solution. This is why this kind of photoresist is called "negative photoresist". The negative photoresist SU-8 2100 enables the fabrication of novel microchannels [188]. Meanwhile, this kind of photoresist has the advantages like high sensitivity, high thermal stability and excellent chemical resistance [189]. By using different parameters, the channels with different heights of 41~250 microns can be fabricated.

In the spin coating procedure, the photoresist was loaded manually and covered almost 2/3 clean substrates which were well prepared by the previous part. Then the Delta 10 spin coater (Karl Suss) was used to finish the spin coating step (Fig 2.7). A thin layer of photoresist covered the glass wafers after spin coating. The thickness of the photoresist depends on the viscosity of the photoresist, the various parameters of the spin coater as well as the soft-baking and hard-baking time. The detailed information of the setting up parameters will be shown later in table Table 2.2 and Table 2.3.
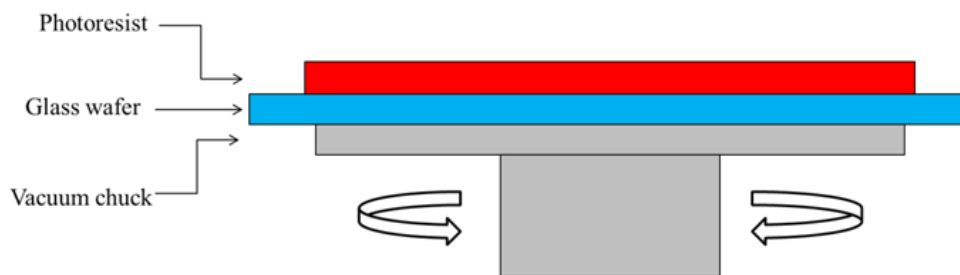
Fig 2.7 Spin coating

- Step 3. Soft bake (Pre-bake)

In order to stabilize the photoresist layer, the wafers were heated on the hot plate with the specific temperatures. This step aims to evaporate vapour in the coating solvent and to densify the photoresist which is shown in Fig 2.8. In this part, to keep the hot plate surface even is quite significant. If the surface is uneven, the asperous part cannot offer the good thermal

condition. In this case, it will influence the evaporation of the photoresist which may do harm to the quality of the final products.

Another crucial item of the soft bake step is the temperature and time control. Apart from the equipment for the soft bake procedure, an accurate soft bake temperature and time are also crucial for a better exposure fidelity and minimization of the edge bead problem. The specific soft bake temperature and time depend on the different photoresist and the desirable thickness, which will be illustrated in Table 2.2 and Table 2.6.
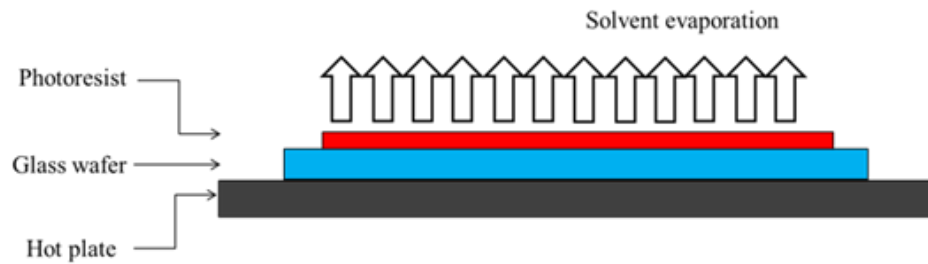
Fig 2.8 Soft bake

- Step 4. Exposure

When the photoresist layer was soft baked, it was ready to be exposed and a mask aligner (Karl Suss, MJB3) was used to achieve this. Based on the patterns needed whether for the microelectrodes or the microchannels, different masks (Micro-lithography Services Ltd) were prepared. Next an ultraviolet light source was projected through the mask to the photoresist layer. Then the solubility of the exposed area and the unexposed one were different according to which kind of photoresist was used.
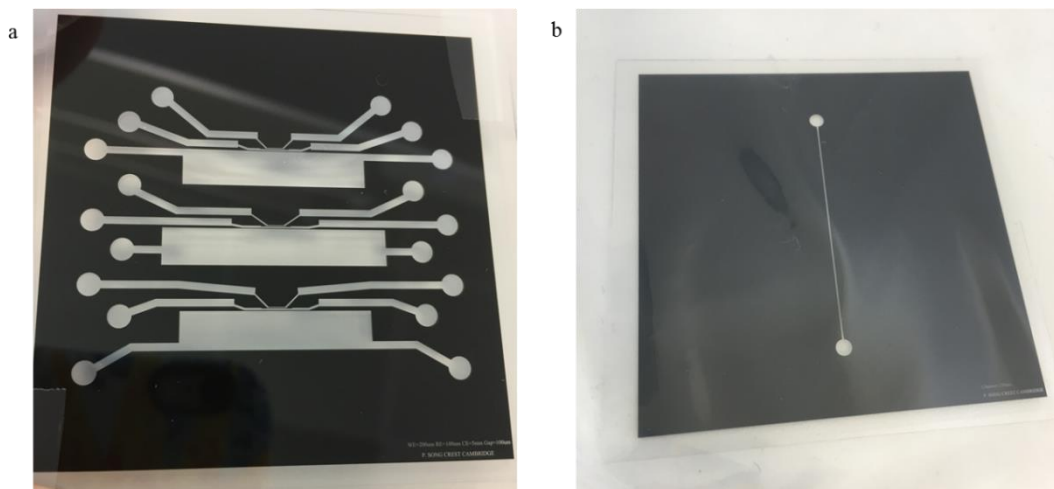
Fig 2.9 Photo mask film for (a) microelectrode; (b) microchannel

This step determines the shape that remains on the wafers. One trick of this step is to let the wafer soft contact with the mask. If the wafer is too close to the mask, the thickness of the photoresist layer will be depressed and the photoresist will pollute the mask pattern. In contrast, if there is a gap between the mask and the wafer, the scattering will happen. Both of these two situations will reduce the quality and the precision of the microstructure.

- Step 5. Hard bake (Post-bake)

This step took place approximately 60 seconds after exposure to cross-link the exposed portions of the negative photoresist. Hard baking is in order to stabilized the photoresist to the wafer and hardens it as well. The detailed post baking time will be shown in Table 2.2 and Table 2.3.

- Step 6. Development

After post-bake, all the wafers were held at the room temperature for at least 10 minutes to cool down. Then the wafers were developed to rinse off the part which is not needed with the specific development solution.

The development for the positive photoresist is AZ351 developer (Shipley) and that of the negative one is the EC solvent developer (MicroChem). The developing time varies from the types and the thickness of the photoresist. The details will be given in the Table 2.2 and Table 2.3.

Fig 2.10 showed the summary of lithography with positive and negative photoresist.
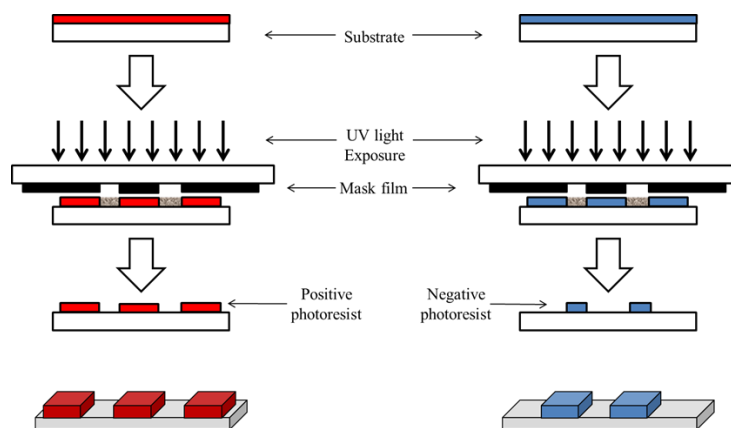
Fig 2.10 Summary of UV-lithography

Table 2.2 Experimental parameters for positive photoresist S1828

Positive Photoresist S1828					
Thickness: 2.5μm					
Spin speed (rpm)	Acceleration time (s)	Duration (s)	Pre bake time at 115℃ (min)	Exposure time (s)	Development time (min)
4000	0	60	1	27	1

Table 2.3 Experimental parameters for negative photoresist SU8-2100

Negative Photoresist SU-8 2100											
Thickness: 100μm											
Spin speed (rpm)	Acceleration time (s)	Duration (s)	Spin speed (rpm)	Acceleration time (s)	Duration (s)	Pre exposure bake time at 65℃ (min)	Pre exposure bake time at 95℃ (min)	Exposure time (s)	Post exposure bake time at 65℃ (min)	Post exposure bake time at 95℃ (min)	Development time (min)
500	9	10	3000	4	30	5	20	26.2	1	10	5-6
Thickness: 140μm											
Spin speed (rpm)	Acceleration time (s)	Duration (s)	Spin speed (rpm)	Acceleration time (s)	Duration (s)	Pre exposure bake time at 65℃ (min)	Pre exposure bake time at 95℃ (min)	Exposure time (s)	Post exposure bake time at 65℃ (min)	Post exposure bake time at 95℃ (min)	Development time (min)
500	9	10	2000	4	30	5	35	29.2	1	15	8-9
Thickness: 250μm											
Spin speed (rpm)	Acceleration time (s)	Duration (s)	Spin speed (rpm)	Acceleration time (s)	Duration (s)	Pre exposure bake time at 65℃ (min)	Pre exposure bake time at 95℃ (min)	Exposure time (s)	Post exposure bake time at 65℃ (min)	Post exposure bake time at 95℃ (min)	Development time (min)
500	9	10	1000	4	30	12	60	5*10.5 1min between	1	15	20-25

2.3.2 Microelectrode fabrication

By utilizing the photolithography with positive photoresist, the wafers with different kinds of patterns can be obtained. Then the wafers were coated with the specific metals by evaporation (Auto 306 vacuum coating systems) procedure to form the microelectrodes. The patterns on the wafer were coated with Titanium thin film (approximate 30 nm) following by a thin film of gold (approximate 120 nm) in this research. Then the wafers were developed again with acetone solution. Only the patterns with the metals coated remained. The details of microelectrode fabrication are given in Fig 2.11.
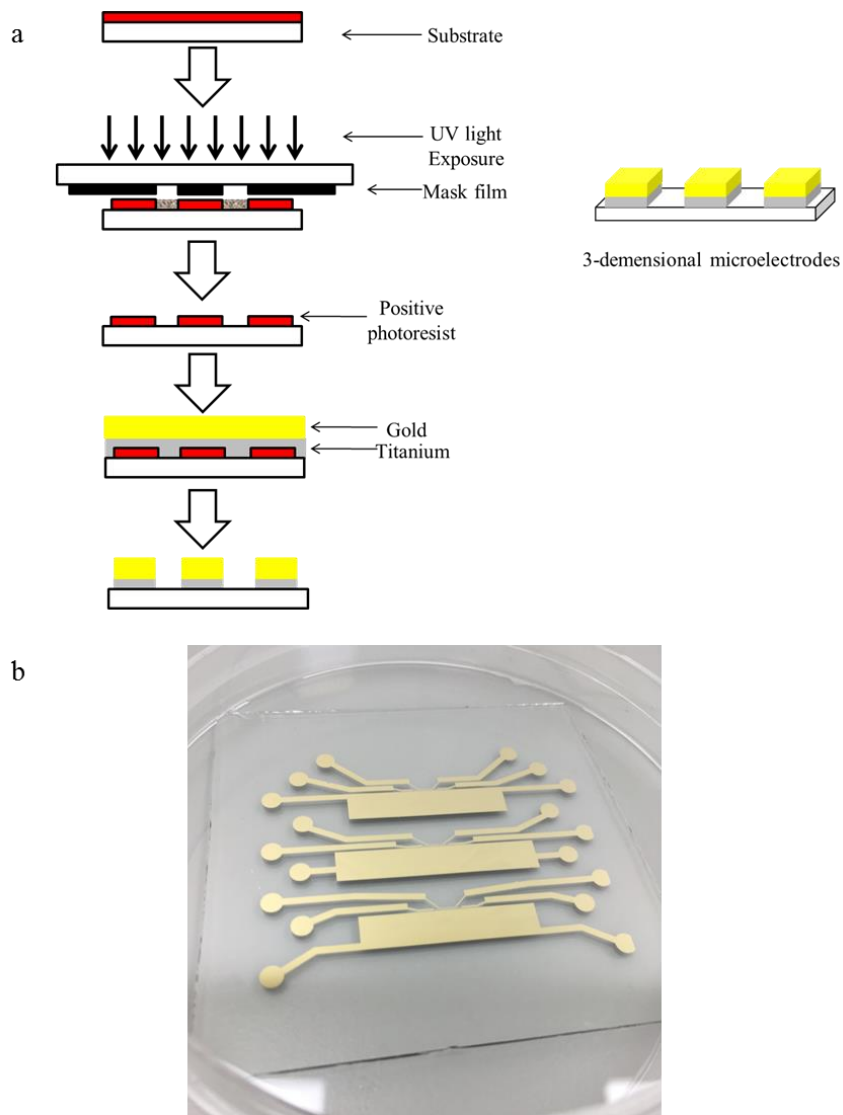
Fig 2.11 (a) The process of microelectrodes fabrication (b) The gold coated electrodes fabricated by UV-LIGA

2.3.3 Microchannel fabrication

By utilizing the photolithography process, the different microchannel moulds can be obtained with the negative photoresist. Then, the wafers with the microchannel mould on were covered by PDMS (polydimethylsiloxane). PDMS is a widely used elastomer which provides a good liquid-tight seal on many kinds of substrates. In addition, it is a transparent material so it is easy to monitor the liquid flowing inside. Fig 2.12 showed the process of the microchannel fabrication with PDMS.
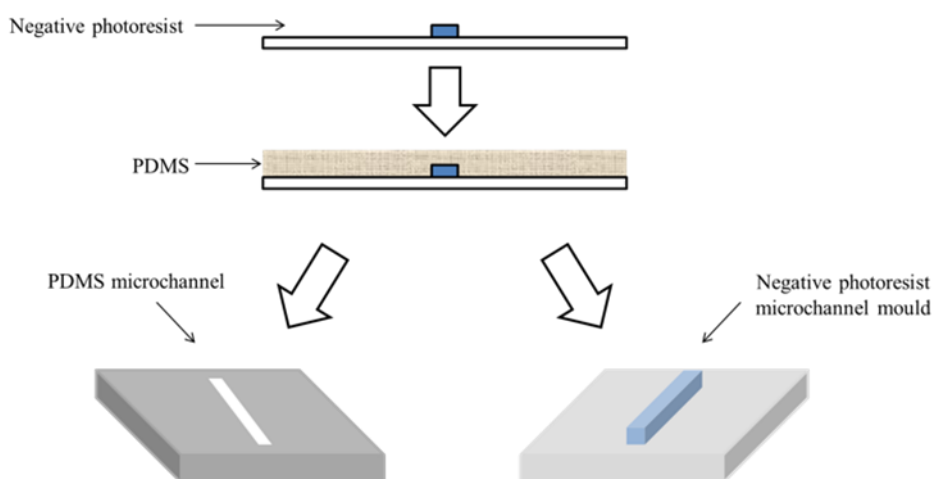
Fig 2.12 Process of microchannel fabrication with PDMS

2.3.4 Electrochemical microreactor assembly

The assembly method takes a really important part in microreactor fabrication. A good assembly can assure the best performance of the microreactors for long-time use. The assembly method used in this thesis is adhesive bonding between PDMS and glass substrate by oxygen plasma technique.

A low pressure plasma system (Femto, Diener Electronic) was used to assemble glass wafer on which the micro-gold electrodes lied and PDMS channel part with liquid inlet and outlet holes. An oxygen plasma was applied to oxidize the surface of both the glass substrate and PDMS. Then these two parts can be adhered permanently.

After that, the PTFE tubing was connected and sealed with epoxy glue, followed with the copper wires soldered onto the electrode welding spots.

2.4   Instrumentations

Details of the chemical reagents used in this thesis are given in the Table 2.6.

Table 2.4 List of instrumentations

Apparatus	Supplier	Model
Analytical balance	Precisa	XT 120A
Diamond glass cutter	Diamond tech	DL 3000XL
Spin coater	Karl Suss	Delta 10 TT
Hot plate	Heidolph	HG 3001 K
Mask aligner	Karl Suss	MJBS 340
Thermal evaporator	Edwards	AUTO 306
Plasma system	Diener Electronic	FEMTO
Syringe pump	Harvard Apparatus	PHD ULTRA 70-3009
Potantiostat/ Galvanostat	AUTOLAB	PGSTAT100
Alternating current potentiostat [108]	N/A	N/A

2.5   Chemical reagents and summary of reactions

Details of the chemical reagents used in this thesis are given in the Table 2.5.
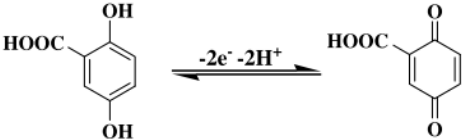
Table 2.5 List of chemical reagent

Chemicals	Supplier	Grade
2,5-Dihydroxybenzoic acid	Aldrich	98%
Acetone	Aldrich	HPLC
AZ 351Developer	Shipley	Clean room quality
Borate buffer solution pH 9.2	ACROS	-
D-(-)-Isoascorbic acid	Aldrich	98%
EC solvent	MicroChem	Clean room quality

Ferrocenecarboxylic acid	Fluka	97%
Gold	Advent Materials	99.99%
Hydrogen peroxide	Aldrich	30 wt.%
L-cysteine	Aldrich	98.5%
Microposit S1828	Shipley	Clean room quality
N,N,N',N'-tetramethyl-p-phenylene-diamine	ACROS	98%
Phosphate buffer solution pH 7	ACROS	-
Poly(dimethylsiloxane)	Dow Corning	-
Platinum	Advent Materials	99.99%
Potassium chloride	Aldrich	99.999%
Potassium ferrocyanide	Aldrich	99.0%
Sodium borohydride	Aldrich	96%
Sodium hydroxide	Aldrich	98%
SU8-2100	MicroChem	Clean room quality
Sulphuric acid	BDH	95%
Titanium	Advent Materials	99.9%

In this thesis, some electrochemical reactions were studied. Details of the reactions, including the chemicals involved and reversibility are given in Table 2.6.

Table 2.6 List of reactions

Chemicals	Redox	Reversibility
Potassium ferrocyanide	$Fe(CN)_6^{4-} - e^- \rightleftharpoons Fe(CN)_6^{3-}$	Quasi-reversible
Ferrocenecarboxylic acid	$FCA - e^- \rightleftharpoons FCA^+$	Reversible
2,5-Dihydroxybenzoic acid		Quasi-reversible
N,N,N',N'-tetramethyl-p-phenylene-diamine	$TMPD - e^- \rightleftharpoons TMPD^{*+}$ $TMPD^{*+} - e^- \rightleftharpoons TMPD^{2+}$	Quasi-reversible
Sodium borohydride	$BH_4^- - 8e^- + 8OH^- \rightarrow BO_2^- + 6H_2O$	Irreversible
Potassium ferrocyanide/ L-cysteine	$Fe(CN)_6^{4-} - e^- \rightleftharpoons Fe(CN)_6^{3-}$ $Fe(CN)_6^{3-} + L - cysteine \rightarrow Fe(CN)_6^{4-} + L - cystine$	Homogeneous irreversible
Ferrocenecarboxylic acid/ L-cysteine	$FCA - e^- \rightleftharpoons FCA^+$ $FCA^+ + L - Cysteine \rightarrow FCA + L - cystine$	Homogeneous irreversible
N,N,N',N'-tetramethyl-p-phenylene-diamine/ ascorbic acid	$TMPD^{*+} + AA \rightleftharpoons TMPD + AA^+$ $TMPD^{*+} + AA^+ \rightleftharpoons TMPD + AA^{2+}$ $AA^+ + AA^+ \rightleftharpoons AA + AA^{2+}$	Homogeneous irreversible

Chapter 3   Hydrodynamic   System   with   Large Amplitude   Fourier   Transformed   Alternating Current Voltammetry in Microreactors

3.1   Introduction

Based on previous research, large amplitude Fourier transformed alternating current voltammetry (FTACV) has been utilized in stagnant system to conduct mechanistic study. In this chapter, a broad range of electrochemical reactions have for the first time been investigated with FTACV in microfluidic system. The micro-engineered devices which contain micro-gold electrodes, micro-channels with 100 µm height, liquid inlet(s) and outlet(s) were produced with microfabrication methodology. All of the electrochemical reactions mentioned before in Chapter 1 have been examined under either stagnant or hydrodynamic system. In the hydrodynamic system, a wide range of flow rates have been applied by controlling a syringe pump. As for the homogeneous reactions, different substrate concentrations have been selected to examine the response from the system.

3.2   Hydrodynamic   system   with   large   amplitude   Fourier transformed AC voltammetry

The channel flow cell has been shown to be a powerful tool to study analytical, mechanistic and kinetic processes [190]. The development of microfabrication technique makes possible the production of micro-electrochemical reactors with significantly enhanced transport rates, resulting in access to faster kinetic regimes [191], as well as improved performance in applications related to the study of chemical analysis[192], organic synthesis [193], processes at an immiscible liquid/liquid interface, biosensing [194], and gas sensing [195]. In order to enhance the selectivity, sensitivity and better understanding of the performance of micro-

electrochemical reactors, different kinds of potential waveforms have been applied to investigate the perturbation of the system [144]. Fourier transformed alternating current voltammetry is an interest in the present study.

Based on previous research [196], fast Fourier transformed (FFT) methods can enhance the capability of electrochemical admittance techniques by resolving the entire frequency spectrum of an AC electrochemical system in considerably less time, and often with great accuracy. In impedance spectroscopy, small amplitude perturbations were mainly used by researchers in attempt to minimize second to higher terms so that the modelling work can be linearized. However the signal-to-noise ratio may be poor and the peaks in the higher harmonics cannot be easily obtained when small amplitude signal is applied [115]. Further, some valuable information, for example, uncompensated resistance and double layer capacitance can only be evaluated from second to higher harmonics [108]. According to Engblom's research [197], there is no cogent reason for restricting experimental AC voltage amplitudes to small values and on the contrary, the use of large amplitude can lead to better sensitivity. The merit to utilize larger amplitude is evident in higher harmonics, *e.g.* after fourth harmonic, and the peaks are significantly more visible comparing to those with small amplitude. This technique has been used in stagnant system to undertake mechanistic study with large amplitude applied [198]. Researchers have found that the large amplitude FTACV technique readily revealed the presence of significant Faradaic processes at potentials within the double-layer region of gold electrodes in acidic and basic media, where the current has often been assumed to be purely capacitive in nature [199].

Large amplitude Fourier transformed AC voltammetry has been utilized in hydrodynamic system by several researchers. Based on Walker's work [200], AC voltammetry is not so sensitive to stirring effects in solution and is a promising key to the continuous process-stream monitoring. According to Japanese researchers [201,202], the measurement under steady state can provide a well-defined convective regime and suppressed effect of natural convection. The use of a rotating disk electrode rather than a stationary electrode in AC voltammetry make the steady state can be achieved easily, so that an AC signal with a frequency as low as 1 Hz can be used. Followed by which, it was proved that this technique is a vast, accurate and simple method for analysing linear hydrodynamic modulation voltammetry systems, and is also a powerful tool for studying non-linear system response [145]. Matthews *et al.* [203] reported that large amplitude AC voltammetry can be advantageously applied to assist in the understanding of the mass transport, electrode kinetic, and double layer capacitance behaviour of a microfluidic electrode device. Even in the

presence of solution flow, AC harmonic responses retain excellent signal-to-noise ratio allowing higher order harmonics to be accessed. However, large amplitude FTACV has little been applied to probe the mechanism study in hydrodynamic system. In this chapter, the technique was used to study different electrochemical reactions in hydrodynamic environment.

3.3   Experimental setup

The electrochemical microreactors were produced and assembled by microfabrication methodology mentioned in Chapter 2. Fig 3.1 shows a well-made electrochemical microreactor which was mainly used in this thesis. On the glass substrate, there were three sets of microelectrodes and each set contained a reference, working and counter electrode with width of 100 μm, 100 μm and 5 mm, respectively. The microchannel covered all sets of electrodes and the width and height of the microchannel was 1 mm, 100 μm, respectively. The diameter of the PTFE tubing was 1 mm. The cables were soldered with the electrodes on the soldering points.
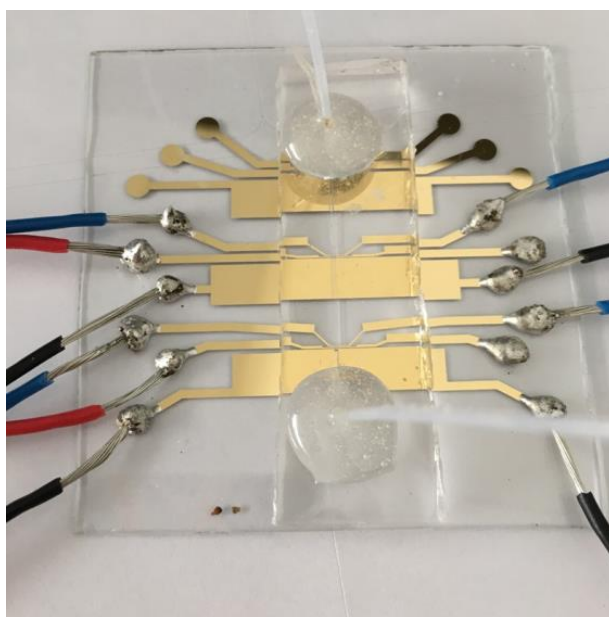
Fig 3.1 Electrochemical microreactor

The supporting electrolyte contained 0.5 M potassium chloride was used in every measurements excluding specific statement. The solution was pumped into the microreactors

and controlled flow rates with the syringe pump (Harvard PHD ULTRA 70-3009). All the experiments were carried out under room temperature (25 ± 1℃)

The electrochemical detection was carried out with large amplitude Fourier transformed alternating current voltammetry by home-built instrumentation [108]   to study different electrolysis mechanisms in both stagnant and hydrodynamic system.

3.4   Electrochemical detection of pure electron transfer reactions in microfluidic system

In this section, the pure electron transfer reaction is reported in a microfluidic system. Firstly, the single electron transfer reactions with total reversibility and quasi-reversibility were examined in section 3.4.1. Then multiple electron transfer reactions are studied in section 3.4.2.

3.4.1 Single electron transfer reaction

3.4.1.1   Detection of potassium ferrocyanide

The redox system of $Fe(CN)_6^{4-}$/ $Fe(CN)_6^{3-}$ is a classical alternative for the electrochemistry. This redox system is often used to probe the reactivity of electrodes, and it is often presumed that this redox couple undergoes electron transfer via a simple outer-sphere mechanism [204]. It is believed that the redox undergoes a quasi-reversible reaction.

$$Fe(CN)_6^{4-} - e^- \rightleftharpoons Fe(CN)_6^{3-} \tag{3.1}$$

Firstly, the Levich behaviour was obtained with different volume flow rates. Fig 3.2 shows the limiting current obtained detailing with various flow rates, which was extracted directly from data generated with FTACV. The plot of limiting current values versus volume flow rates was shown in Fig 3.2 (b). Good linear relationship can be found from the figure, which reveals the Levich behaviour. The linear trend line nearly crossed the origin of coordinate axis showed that the device was properly fabricated and reliable to use.

Fig 3.2 (a) linear sweep voltammogram (potential range: -0.1-0.6 V, scan rate: 13.04 mV/s) detailing with the response of 2 mM potassium ferrocyanide to increasing flow rates (from 0.01 to 0.10 mL/min); (b) limiting current with various cubic root of flow rates.

Fig 3.3 The large amplitude FTACV (potential range: -0.2-0.4 V, scan rate: 11.18 mV/s, frequency: 1 Hz, amplitude: 50 mV) detailing with the response of 2 mM potassium ferrocyanide in absence of L-cysteine (a) first harmonic; (b) second harmonic; (c) third harmonic; (d) DC signal.

Fig 3.3 shows the large amplitude FTACV signal response of potassium ferrocyanide (2 mM, in 0.5 M KCl electrolyte solution) on the 100 μm gold electrode in the stagnant system. The

parameters setting in the FTACV are: potential range: -0.2-0.4 V, scan rate: 11.18 mV/s, frequency: 1 Hz and amplitude as 50 mV. The DC signal and harmonic components can be obtained at the same time by utilizing FTACV.

As it can be seen from Fig 3.3, the peaks of the back sweep from all harmonics are slightly smaller than the forward ones because the redox reaction of potassium ferrocyanide is quasi-reversible. In the second harmonic, two peaks from both oxidative and reductive process were obtained clearly. The reductive peaks are slightly smaller than the oxidative one can be found in this and higher harmonics as well due to the relatively small rate constant of redox of ferrocyanide, which is about 0.10 cm s^{-1} according to literature [205–207]. The DC signal showed a classic duck shape voltammogram, which indicated that the both the AC components and DC signal can be obtained in a short time measurement.

Fig 3.4 shows the signal response extracted from large amplitude FTACV for the redox of potassium ferrocyanide in the microfluidic system. As the flow rates increased in the microchannel, the peak heights in fundamental harmonic increased due to the thickness of diffusion layer decreased, but the peak didn't shift with the change of flow rates. Similar phenomena can be found in higher harmonic as well. Also the diffusion coefficient can be obtained from the DC signal extracted from the overall response based on Equation (1.31). The diffusion coefficient value was revised and calculated as $7.70 \pm 0.20 \times 10^{-6}$ cm^{2}s^{-1} for 2 mM potassium ferrocyanide in 0.5 M KCl supporting electrolyte.
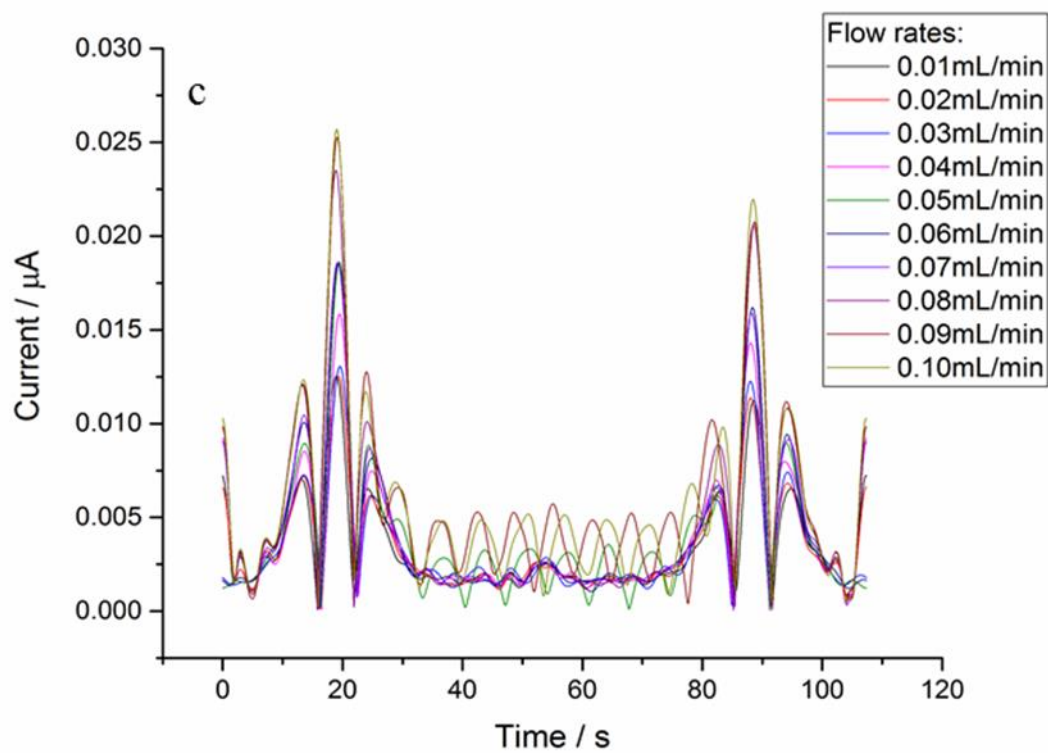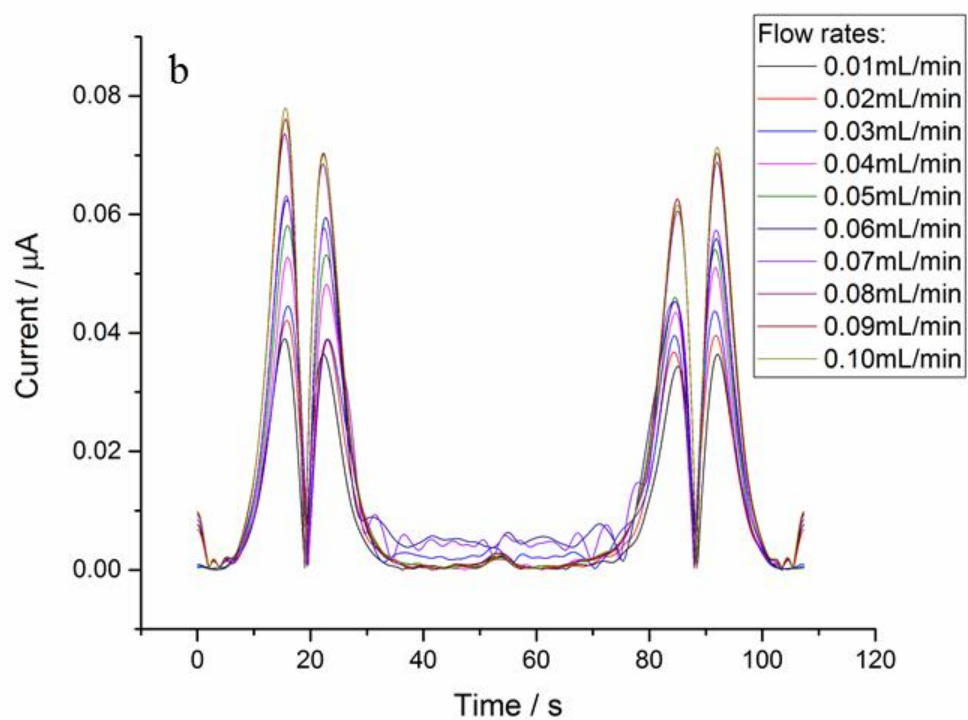
Fig 3.4 The large amplitude FTACV (potential range: -0.1-0.6 V, scan rate: 13.04 mV/s, frequency: 1 Hz, amplitude: 50 mV) detailing with the response of 2 mM potassium ferrocyanide to increasing flow rates (from 0.01 to 0.10 mL/min) (a) first harmonic; (b) second harmonic; (c) third harmonic; (d) peak current with various flow rates; (e) integral of peaks generated from forward scans with various flow rates.

The plot of peak current values versus cubic flow rates in each harmonic was shown in Fig 3.4 (d). As it can be seen from the figure, good linear relationship can be found between the

peak current values and cube root of flow rates, which is analogue with the Levich behaviour in DC technique. The correlation between peak current values and flow rates became weaker in the higher harmonic, which means that the peak current values became independent of the flow rates in the higher harmonics. This phenomenon has been noted previously [203]. In the higher harmonics, the Levich-like behaviour breaks down and the mass transport becomes dominated by the diffusion rather than convection contribution.

The integral of each curve was calculated and plotted in Fig 3.4 (e) as well. The integral of the harmonic peaks represented the electric charge within the measurement time. The plot showed good linear relationship between the peak integral and cubic flow rates which is similar with the Levich-like behaviour mentioned before. The analysis of peak integral has been done in all sections and found similar results. For convenient and intuitional aspect, only the peak current value versus cubic flow rates plot will be shown in the later sections for discussion.

3.4.1.2   Detection of ferrocenecarboxylic acid

Ferrocenecarboxylic acid (FCA) has been reported to undergo a reversible oxidation in aqueous solution. Fig 3.6 shows the electrochemical response of 2 mM FCA with 0.5 M KCl supporting electrolyte in pH 9.2 borate buffer solution in AC components. The parameters setting in FTACV are: potential range -0.1-0.6 V, scan rate: 13.04 mV/s, frequency: 1 Hz and amplitude as 50 mV.

From fundamental through fourth harmonics, the peak current values rose up with the increase of the flow rates, consistent with the behaviour noted in section 3.4.1.1.

$$FCA - e^- \rightleftharpoons FCA^+ \tag{3.2}$$

The DC signal was extracted firstly from the overall AC data to examine the Levich behaviour. Fig 3.5 shows the limiting current obtained under different volume flow rates. The good linear relationship between limiting current values and various cubic roots of flow rates shows that the Levich behaviour had been achieved in the measurements.
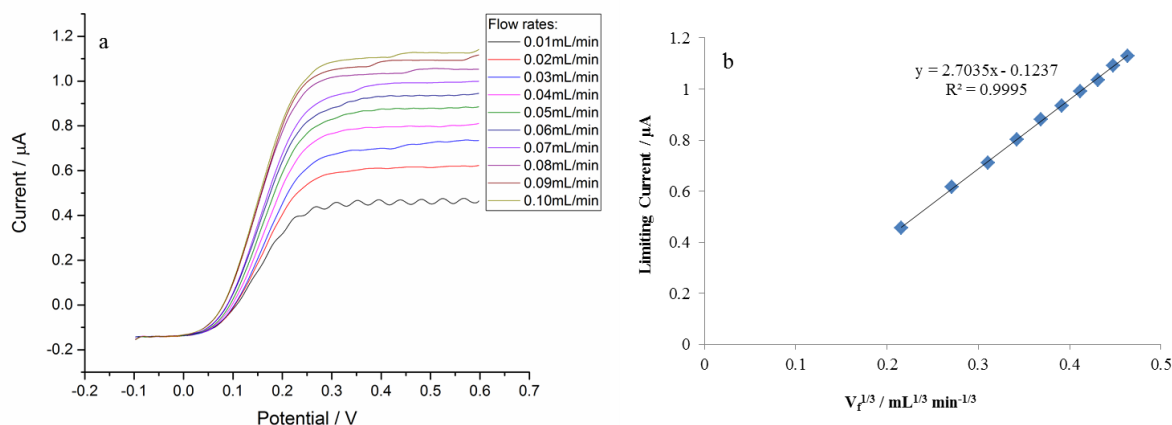
Fig 3.5 (a) linear sweep voltammogram (potential range: -0.1-0.6 V, scan rate: 13.04 mV/s) detailing with the response of 2 mM FCA in pH 9.2 borate buffer to increasing flow rates (from 0.01 to 0.10 mL/min); (b) limiting current with various cubic root of flow rates.
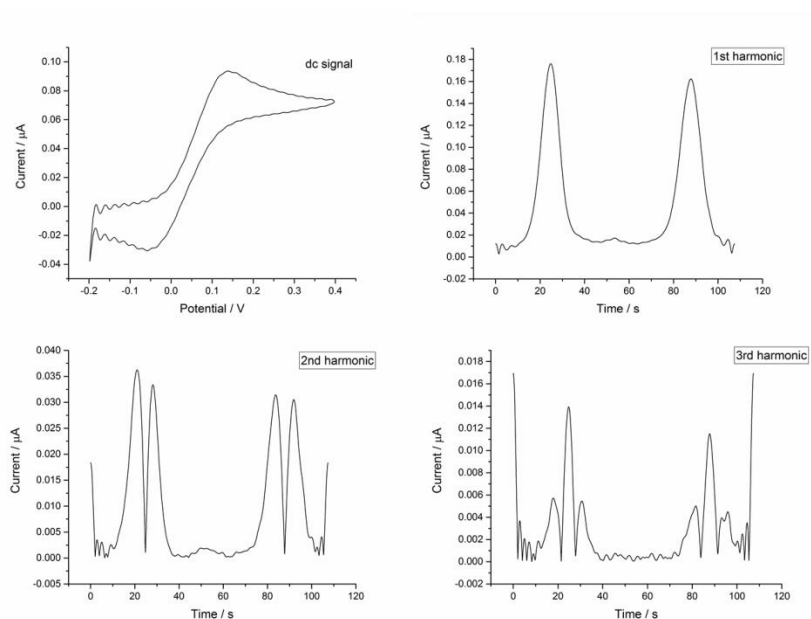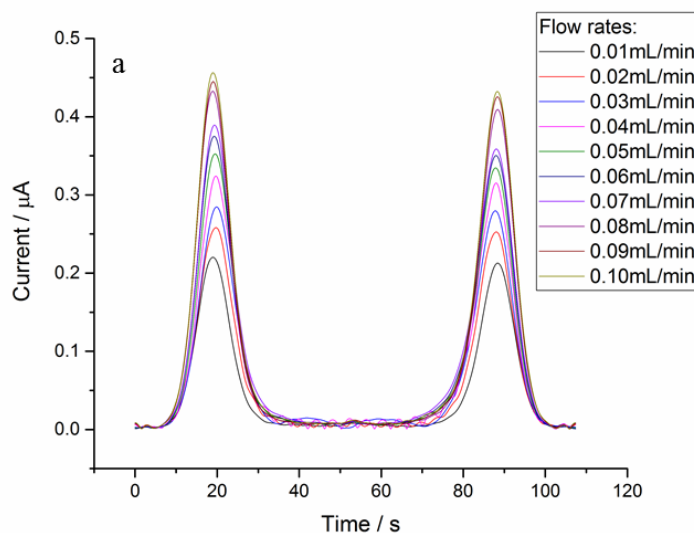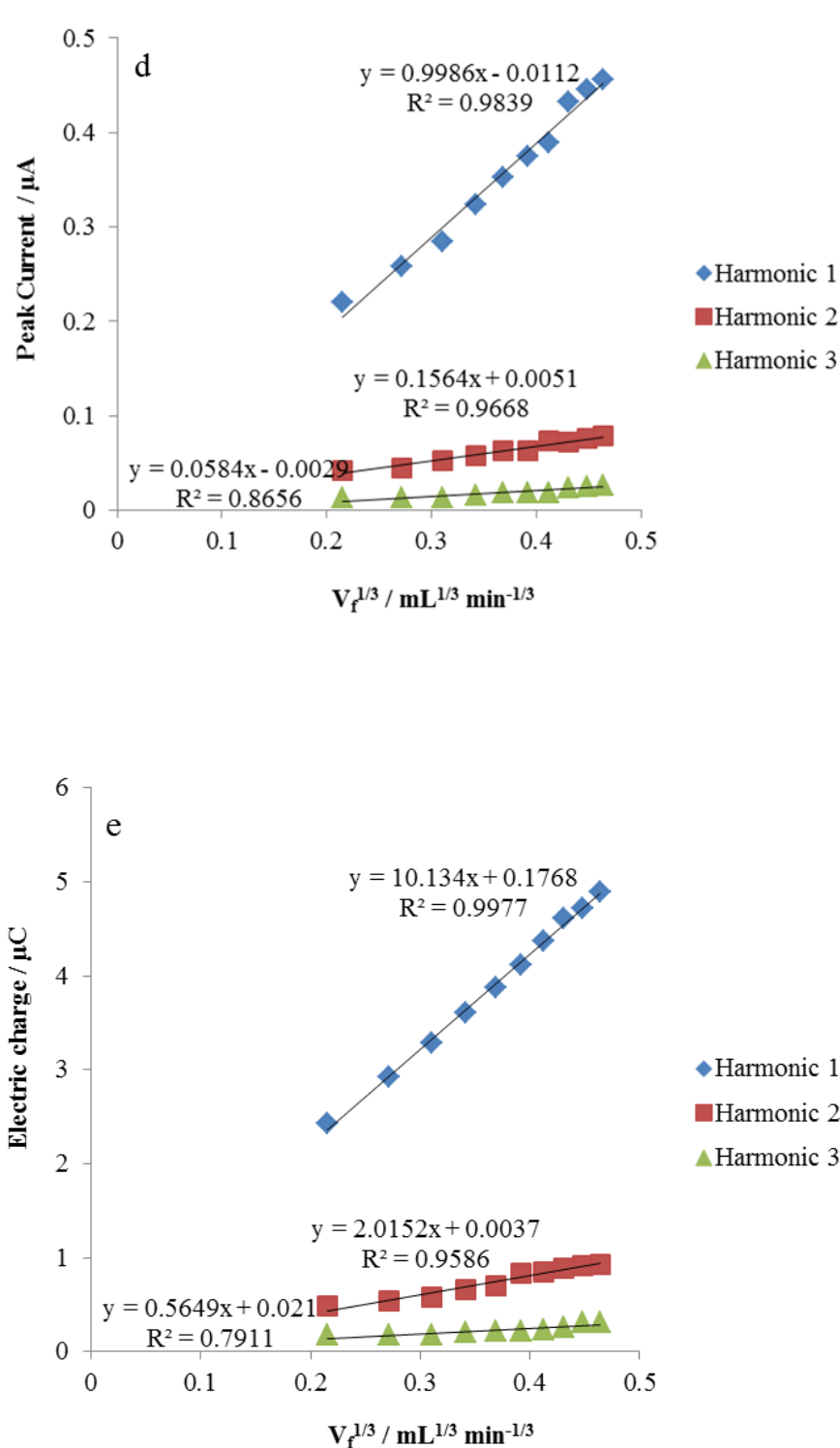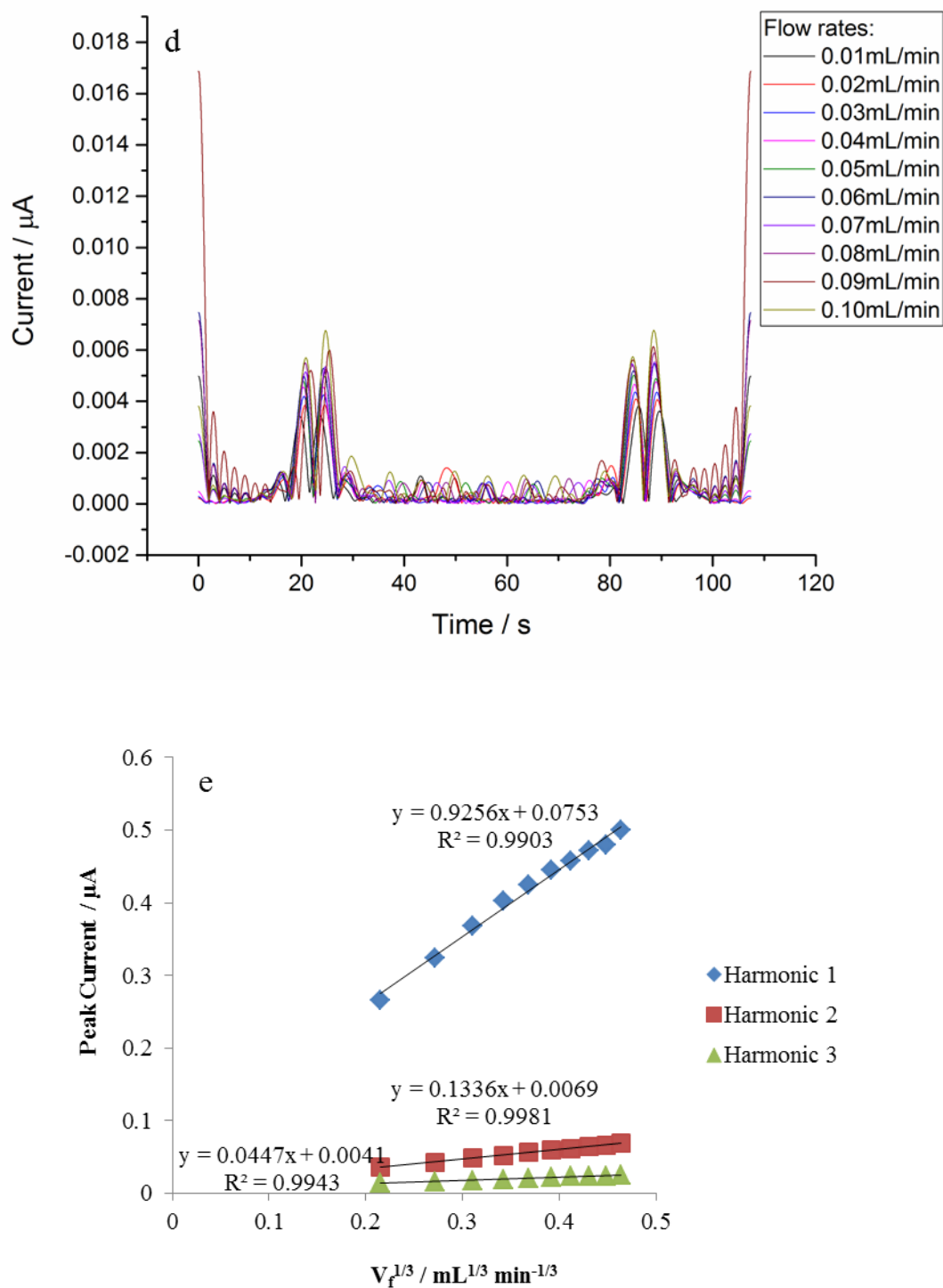
Fig 3.6 The large amplitude FTACV (potential range: -0.1-0.6 V, scan rate: 13.04 mV/s, frequency: 1 Hz, amplitude: 50 mV) detailing with the response of 2 mM FCA in pH 9.2 borate buffer to increasing flow rates (from 0.01 to 0.10 mL/min) (a) first harmonic; (b) second harmonic (c) third harmonic; (d) fourth harmonic; (e) peak current with various flow rates.

As it can be seen from Fig 3.6, the peaks generated from the backward sweep showed the same height with the ones from forward sweep, which revealed that the oxidation of FCA is a reversible reaction. The signal-to-noise ratio is relatively high in higher harmonics compared with the same measurement of potassium ferrocyanide, which may due to the better reversibility of FCA. The diffusion coefficient value can be calculated from the DC signal extracted from overall response based on Levich equation. The value was obtained as $8.10 \pm 0.20 \times 10^{-6}$ cm^{2}s^{-1}, which is consistent with literature [208].

Fig 3.6 (e) showed the good linear relationship between peak current of FCA in each harmonic and cube root of flow rates. Within this flowing region, the system is under laminar flow and the resulting current is under diffusion control. Compared with ferrocyanide, FCA showed better electrochemical reversibility even in the higher harmonics.

3.4.2 Dual electron transfer reaction

In this section, two different dual reactions were studied. The first one is redox of 2,5-dihydroxybenzoic acid, which undergoes a direct two electron transfer reaction. The other one is N,N,N',N'-tetramethyl-*para*-phenylene-diamine, which shows a typical two consecutive one-electron steps.

3.4.2.1   Detection of detection of 2,5-dihydroxybenzoic acid

2,5-dihydroxybenzoic acid (also named gentisic acid or DHB) is a dihydroxybenzoic acid. It is a derivative of benzoic acid and a minor (1%) product of the metabolic break down of aspirin. It is also found in the African tree and in wine [209].

The most famous application of DHB is that it can be utilized as sample matrix in matrix-assisted laser desorption/ionization (MALDI) mass spectrometry [210–212]. The use of DHB in MALDI mass spectrometry was showed to improve ion yields and signal-to-noise ratio of analyte molecules, especially for the high-mass range [213]. Also, as one of catechol derivatives, it plays an important role in mammalian metabolism. Many compounds of this type are known to be secondary metabolites of higher plants [214].

The electrochemical redox of DHB shows a typical two-electron transfer in one single step reaction [215]. Researchers have also found out that the electrochemical behaviour of DHB is dependent on the change of pH values of the electrolyte due to the protons were involved in the whole process [216].
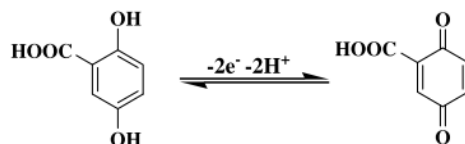
Fig 3.7 Scheme of redox of DHB

As it can be seen from Fig 3.8, the limiting current under different volume flow rates were obtained from the overall AC data. Compared to the previous reactions, it took longer time for DHB to achieve steady-state under microfluidic conditions due to the quasi-reversibility of the reaction on gold electrode.
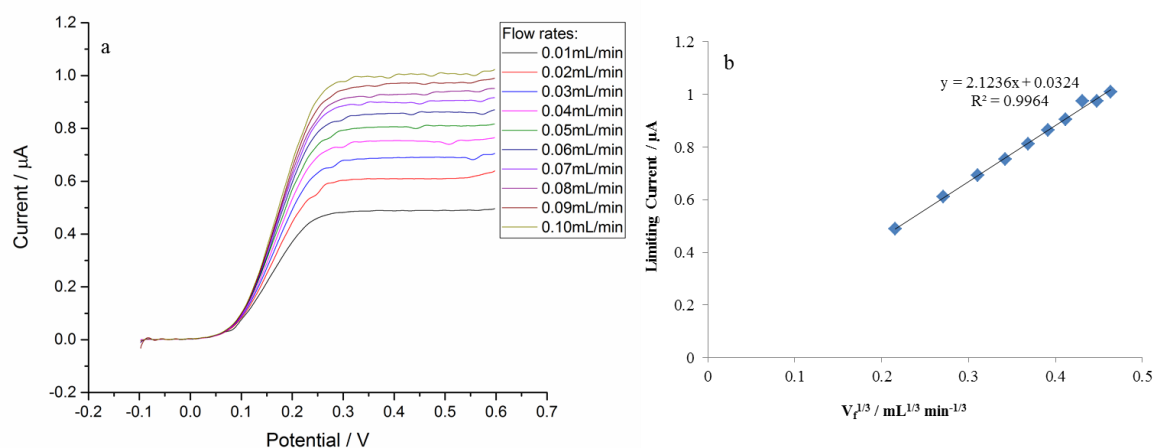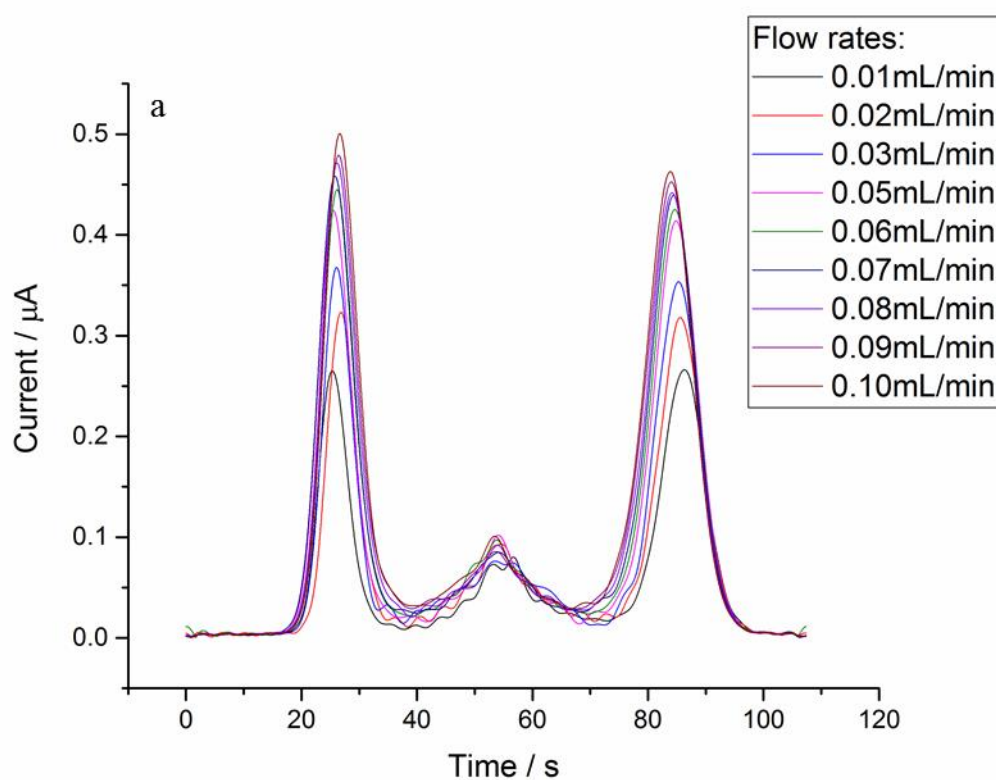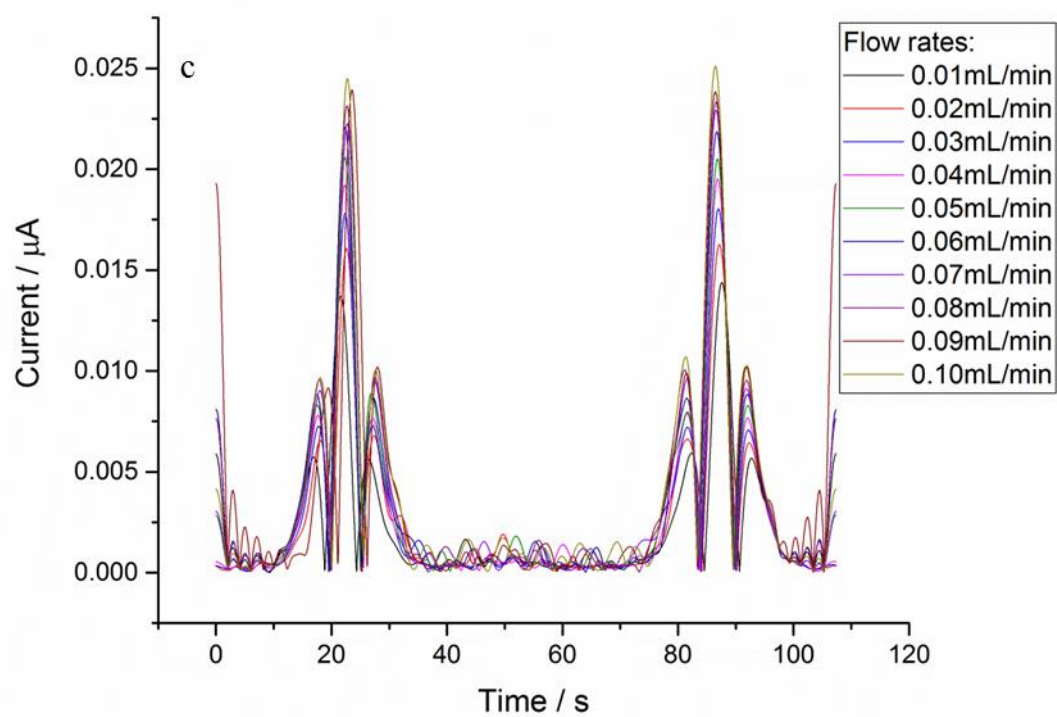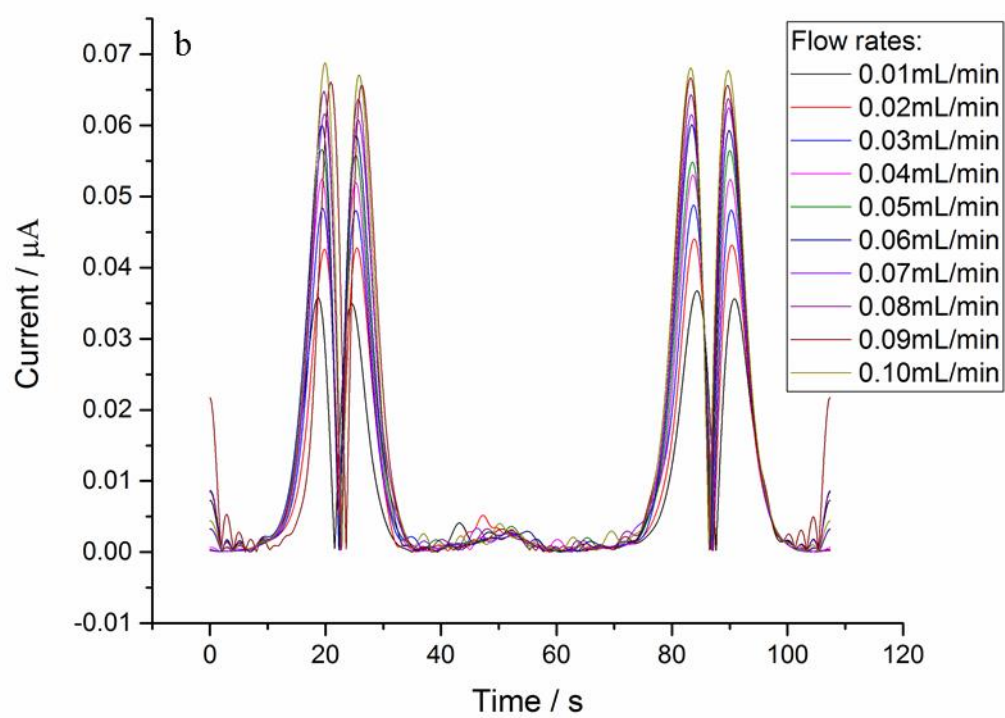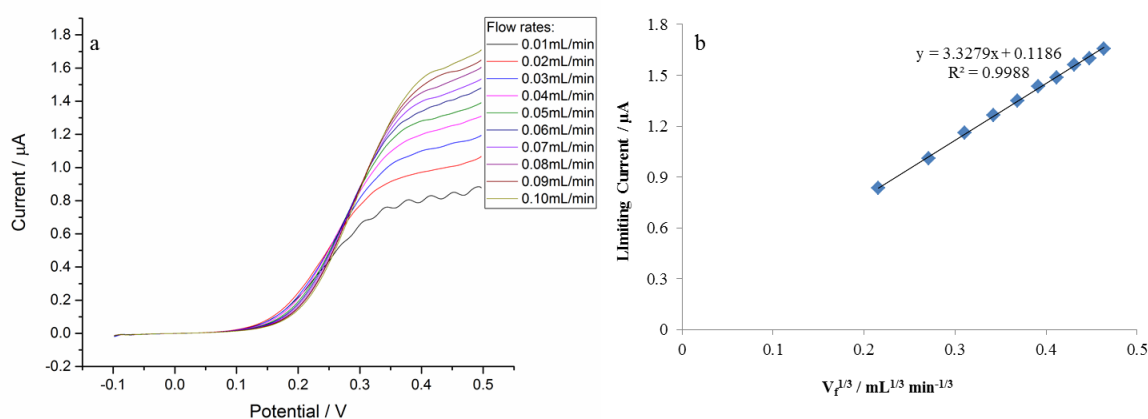

Fig 3.8 (a) linear sweep voltammogram (potential range: -0.1-0.5 V, scan rate: 11.18 mV/s) detailing with the response of 2 mM DHB in pH 5 acetate buffer to increasing flow rates (from 0.01 to 0.10 mL/min); (b) limiting current with various cubic root of flow rates.

Fig 3.9 showed the electrochemical response of 2 mM DHB in pH 5 acetate buffer. As it was expected, the peak current values rose with the increase of the flow rates. In the DC technique, based on Levich equation (1.31), the peak current has a linear relationship with cubic root of flow rates when the flowing stream reaches the steady state. In FTACV, unfortunately there is no such a theory that can be depicted the algebraic relationship. In Fig 3.9 (c), the peak current in each harmonic with the cube root of chosen flow rates has been shown. When the flow in the channel was fast enough and reached the convective controlled condition, the current of the harmonic components behaved in a Levich-like manner as expected. The peaks in the second harmonic did not show the typical bell shape compared

with the figures in previous section, the reason for which could be the effect caused by proton transfer.

According to Nematollahi's work [217], the side reactions such as hydroxylation and/or dimerization reactions are too slow to be observed under cyclic voltammetry when a scan rate at 100 mV/s was used. However, in FTACV, a relatively slow scan rate at 11.18 mV/s was used to enable the system to achieve steady-state. In this case, the side reactions could take place with enough time. The hydroxylation and/ or dimerization reactions could be one of the possibilities of the noise which was detected during the measurements and the incomplete bell shape.
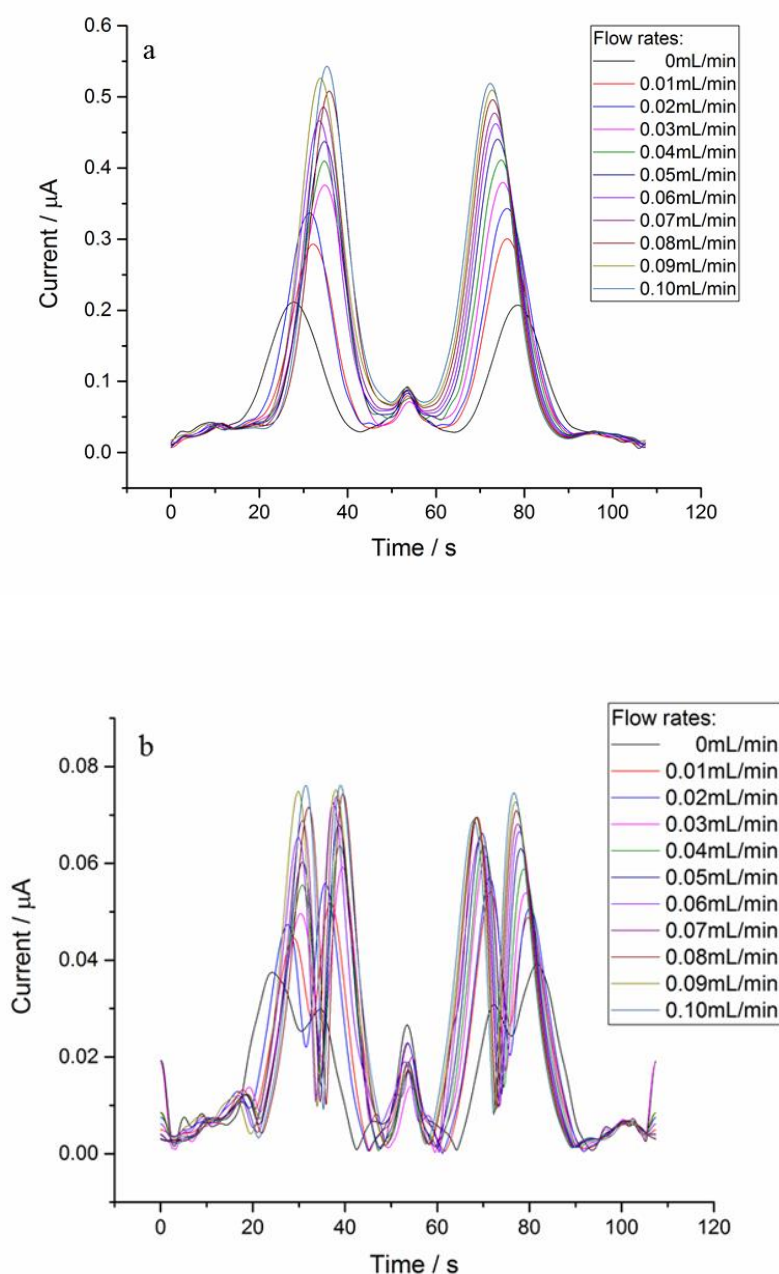
Fig 3.9 The large amplitude FTACV (potential range: -0.1-0.5V, scan rate: 11.18mV/s, frequency: 1 Hz, amplitude: 50 mV) detailing with the response of 2 mM DHB in pH 5 acetate buffer to increasing flow rates (from 0.01 to 0.10 mL/min) (a) first harmonic; (b) second harmonic (c) peak current with various cubic root of flow rates.

3.4.2.2   Detection of N,N,N',N'-tetramethyl-*para*-phenylene-diamine (TMPD)

N,N,N',N'-tetramethyl-*para*-phenylene-diamine, also named as TMPD, is well-known to undergo a two-electron transfer oxidation pathway: upon removal of the first electron a delocalized radical cation results and removal of the second electron forms a p-quinonediimine dication [218]. It can be shown as

$$TMPD - e^- \rightleftharpoons TMPD^{*+} \tag{3.3}$$

$$TMPD^{*+} - e^- \rightleftharpoons TMPD^{2+} \tag{3.4}$$

Based on that, the oxidation of TMPD on cyclic voltammogram shows two individual oxidation and reduction peaks at different potentials, which was shown in Fig 3.10.
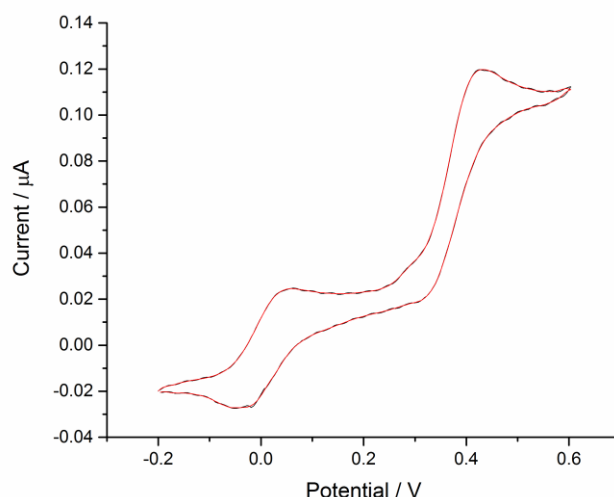
Fig 3.10 Cyclic voltammogram of 2 mM TMPD in pH 7 phosphate buffer (potential range: -0.2-0.6, scan rate: 50 mV/s)

As it can be noted from the figure, there is a small wave between the two primary waves. This is a result of ipso attach of water on the electrogenerated dication [219]. The use of microelectrode and hydrodynamic voltammetry eliminated this phenomenon to an extent compared with the situation when a macro electrode is involved. In this thesis, the research primarily concentrated on the primary waves generated due to the electron transfer.
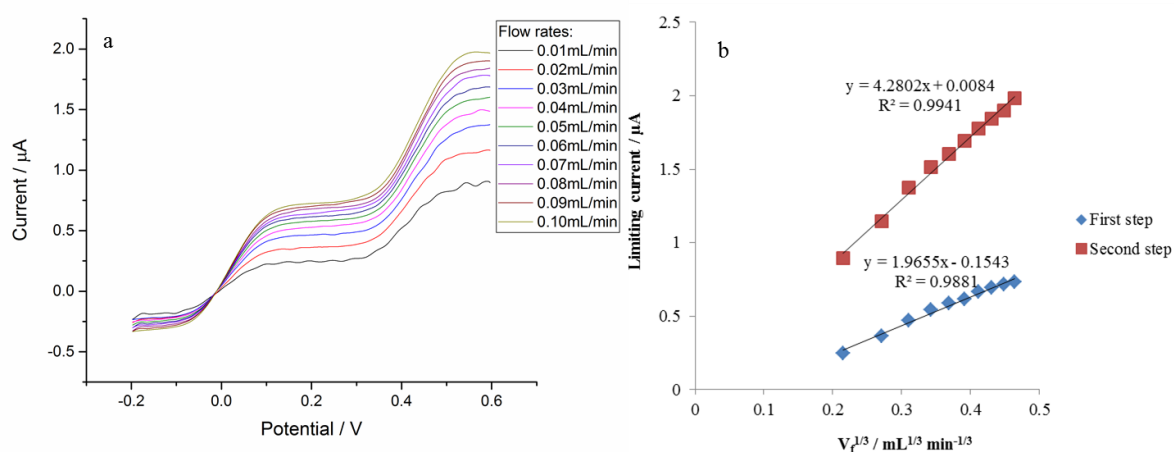
Fig 3.11 (a) linear sweep voltammogram (potential range: -0.2-0.6 V, scan rate: 14.90 mV/s) detailing with the response of 2 mM TMPD in pH 7 phosphate buffer to increasing flow rates (from 0.01 to 0.10 mL/min); (b) limiting current with various cubic root of flow rates.

Fig 3.11 shows that under different volume flow rates electrochemical oxidation of TMPD presented two limiting current due to two consecutive electron transfer steps. Levich behaviour can be obtained from both electron transfer steps evidenced by the linear relationship between limiting current values versus cubic roots of flow rates, which can be found in Fig 3.11 (b).

The typical electrochemical characteristic of TMPD triggered the research interest in the electrochemical response of two consecutive oxidation steps in large amplitude Fourier transformed alternating current voltammetry. Fig 3.12 showed the two consecutive one-electron transfer steps of TMPD. Similar with cyclic voltammogram, in AC component, it showed two individual peaks either in oxidation or reduction sweep. As it can be seen from the figure, the change of the peak current was the result from the increasing controlled flow rates. And the reverse peak(s) was almost as high as the forward one, which indicates a reversible reaction. The diffusion coefficient value was obtained as $6.30\pm0.10 \times 10^{-6}$ cm^2s^{-1}, which was noted in literature previously as well [220].

The peak current value of second oxidative peak is slightly higher than the first one, which means that the intermediate TMPD*$^+$ is thermodynamically unstable and it is easier to be oxidized with overpotential. Based on that, most of the electrocatalytic methods utilize TMPD*$^+$ as a mediator to continue the following (electro)chemical reactions. In conventional cyclic voltammetry, the baseline of the first peak and the second one is not the same, so it takes more efforts to fix the baselines for measuring the peak current. However in FTACV, both of the peaks shared the same baseline, it is more intuitional to compare the two steps at the same time.

As it can be seen from the second harmonic, the second peak generated due to the second step of electron transfer (TMPD^{*+}/ TMPD^{2+}) was relatively lower than the first peak. This indicated that the second step oxidation of TMPD represented a quasi-reversible reaction, which was the result of competition of kinetic control and diffusion control. The similar phenomena can be obtained from third to higher harmonics due to the quasi-reversibility of the reaction as well.
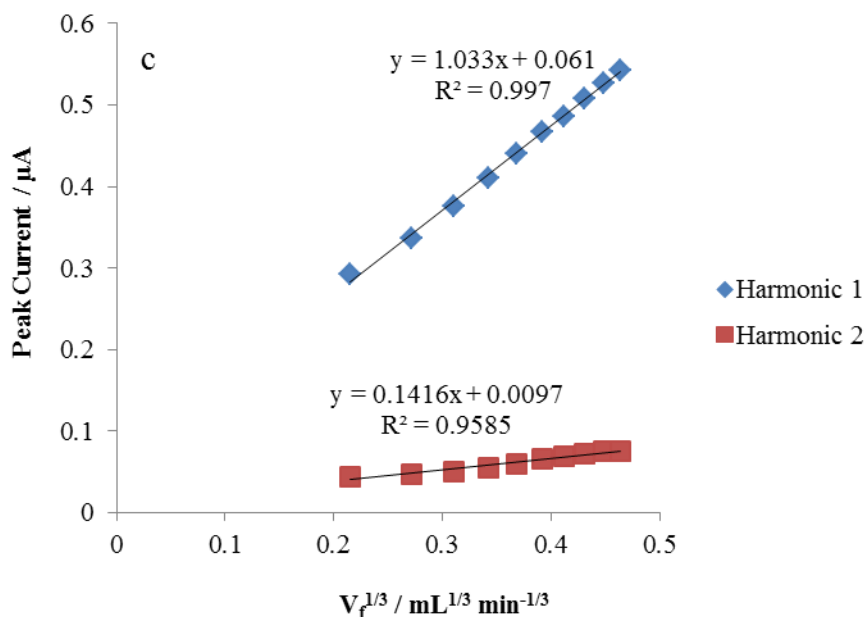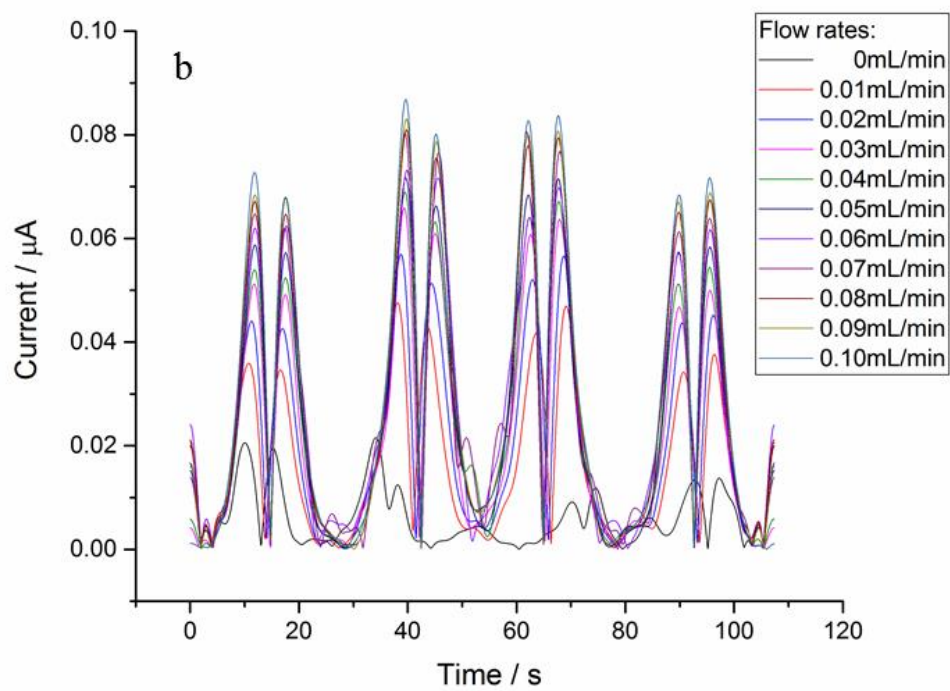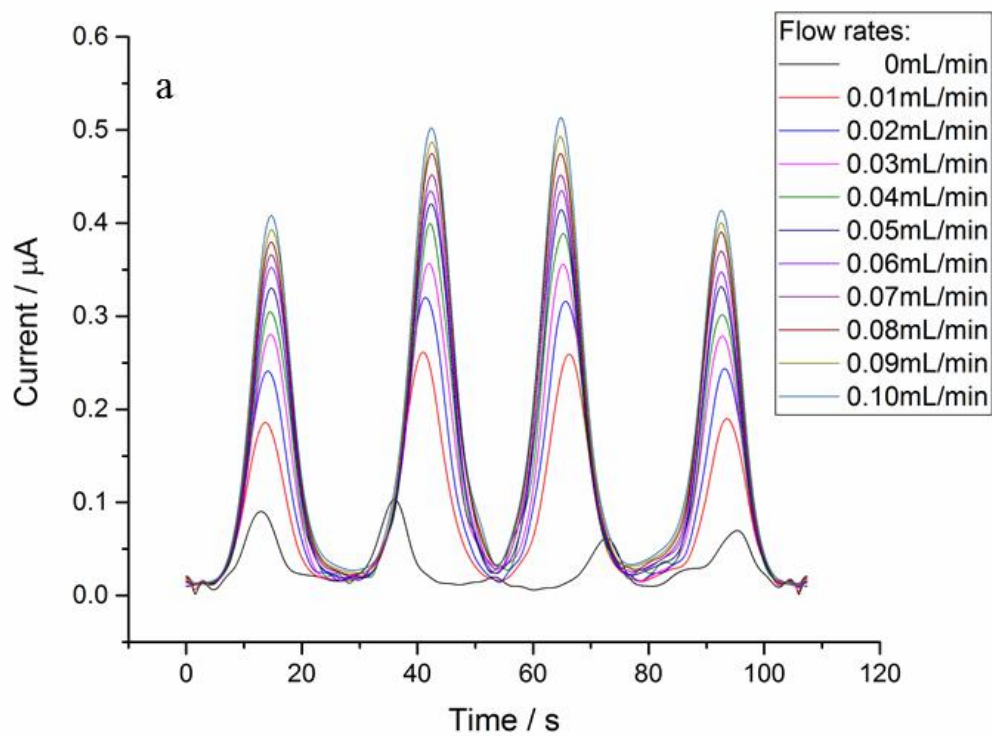
Fig 3.12 The large amplitude FTACV (potential range: -0.2-0.6V, scan rate: 14.90mV/s, frequency: 1 Hz, amplitude: 50 mV) detailing with the response of 2 mM TMPD in pH 7 phosphate buffer to increasing flow rates (from 0.01 to 0.10 mL/min) (a) first harmonic; (b) second harmonic (c) third harmonic; (d) fourth harmonic.

3.4.3 Irreversible reaction

Sodium and other borohydrides have been used as the reducing agents in many inorganic and organic reactions [221]. The earliest methods for analysing borohydrides cannot meet the standard for rapid, accurate and simple determination. The most accurate hydrogen evolution method [222] is very complicated while the titration technique [223] and argentimetric method [224] are not that accurate. Some other methods, such as polarography [225] and spectrophotometry [226] cannot be used directly in a reaction system.

Later on, electrochemical method was introduced to detect borohydrides. The electrode reaction of sodium borohydride elucidates a complicated irreversible reaction [227]

$$BH_4^- + 8OH^- - 8e^- \rightarrow BO_2^- + 6H_2O \qquad (3.5)$$
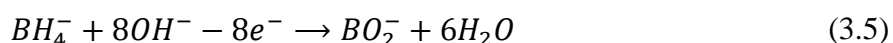
Based on previous study of aqueous solutions of borohydride, the hydrolysis will result in the BH_4^- reacting rapidly with water at pH below 12 which makes the analysis complicated. To eliminate this effect, in this experimental part, the supporting electrolyte solution used was sodium hydroxide and the pH value was controlled strictly higher than 12.

Fig 3.13 showed the electrochemical response of 10mM sodium borohydride in NaOH solution as supporting electrolyte from cyclic voltammetry. As it can be seen from the figure, a typical irreversible reaction was shown. There was an oxidation peak of borohydride can be found at +0.089 V while no reduction peak can be detected, which showed a great agreement to literature.
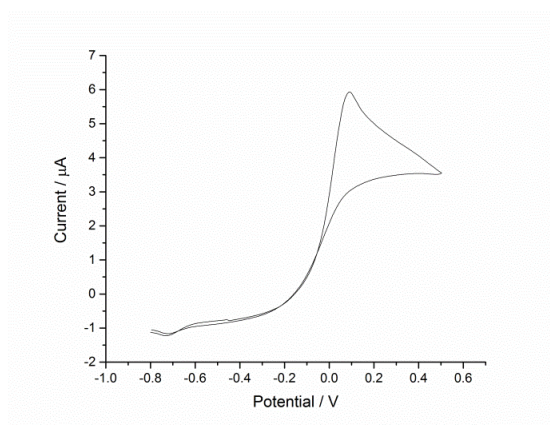
Fig 3.13 Cyclic voltammogram detailing of the response of 10mM sodium borohydride in 3M NaOH solution on micro-gold electrode (potential range: -0.8-0.5V, scan rate: 30mV/s)

Firstly the DC signal was extracted from overall AC data to study the Levich behaviour. As it can be seen from Fig 3.14, the steady-states phenomena can be obtained under different flow rates, which showed the diffusion-control process. Also, the limiting current values were proportional with the cubic roots of volume flow rates, which showed the Levich behaviour.
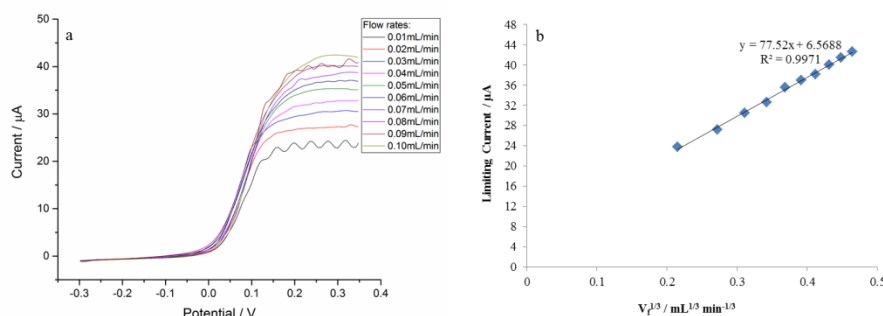
Fig 3.14 (a) linear sweep voltammogram (potential range: -0.3-0.35 V, scan rate: 12.11 mV/s) detailing with the response of 10 mM sodium borohydride in 3 M NaOH supporting electrolyte to increasing flow rates (from 0.01 to 0.10 mL/min); (b) limiting current with various cubic root of flow rates.

Next, the large amplitude FTACV was utilized to study the redox reaction of borohydride both in stagnant and microfluidic system. Fig 3.15 showed the AC components extracted from overall signal of large amplitude FTACV. The peaks generated from the backward sweep were obviously smaller than the forward ones, which indicates the kinetics of this reaction. Also, the peak current increased when higher flow rates have applied. Further the complexity of the reaction and the possible unstable intermediates resulted in the poor signal-to-noise ratio, so that the noise in the harmonics cannot be eliminated and higher harmonics are hard to analyse accurately. Fig 3.15 (c) showed the relationship of the peak current values in the first and second harmonic and the cubic root of flow rates. A Levich-like manner can still be obtained even if the ratio of signal-to-noise is relatively poor compared with reversible reactions. In spite of that, the diffusion coefficient value was obtained as $1.06 \pm 0.09 \times 10^{-5}$ $cm^2 s^{-1}$ in 3 M NaOH supporting electrolyte, which has a good agreement with literature [228].

Based on the previous research, the overall irreversibility of the process is caused by very unstable intermediate products that can be reduced only under conditions of a sufficiently fast electrochemical method [227]. The unstable intermediate products can also result in the unexpected noise in large amplitude FTACV measurement.
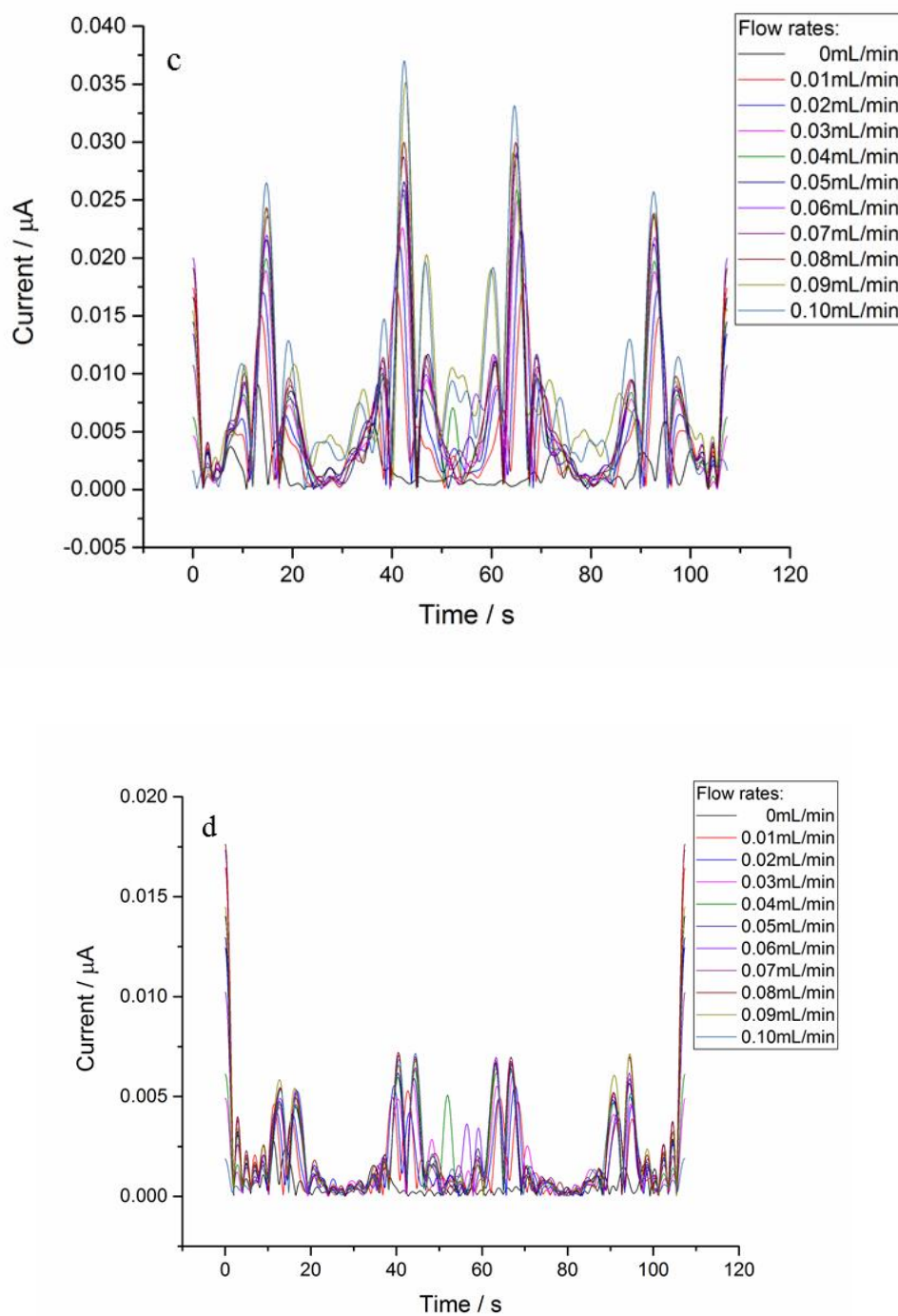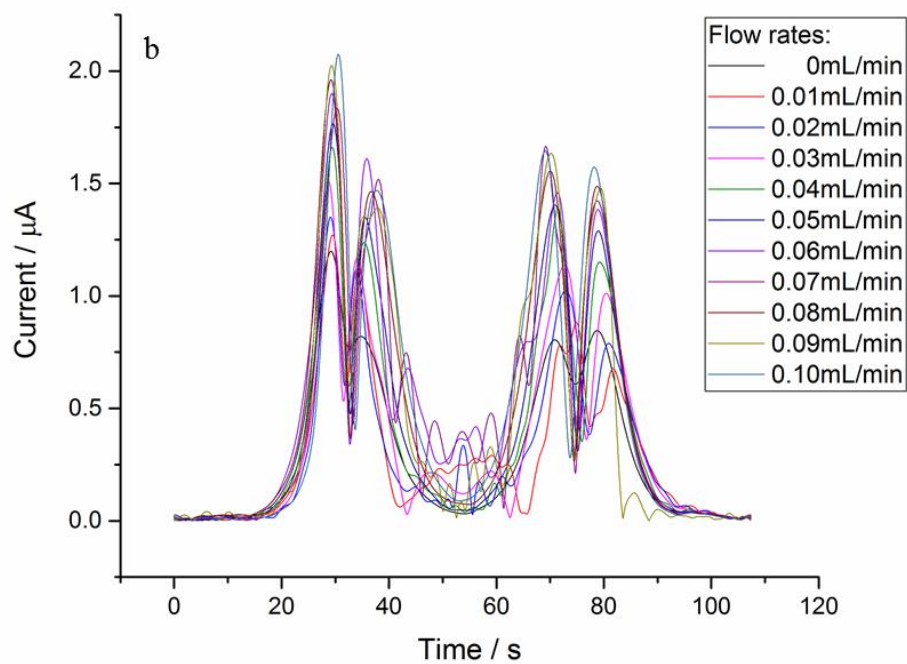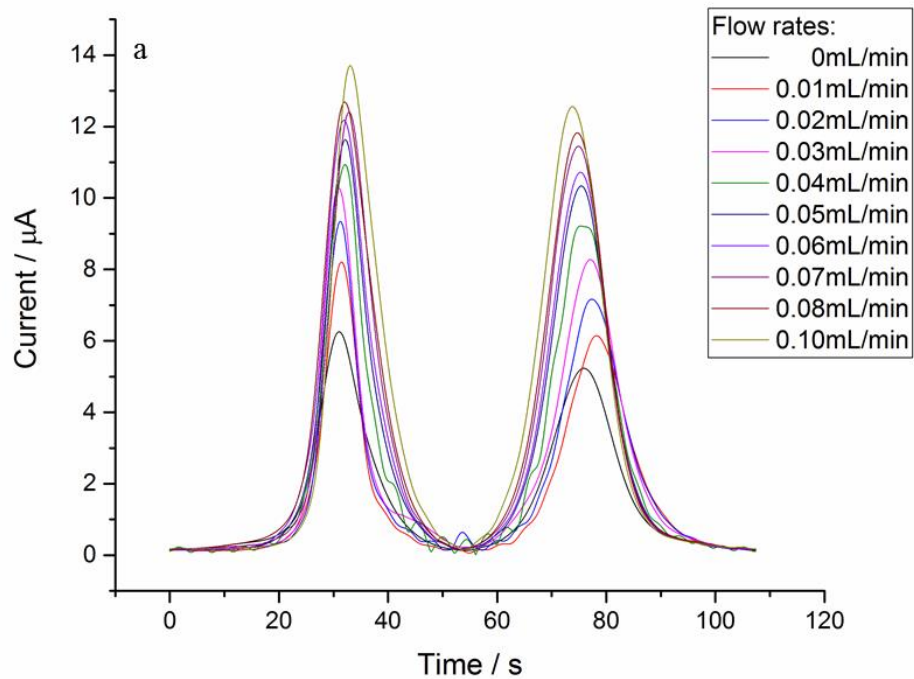
Fig 3.15 The large amplitude FTACV (potential range: -0.3-0.35V, scan rate: 12.11mV/s, frequency: 1 Hz, amplitude: 50 mV) detailing with the response of 10mM sodium borohydride in 3M NaOH supporting electrolyte to increasing flow rates (from 0.01 to 0.10 mL/min) (a) first harmonic; (b) second harmonic (c) peak current with various cubic root of flow rates.

3.5 Electrochemical detection of coupled homogeneous reactions in microfluidic system

3.5.1 Electrochemical detection of L-cysteine by using Fe^{2+} mediated oxidation

Hydrogen sulfide often results from the microbial breakdown of organic matter in the absence of oxygen gas, such as in swamps and sewers. It also occurs in volcanic gases, natural gas, and in some sources of well water. Recently , the use of hydrogen sulfide gets researchers' attention in pharmaceutical [229], industrial fields especially in neuron science [230–233]. The detection of hydrogen sulfide gained significant importance due to its high toxicity and the corresponding risks associated with exposure in a number of occupational settings. The various routes that have been considered in the analysis of sulfide are broadly summarised in Fig 3.16.

This Figure is not shown due to copyright issues

Fig 3.16 Analytical pathways for the detection of sulfide [234]

Compared with classical techniques, such as iodine titration [235] and spectroscopic detection [236], electrochemical sensing method provides advantages of low cost, simplicity of design, high sensitivity, and rapid response as well as suitability in some extreme environments [237–240].

L-cysteine is an amino acid, which has been studied because of its importance in biological system [241]. The sulfhydryl functional group gives L-cysteine significant redox characteristics [242], therefore it is utilized as a replacement of H_2S in the laboratory. Furthermore, it is a solid material, which means it is much safer to undergo the experiments other than applying hydrogen sulfide gas directly. This redox reaction involved L-cysteine has the potential application in H_2S or other hazardous gas sensing in oil extracting industry [243].

There some research based on electrochemical sensing of L-cysteine. People found that although L-cysteine showed electroactive characteristic, the drawbacks of large overpotential, low sensitivity and potential to cause electrode fouling were still needed to take into consideration [244]. Fig 3.17 showed the cyclic voltammogram of L-cysteine on glassy carbon electrode, which showed good agreement with literature [245]. The electrochemical peak can be hardly found when there is absence of other electroactive species and unmodified electrode.
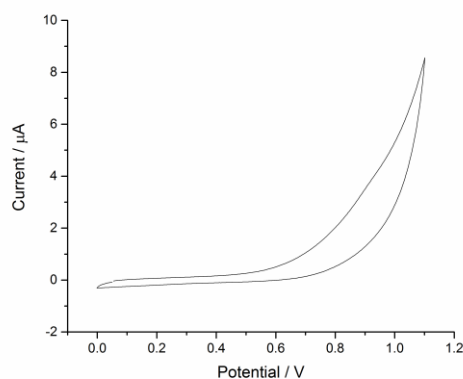
Fig 3.17 Cyclic voltammogram of 1 mM L-cysteine in 0.5 M KCl electrolyte at 3.0 mm diameter glassy carbon electrode

On the basis of that, some efforts have been developed to overcome the obstacles including modified the electrode surface [246–249] or utilize intermedia to achieve electrocatalytic process to determine L-cysteine.

The consistent reduction potential of $Fe(CN)_6^{4-}$/ $Fe(CN)_6^{3-}$ over a wide pH range and both stable oxidized and reduced forms proved that ferricynaide can be an efficient oxidant of a wide variety of organic substrate. The oxidation of cysteine by ferricyanide is well established [250–252]. Fig 3.18 showed the system response when L-cysteine was added to $Fe(CN)_6^{4-}$ solution. It can be seen obviously that the oxidative peak current increased while the reductive peak current decreased when L-cysteine was induced to the system due to the EC' reaction. Furthermore, the peak current values can be traced according to the change of L-cysteine concentrations.
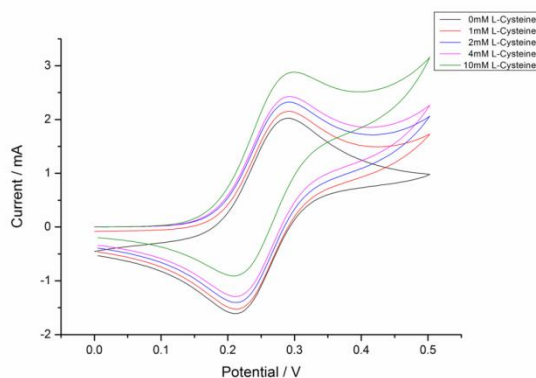
Fig 3.18 Cyclic voltammogram detailing with the response of 2 mM potassium ferrocyanide to increasing concentrations of L-cysteine on macro gold electrode

94

Large amplitude FTACV was carried to investigate the influence of sulfide under the hydrodynamic condition. Fig 3.19 shows the electrochemical response with L-cysteine added to the system. Also, the peak height changed according to the increase of the controlled flow rates. But it can be seen from the figure that the peak shifted slightly to more positive direction. One possible reason for this phenomenon is less stable nature of the gold pusedo reference was used in the microfabrication process. Measurements were repeated with different concentration of L-cysteine, and same phenomena can be obtained from Fig 3.19 to Fig 3.22.
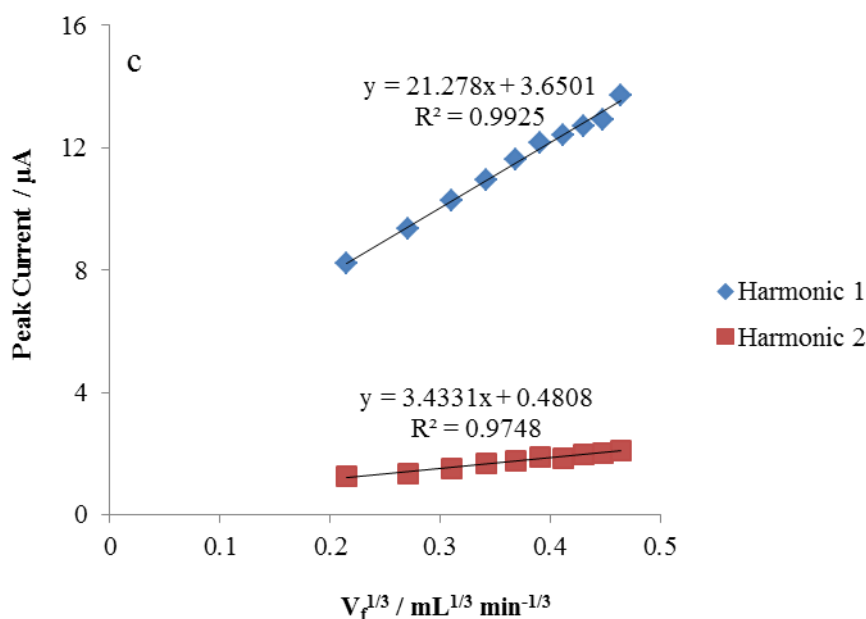

Fig 3.19 The large amplitude FTACV (potential range: -0.1-0.6 V, scan rate: 13.04 mV/s, frequency: 1 Hz, amplitude: 50 mV) detailing with the response of 2 mM potassium ferrocyanide with 1 mM L-cysteine to increasing flow rates (from 0.01 to 0.10 mL/min) (a) first harmonic; (b) second harmonic.

Fig 3.20 The large amplitude FTACV (potential range: -0.1-0.6 V, scan rate: 13.04 mV/s, frequency: 1 Hz, amplitude: 50 mV) detailing with the response of 2 mM potassium ferrocyanide with 2 mM L-cysteine to increasing flow rates (from 0.01 to 0.10 mL/min) (a) first harmonic; (b) second harmonic.

Fig 3.21 The large amplitude FTACV (potential range: -0.1-0.6 V, scan rate: 13.04 mV/s, frequency: 1 Hz, amplitude: 50 mV) detailing with the response of 2 mM potassium ferrocyanide with 3 mM L-cysteine to increasing flow rates (from 0.01 to 0.10 mL/min) (a) first harmonic; (b) second harmonic.

Fig 3.22 The large amplitude FTACV (potential range: -0.1-0.6 V, scan rate: 13.04 mV/s, frequency: 1 Hz, amplitude: 50 mV) detailing with the response of 2 mM potassium ferrocyanide with 4 mM L-cysteine to increasing flow rates (from 0.01 to 0.10 mL/min) (a) first harmonic; (b) second harmonic.

Fig 3.23 shows the pathway in the electrochemical sensing of L-cysteine involving ferrocyanide. This method shows a typical EC' process since the electrochemically generated ferricynaide will react with L-cysteine and reduces back to ferrocyanide. The equations as following

$$Fe(CN)_6^{4-} - e^- \rightleftharpoons Fe(CN)_6^{3-} \tag{3.6}$$

$$Fe(CN)_6^{3-} + L - cysteine \longrightarrow Fe(CN)_6^{4-} + L - cystine \tag{3.7}$$

This Figure is not shown due to copyright issues

Fig 3.23 Oxidation of cysteine by electrochemically generated ferricyanide [253]

Furthermore, the influence of L-cysteine concentrations was studied in large amplitude FTACV. Fig 3.24 shows the AC component extracted from overall signal in the stagnant system. When the concentration of L-cysteine increased, the peak height of the fundamental harmonic increased as well. The current rise according to the substrate concentration was resulted from the current contribution from the oxidation of the regenerated potassium ferricynaide in the catalytic step. Fig 3.24 (c) demonstrated the linear relationship between the peak current in AC component and concentrations of L-cysteine, which is analogous with previous research based on DC technique [253].

According to the literature, there are two possible pathways of cysteine by ferricyanide, depending on whether the de-protonation stage takes place before the oxidation step [253]. The modelling result showed that both forms of cysteine could be oxidized by ferricyanide and the rate constant of the electrocatalytic step was found to increase with pH values.

Fig 3.25 shows the same measurements in the hydrodynamic system. As the flow rated increased, the heights of peak current rose up as well but the peaks did not shift. Similar with stagnant system, Fig 3.25 (c) showed a great linear relationship between peak current and the concentrations of L-cysteine.

Fig 3.24 The large amplitude FTACV (potential range: -0.1-0.6V, scan rate: 13.04mV/s, frequency: 1 Hz, amplitude: 50 mV) detailing with the response of 2 mM potassium ferrocyanide to increasing concentration of L-cysteine in stagnant system (a) first harmonic; (b) second harmonic; (c) peak current with different concentrations of L-cysteine.

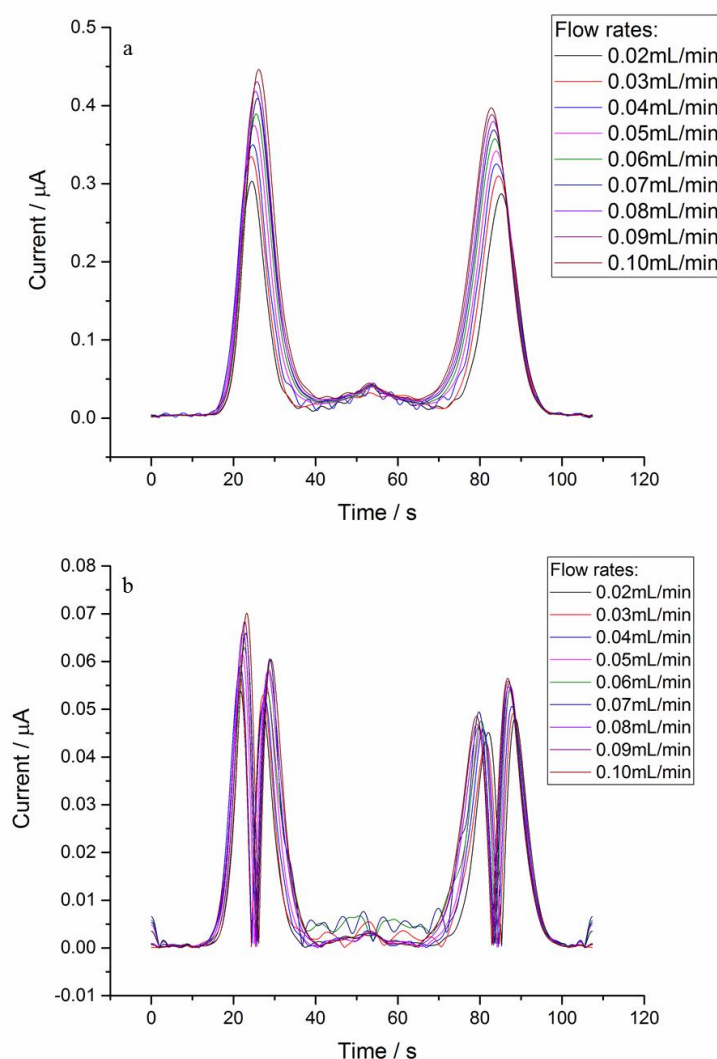Fig 3.25 The large amplitude FTACV (potential range: -0.1-0.6V, scan rate: 13.04mV/s, frequency: 1 Hz, amplitude: 50 mV) detailing with the response of 2 mM potassium ferrocyanide to increasing concentration of L-cysteine under flow rate at 0.10 mL/min (a) first harmonic; (b) second harmonic; (c) peak current with different concentrations of L-cysteine.

3.5.2 Electrochemical detection of L-cysteine by using FCA mediated oxidation

Ferrocenes often exhibit simple electrochemical behaviour and the oxidation to the ferricinium is reversible and uncomplicated [208]. Based on that, in this section ferrocenecarboxylic acid (FCA) was used as a mediator to electrocatalytically oxidize L-cysteine. Song *et al.* published that the split wave behaviour can be investigated on both macro- and micro- glassy carbon electrodes when FCA was used as a mediator [254].

Fig 3.26 shows the electrochemical behaviour of FCA and L-cysteine in the hydrodynamic system. As it can be predicted, the peak current increase with higher controlled flow rates and was consistent through the fundamental to fourth harmonic while the split wave behaviour was not found due to the utilization of gold electrode and the microfluidic conditions.

It can be concluded that the large amplitude FTACV is sensitive to the change of flow rates and then concentrations of substrate. The linear relationship between peak current values and concentrations of L-cysteine is observed with DC technique.

The use of mediator ($Fe(CN)_6^{4-}$ or FCA) as a catalyst showed a promising way to determine the L-cysteine since that the overpotential value is relatively small compared with direct oxidizing L-cysteine and it can prevent electrode fouling which is more efficient and economically friendly.
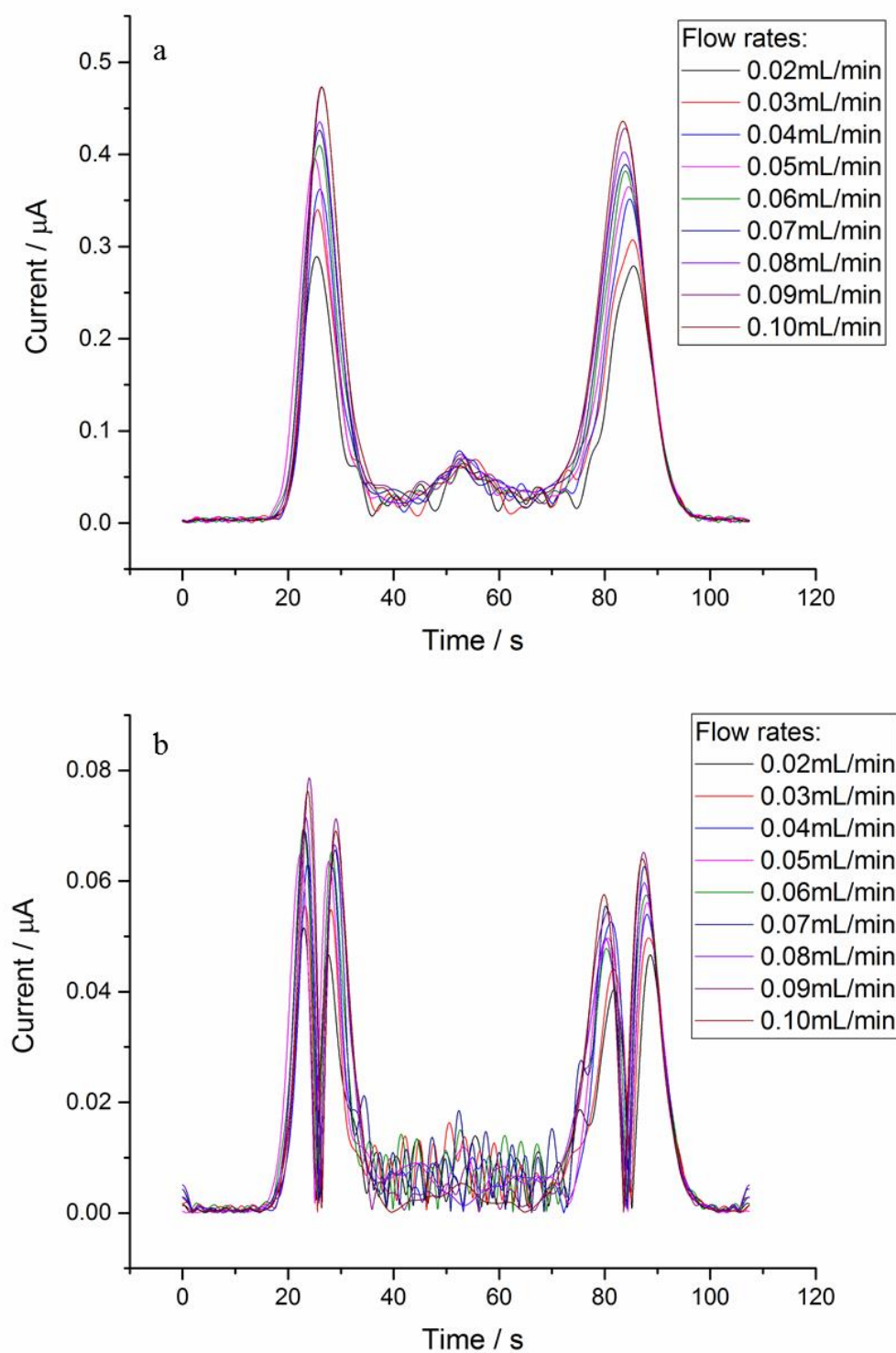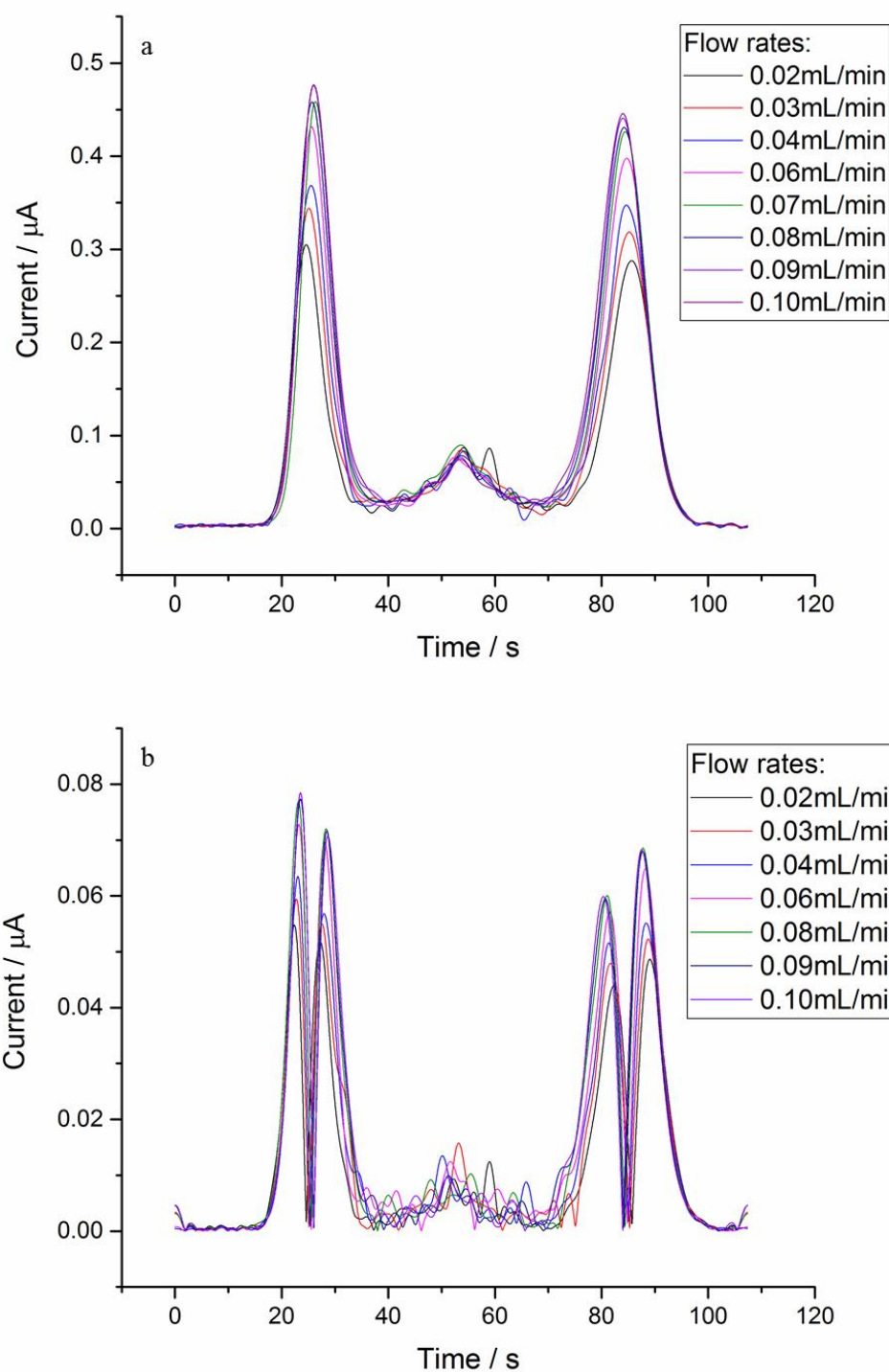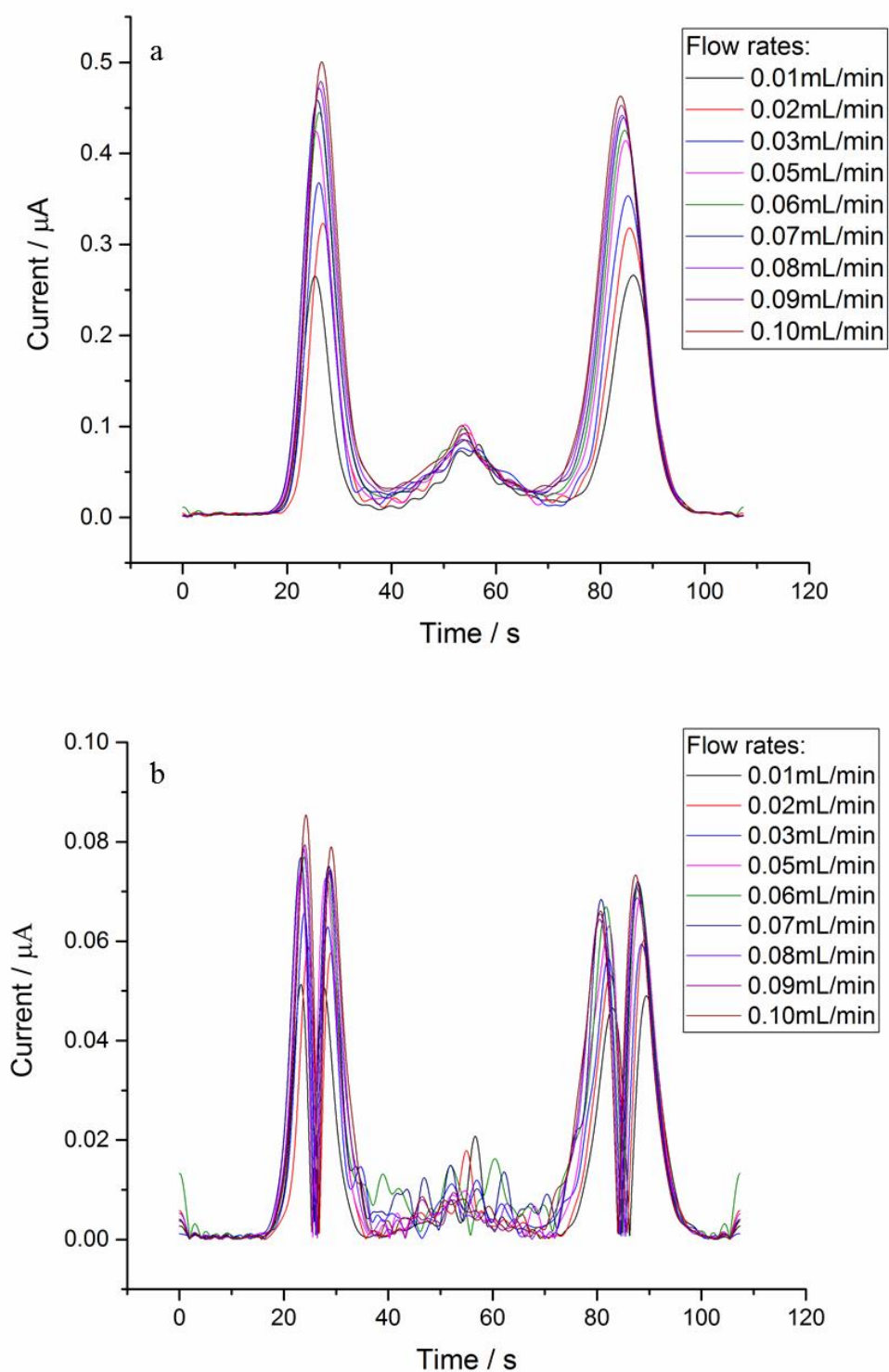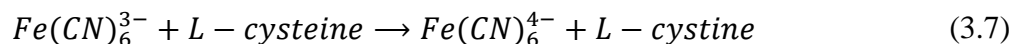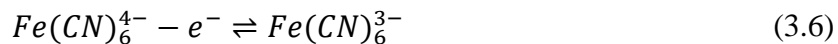
103
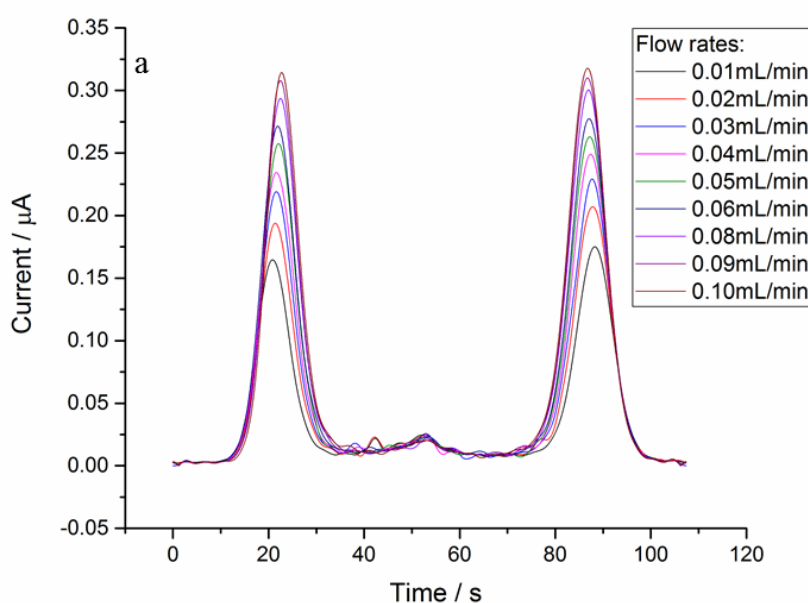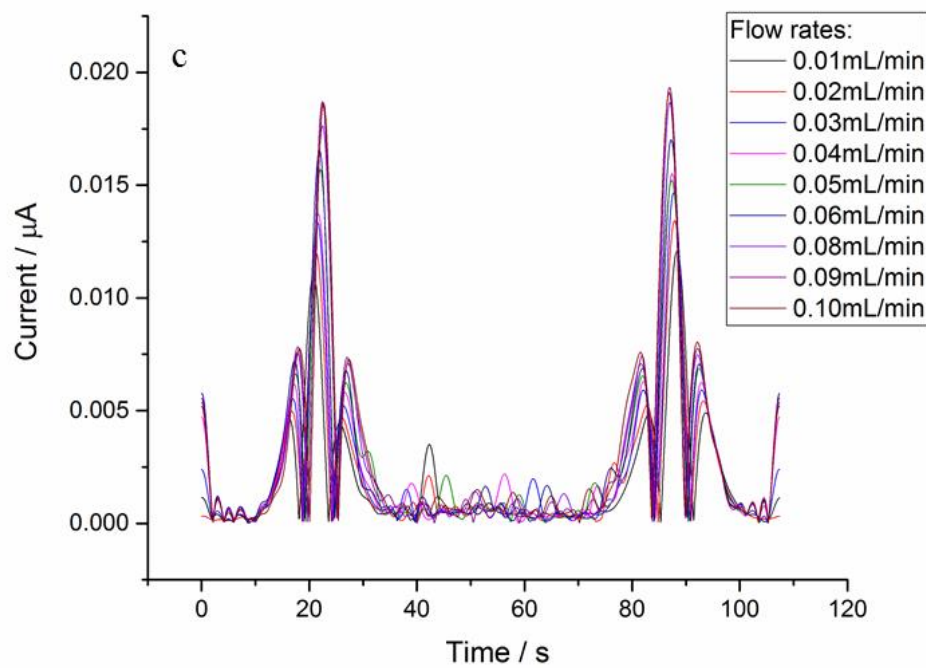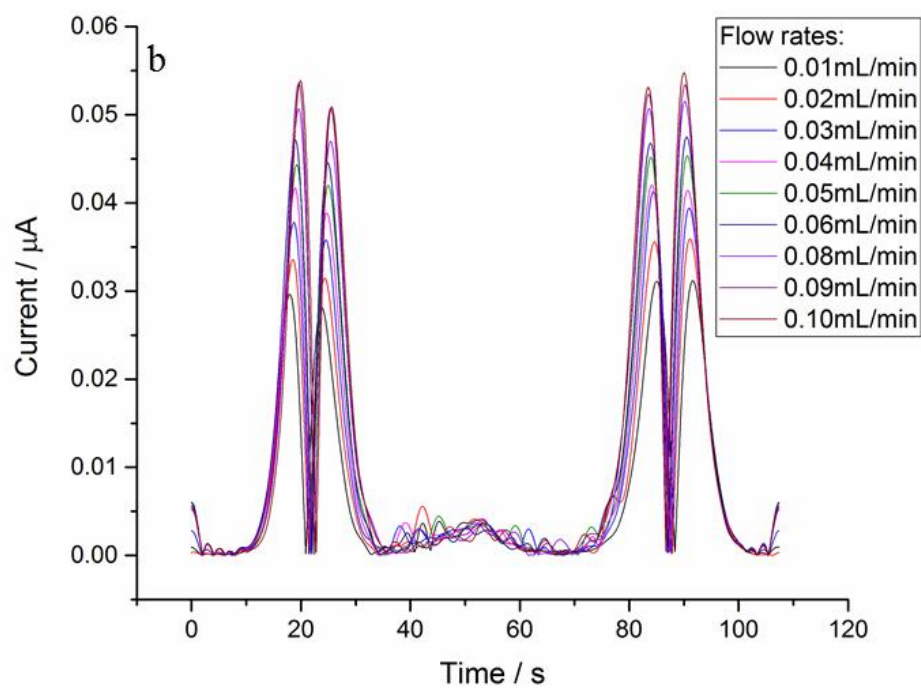
Fig 3.26 The large amplitude FTACV (potential range: -0.1-0.6V, scan rate: 13.04mV/s, frequency: 1 Hz, amplitude: 50 mV) detailing with the response of 2 mM FCA in pH 9.2 borate buffer with 0.2 mM L-cysteine to increasing flow rates (from 0.01 to 0.10 mL/min) (a) first harmonic; (b) second harmonic (c) third harmonic; (d) fourth harmonic.

3.5.3 Electrochemical detection of ascorbic acid by using N,N,N',N'-tetramethyl-*para*-phenylene-diamine mediated oxidation

Ascorbic acid, also known as Vitamin C, is a vital substance for human being. Unlike most mammalian species, human cannot synthesize ascorbic acid from glucose, hence its uptake from food sources, mainly vegetables [255]. The concentration of ascorbic acid in food industry can be varied according to climate change and methods of harvest, storage and processing conditions [256], hence reliable and accurate detection of ascorbic acid is required in agricultural area.

The methods for detection of ascorbic acid include HPLC [257], titration [258], molecular spectroscopic techniques [259] such as spectrophotometry, chemiluminescence and fluorescence techniques, sorption–spectroscopy, visual-test, colorimetry [260] , photometric method [261], electrochemical technique [262]. In electrochemistry, ascorbic acid shows a typical irreversible two-electron transfer reaction with the poor reproducibility and electrode

104

fouling. The current trendy way to detect ascorbic acid indicates that the electrode modification can be a good solution [263], while it often involves some expensive materials.

Electrocatalytic methods have shown promise as a rapid response and economically friendly approach to ascorbic acid monitoring. Kuss [264] demonstrated an electrocatalytic way to detect ascorbic acid by using TMPD as a mediator. In presence of TMPD, ascorbic acid can be oxidized at a low overpotential [265] and the products are formed in the solution to avoid the electrode fouling and the reliable electrochemical signal can be recorded on unmodified electrode. Also, the applicability of this technique can be reproducible on commercial orange juice, offering a straight forward, inexpensive and precise alternative to other ascorbic acid determination strategies.

First of all, the electrochemical detection of 2 mM TMPD to TMPD$*^+$ in pH 7 phosphate buffer solution was processed under large amplitude FTACV with potential range of -0.2-0.25 V, scan rate as 8.38 mV/s, frequency as 1 Hz and amplitude as 50 mV.

In Fig 3.27, the electrochemical response of TMPD to TMPD$*^+$ was shown. Similar to Fig 3.12, the good current response to the flow rates change can be found. But as it mentioned before, due to TMPD$*^+$ is thermodynamically unstable. The signal-to-noise ratio in higher harmonic components is relatively poor compared with fully oxidation of TMPD. However the active TMPD$*^+$ performs as a good catalysis to later homogeneous reaction.
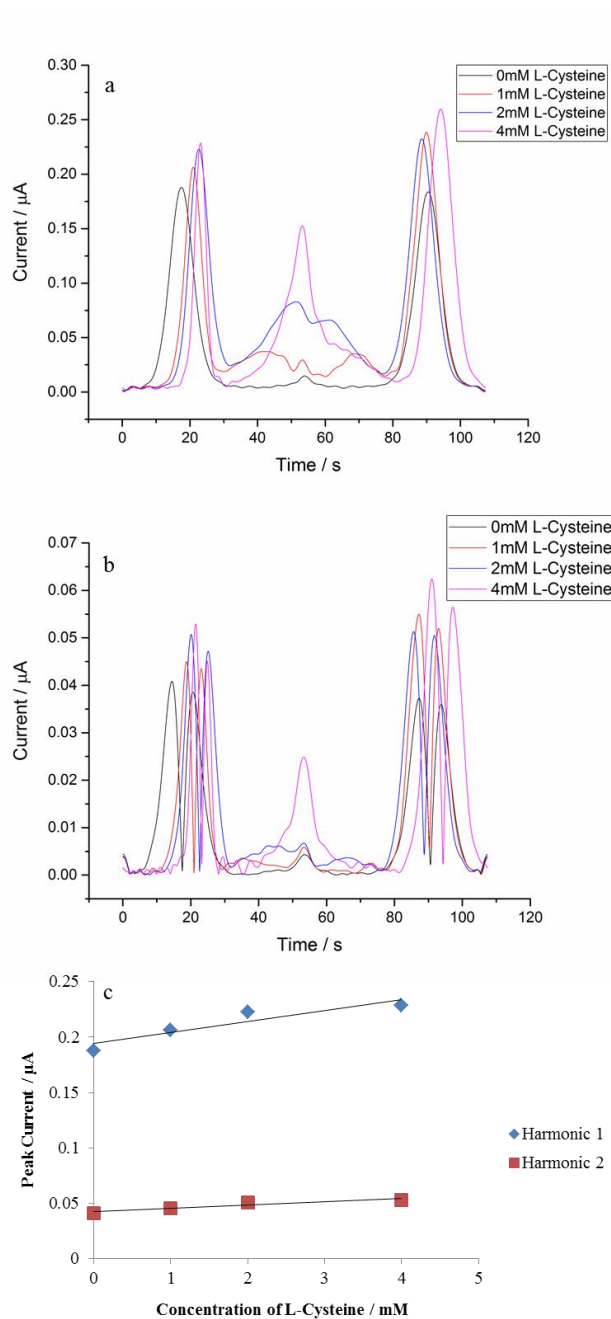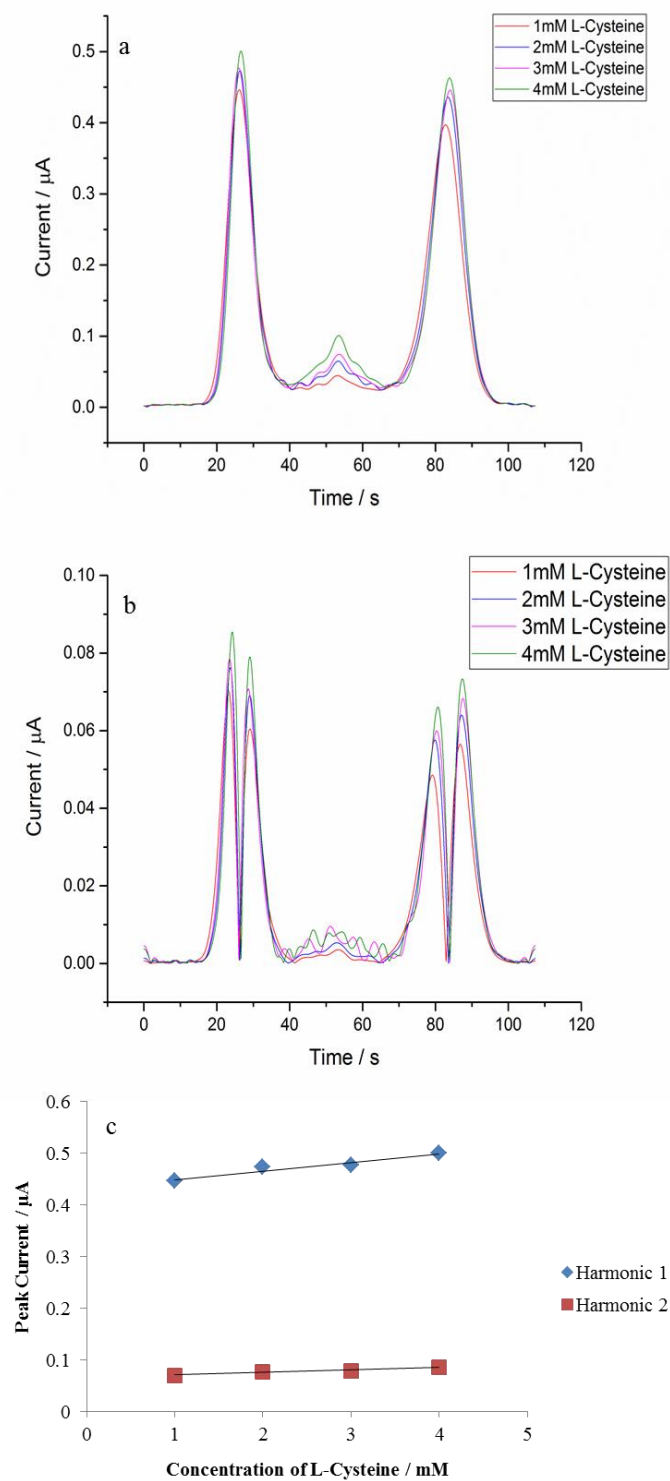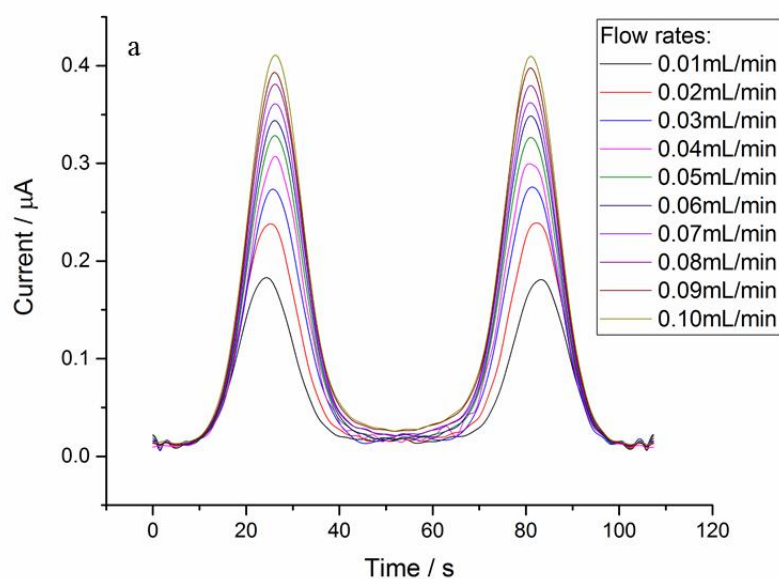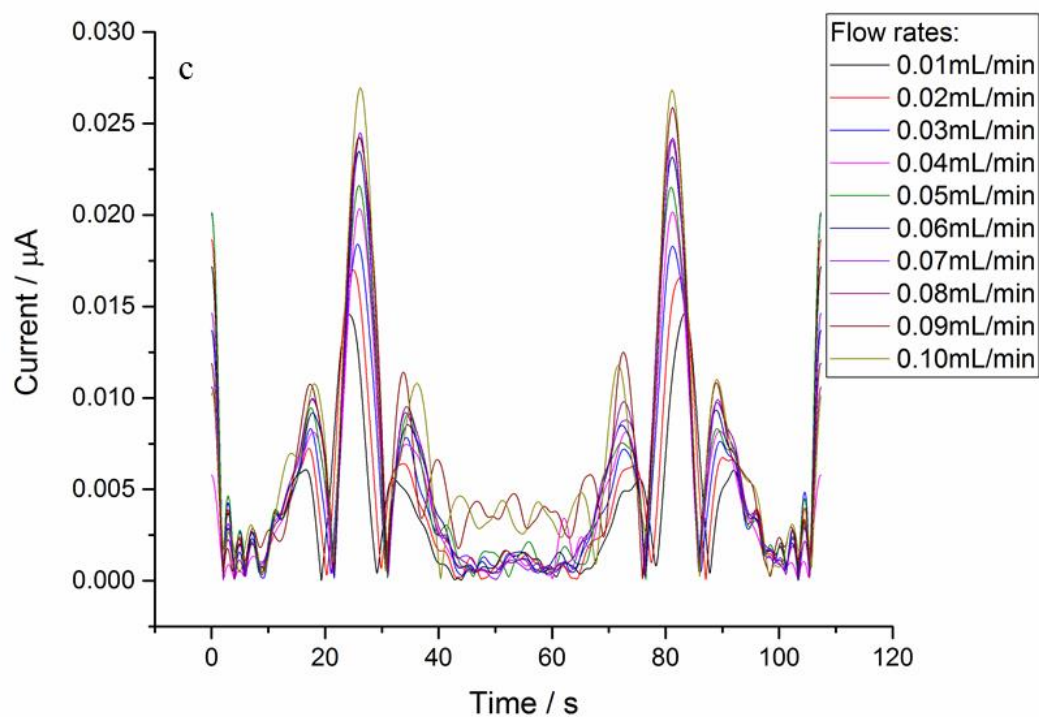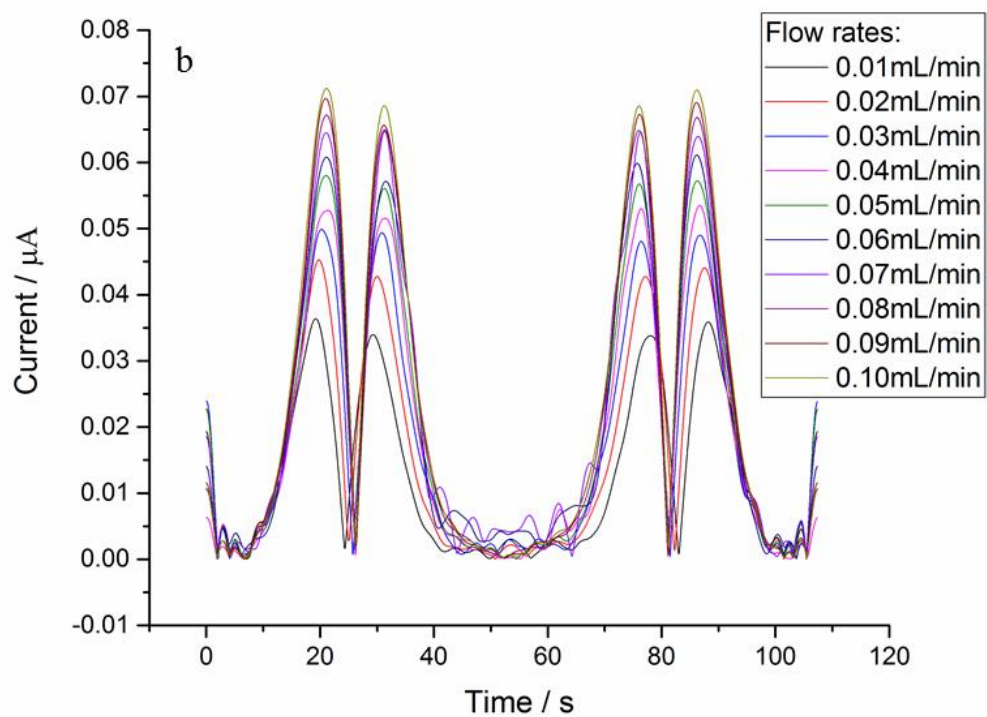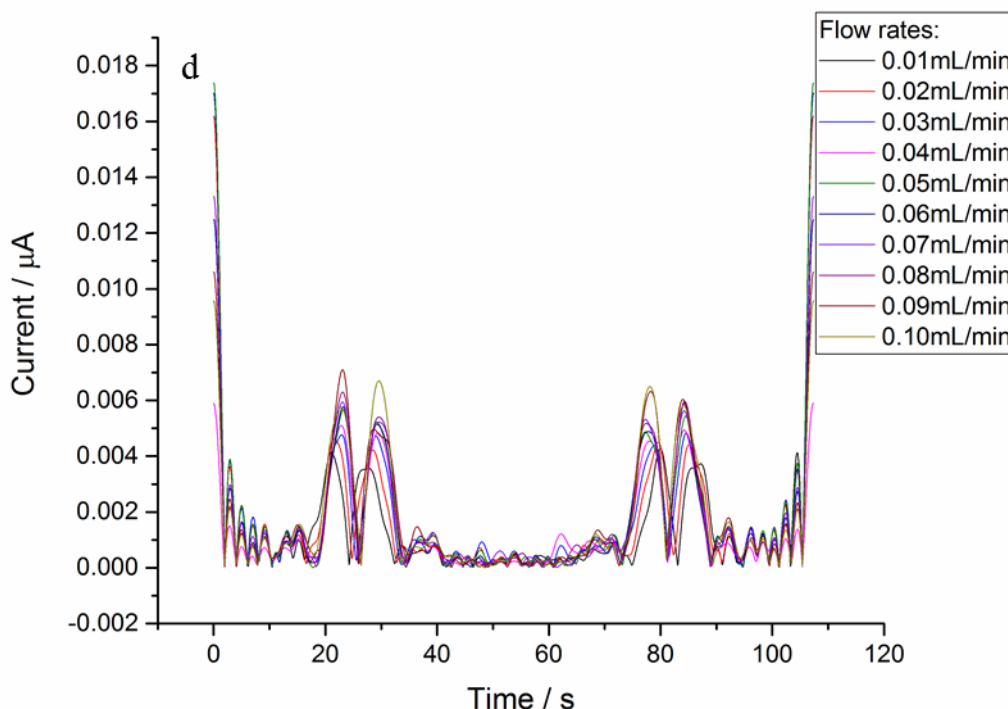
Fig 3.27 The large amplitude FTACV (potential range: -0.2-0.25 V, scan rate: 8.38 mV/s, frequency: 1 Hz, amplitude: 50 mV) detailing with the response of 2 mM TMPD in pH 7 phosphate buffer to increasing flow rates (from 0.01 to 0.10 mL/min) (a) first harmonic; (b) second harmonic (c) third harmonic; (d) fourth harmonic.

Next, ascorbic acid was introduced to the system. The concentrations of ascorbic acid were chosen in excess of TMPD to ensure stability of experimental measurements. Fig 3.28 to Fig 3.30 showed the AC components extracted from overall signal of TMPD with different concentrations of ascorbic acid. As it can be seen from these figures, when ascorbic acid was added to the microfluidic system, the peaks shifted. This phenomenon is quite similar with that happened in previous section when L-cysteine was introduced into potassium ferrocyanide environment. The added substrate in the system did have the influence to the gold reference electrode, which is not that stable compared with other commercial reference electrode materials.
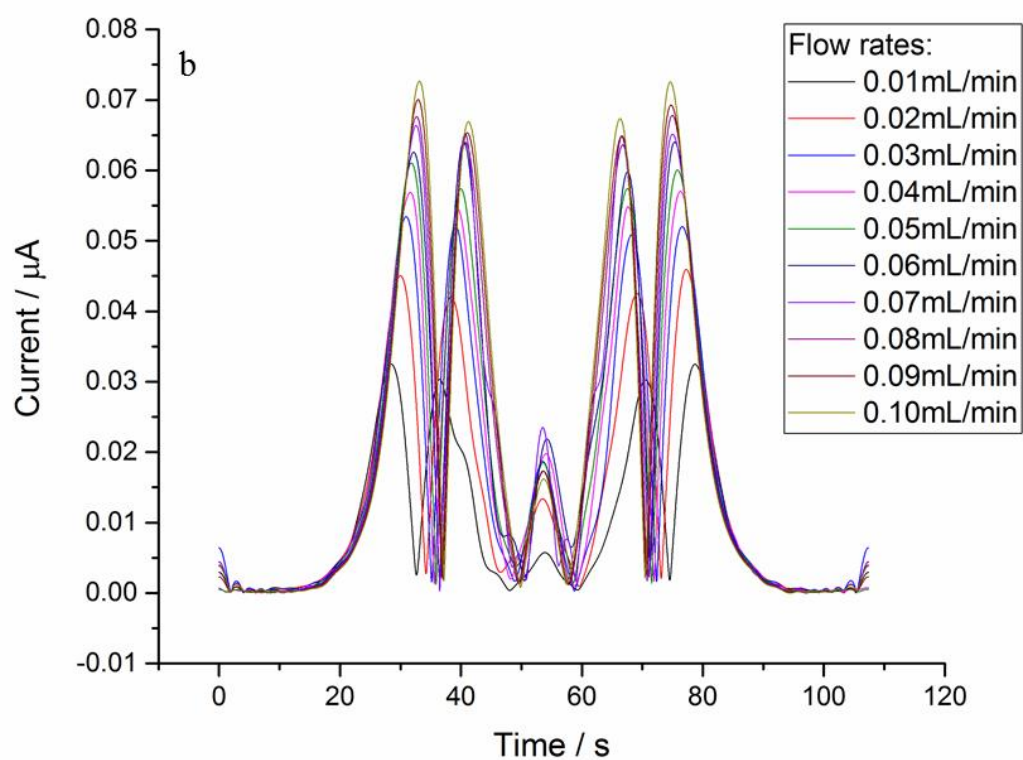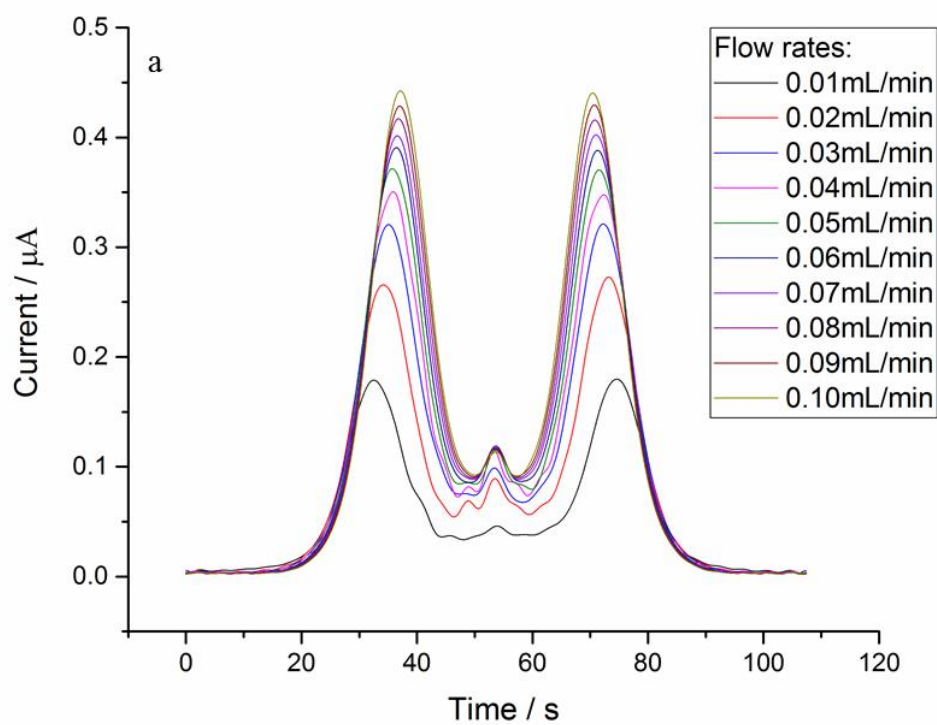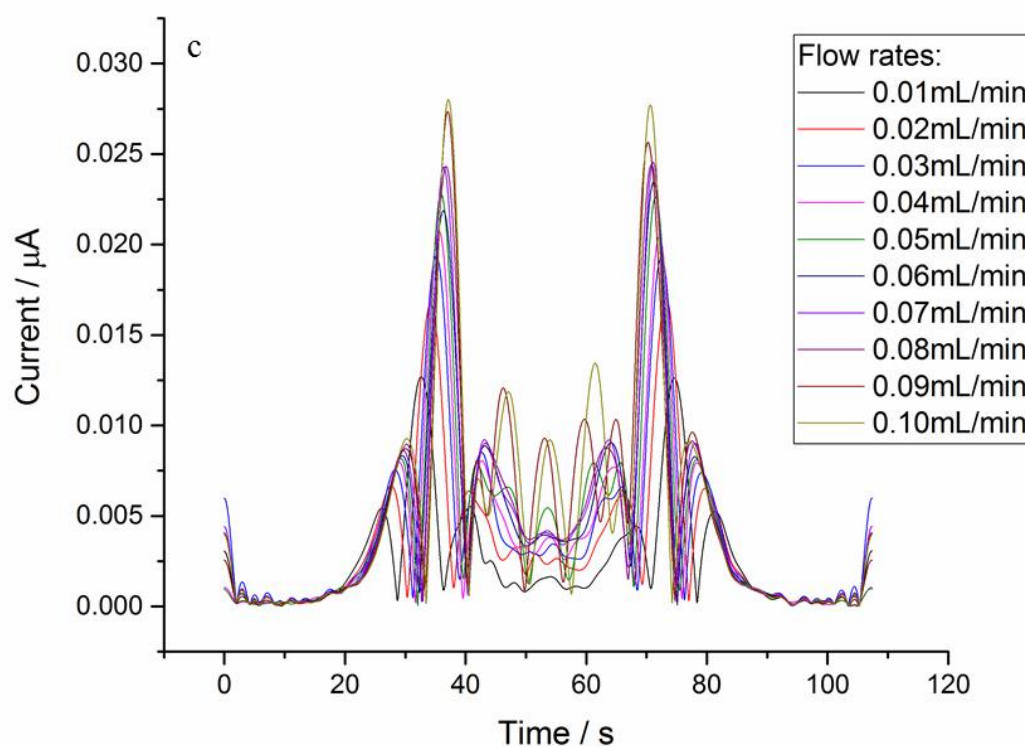
Fig 3.28 The large amplitude FTACV (potential range: -0.2-0.35 V, scan rate: 10.24 mV/s, frequency: 1 Hz, amplitude: 50 mV) detailing with the response of 2 mM TMPD with 2 mM ascorbic acid in pH 7 phosphate buffer to increasing flow rates (from 0.01 to 0.10 mL/min) (a) first harmonic; (b) second harmonic; (c) third harmonic.
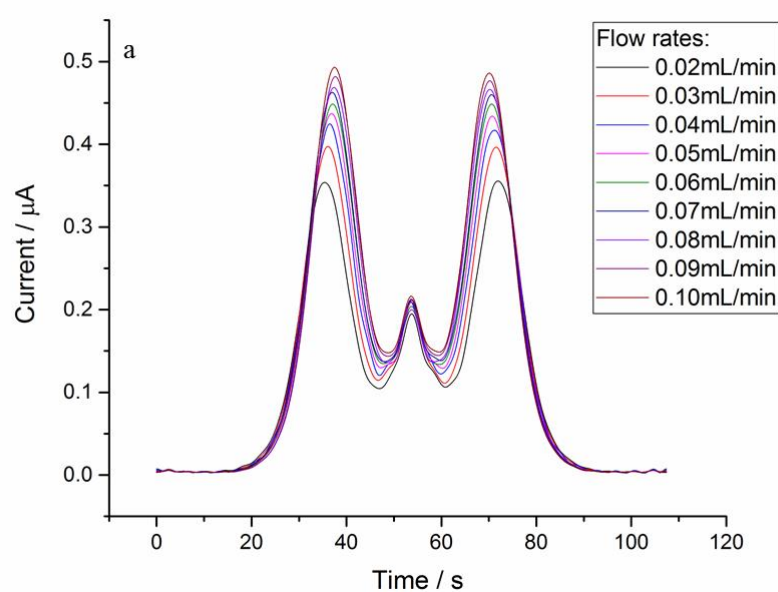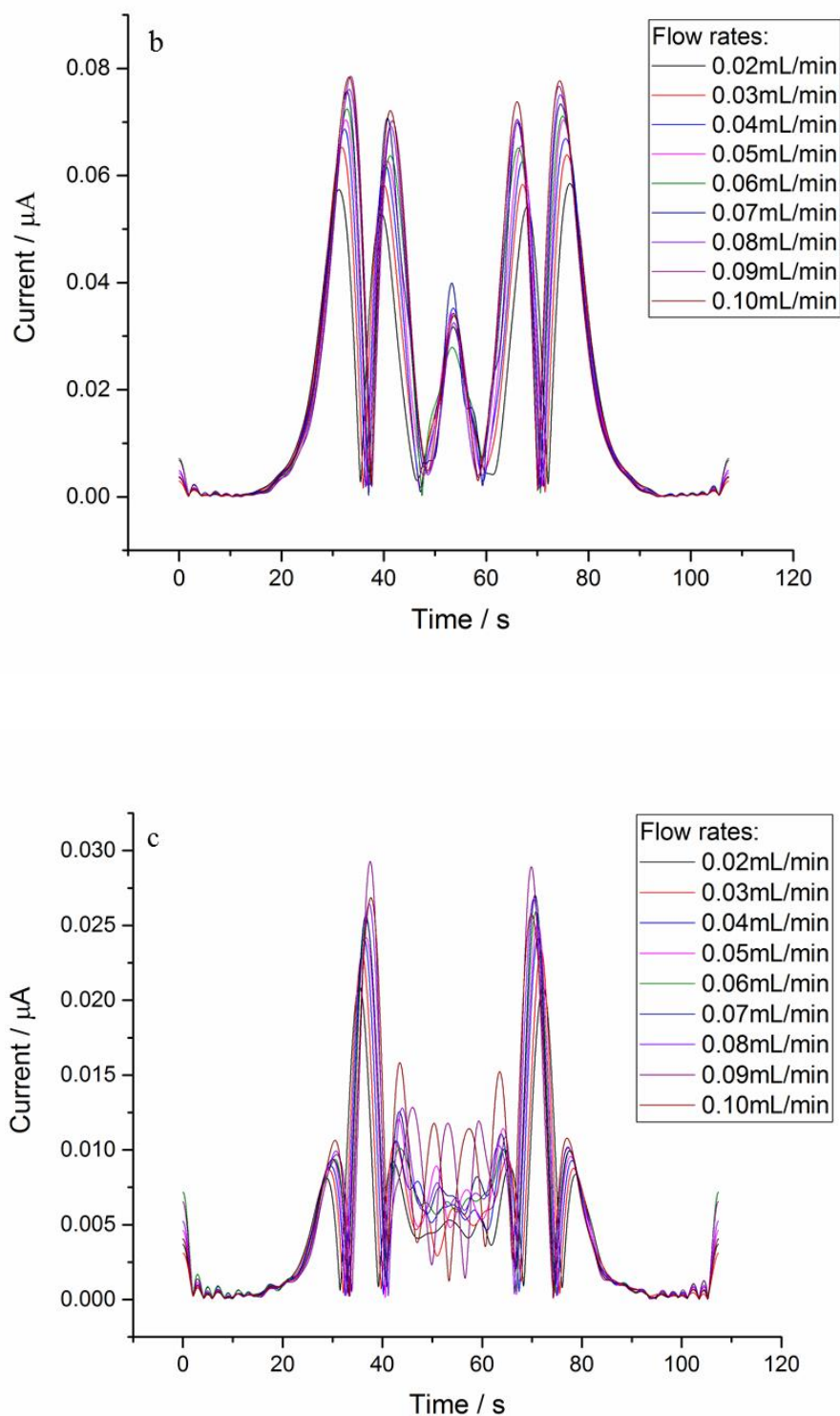
Fig 3.29 The large amplitude FTACV (potential range: -0.2-0.35 V, scan rate: 10.24 mV/s, frequency: 1 Hz, amplitude: 50 mV) detailing with the response of 2 mM TMPD with 4mM ascorbic acid in pH 7 phosphate buffer to increasing flow rates (from 0.01 to 0.10 mL/min) (a) first harmonic; (b) second harmonic; (c) third harmonic.
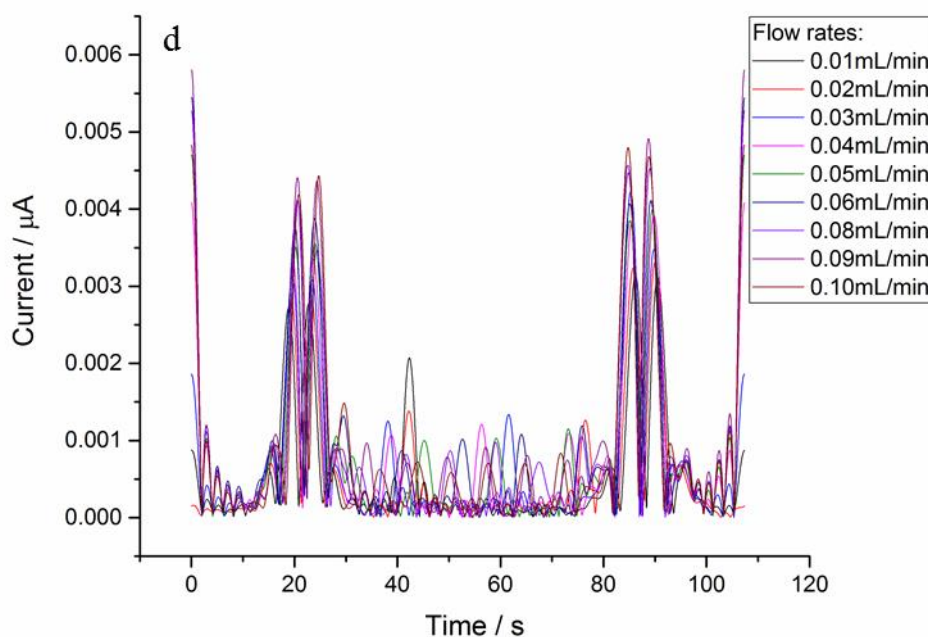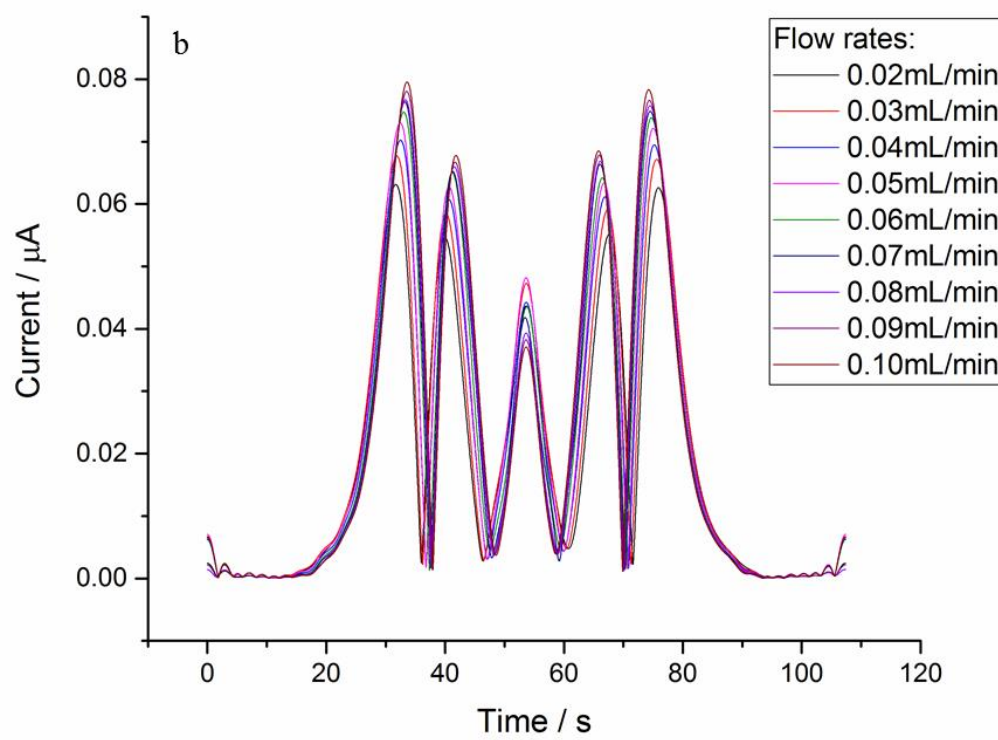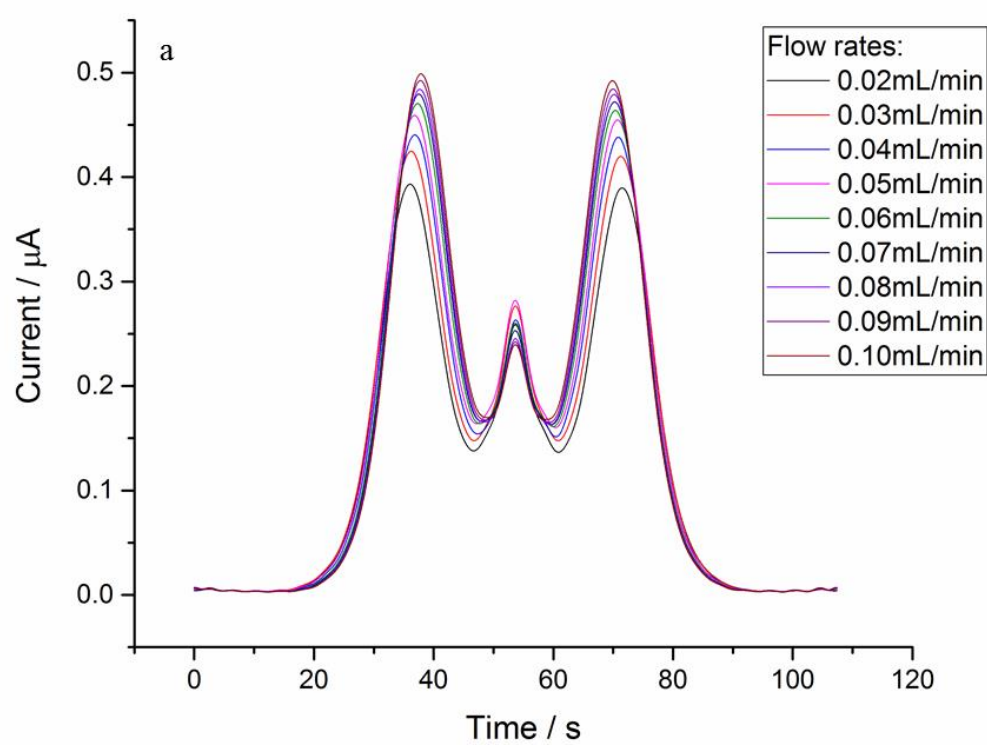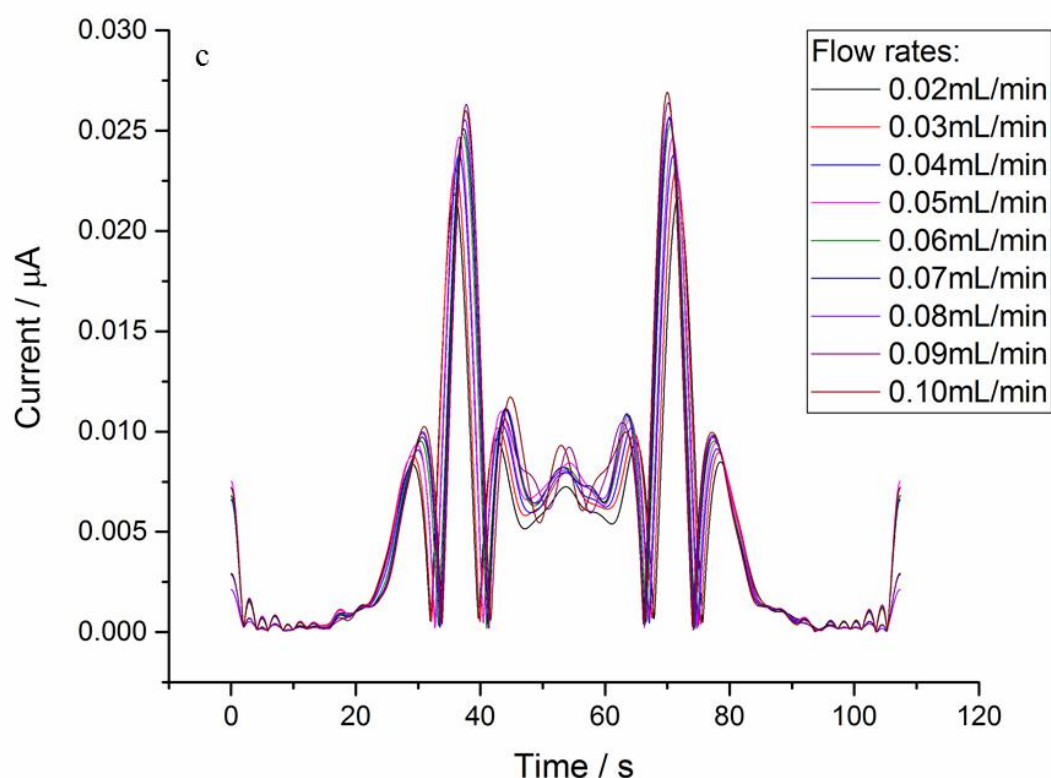
Fig 3.30 The large amplitude FTACV (potential range: -0.2-0.35 V, scan rate: 10.24 mV/s, frequency: 1 Hz, amplitude: 50 mV) detailing with the response of 2 mM TMPD with 6 mM ascorbic acid in pH 7 phosphate buffer to increasing flow rates (from 0.01 to 0.10 mL/min) (a) first harmonic; (b) second harmonic; (c) third harmonic.

The influence of concentrations of ascorbic acid was also investigated. Fig 3.31 (a-c) shows the change of peak current in the AC components with different concentrations of ascorbic acid under microfluidic conditions. It shows clearly when more ascorbic acid was introduced into the system, the peak current increases. In the presence of ascorbic acid, TMPD reacts homogeneously with AA, resulting in an enhanced current signal. Also, the relationship between peak current value and ascorbic concentration was plotted in Fig 3.31 (d-f). A good linear relationship can be found between peak current value and various concentrations of ascorbic acid. According to Kuss [264], they believe that other than EC' or EC'-disproportionation mechanisms, TMPD/ascorbic acid system exhibits a combination of two catalytic steps and singly oxidized ascorbic acid disproportionation as

112

$$TMPD^{*+} + AA \rightleftarrows TMPD + AA^{+} \tag{3.8}$$

$$TMPD^{*+} + AA^{+} \rightleftarrows TMPD + AA^{2+} \tag{3.9}$$

$$AA^{+} + AA^{+} \rightleftarrows AA + AA^{2+} \tag{3.10}$$
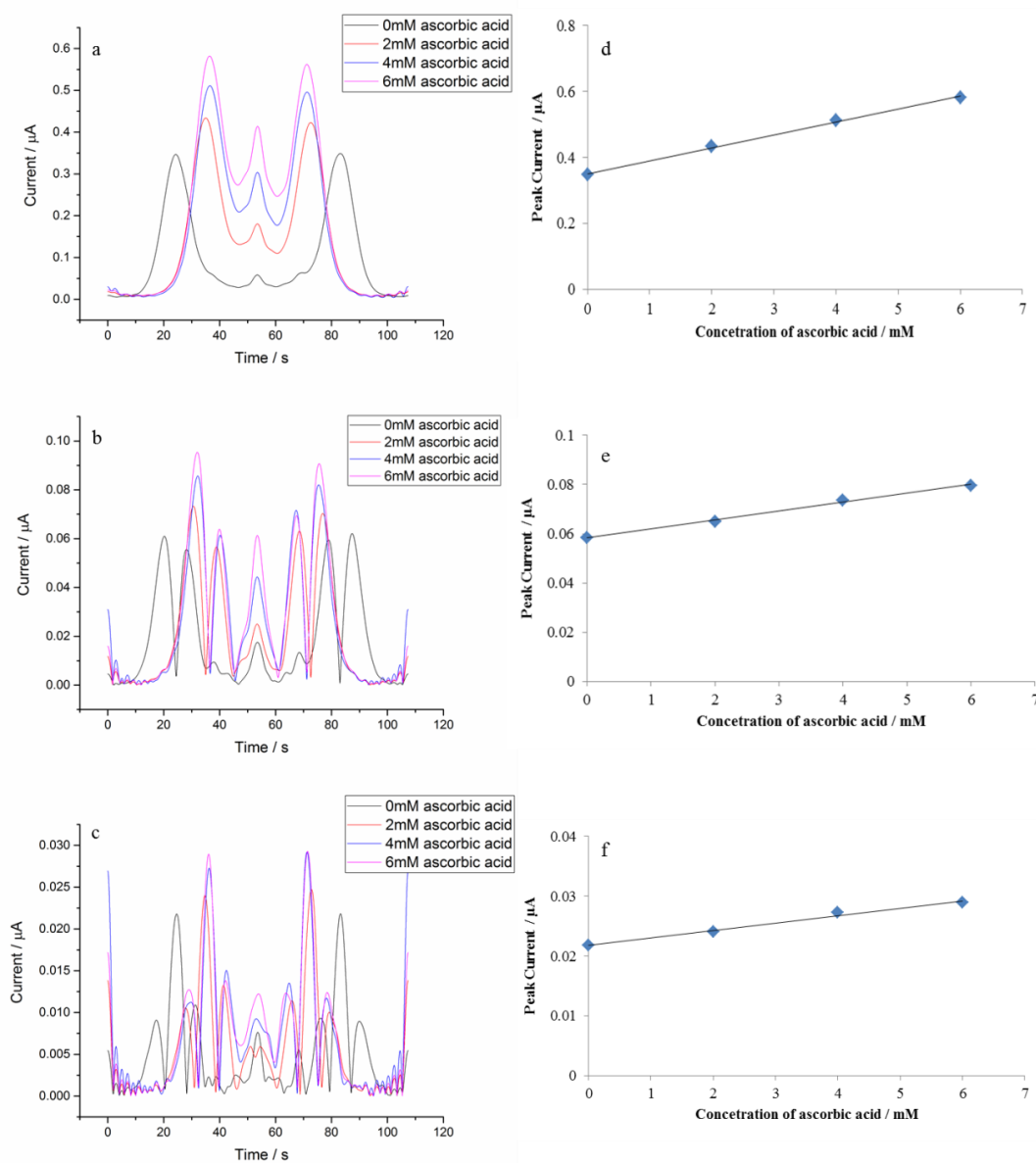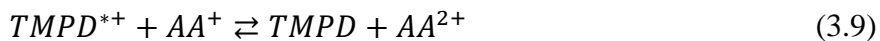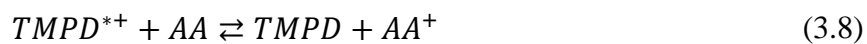
Fig 3.31 The large amplitude FTACV (potential range: -0.2-0.35V, scan rate: 10.24mV/s, frequency: 1 Hz, amplitude: 50 mV) detailing with the response of 2 mM TMPD to increasing concentration of ascorbic acid under flow rate of 0.05mL/min (a-c) first to third harmonic; (d-f) peak current with different concentrations of ascorbic acid in each related harmonic.

3.6 Conclusions

In this chapter, electrochemical microreactors were fabricated and utilized as electrochemical cells to study different electrochemical mechanisms in microfluidic system. Large amplitude Fourier transformed alternating current voltammetry was used as electrochemical detection method.

The input signal of large amplitude FTACV was comprised of a DC signal and AC sinusoidal waveform, so that both DC signal and AC components can be obtained in a short time. The raw data was processed by using a Fourier transform analysing technique, different order harmonics were extracted along with the corresponding with DC signal.

First experiments explored traditional pure electron-transfer reactions, such as quasi-reversible, irreversible and different electron-transfer reaction. The experiments were carried out both in stagnant and microfluidic systems. The DC signal extracted from the overall signal had a good agreement with the classical cyclic voltammogram and the diffusion coefficient values were calculated. Both the DC signal and AC components reflected the reversibility of the reaction. Further, when controlled flow rates were applied to the system, the resulting signal showed that the AC components were sensitive with the change of the flow rates. And the peak current in lower components showed a Levich-like manner analogue with the steady state theory applied in CV technique, which diminished with increasing harmonic order due to the diffusion rather than convection contribution.

Later, the coupled homogeneous reactions were investigated in such systems. As the EC' reaction processed, the AC signal was enhanced when the L-cysteine was introduced to the system due to the chemical reaction following after the electron-transfer. In microfluidic system, the AC components stilled obeyed the Levich-like manner as the peak current value increased with faster flow stream. A good linear relationship of peak current values and different concentrations of L-cysteine can be got in each harmonic.

When ascorbic acid was added to TMPD, the unstable TMPD^{*+} reacted with ascorbic acid immediately when it was electrochemically generated from TMPD. Also, with excess ascorbic acid, the TMPD was fully reacted and the linear relationship of substrate concentrations and peak current can be obtained. A combination of two catalytic steps and singly oxidized ascorbic acid disproportionation was studied based on previous research.

Chapter 4   Modulated Hydrodynamic System with Large Amplitude Fourier Transformed Alternating Current Voltammetry in Microreactors

4.1   Introduction

In the previous chapter, the different electrochemical mechanisms in a hydrodynamic system with large amplitude Fourier transformed alternating current voltammetry under steady flow conditions. In this chapter, the modulated technique was applied to hydrodynamic system and all the electrolysis mechanisms mentioned before were studied with large amplitude FTACV in modulated hydrodynamic system.

4.2   Hydrodynamic modulation methods in electrochemical detection

The benefit of utilizing hydrodynamic systems to study reaction kinetics have been addressed by researchers [266–269]. In the case of microfluidic channels, convection and diffusion operate in two or three dimensions, the channel electrode surface is non-uniformly accessible [270]. The current density varies over the electrode surface [271], and under laminar flow conditions the flow is well defined and calculable so that electrode processes can be accurately simulated so as to permit discrimination between candidate mechanisms [134]. It has been noted that introduction of hydrodynamic modulation voltammetry can enhance the non-uniform diffusion layer at the electrode surface, which can result in better understanding and resolution of the mechanisms and reaction kinetic studies.

This Figure is not shown due to copyright issues

Fig 4.1 A concentration profile of a species undergoing transport-limited oxidation or reduction at a channel electrode [134].

Furthermore, researchers have shown that hydrodynamic modulation voltammetry is a powerful method for enhancing detection limit and the potential window in which dynamic electroanalytical measurements can be made. The quantitative limiting current measurements can be made either for analytes at low concentration, or close to the solvent window, where DC measurements are often dominated by background currents. A significant goal of HMV is to implement high modulation frequencies, thereby reducing detection times and enhancing detection sensitivity [272].

In Chapter 1, some previous research related to hydrodynamic modulation voltammetry has been reviewed. The early year research about hydrodynamic modulation voltammetry can be divided into two parts: the first one is the electrode motion modulation, which can be achieved with mechanical techniques, such as ultrasonic modulation[143], switching the rotating speed or modulating the rotating frequency of RDE [273–276] and vibrating the electrode [277–280]. The other approach includes various methods involving interruption or periodic variation of solution flow [281].

With the robust development of UMEs, the HMV related research went to a new era, and some new techniques have been studied in hydrodynamic modulation voltammetry. The variable-height radial flow microring electrode was proposed by Macpherson and the co-worker [282]. This technique coupled with in-phase current detection represents a new hydrodynamic modulation approach, by which the mass transfer characteristics of the electrode are well-defined and calculable in terms of steady state laminar radial channel flow theory. The fast response time of the device, coupled with in-phase current detection, and the experimental simplicity made this variable-height radial flow microring electrode an useful

prospect as an end-of-column electrochemical detector for flow injection analysis or HPLC with electrochemical detection.

This Figure is not shown due to copyright issues

Fig 4.2 Schematic cross-section of the radial flow microring electrode arrangement [282].

A dual disk chopped flow-microjet electrode was then developed by the same group. This device contains a rotating blade positioned between the nozzle and the UME probe, which is used to periodically interrupt flow to the electrode surfacing, resulting in modulation of the overall mass transfer rate [283]. The use of a dual-disk microelectrode probe enables the current for two electroactive solutes to be recorded simultaneously.

This Figure is not shown due to copyright issues

Fig 4.3 (a) experimental arrangement for chopped flow-microjet electrode; (b) mass transport controlled current responses recorded simultaneously for both UMEs [283]

Another concept was proposed by Gooch [284] about applying pressure driven flow control over a channel cell. It is reported that the modulation referred to a stepped change in the

pressure between two limits. In the concept, first at a fixed volume flow rate, a potential step experiment was performed. Once the steady state current had been established the applied pressure was stepped instantly to a new value and the transient current response monitored.

This Figure is not shown due to copyright issues

Fig 4.4 Current/Time Graph, showing the effect of a pressure step [284]

As it can be seen from the examples above, the electrochemical detection is quite sensitive to the hydrodynamic modulation. According to Wong [135], HMV could be utilized under some specific conditions and it was proved to obtain more useful information while conventional electrochemical technique was unable to do so.

For the development of HMV mentioned above, all of the measurements only involved DC mode detection such as chronoamperometry and cyclic voltammetry. The reason for that is the voltammetry related to DC mode is relatively intuitive. Also it is fast and easy for researchers to process compared with some advanced electrochemical detection technique. However, sometimes the DC voltammetry fails to give more accurate and interesting information due to the limitation of detection time and potential range. The Faradaic current cannot be distinguished from the residual current on the i-E scan as well, which indicated that to develop new electrochemical detection method combined with hydrodynamic modulation is a promising way. Compton and co-workers have shown that AC impedance measurements can be used to precisely characterize the dominant mass transport regime in experimental channel electrodes to develop both mechanistic and electroanalytical studies [104].

Researchers have also managed to prove that the modulation techniques involving sine wave signals of low level are very powerful tools for identifying the elementary processes

characterizing a physical system and determining the time constants associated to each of them [285]. They also demonstrated that the AC impedance was a powerful tool to study interfacial kinetics with modulated rotation disc electrode system.

There was little or no research has been done in hydrodynamic modulation with alternating current voltammetry. The merit of utilizing FTACV has been explicated before, therefore to investigate the influence of hydrodynamic modulation to different electrochemical mechanisms with large amplitude FTACV is a worthy attempt.

4.3   Experimental procedures

In this chapter, the hydrodynamic system was built similarly as Chapter 3. The hydrodynamic modulation was achieved by programming the flow procedure on the syringe pump.

For normal hydrodynamic measurement in Chapter 3, the flow rate was kept as a fixed value during the measurement as Fig 4.5 (a). In this chapter, the step hydrodynamic modulation was introduced during the measurement. The flow rate was first set as a fixed value when the electrochemical measurement started simultaneously, the flow rate jumped to another value when the time reached t_s as Fig 4.5 (b) showed.
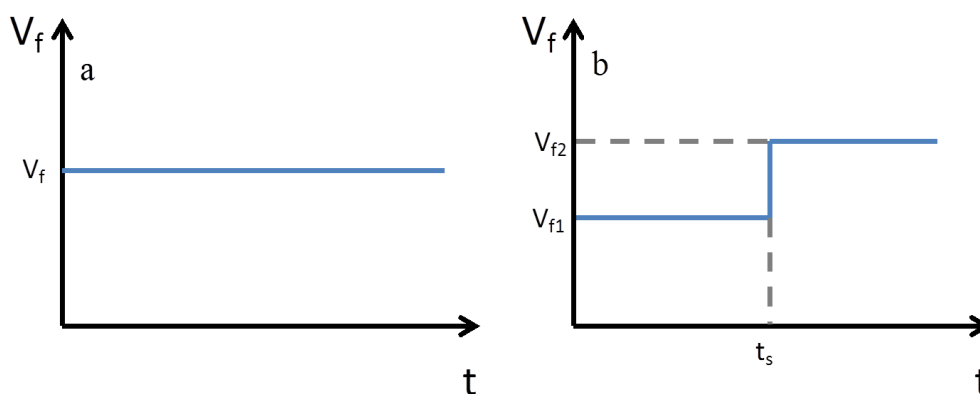
Fig 4.5 Flow rate setup in hydrodynamic system (a) normal setup; (b) step modulation setup

With the hydrodynamic modulation, the previous steady state will be interrupted due to the changed flow rate. With a higher flow rate, the new diffusion layer will be achieved. The resulting current therefore increased as showed in Fig 4.6 due to a thinner diffusion layer.
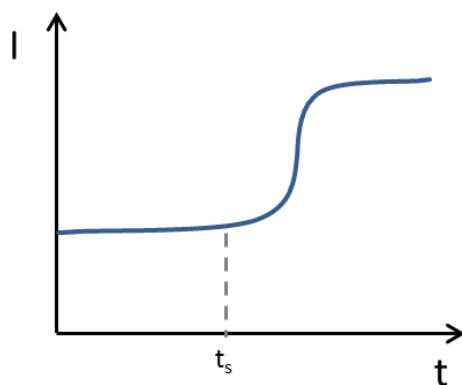
Fig 4.6 Current/time graph, showing the effect of step increasing flow rate

The same detection was processed in large amplitude FTACV as well. Fig 4.7 showed the electrochemical response of step increasing flow rate in large amplitude FTACV. The step increasing flow rate took place when the time reached t_s. It can be seen that from first through fourth harmonic, the peaks generated from the reverse sweep were higher than the ones from the forward sweep due to the higher flow rate.
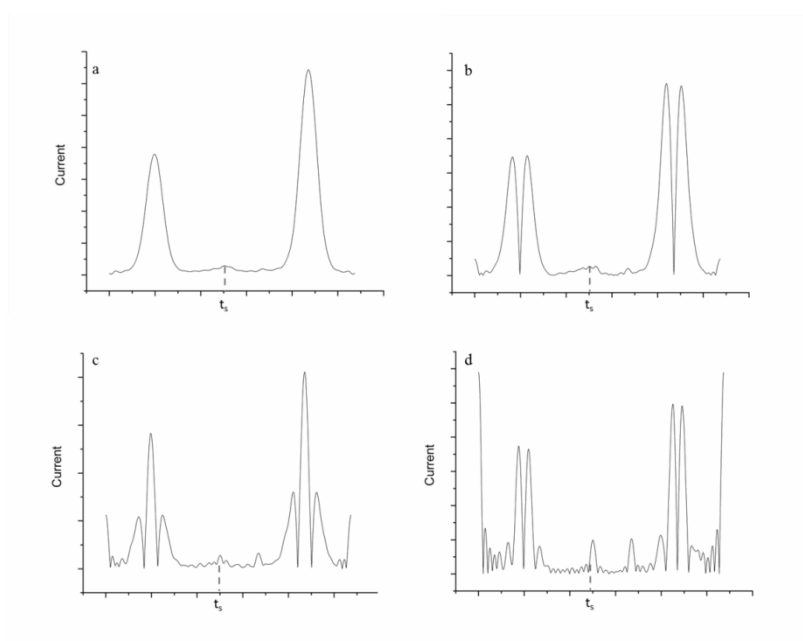
Fig 4.7 Large amplitude FTACV of increasing step flow rate (a)-(d) first to fourth harmonic

The different ratios of second-to-first flow rates can be obtained by programming on the syringe pump. All electrolysis mechanisms mentioned in Chapter 3 will be investigated in hydrodynamic modulation system with large amplitude FTACV in this chapter.

4.4 Electrochemical detection of pure electron transfer reaction in hydrodynamic modulation system

4.4.1 Single electron transfer reaction

4.4.1.1 Detection of potassium ferrocyanide

Firstly, the pure electrochemical reaction of $Fe(CN)_6^{4-}$/ $Fe(CN)_6^{3-}$ redox was studied with HMV. Fig 4.8 (a) showed the first experiment of hydrodynamic modulation effect with 2 mM potassium ferrocyanide in 0.5 M KCl supporting electrolyte solution.

First, the flow rate in the microchannel was set as 0.01 mL/min, the applied potential was kept as +0.25 V (at this potential the conversion has completed) all the time. After the steady state was achieved, the controlled flow rate increased which was programmed on the syringe pump in advance. Every step of flow rate was kept for 20 s then jumped into next step automatically. It can be seen that the steady states were achieved in a short time for every step. Fig 4.8 (b) showed a good Levich manner of limiting current and cubic root of flow rates.
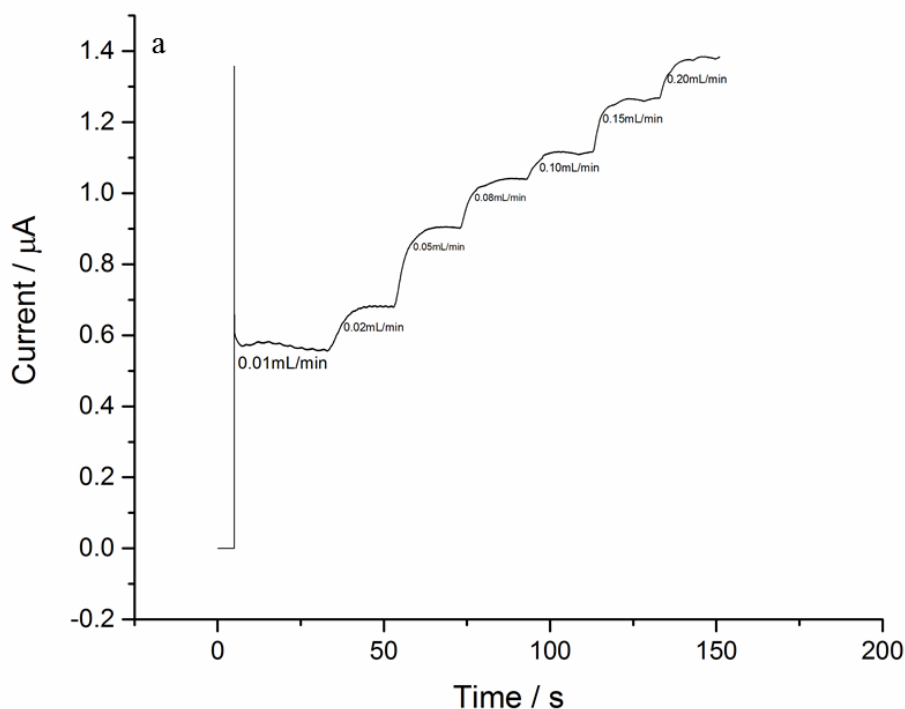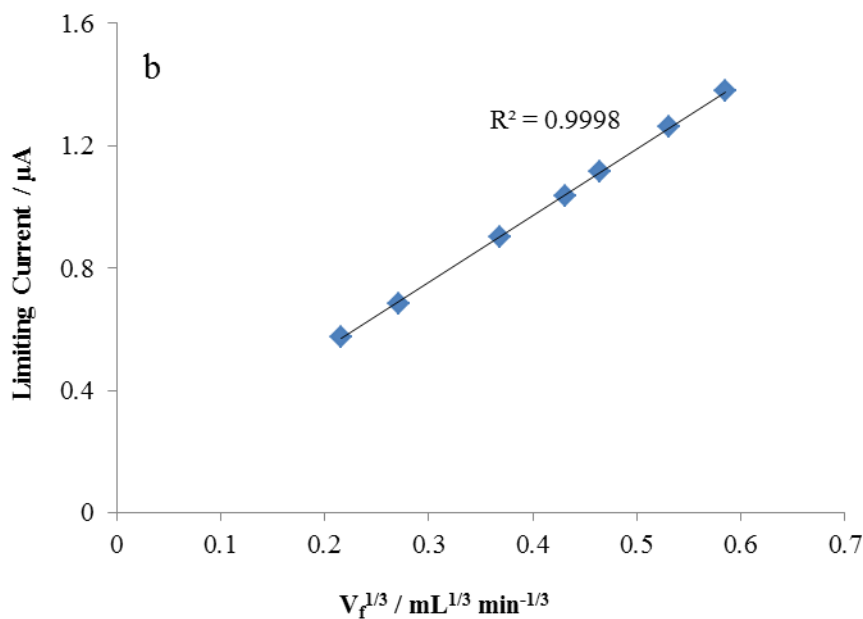
Fig 4.8 (a) Chronoamperometry of potassium ferrocyanide to increasing flow rate steps; (b) limiting current with various cubic root of step flow rates.

After that, the large amplitude FTACV was utilized to study the effect of hydrodynamic modulation. During the experimental process, the flow rate was firstly set as 0.01 mL/min as well, after 50 seconds (t_s=50 s) the flow rate was increased to another value and kept till the measurement ended. Fig 4.9 showed the electrochemical response of the hydrodynamic modulation effect in the microfluidic system. As it can be seen from the figure, the oxidation peaks of all harmonic were all under flow rate as 0.01 mL/min and the output signal overlapped with each other in each harmonic. After 50 seconds, the flow rate was increased to a higher value. The response in the AC components demonstrated that the peak values generated from the backward sweep increased due to the change of the controlled flow rates.

Fig 4.9 (d) showed the relationship between the peak current generated from the backward sweep in each harmonic and cubic flow rates. The good Levich-like manner indicated that under the hydrodynamic modulation control, the system showed great response in electrochemical measurement.

Under hydrodynamic modulation control, the diffusion coefficient can be revised and calculated based on one measurement. The first limiting current in DC signal can be used to revise the efficient electrode area and the calculated diffusion coefficient can be obtained from the second limiting current. With this setup, the calculation and analysis can be achieved in a shorter time compared with normal hydrodynamic system.

122
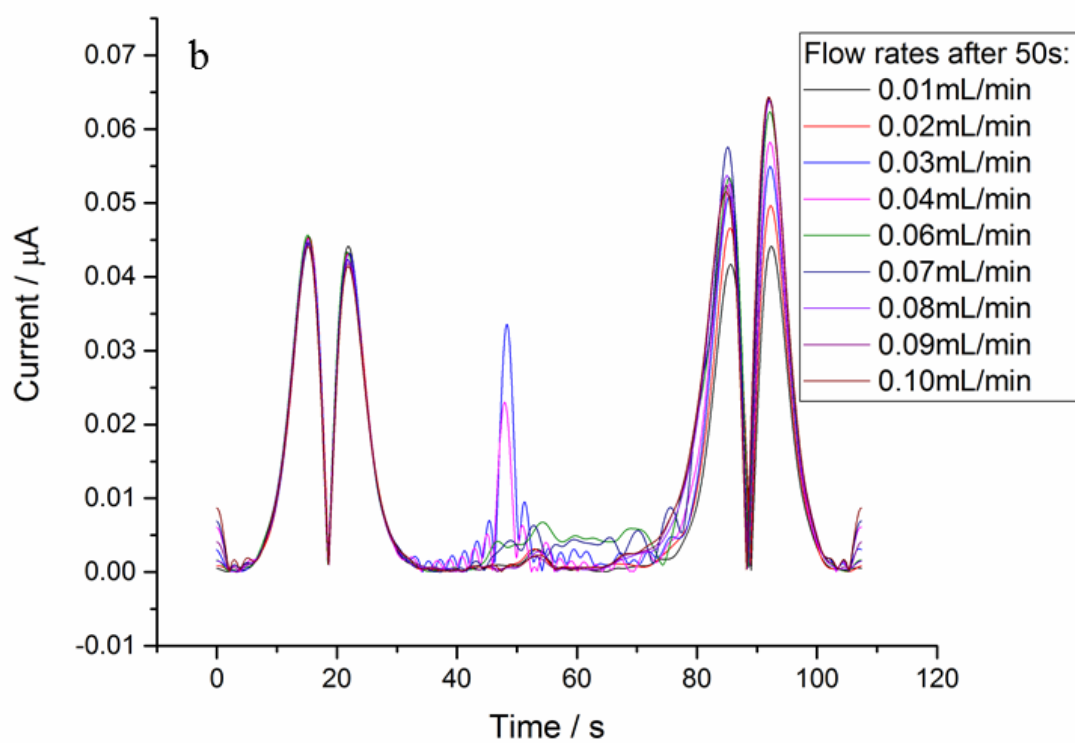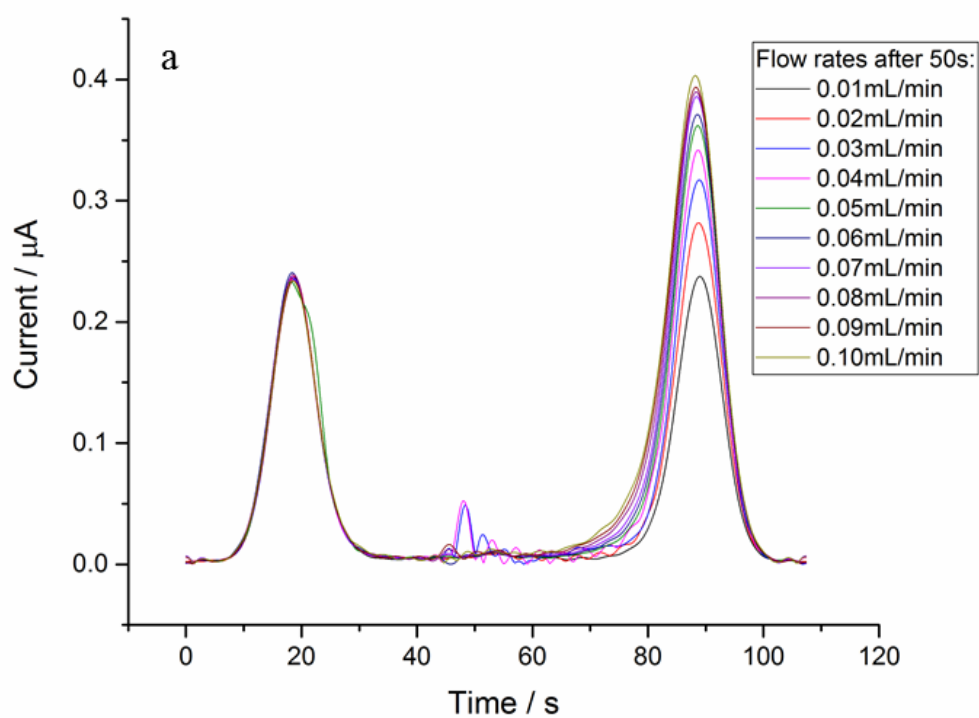
Fig 4.9 The large amplitude FTACV (potential range: -0.1-0.6 V, scan rate: 13.04 mV/s, frequency: 1 Hz, amplitude: 50 mV) detailing with the response of 2 mM potassium ferrocyanide to increasing step flow rates (from 0.01 to 0.10 mL/min) (a) first harmonic; (b) second harmonic; (c) third harmonic; (d) backward peak current with various cubic root of flow rates.

4.4.1.2　　Detection of ferrocenecarboxylic acid

Analogously, the FCA was examined under condition of hydrodynamic modulation. Fig 4.10 showed the electrochemical response of 2 mM FCA in pH 9.2 borate buffer solution in the hydrodynamic modulation system.

Fig 4.10 The large amplitude FTACV (potential range: -0.1-0.6 V, scan rate: 13.04 mV/s, frequency: 1 Hz, amplitude: 50 mV) detailing with the response of 2 mM FCA in pH 9.2 buffer to increasing step flow rates (from 0.01 to 0.10 mL/min) (a) first harmonic; (b) second harmonic; (c) third harmonic; (d) fourth harmonic.

According to the signal response, when the flow rate was firstly set to a fixed value, the forward peak overlapped with each other which indicats a uniform diffusion layer thickness can be obtained. When the flow rates were increased deliberately, the backward peak grew due to the thinner diffusion layer achieved with the faster flow rates.

4.4.2 Dual electron transfer reaction

4.4.2.1   Detection of 2,5-dihydroxybenzoic acid

The two-electron transfer reaction of DHB was examined under hydrodynamic modulation condition with large amplitude FTACV as well. The experimental setting up was as before, the flow rates were fixed at 0.01mL/min for 50 seconds first, then increased to a higher value. Both DC signal and AC components can be obtained simultaneously with large amplitude FTACV.
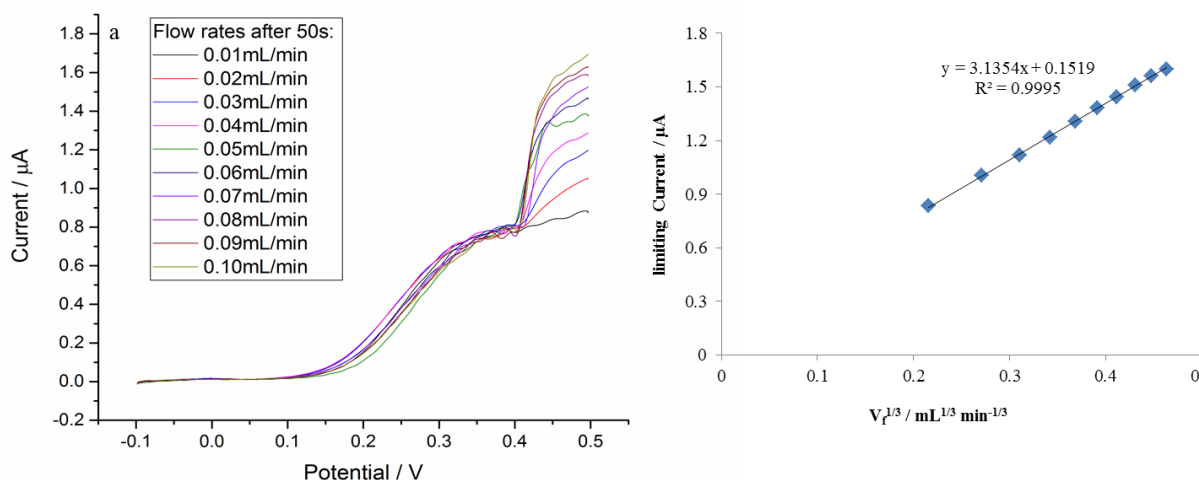
Fig 4.11 (a) cyclic voltammogram of 2 mM DHB in pH 5 acetate buffer (scan rate: 11.18 mV/s) to increasing step flow rates (from 0.01 to 0.10 mL/min) extracted from large amplitude FTACV; (b) limiting current of second steady state with various cubic root of step flow rates.

First, the DC signal was studied. Fig 4.11 (a) showed the DC component extracted from the overall electrochemical signal. The first steady state was achieved with the fixed small flow rate, then with the flow rates increased according to the programme on the syringe pump. With larger flow rates, the thinner diffusion layer can be obtained, where the second steady

127

state can be achieved and the resulting current jumped onto a higher value. Fig 4.11 (b) showed the plot of limiting current of second steady state and cubic root of corresponding flow rates. The good linear relationship indicated a Levich manner was achieved.

Then the AC components were extracted and analysed. Fig 4.12 showed the first two harmonics of electrochemical response of DHB under hydrodynamic modulation. Unsurprisingly, the forward peaks overlapped with each other due to the same flow rate and the backward current increased with the change of the controlled flow rates.

In the second harmonic, the second peak of the forward peaks was slightly smaller than the first one, illustrating the partial reversibility of the two-electron transfer that could be assigned to the 2,5-dihydroxybenzoic acid. Further, the peaks shifted in the second harmonic, which is indicative that with two protons transfer, the system underwent unexpected disturbance.
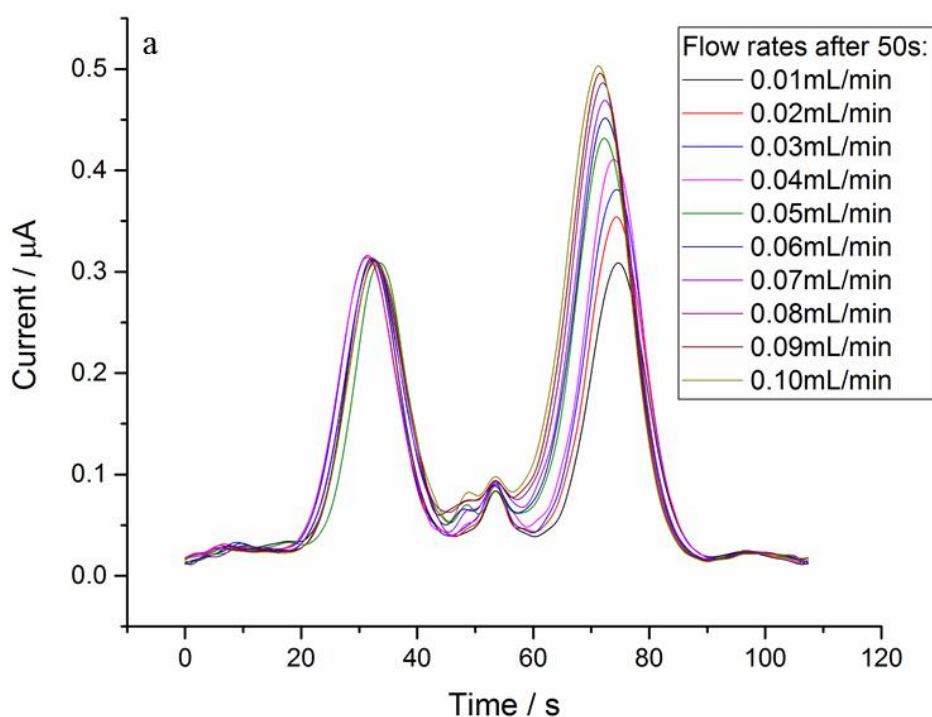
Fig 4.12 The large amplitude FTACV (potential range: -0.1-0.5 V, scan rate: 11.18 mV/s, frequency: 1 Hz, amplitude: 50 mV) detailing with the response of 2 mM DHB in pH 5 acetate buffer to increasing step flow rates (from 0.01 to 0.10 mL/min) (a) first harmonic; (b) second harmonic; (c) backward peak current with various cubic root of flow rates.

4.4.2.2 Detection of N,N,N',N'-tetramethyl-*para*-phenylene-diamine (TMPD)

As noted above, the oxidation of TMPD undergoes two consecutive one-electron steps. With hydrodynamic modulation control, the electrochemical investigation of TMPD involves two parts: the first one is the first electron transfer from TMPD to TMPD^{*+} and the second part is two-electron transfer from TMPD to TMPD^{2+}.

Fig 4.13 The large amplitude FTACV (potential range: -0.2-0.25 V, scan rate: 8.38 mV/s, frequency: 1 Hz, amplitude: 50 mV) detailing with the response of 2 mM TMPD in pH 7 phosphate buffer to increasing step flow rates (from 0.01 to 0.10 mL/min) (a) first harmonic; (b) second harmonic; (c) third harmonic.

Fig 4.13 showed the electrochemical response of TMPD under conditions of hydrodynamic modulation. The resulting current of first electron transfer showed good response with the modulation control. The noise in the figures indicated that before the second steady state formed, there was a time for the solution stream in the channel to be stabilized. The stabilization time typically occurred over 9 s, and the similar phenomenon can be found in the DC signal as well.
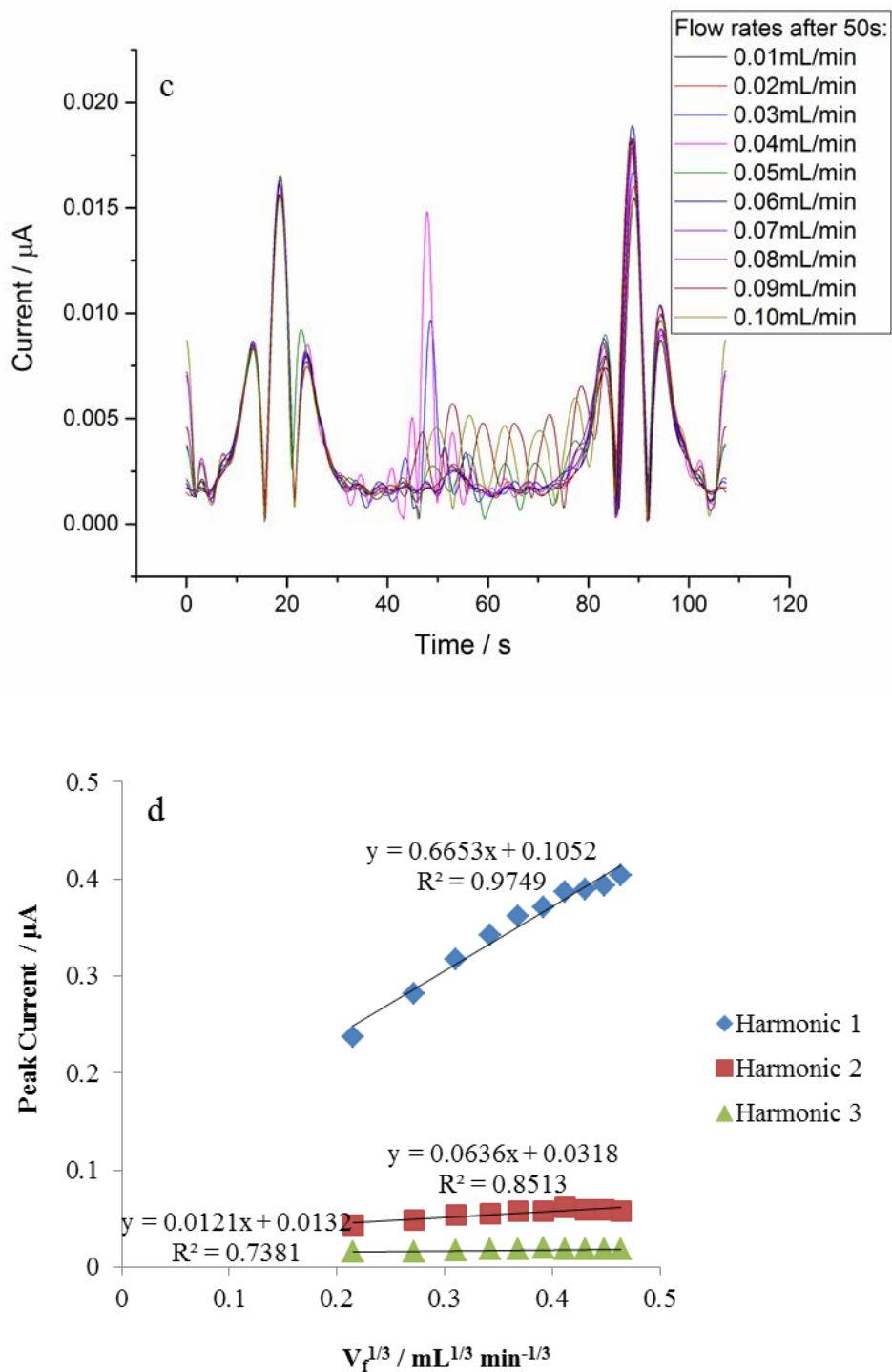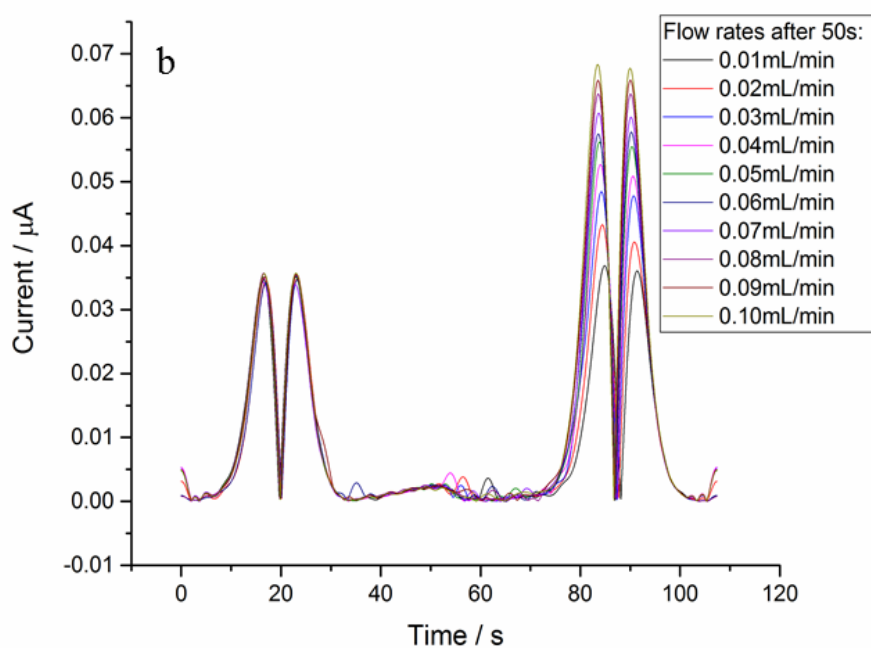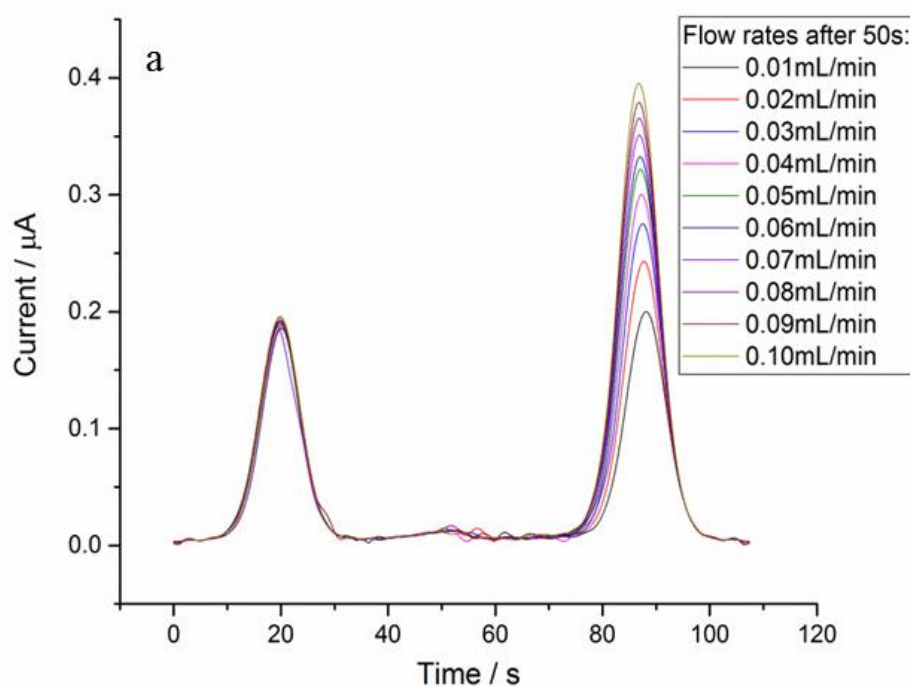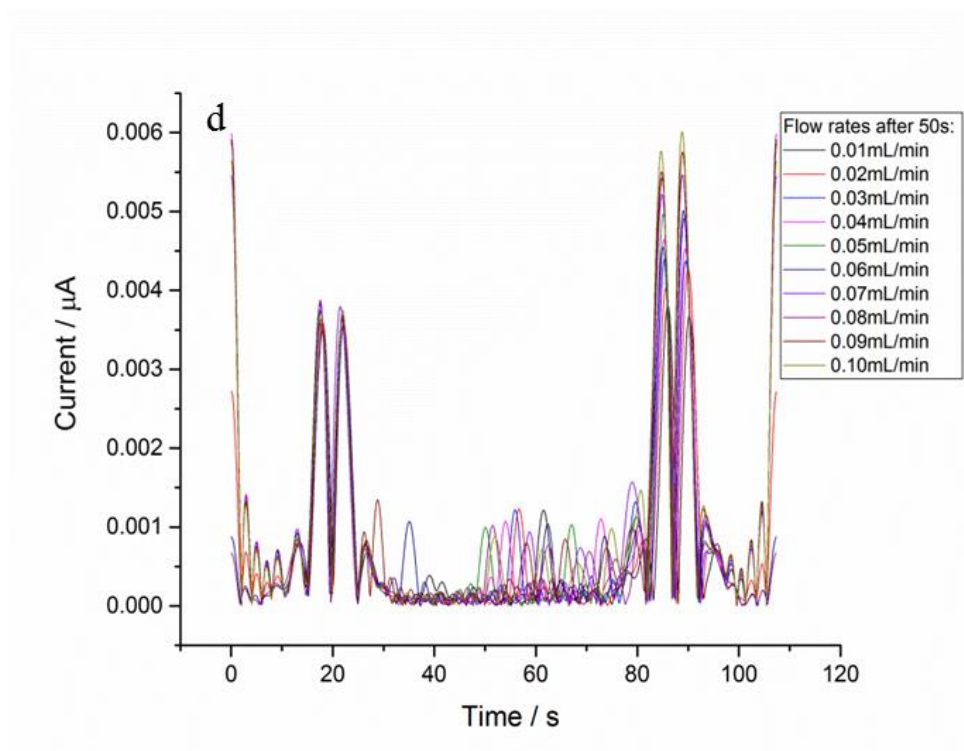
Fig 4.14 The large amplitude FTACV (potential range: -0.2-0.6 V, scan rate: 14.90 mV/s, frequency: 1 Hz, amplitude: 50 mV) detailing with the response of 2 mM TMPD in pH 7 phosphate buffer to increasing step flow rates (from 0.01 to 0.10 mL/min) (a) first harmonic; (b) second harmonic; (c) backward peak current with various cubic root of flow rates.

Fig 4.14 showed the two-electron transfer of TMPD to TMPD^{2+}. The AC components showed a complete two consecutive electron transfer step of TMPD. The turbulence after the first electron transfer indicated that TMPD*$^{+}$ is thermodynamically unstable. Also, the backward peaks were slightly smaller than the forward ones explicated both of these two steps were quasi-reversible reaction.

Also, it can be seen from Fig 4.14 (c), the peak current of reverse peaks, which were generated in the modulation step, and the cubic root of flow rates showed a Levich-like manner for both electron transfer step.

4.4.3 Irreversible reaction

The irreversible electrochemical reaction was examined in hydrodynamic modulation system with large amplitude FTACV lastly. The pH of the analyte solution was controlled beyond 12 to ensure the borohydride would not react with water.

Fig 4.15 showed the AC components extracted from the overall signal from large amplitude FTACV. In first harmonic, the typical response under hydrodynamic modulation was shown. The peaks generated from the forward sweep overlapped with each other due to the same

controlled flow rate. The backward peak current increased with the change of the flow rates of the analyte stream in the microchannel.

In the second harmonic, the same phenomena as in the first harmonic can be found. Meanwhile, the second peak from the forward scan was much smaller than the first one, which indicated the overall thermodynamically irreversibility of sodium borohydride.

The signal-to-noise ratio is relatively poor in this measurement. The one possibility is that the noise is caused from the very unstable intermediate products, which can only be detected under sufficiently fast scan rate [227].
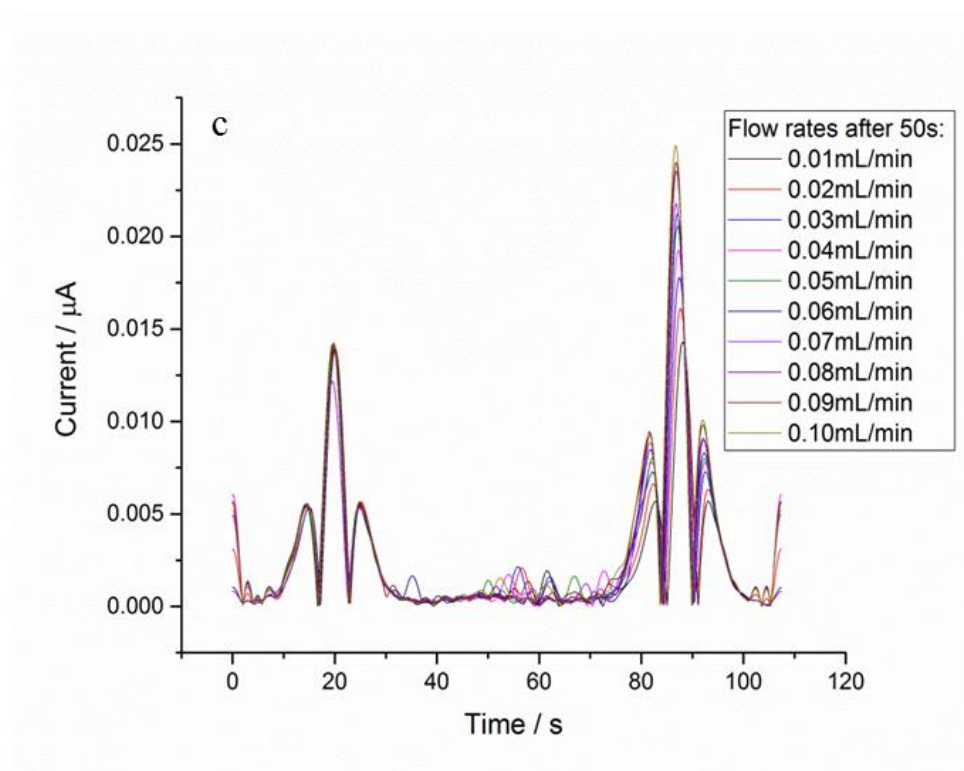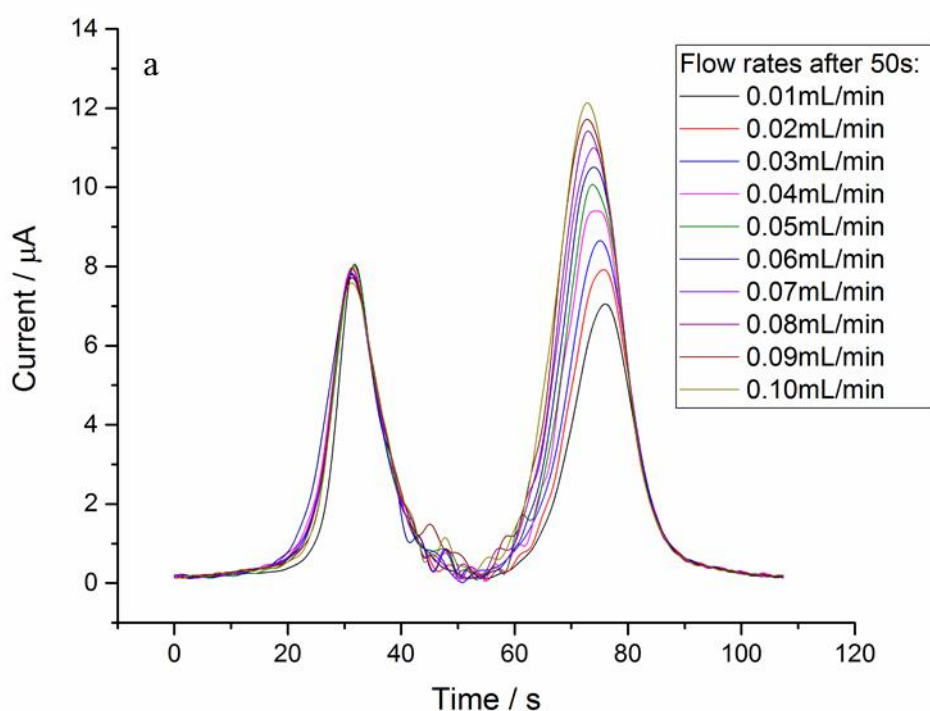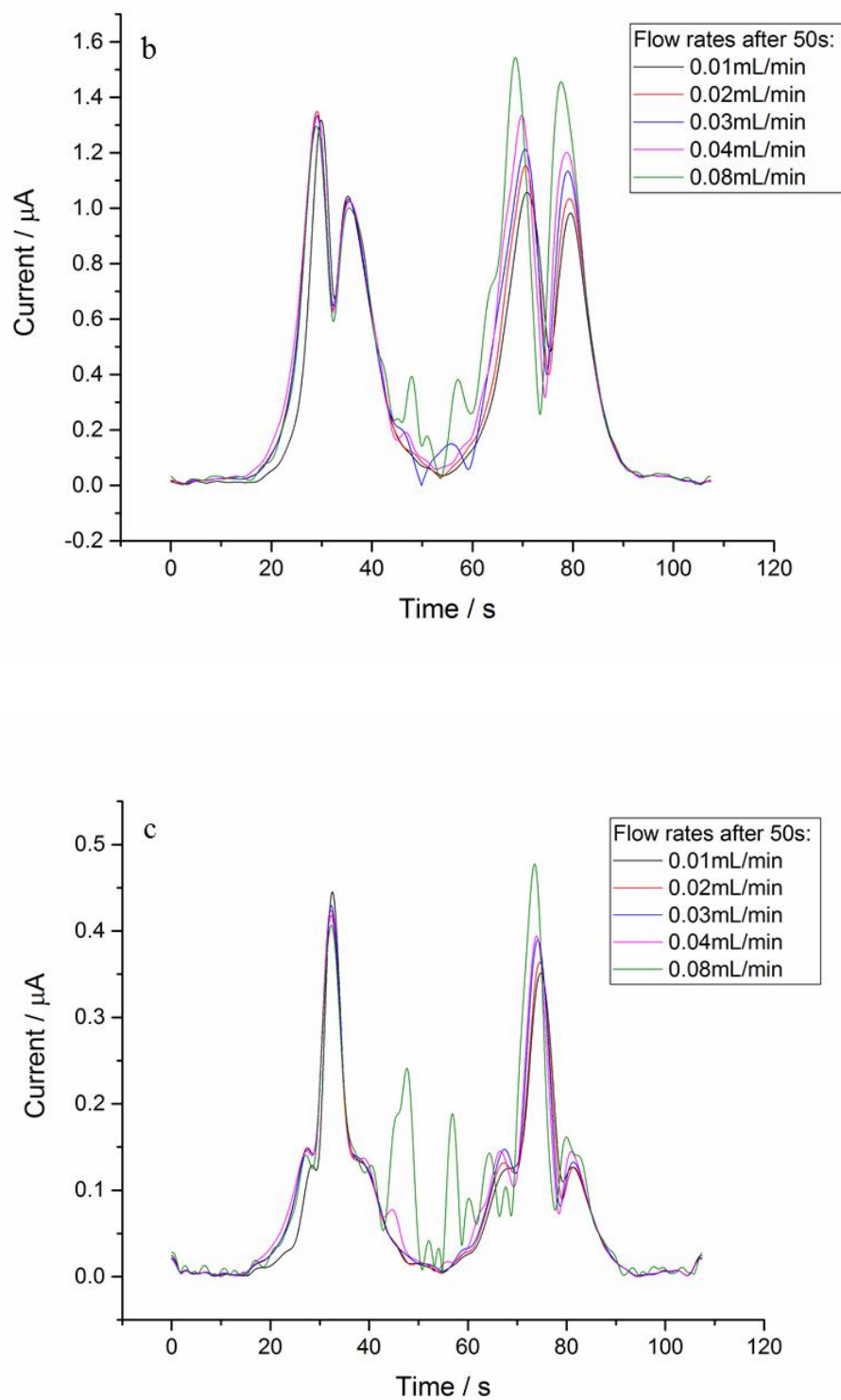
Fig 4.15 The large amplitude FTACV (potential range: -0.3-0.35 V, scan rate: 12.11 mV/s, frequency: 1 Hz, amplitude: 50 mV) detailing with the response of 10 mM sodium borohydride in 3 M NaOH to increasing step flow rates (from 0.01 to 0.10 mL/min) (a) first harmonic; (b) second harmonic; (c) third harmonic.

4.5 Electrochemical detection of coupled homogeneous reaction in hydrodynamic modulation system

Coupled homogeneous reactions have been studied in microfluidic with large amplitude FTACV in the previous chapter. To study the coupled homogeneous reactions with hydrodynamic modulation control, the EC' mechanism was chosen to be examined in the system with large amplitude FTACV. Both potassium ferrocyanide and ferrocenecarboxylic acid were electrochemically oxidized and utilized as mediator to react with L-cysteine.

4.5.1 Detection of L-cysteine by using $Fe(CN)_6^{4-}$ mediated oxidation

Fig 4.16 showed the first AC components of potassium ferrocyanide with different concentrations of L-cysteine in hydrodynamic modulation system. Similar with the previous reactions, the peaks generated from forward sweep showed good coordination with each other and the resulting current rose up due to increasing the second step flow rates. The backward peaks shifted a little bit due to the substrate added into the system, which resulted in the unstable signal of the gold reference electrode. Also, the signal-to-noise ratio seemed to be poorer when more L-cysteine was added to the system.
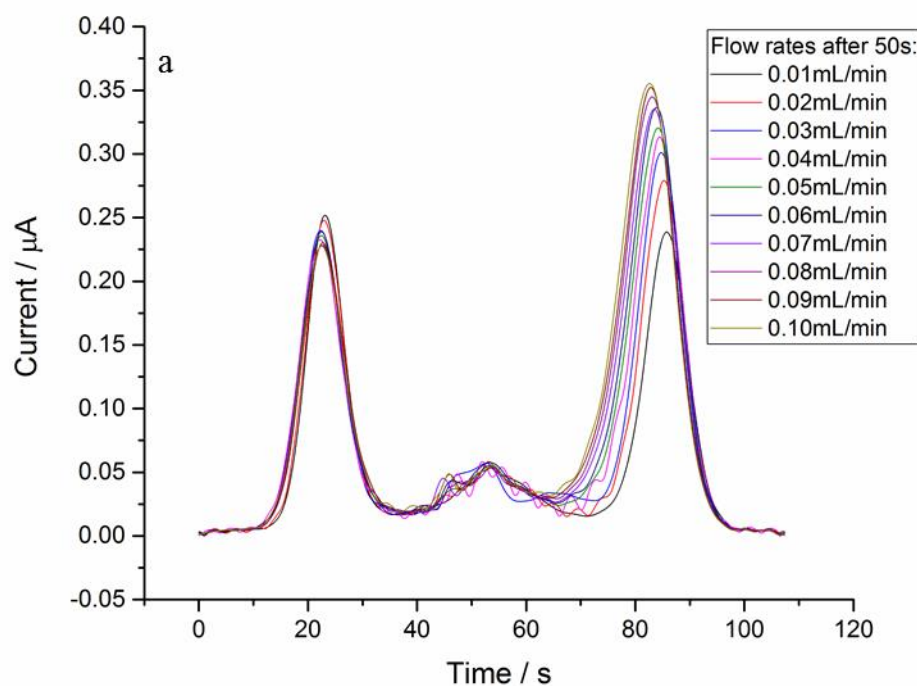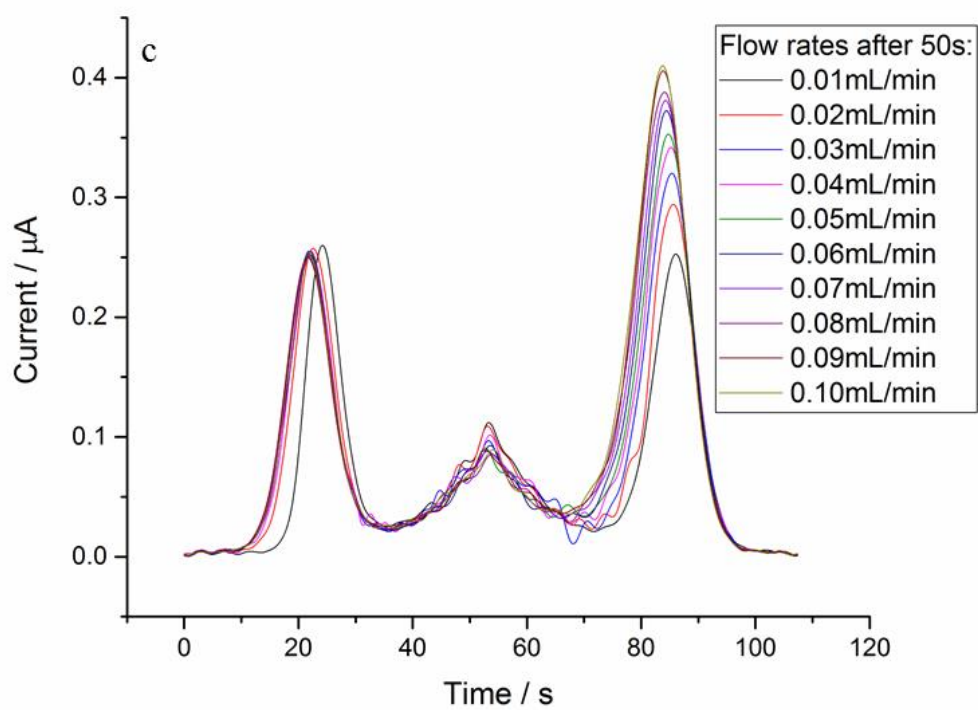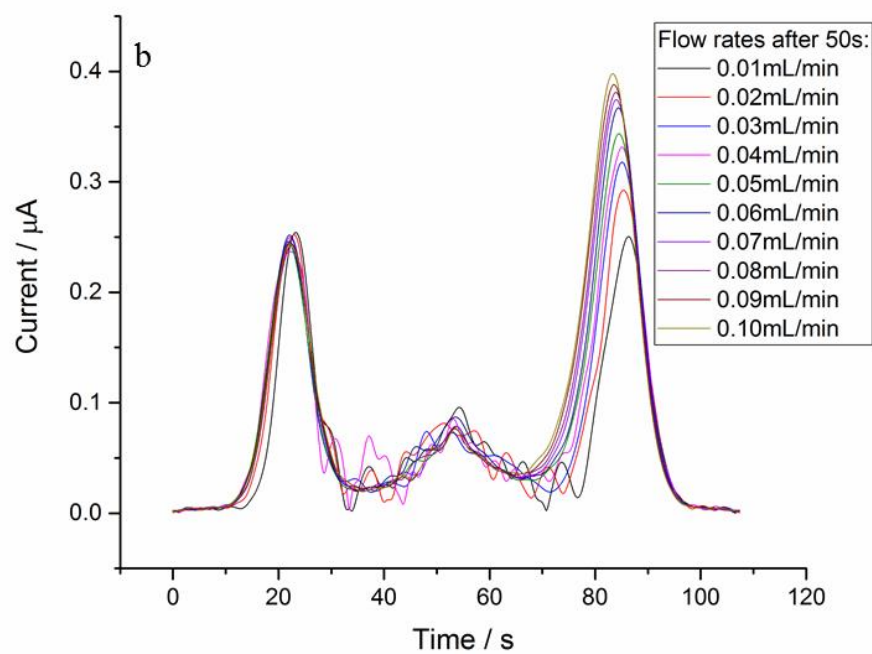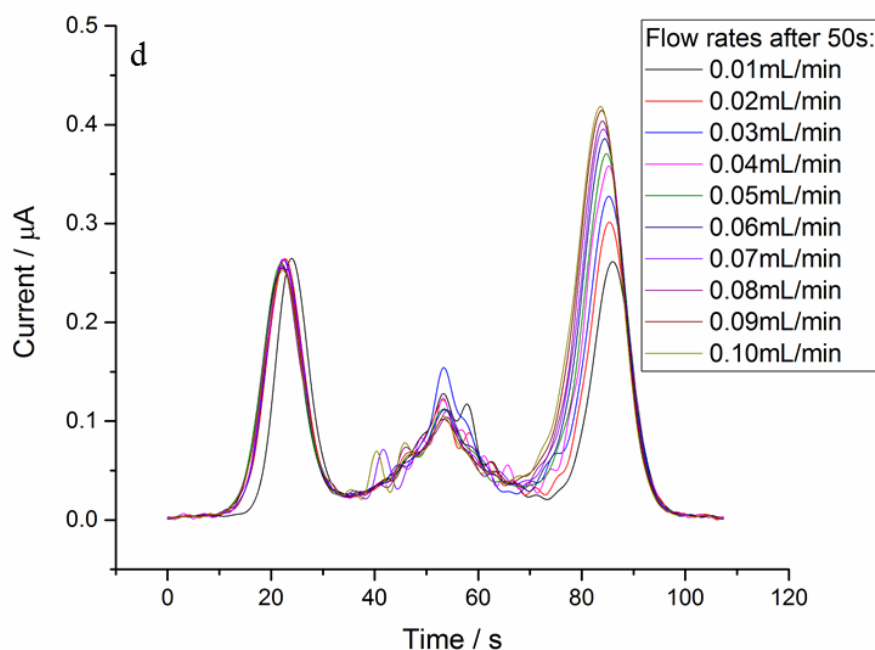
Fig 4.16 The large amplitude FTACV (potential range: -0.1-0.6 V, scan rate: 13.04 mV/s, frequency: 1 Hz, amplitude: 50 mV) detailing with the response of 2 mM potassium ferrocyanide with different concentrations of L-cysteine to increasing step flow rates (from 0.01 to 0.10 mL/min) in first harmonic (a) with 1 mM L-cysteine; (b) with 2 mM L-cysteine; (c) with 3 mM L-cysteine (d) with 4 mM L-cysteine.

Under hydrodynamic modulation conditions, the influence of different concentrations of substrate was investigated. As it can be seen from Fig 4.17 (a) and (b), with the increase of L-cysteine concentration, the signal of peak current enhanced as well. Differentially from the normal hydrodynamic system, in hydrodynamic modulation voltammetry, the relationship of peak current and the substrate concentrations can be obtained from two different flow rates at the same time in one measurement. Both of the forward and backward peaks generated can be evaluated as function of substrate concentrations. In Fig 4.17 (c) and (d), the linear relationship of peak current and L-cysteine concentrations in both forward and backward sweep were displayed. It revealed the advantage to utilize hydrodynamic modulation voltammetry is that more information can be obtained in a short time measurement.
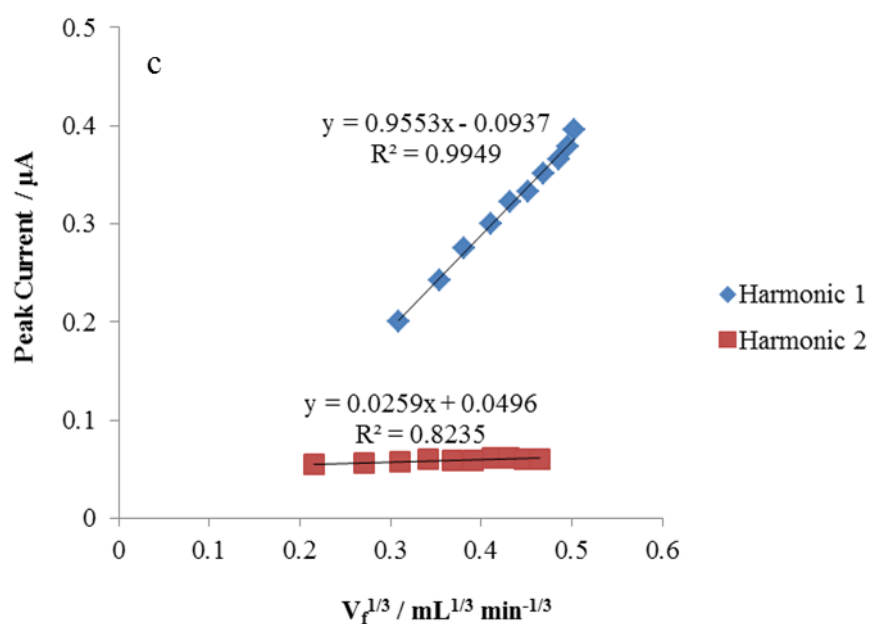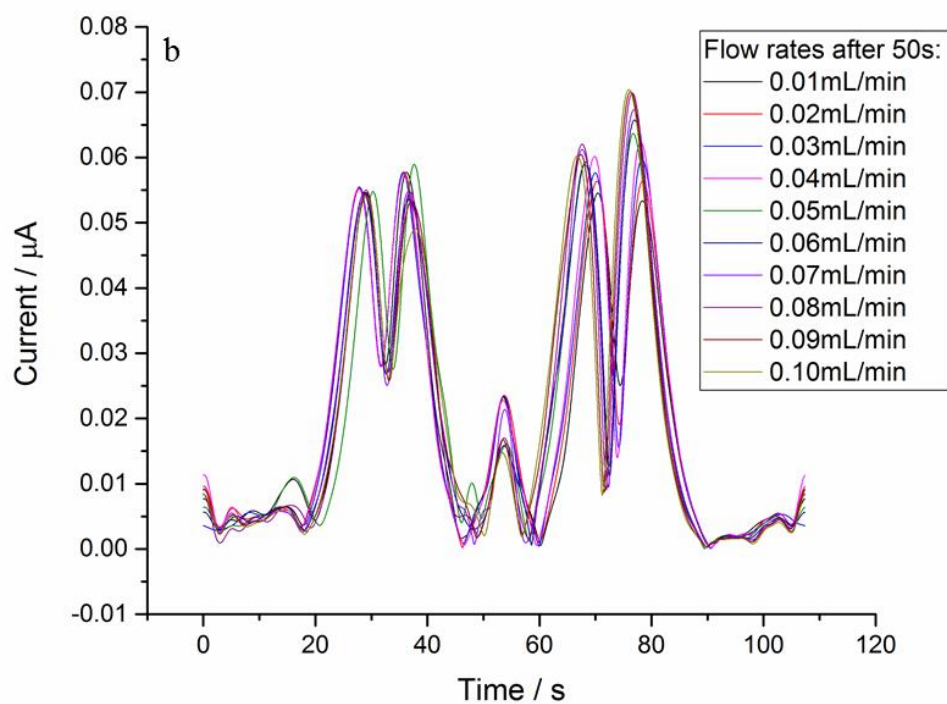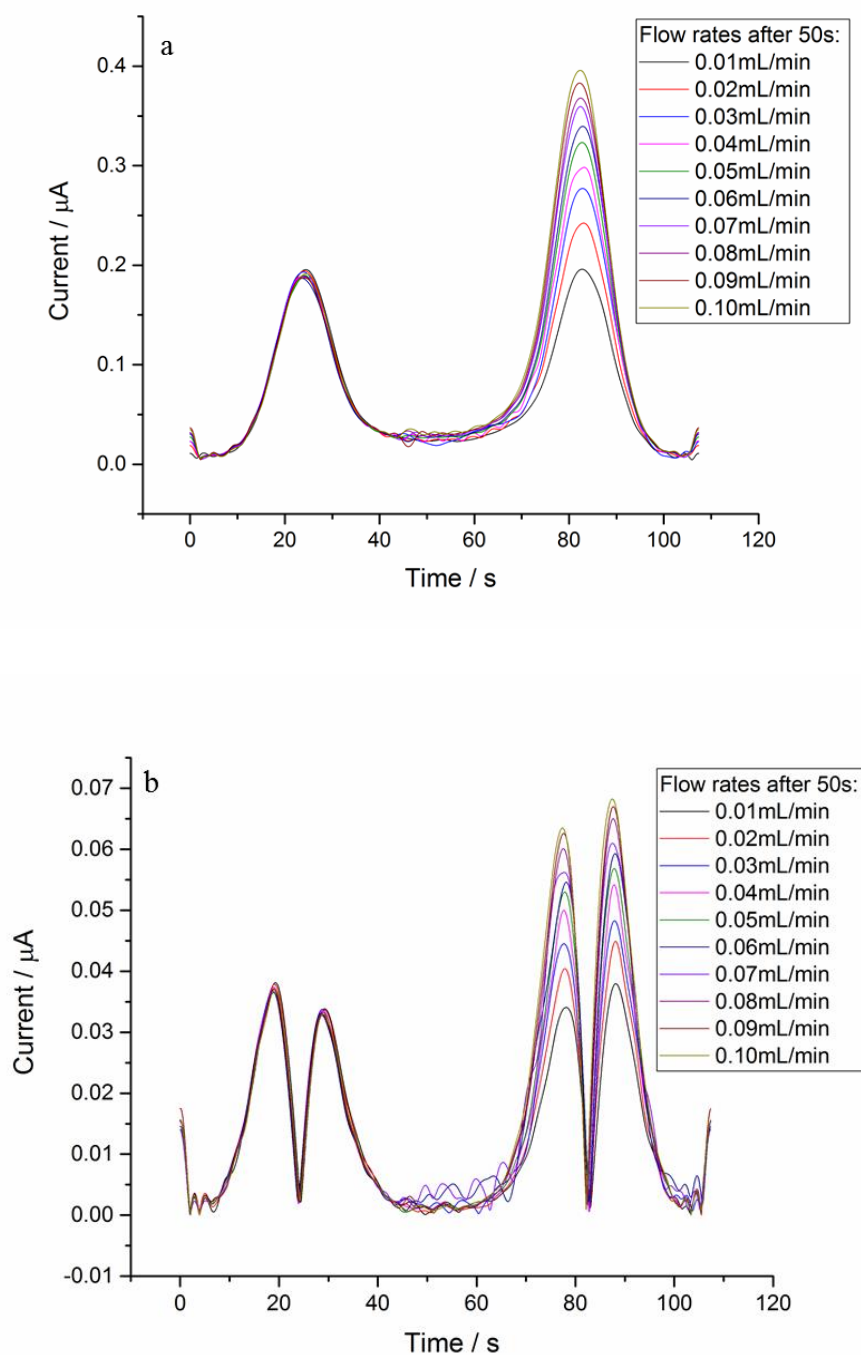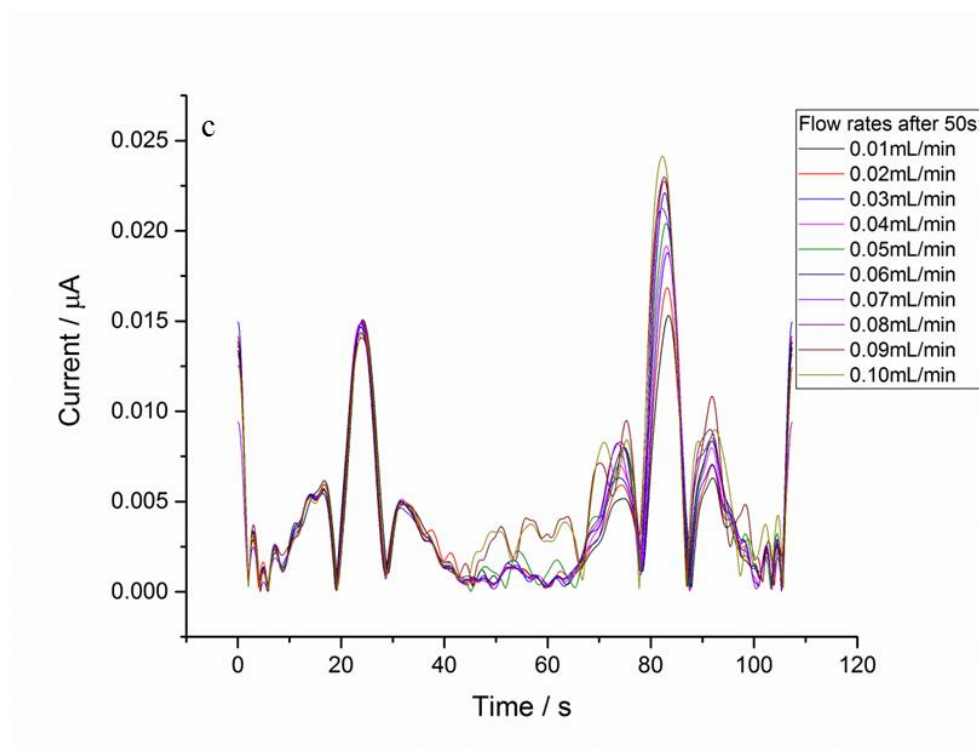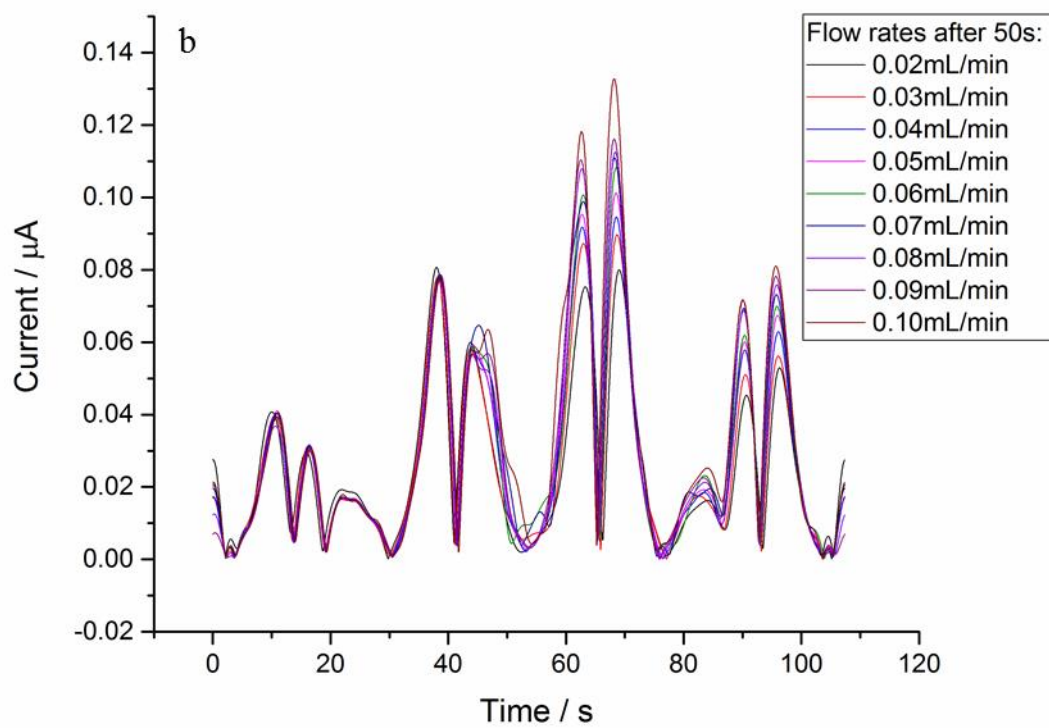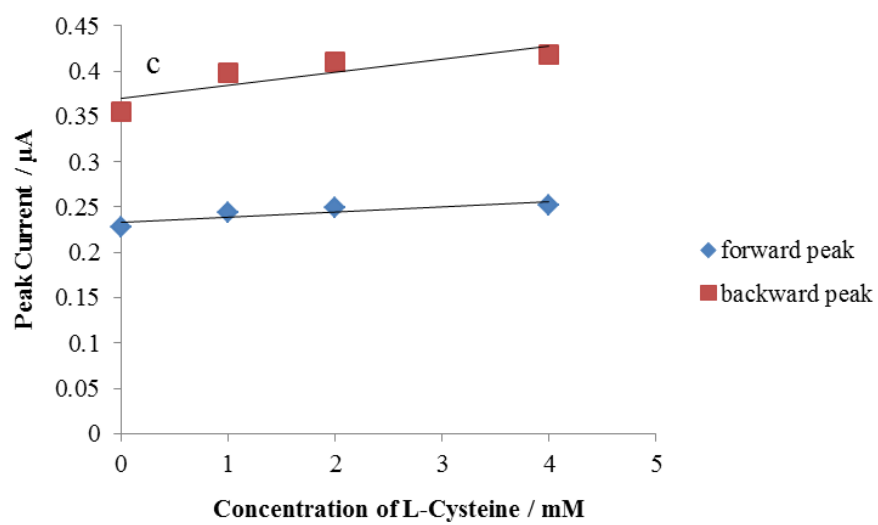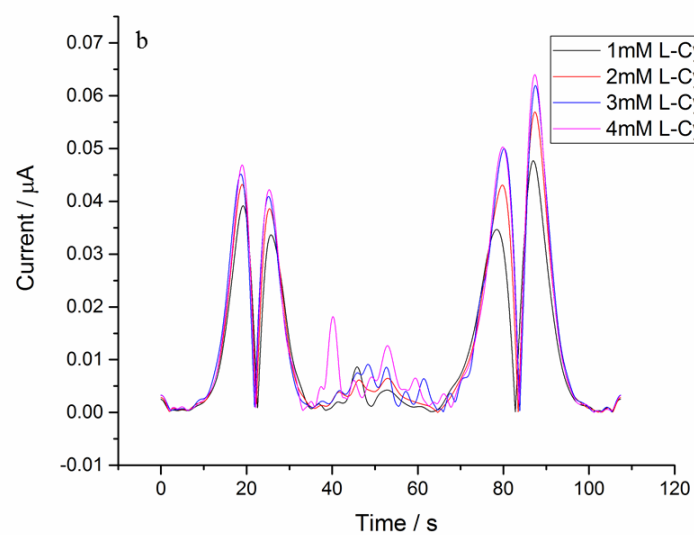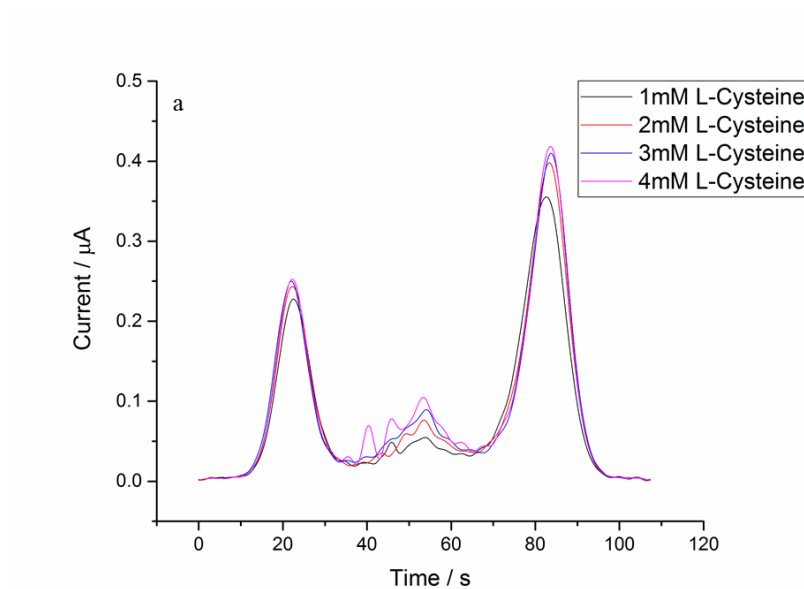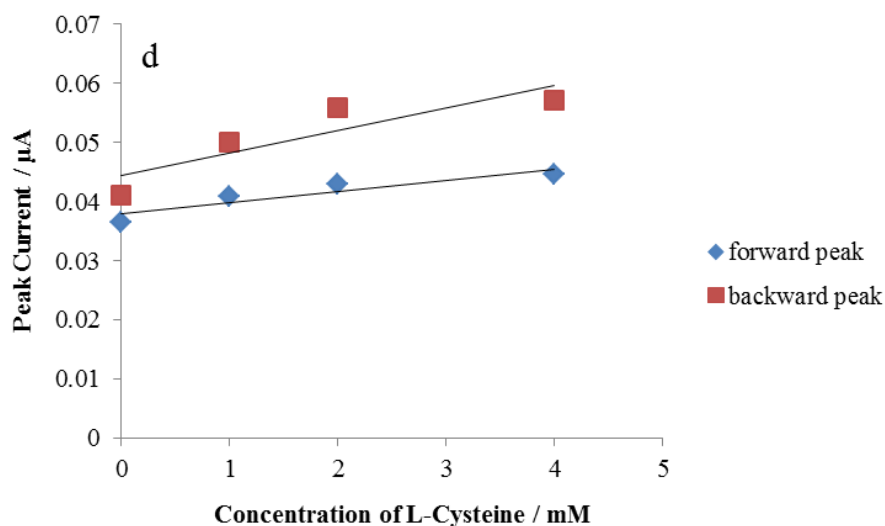
Fig 4.17 The large amplitude FTACV (potential range: -0.1-0.6 V, scan rate: 13.04 mV/s, frequency: 1 Hz, amplitude: 50 mV) detailing with the response of 2 mM potassium ferrocyanide to various concentrations of L-cysteine under hydrodynamic modulation step (flow rate change from 0.01mL/min to 0.10 mL/min after 50 s) (a) first harmonic; (b) second harmonic; peak current with various concentrations in (c) first harmonic and (d) second harmonic.

4.5.2 Detection of L-cysteine by using ferrocenecarboxylic acid mediated oxidation

Similarly, L-cysteine was introduced into the FCA/FCA$^+$ system to study the EC' mechanism under the condition of hydrodynamic modulation. Fig 4.18 to Fig 4.20 showed that in the presence of L-cysteine, the AC components extracted from the overall current signal. As it can be seen from the figures, FTACV is sensitive for both the changes of flow rates or concentrations of substrate. The substrate induced the peaks shift. During the experiment, the electrode fouling could take place due to excess amount of L-cysteine, which might cause errors to analysis. There was some noise can be observed where the modulation step was initiated.

The second harmonic component was more sensitive to the Faradaic signal and the effect of catalytic reaction was mainly on the first peak, it can be seen from the figures that, with the concentrations of L-cysteine increased, the second peak of forward sweep in second harmonic

was significantly smaller than the first one (especially in Fig 4.20 (b)), which demonstrates an irreversible reaction resulting from the C' step.
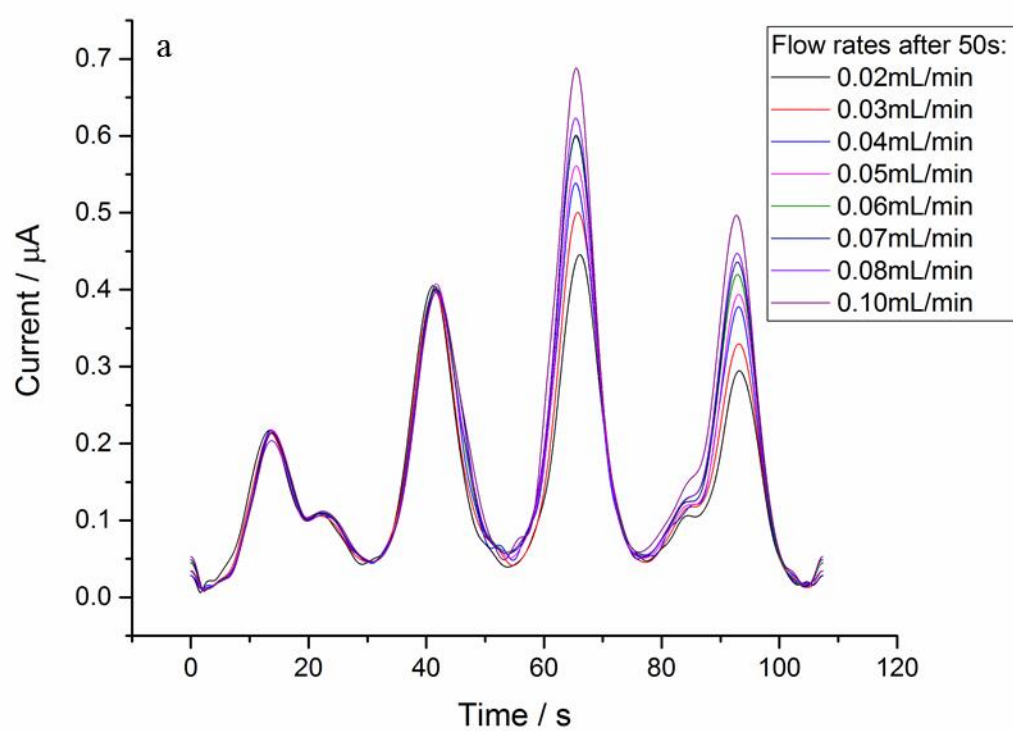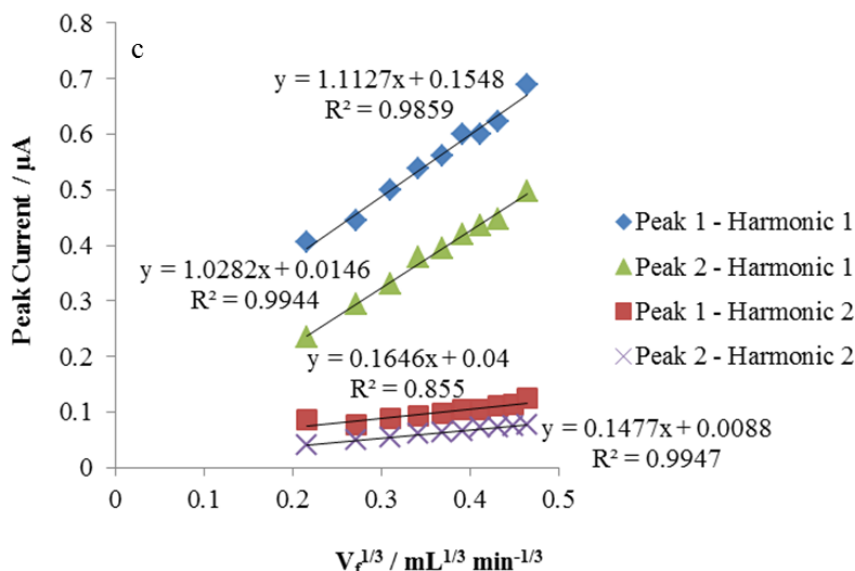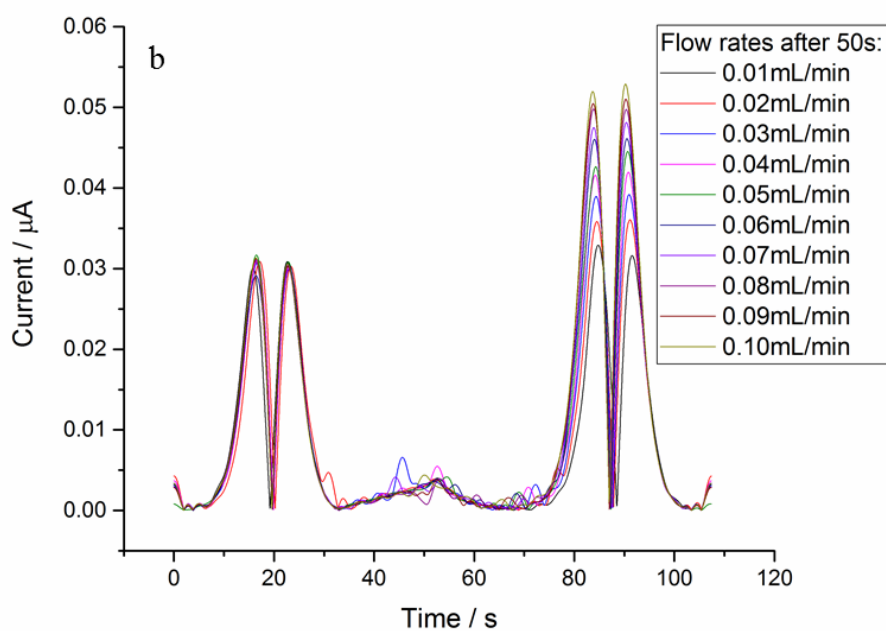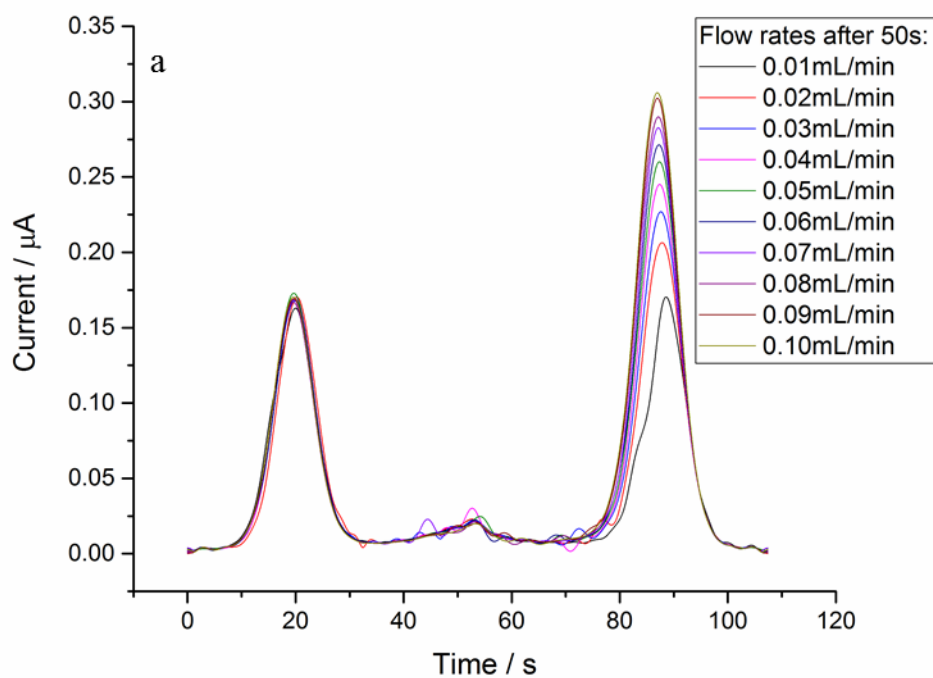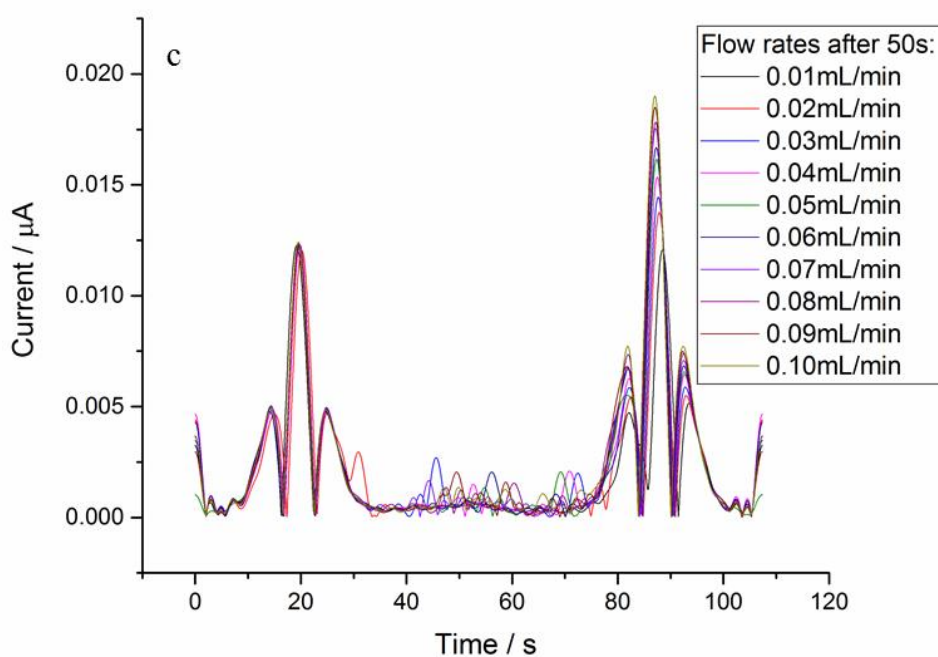
Fig 4.18 The large amplitude FTACV (potential range: -0.1-0.6 V, scan rate: 13.04 mV/s, frequency: 1 Hz, amplitude: 50 mV) detailing with the response of 2 mM FCA and 0.2 mM L-cysteine to increasing step flow rates (from 0.01 to 0.10 mL/min) in first harmonic (a) first harmonic; (b) second harmonic; (c) third harmonic.
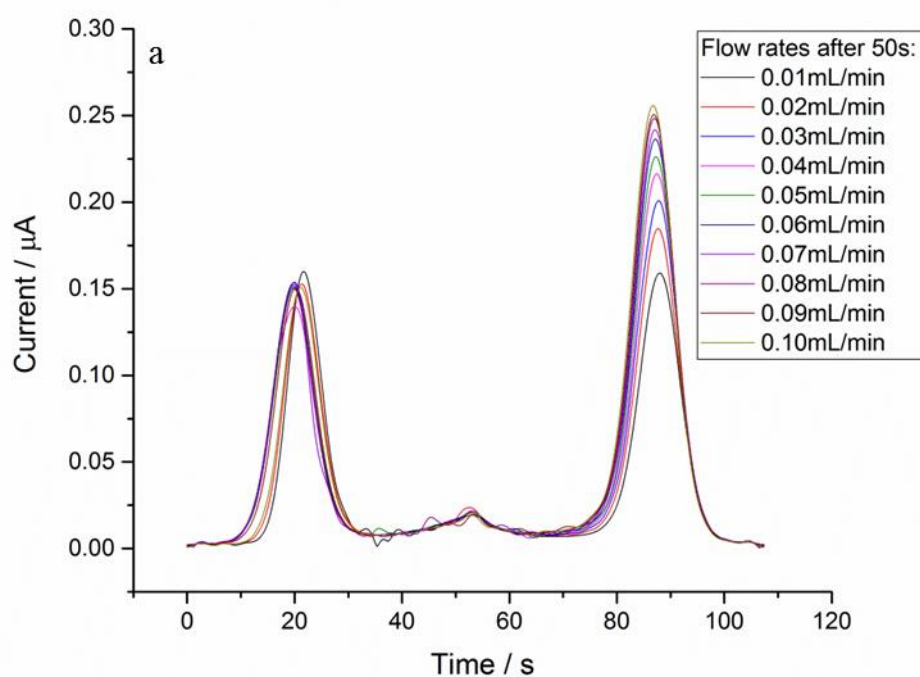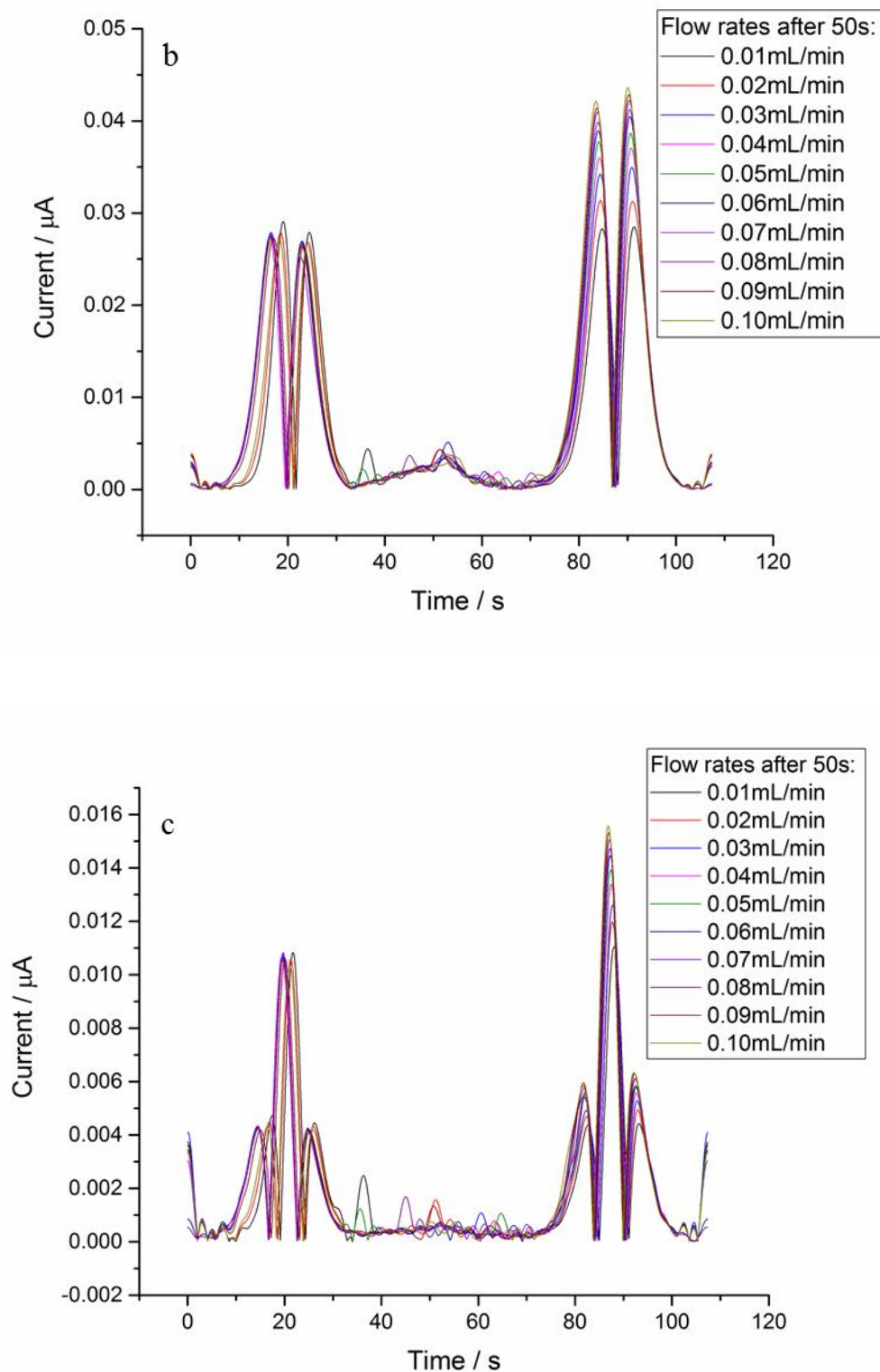
Fig 4.19 The large amplitude FTACV (potential range: -0.1-0.6 V, scan rate: 13.04 mV/s, frequency: 1 Hz, amplitude: 50 mV) detailing with the response of 2 mM FCA and 0.5mM L-cysteine to increasing step flow rates (from 0.01 to 0.10 mL/min) in first harmonic (a) first harmonic; (b) second harmonic; (c) third harmonic.
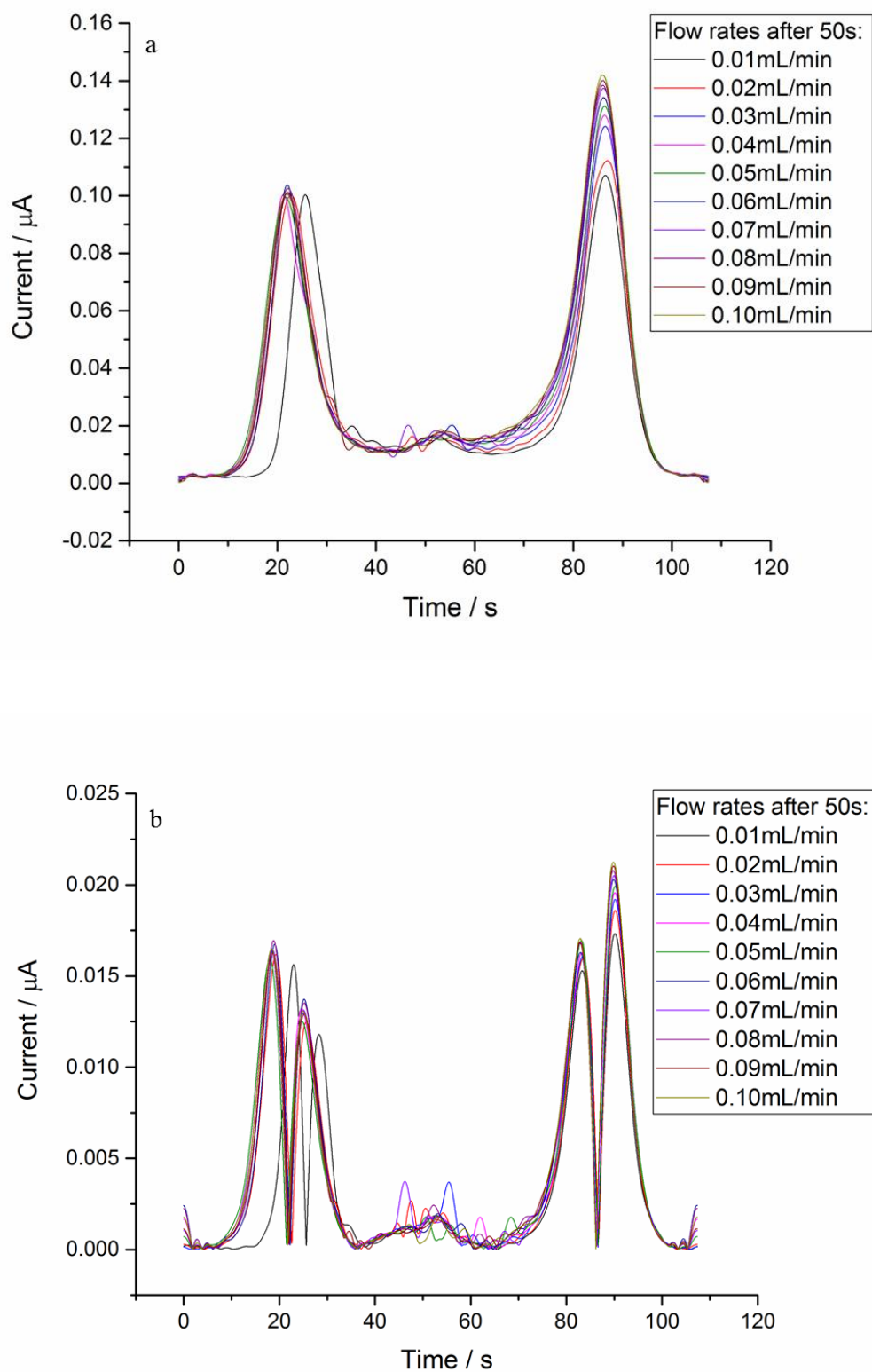
Fig 4.20 The large amplitude FTACV (potential range: -0.1-0.6 V, scan rate: 13.04 mV/s, frequency: 1 Hz, amplitude: 50 mV) detailing with the response of 2 mM FCA and 1mM L-cysteine to increasing step flow rates (from 0.01 to 0.10 mL/min) in first harmonic (a) first harmonic; (b) second harmonic.

4.6 Conclusions

The aim of this chapter was to investigate the electrochemical response of various electrolysis mechanisms in a hydrodynamic modulation system, using FTACV to monitor the reactions.

In this chapter, all the flow rates in the measurements were controlled by the programmable syringe pump. In each measure measurement, first a steady state was achieved due to the initial flow rate then the second steady state was achieved after a defined period when the controlled flow rates increased according to a program controlled by the pump. The linear relationship of peak current and corresponding flow rates can be obtained in each harmonic.

Based on the results, it can be deduced that the signal of hydrodynamic keep consistently when the analyte stream was under fixed flow rate and the system response fast with the change of controlled flow rates. Also, with the hydrodynamic modulation, both the relationships between peak current and flow rates or substrate concentrations can be obtained simultaneously, which reveals a promising approach to get more information in a short time measurement.

Chapter 5   Advanced   Hydrodynamic   Modulation Voltammetry

5.1   Introduction

In chapter 4 a hydrodynamic modulation step was introduced to the microfluidic system, two steady states can be achieved by altering the flow rate during the measurements. In this chapter, a new approach was introduced by not only increasing the stream flow rates, but also forcing the stream to flow in a reverse direction. Both DC technique and large amplitude FTACV were applied to detect the electrochemical signal in the advanced hydrodynamic modulation system.   The simulation work has been established by Dr Ashoke Raman for understanding the influence of transition time and depletion layer to the current response by using the commercial finite element solver Comsol Multiphysics 5.3.

5.2   Oscillatory flow

In chemical and biochemical engineering operations, the good fluid mixing and efficient mass and energy transport are key factors. The oscillatory flow reactors were designed for providing a mechanism for mixing, enhanced radial transport, improved surface purging properties and also providing a route towards obtaining a near plug flow residence time distribution within a baffled tube [286].

The idea of oscillatory flow reactors is to superimpose oscillatory flow onto a steady state flow in a tube with periodic, sharp-edged baffles. The series of experimental observations including flow patterns, mixing, energy loss and heat transfer were reported by Mackley and co-workers [287–289]. Fig 5.1 shows a typical oscillatory flow reactor prototype with baffles evenly implemented alongside the tube wall.

Fig 5.1 Schematic diagram of oscillatory flow reactor [288]

The outstanding features to apply oscillatory flow reactor for chemical engineering industry are firstly they are able to significantly enhance heat and mass transfer rates. The implementation of baffles in the tube increases the surface area which effectively enhances the heat and mass transfer. According to Hewgill's research [290], the column operated more efficiently by using oscillatory flow in a baffled tube which represented that this type of device has excellent potential for application in industry, for example fermentation technology, and it is useful in gas-liquid reactions.

With the development of microfabrication technology, the oscillatory flow can be achieved in the microchannel. Kabaschi and the co-workers [291] reported their work of oscillatory flow in the microchannel with oscillating drop and bubble setup based on the capillary pressure technique. The particular flow field causes a higher pressure loss as compared to the expected maximum pressure due to the maximum instant flow rate obtained from the conventional fluid mechanics formulations.

Oscillatory flow reactors have been used as electrochemical reactors to investigate mass transfer and resident time distribution characteristics [292]. It is reported by Cognet [293] that the mass transfer under pulsed flow conditions showed that pulsation increased mass transfer coefficient especially in the case of the low flow rates often required to achieve reasonable residence times.

Carpenter and Roberts [292] used a parallel-plate oscillatory flow electrochemical reactor (as Fig 5.2 shows) and redox couple $Fe(CN)_6^{4-}$/ $Fe(CN)_6^{3-}$ to investigate the influence of various experimental factors towards mass transfer and residence time distributions.

This Figure is not shown due to copyright issues

Fig 5.2 Cross-sectional schematic view of the oscillatory flow electrochemical reactor used for (a) mass transfer measurements; (b) resident time distribution studies. [292]

The results showed that the superimposed of an oscillatory flow onto a net flow with appropriate turbulence promoter can efficiently enhance the surface mass transport and under such conditions, the mass transport was dominated by the oscillatory flow. The net flow showed little effect even with increasing flow rates. The study of residence time distribution showed that the mean residence times were controlled mainly by the net flow where the oscillatory flow had little effect on these times.

The investigation based on oscillatory flow electrochemical reactors implied that with the hydrodynamic modulation, different flowing factors can be considered in one set of experiments. By appropriately designing the oscillatory flow reactor and setting up parameters, different intensification goals can be achieved.

Although the baffles in oscillatory flow reactors cannot be implemented in the microchannel due to the difficulties of fabrication, the concept of oscillatory flow provides a new approach to conduct electrochemical experiment with microfluidics to take mechanism study.

5.3   Flow-controlled methods in HMV

The concept of hydrodynamic modulation voltammetry has been introduced in section 1.4.5.7. In recent years, researchers have made efforts to introduce more advanced modulation methods of controlling electrolyte flow to enhance the mass transport in electrochemical detection.

Barker and the co-workers [294] developed a device with a cross-channel design to have different surface charges. This design allowed different assignment of positive and negative arms. Furthermore, by utilizing fluorescently labelled beads, the bi-directional flow in single microchannel has been achieved by this group as well and they indicated that this technique could serve for various applications include transport of analytes to separate detection systems, such as electrochemical and optical sensors positioned at opposite ends of microchannel.

This Figure is not shown due to copyright issues

Fig 5.3 Four flow patterns achieved in cross-devices derivatized to have differing surfaces charges on various arms [294].

Similar with this, a novel flow-focusing microfluidic device was employed to study behaviour of an immiscible liquid/liquid droplet [295]. Different electro-active species can be employed in this method provided that they are soluble in the organic phase and have a strong electrochemical response at the working electrode potential window. This development

allowed the study of droplet formation in opaque devices which traditionally presented a problem for optical measurements.

This Figure is not shown due to copyright issues

Fig 5.4 Images illustrating the effect of total volume flow rate on the shape of the droplets formed in flow-focusing microfluidic device [295]

In the electrochemical machining field, researchers have managed to simulate the circumstance with pulsating electrolyte flow in the electrolytic supply pipe by controlling the input pressure as a sinusoidal function of time [296].

Based on the physical models, the pulsation of electrolyte pressure led to an obvious jump of temperature gradient. When a pulsating electrolyte was applied, flow separation occurred and created regions of reverse flow, which resulted in high mixing and turbulence. Based on the physical models, it indicated that proper pulsating parameters would enhance the heat and mass transfer.

This Figure is not shown due to copyright issues

Fig 5.5 Schematic diagram of electrochemical machining with pulsating electrolyte flow [296]

The research about flow-controlled methods has been carried out by many researchers. Most of the methods mentioned above needs at least two flow streams to be applied to change the flow direction during the measurement, which require more complicated design of the devices and more substance would be wasted during the measurement since normally there are more than one inlets of the reacting chamber. Also, the multiple inlets or channels will result in error in theoretical calculation due to the multiple phase in the detection was involved.

In this chapter, an advanced hydrodynamic modulation is introduced to control the flow stream direction in a single microchannel.

5.4 Results and discussion

5.4.1 Flow strategy and detection method

Different from the previous hydrodynamic strategy, the direction of the flowing stream was changed during one measurement in this section. The flow rate of the analyte was firstly set as a fixed value, after a period of time the flow stream was forced to a reverse direction. Chronoamperometry was mainly used in this chapter to detect the electrochemical signal.
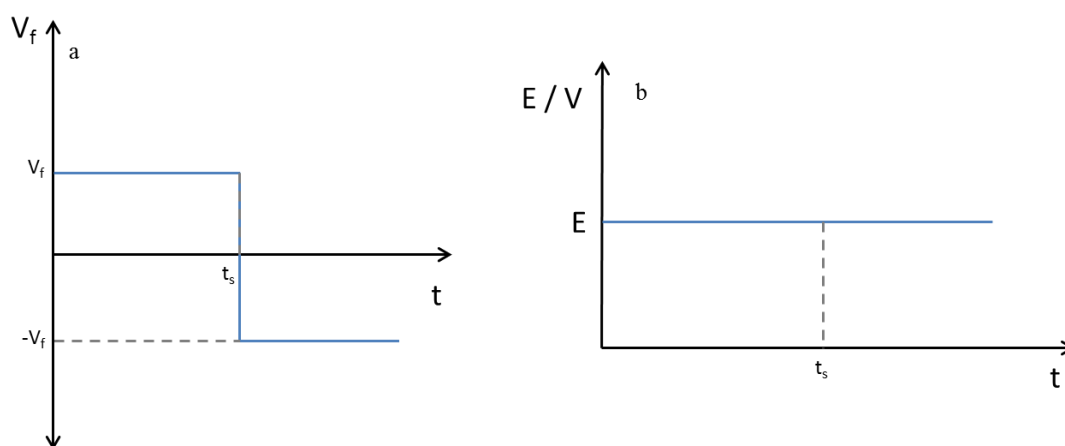
Fig 5.6 (a) Flow rate and (b) applied potential setup in advanced hydrodynamic modulation system (-V indicated the reverse flow direction compared with V)

5.4.2 Simulation

As this is a new flow strategy for hydrodynamic modulation, some prelimary simulations were carried out to explore relevant experimental parameters needed for the data presented in

this thesis. The simulation work has been established by Dr Ashoke Raman to foresee the current response with the advanced hydrodynamic modulation. In this numerical work, the current response of the reverse flow has been demonstrated. The applied potential was set as a fixed value while the analyte stream was controlled to alter the flow direction during the measurement.

5.4.2.1 Problem definition and methodology

The fluid is assumed to be incompressible Newtonian fluid with density ρ and dynamic viscosity v. The geometry of the computational domain is shown in Fig 5.7. The computational domain of $6L_e \times L_c$ was considered, where L_e is the electrode length, L_c is the channel length and 2h is the channel height. The electrode is embedded into the bottom wall of the channel containing an aqueous solution of the electrolyte. The electrolyte is pumped into the channel at a given flow rate (V_f).
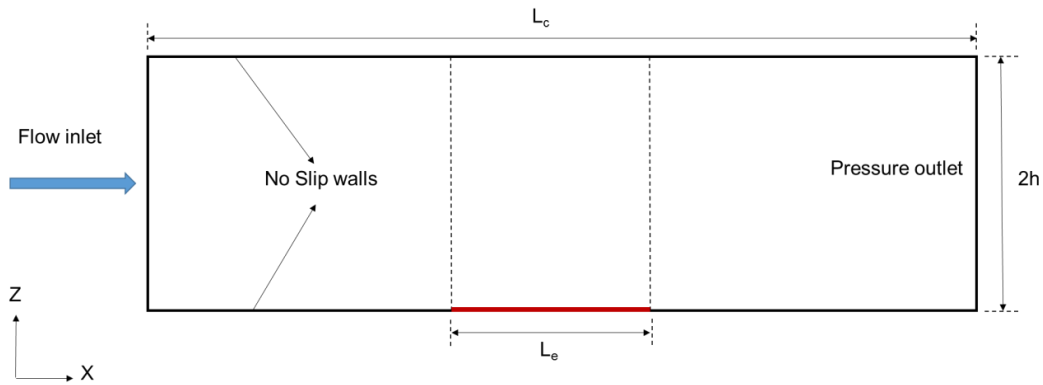
Fig 5.7 A schematic of the two dimensional channel electrode geometry

Excess supporting electrolyte is used and a generalized redox $O + e^- \rightleftharpoons R$ is considered, the continuity equation for incompressible fluids is given by (5.1)

$$\nabla \cdot u_i = 0 \tag{5.1}$$

The momentum conservation for the fluid is given by (5.2)

$$\frac{\partial(u_i)}{\partial t} + u_i \cdot \nabla u_i = -\frac{1}{\rho}\nabla p + v\nabla^2 u_i + f \tag{5.2}$$

The species conversation equation is described as (5.3)

$$\frac{\partial c}{\partial t} = -\nabla \cdot j + r, i = O, R \qquad (5.3)$$

The flux here is defined in (5.4)

$$j = -D\nabla c - z_i uFc\nabla\varphi + u_i c \qquad (5.4)$$

In the above equations, u_i is the velocity vector, p is the pressure, t is the time, ρ is the density of the electrolyte, v is the kinematic viscosity of the electrolyte, c is the concentration of the species, j is the species flux, r is the rate of homogeneous production of species, D is the diffusion coefficient, z_i is the charge number, u is the species mobility F is Faraday constant and φ is the potential in the electrolyte. In equation, (5.4), the first term on the right hand side denotes the diffusive flux. The second term represents the flux due to migration and the third term provides the convective flux. For solutions containing an excess of supporting electrolyte, the ionic migration term can be neglected and hence the second term becomes zero. The liquid phase potential is also set to zero. Without chemical reactions in solution and diffusion coefficients assumed constant, the general convective-diffusion is obtained as

$$\frac{\partial c}{\partial t} = D\nabla^2 c - u_i \cdot \nabla c \qquad (5.5)$$

The boundary and initial conditions can be defined as follow.

At inlet: A laminar inflow boundary condition is used with a time dependent flow rate V_f, $n\cdot j=0$

At the top and bottom channel walls: $u_x=u_y=0$, $n\cdot j=0$

On the electrode surface: $u_x=u_y=0$, $n\cdot j=\frac{s}{F}$

At outlet: Pressure outlet boundary condition is imposed with a gauge pressure $p_0=0$,

$-n\cdot D\nabla c=0$

Constitutive relations: The transfer current density is defined by using Butler-Volmer kinetics

$$i = nF(k_a c_R e^{\frac{(1-\beta)\eta F}{RT}} - k_c c_O e^{\frac{-\beta\eta F}{RT}}) \qquad (5.6)$$

Here the overpotential η is defined as

$$\eta = E_{app} - E^0 \qquad (5.7)$$

where E_{app} and E^0 are the applied and standard electrode potentials, respectively. These two dimensional equations were solved using the commercial finite element solver Comsol Multiphysics 5.3. The parameters used in the simulation work can be found in Table 2.6.

Table 5.1 Parameter used in simulation work

Symbol	Definition	Value
c_0	Bulk concentration	2 mM
c_{R0}	Initial concentration of reductant	2 mM
C_{O0}	Initial concentration of oxidant	0 mM
d	Cell width	1 mm
D_R	Diffusion coefficient for reductant	7.71×10^{-10} m^2/s
D_O	Diffusion coefficient for oxidant	7.71×10^{-10} m^2/s
E^0	Standard electrode potential	0.16 V
E_{app}	Applied potential	0.25 V
F	Faraday constant	96485 C mol^{-1}
h	Half channel height	5×10^{-5} m
k^0	Standard heterogeneous rate constant	0.1 cm/s
L_c	Channel length	6×10^{-4} m
s	Stoichiometric coefficient	1
t	Time	0-35 s
v	Fluid viscosity	8.949×10^{-4} Pa·s
V_f	Input flow rate	0.01 cm^3/min
w	Electrode width	1 mm
x_e	Electrode length	1×10^{-4} m
ρ	Fluid density	1000 kg/m^3

5.4.2.2 Simulation results

As it can be seen from Fig 5.8, the current response experienced a sharp spike when the flow direction of the analyte stream was altered. This is due to the depletion of the electroactive species on the electrode surface. The depleted solution which has been flushed away from the electrode surface was pulled back via the syringe pump during the reverse step. The diffusion layer thickened instantly when the reverse step took place, which was responsible for a sharp spike of the current response. After that a relatively lower liming current was obtained due to the stabilized thicker diffusion layer.

The influence of the transition time was explored in simulation model as well. With longer transition time, the depleted diffusion spread further so the current spike became broader compared to the instant change of the diffusion layer.

The simulation work provides us an insightful analysis of the influence of hydrodynamic modulation to the electrochemical system. By analysing the transition time and depletion layer, more information can be obtained for better understanding the electrolysis mechanisms in the microfluidic system.
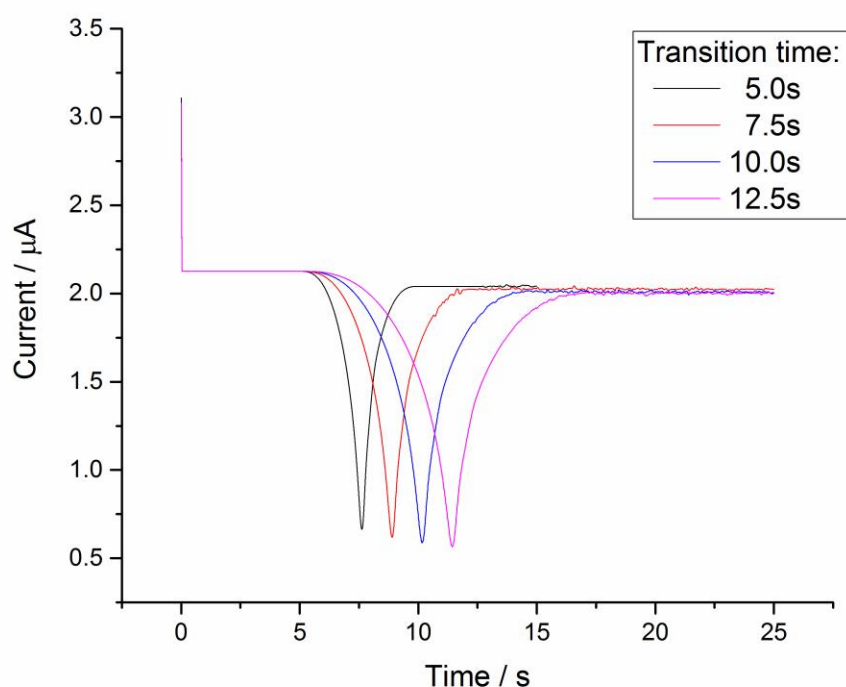
Fig 5.8 Simulated current/time graph of potassium ferrocyanide, showing the effect of a reverse flow step.

5.4.3 Experimental results

The hydrodynamic modulation was introduced into the system during the electrochemical measurement using a function described in section 5.4.2.1. Firstly, the flow stream was pumped into the electrochemical microreactor from a glass syringe and set as a fixed value. After a period of time, the flow stream was forced to a reverse direction (Fig 5.6). The resulting response was recorded to investigate current and flow rate characteristics of the system. The flow direction of the flow stream in the microchannel would be altered for a couple of times and the various flow rates were applied during the measurement. Chronoamperometry was mainly used in this chapter to detect the electrochemical signal.

Firstly, the flowing direction of the stream in the microchannel was altered once to see the response from the system. Fig 5.6 showed the controlled flow rates and applied potential setup for the experiment. The applied potential was kept as +0.5V where there is a complete conversion of $Fe(CN)_6^{4-}$ to $Fe(CN)_6^{3-}$ at the electrode surface.

Fig 5.9 showed the effect of flow direction change on the electrochemical response. The infusing flow rate was firstly set as 0.05mL/min, after 35 second, the pump changed the flow direction from infusing to withdrawing, which resulted in the change of solution flow direction in the microchannel. As it can be seen in Fig 5.9, the first steady stated was achieved due to the fixed flow rate. Then at the point when the flow stream changed the direction, the resulting current dropped immediately and then stabilized at a lower value after several seconds. The reason of that is when the flow stream was first infusing, the steady state achieved with a stable diffusion layer. When the flow stream was withdrawn by the pump, the interface of the stream which just flowed over the electrode surface end was pulled back immediately. The interface of the solution was consisted of $Fe(CN)_6^{4-}$/ $Fe(CN)_6^{3-}$ with the concentration gradient. To form a new diffusion layer, this interface would overlap with the previous diffusion layer, so that the diffusion layer thickness became thicker than the one formed from the infusing step. That is the reason for the current drop. After a period of time, the new diffusion layer has formed and stabilized, so the resulting current reached a stable value again. The shoulder-like behaviour was observed other than the sharp spike obtained from the numerical results, which might be the difference between theoretical setup and internal working system of the syringe pump.

Fig 5.9 Current/time graph of 2 mM potassium ferrocyanide (applied potential: +0.5 V), showing the effect of a reverse flow step, for both directions flow rate at 0.05 mL/min

After that, the direction of flow stream was changed again to investigate the electrochemical response. Fig 5.10 showed the controlled flow rates change with time and the electrochemical response of the flow-controlled steps.

158

Fig 5.10 (a) Flow rate setup; (b) current/time graph of 2 mM potassium ferrocyanide (applied potential: +0.5 V), showing the effect of flow steps, for all directions flow rate at 0.05 mL/min.

After the flow direction was changed after 35 s, the stream was infused again by the pump when the time reached 70 s. As it can be seen from the figure, the resulting current did not increase immediately when the flow stream direction changed to infusing one. The current response fluctuated but stabilized at the value generated from the withdraw direction. Then the current rose up and reached a third steady state which shared the same value as the first infusing step after around 35 seconds when the direction was altered back to infusing. The one possibility of this phenomenon could be that the concentration of electroactive species which flowed over the electrode surface descended due to the same solution fluctuated over the electrode surface which resulted in the stale solution. This is supported by the numerical observations shown in 5.4.2.2. After the stale solution was totally flushed away in the third step, the fresh solution in the syringe was pumped into the microchannel. The new steady state was achieved with the fresh electroactive species flowing over the electrode and the same value of limiting current can be obtained with the first infusing step.

To investigate whether this setup could be replicable, the further detection has been made. Fig 5.11 showed the effect of multiple changes of flow direction of the solution stream inside the microchannel to the electrochemical response. Based on experiment results above, the flow direction was altered again when the second infusing steady state was obtained. The similar

159

phenomenon was achieved that the resulting current dropped dramatically and then stabilized at a value equivalent as the previous withdrawing step.
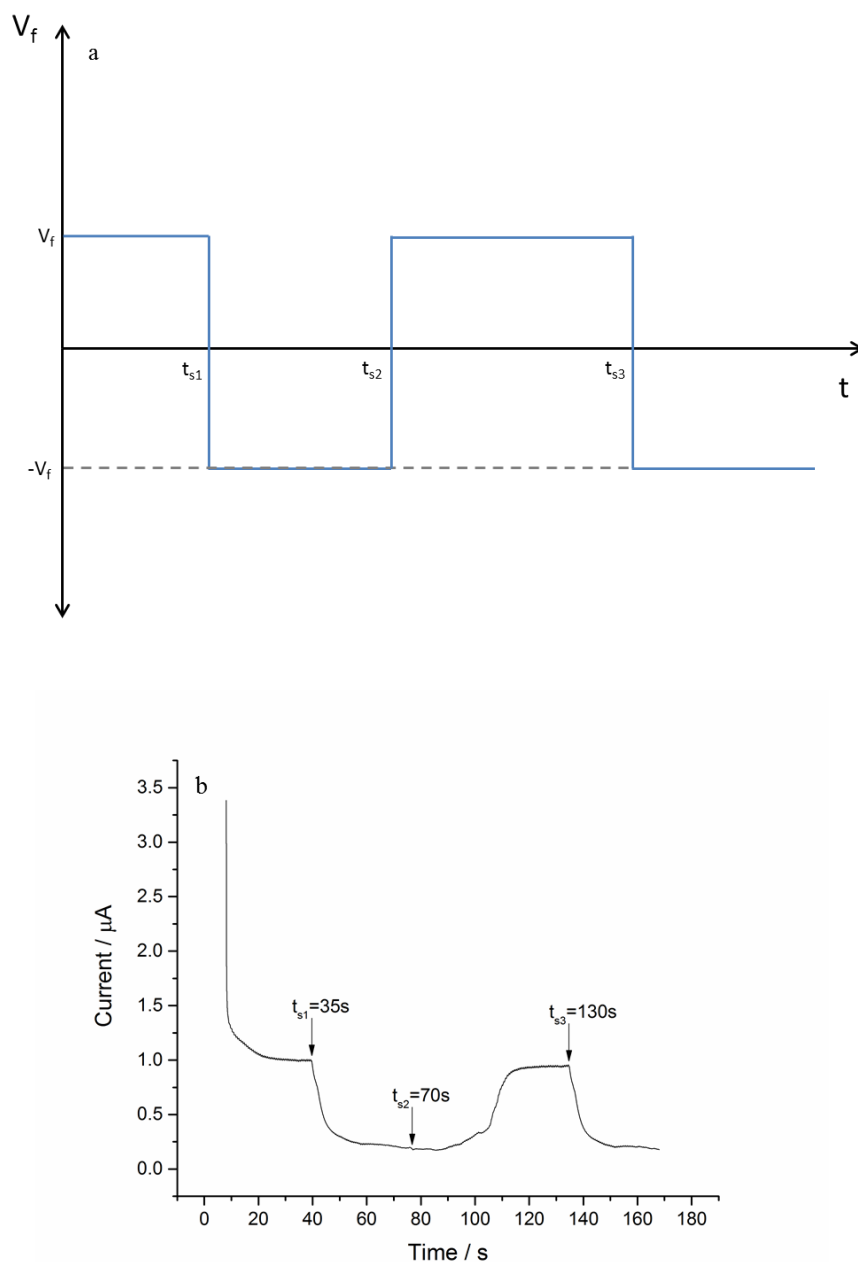
Fig 5.11 (a) Flow rate setup; (b) current/time graph of 2 mM potassium ferrocyanide (applied potential: +0.5 V), showing the effect of different flow direction steps, for all directions flow rate at 0.05 mL/min

The similar phenomena can be found with TMPD as well. Fig 5.12 showed the electrochemical response with the effect of hydrodynamic modulation. The applied potential was kept as +0.3V, at which the TMPD has completely converted to TMPD$*^{+}$ on the

electrode surface. The resulting current showed a good corresponding relationship with the flowing direction of the solution stream inside the microchannel. The limiting current can be measured in each step when the steady state formed.
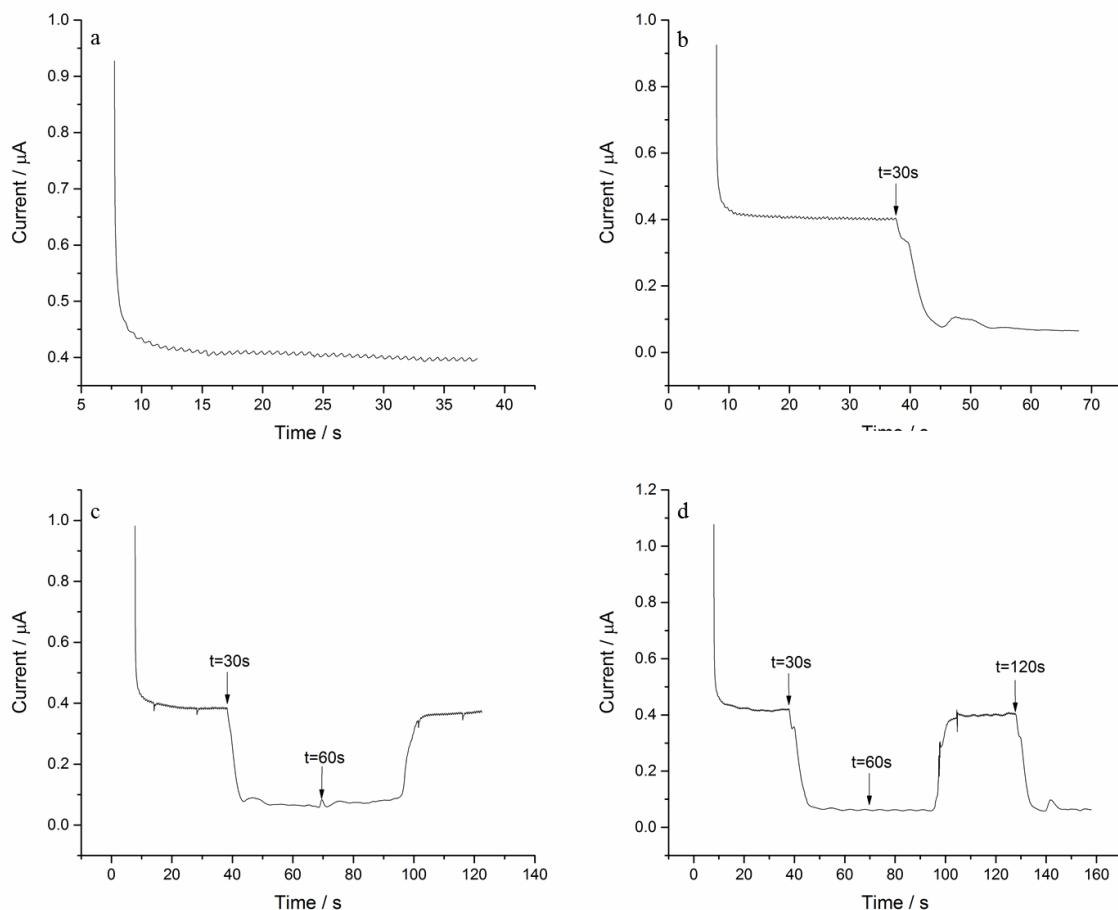
Fig 5.12 Current/time graph of 2 mM TMPD (applied potential: +0.3 V), showing the effect of different flow direction steps, for all directions flow rate at 0.05 mL/min

On the basis of experimental results above, the multiple changes have been made to test the system. As Fig 5.13 showed, the multiple similar shape of the resulting current indicated that the experimental results can be replicated with the setup. The spike behaviour was obtained here, which can be corresponded to the simulation observations.
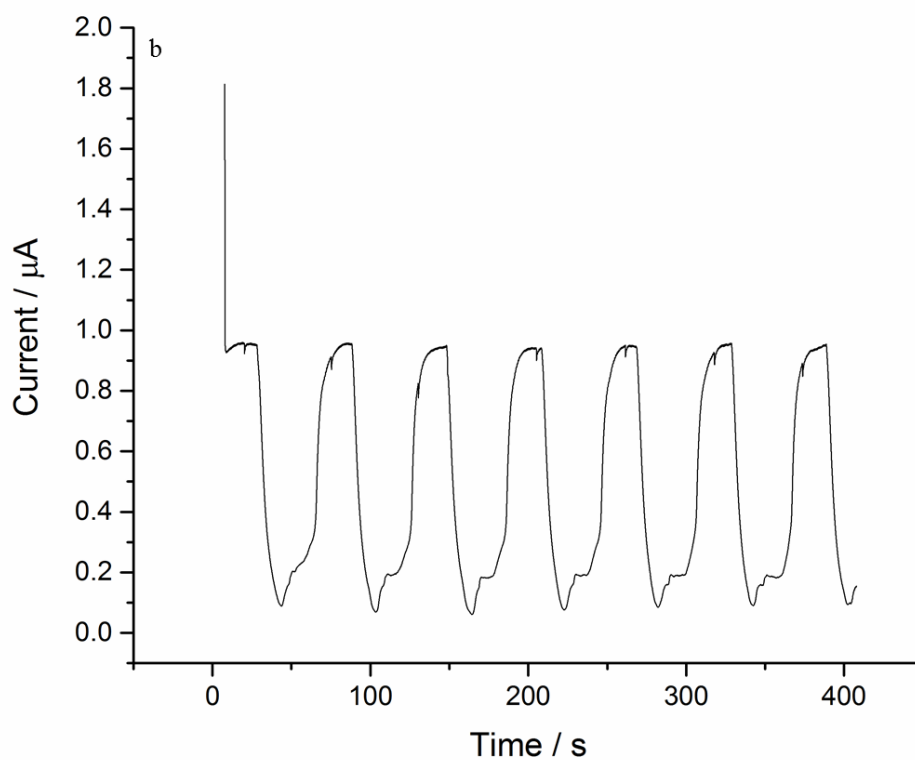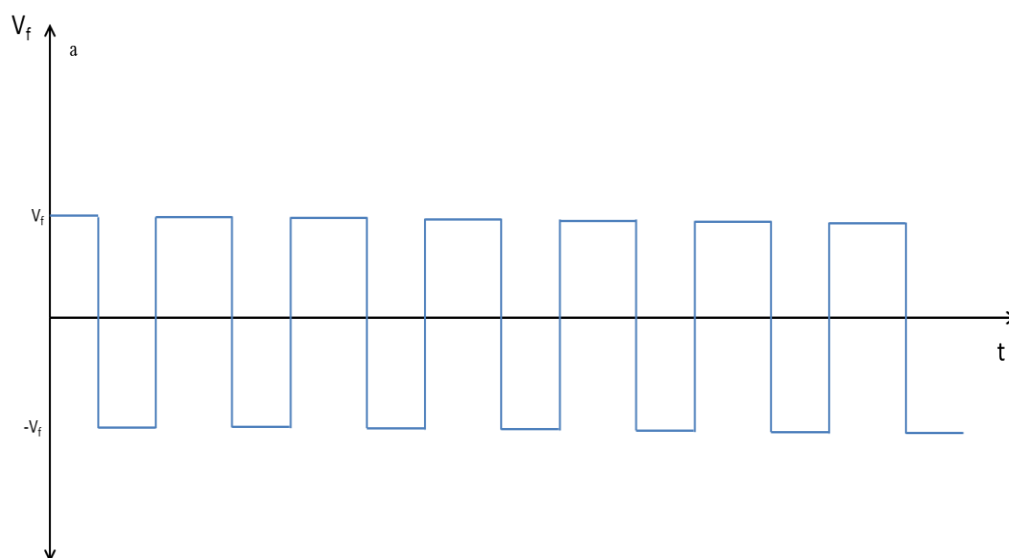
Fig 5.13 (a) Multiple flow rate steps setup; (b) current/time graph of 2 mM potassium ferrocyanide (applied potential: +0.5 V), showing the effect of multiple flow direction steps, for all directions flow rate at 0.05 mL/min.

After that, the different infusing flow rates were applied to the system to examine the response from the hydrodynamic modulation. Fig 5.14 (a) shows the change of controlled

flow rates with time. Fig 5.14 (b) shows the resulting current under the controlled flow rate setup. The resulting current showed good response with the change of different infusing flow rates and the Levich manner can be obtained as Fig 5.14 (c).

$$y = 2.7222x + 0.1594$$
$$R^2 = 0.9996$$
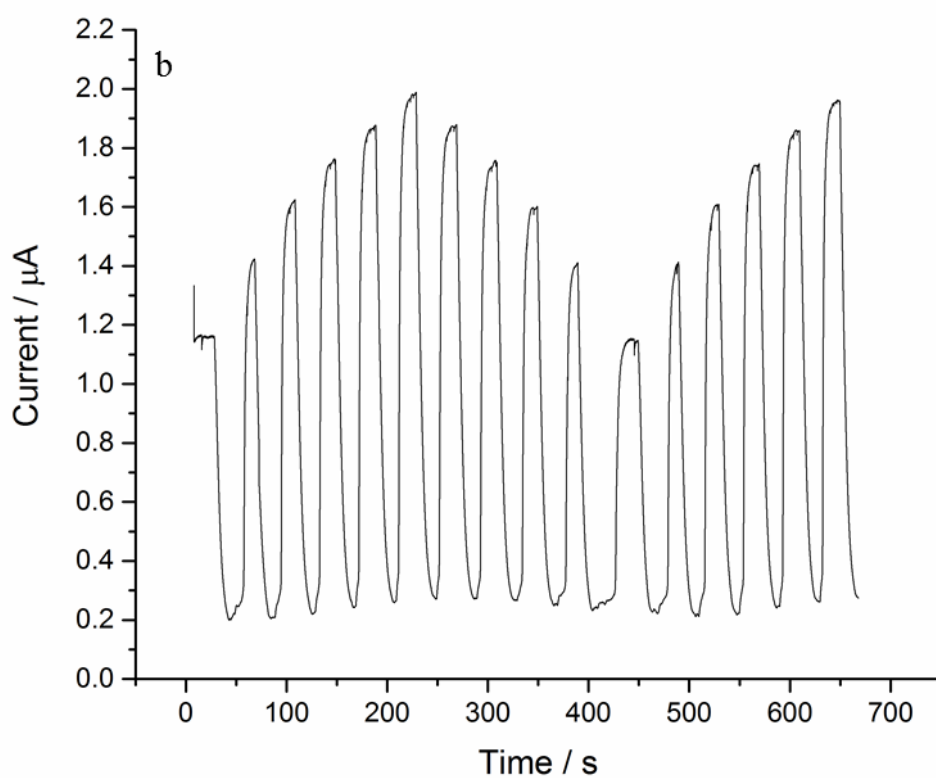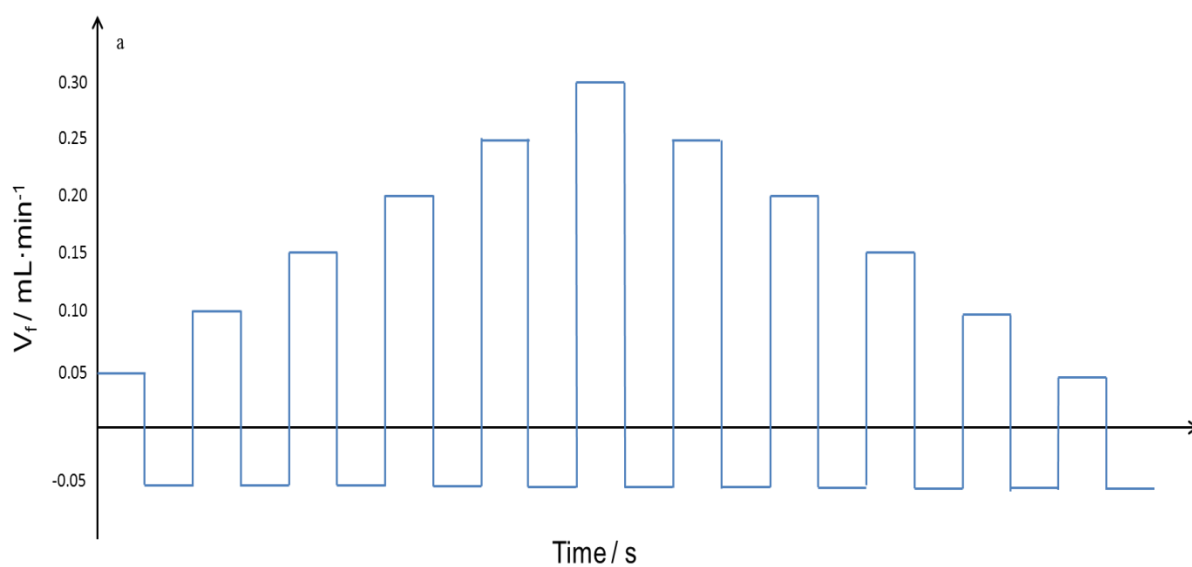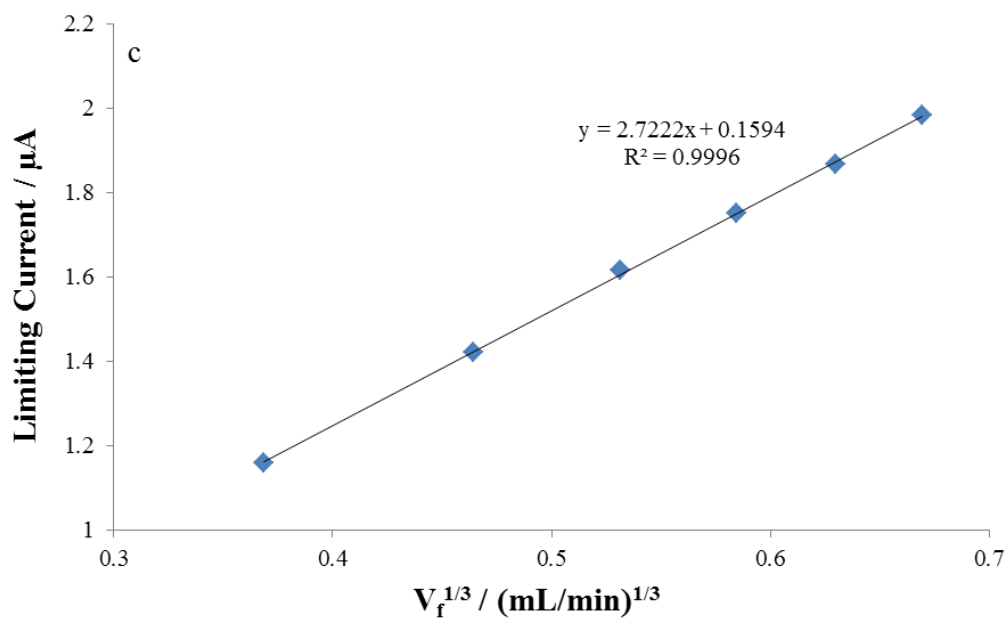
Fig 5.14 (a) Flow rate setup with various infusing flow rates (from 0.05 to 0.30 mL/min) and fixed withdrawing flow rate at 0.05 mL/min; (b) current/time graph of 2 mM potassium ferrocyanide (applied potential: +0.5 V), showing the effect of multiple flow direction steps; (c) liming current with various infusing flow rates.

Similar with that, the infusing flow rates can be set based on a Levich manner. The target Levich flow rates ($V_f^{1/3}$) were calculated first, then the programmed flow rates can be set on the syringe pump. The resulting current was measured with chronoamperometry to exam the hydrodynamic modulation system (Fig 5.15).
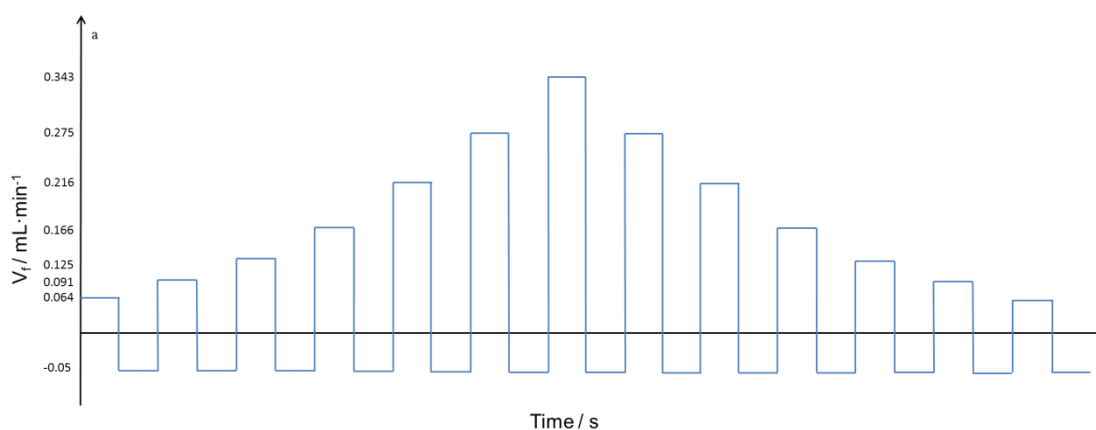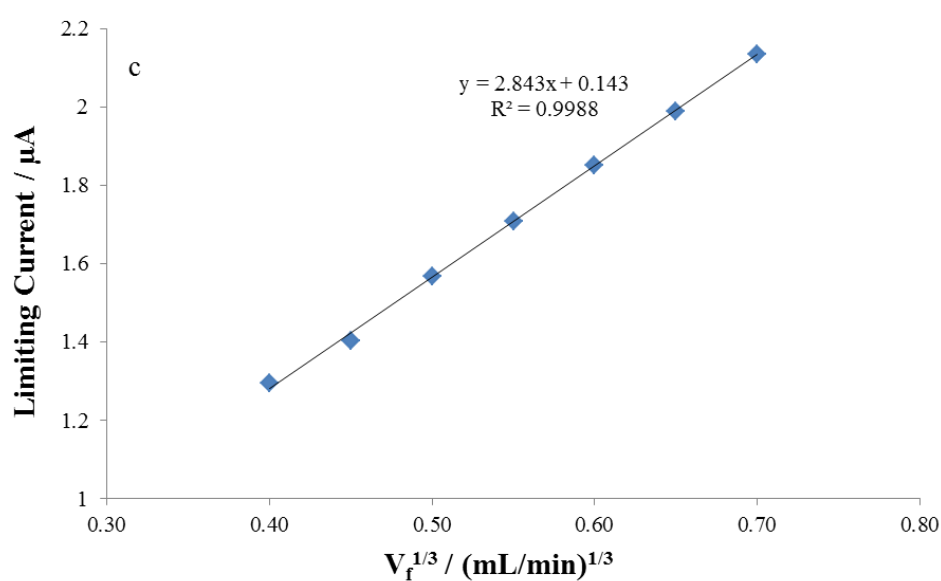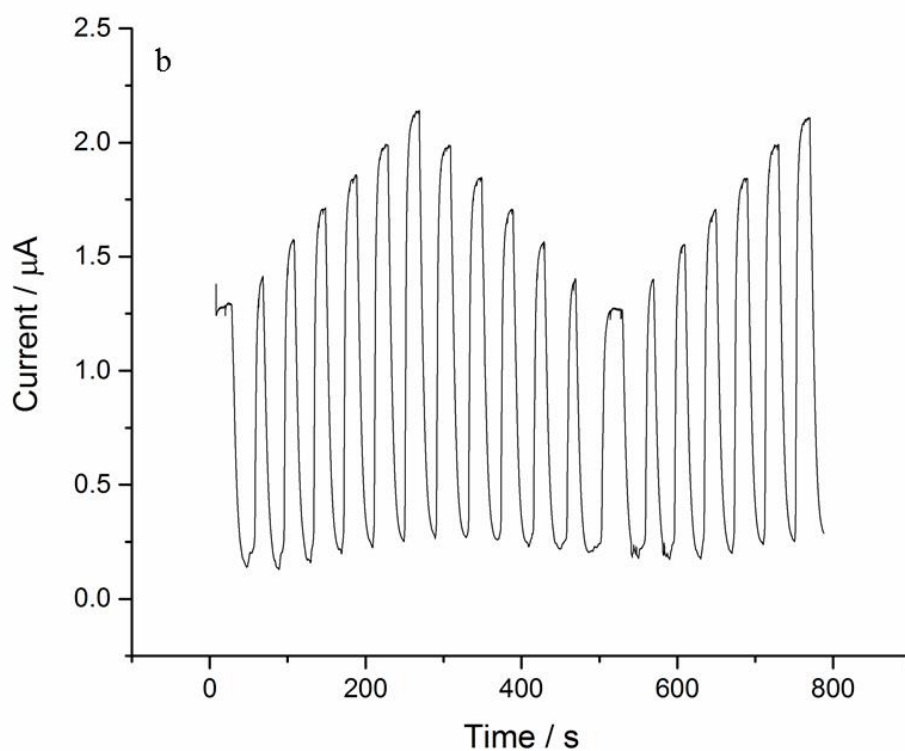
Fig 5.15 Flow rate setup with various infusing flow rates (from 0.064 to 0.343 mL/min) and fixed withdrawing flow rate at 0.05 mL/min; (b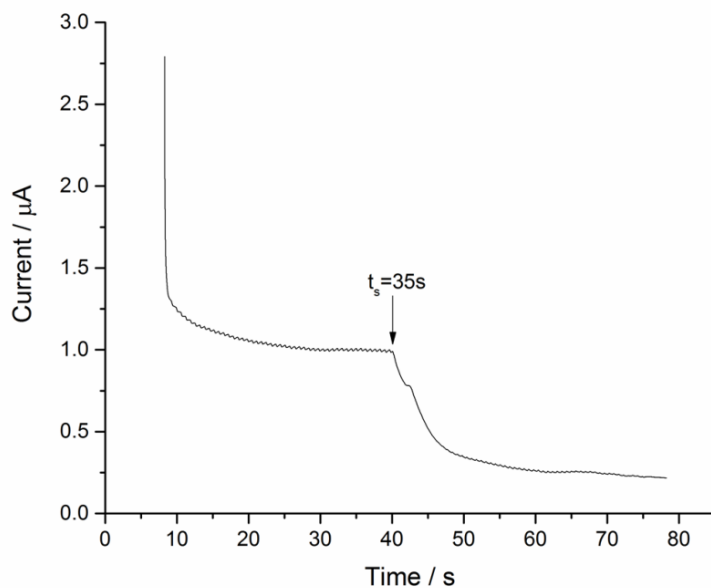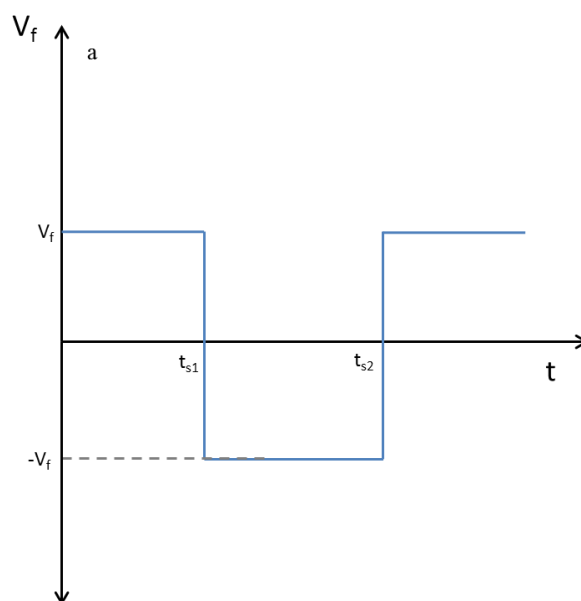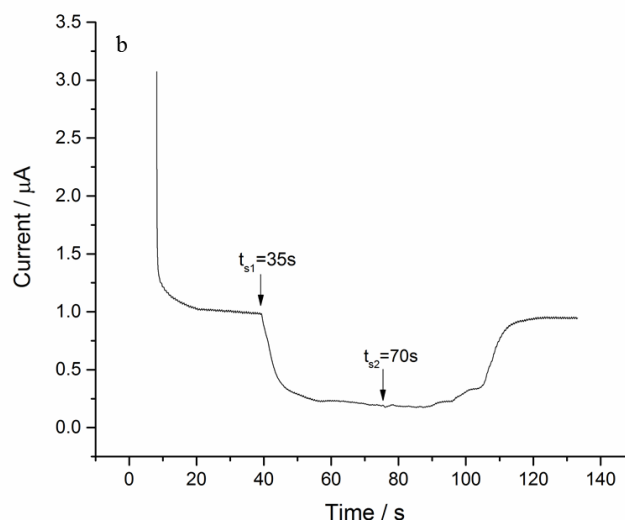) current/time graph of 2 mM potassium ferrocyanide (applied potential: +0.5 V), showing the effect of multiple flow direction steps; (c) liming current with various infusing flow rates.

Based on the results obtained from DC technique, it can be concluded that after the flow direction altering step, the resulting current undergoes an initial rapid variation before

establishing a new steady state value. The concentration of the electroactive species flowed over the electrode surface also contributed to the current response, which can be proved with the multiple changes of the flow directions. With higher infusing flow rates, the shorter stabilized time was needed to achieve the steady state. It is indicative that with the concentration of the solution which flowed by the electrode surface decreased due to the long-time process.

Large amplitude FTACV was also utilized to analyse the system response with advanced hydrodynamic modulation technique. Fig 5.16 (a) shows the fundamental harmonic from the overall electrochemical response of the hydrodynamic modulation system. The infusing process started simultaneously when the electrochemical detection began. After a period of time, the flow direction was altered by syringe pump. The time range was varied to exam the system response. As it can be seen from the figure, the peaks generated from the forward sweep overlapped with each other perfectly due to the same setting up of flow direction and flow rate. The flow direction change took place in the peaks generated from the backward sweep, so that the peaks illustrated the change by showing the shoulder-like shape. Fig 5.16 (b) shows the shoulder-like shape which is enlarged from the fundamental harmonic for clearer observation, where the arrows point out the position of the shoulders in different measurements. After the shoulder shaped achieved, the peak was formed. The value of the second peak which underwent different altering time was similar, which was indicative that the new steady state was formed with reverse flow direction.

The similar phenomenon can be observed with second harmonic and the enlarged part shown in Fig 5.17. Apparently the shoulder-like behaviour can be observed more clearly in the second harmonic, which implies that with large amplitude applied, subtle changes can be addressed better in higher harmonics.
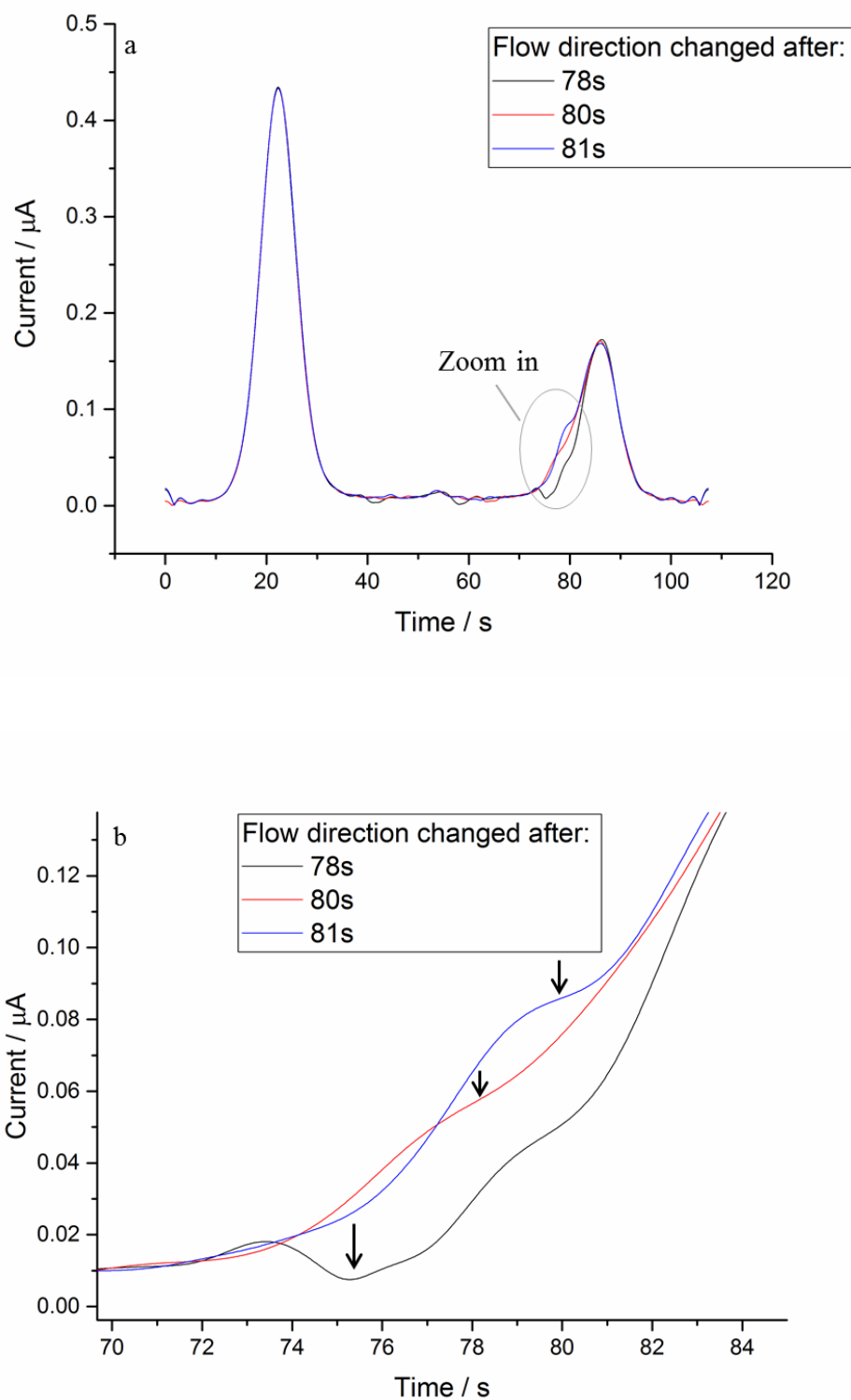
Fig 5.16 The large amplitude FTACV (potential range: -0.2-0.6 V, scan rate: 14.90 mV/s, frequency: 1 Hz, amplitude: 50 mV) detailing with the response of 2 mM potassium ferrocyanide to altering direction step (a) first harmonic; (b) enlarged part from first harmonic.
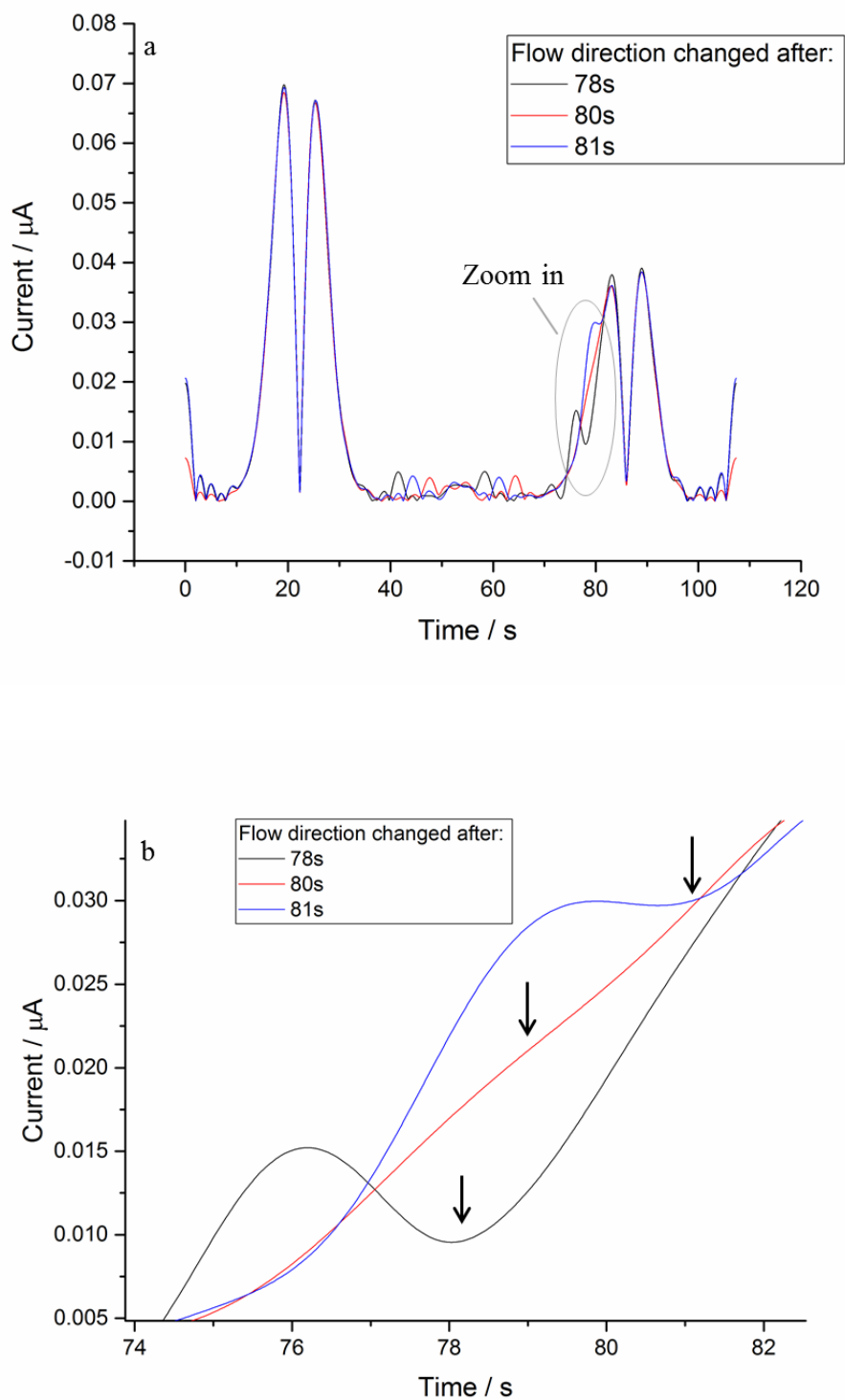
Fig 5.17 The large amplitude FTACV (potential range: -0.2-0.6 V, scan rate: 14.90 mV/s, frequency: 1 Hz, amplitude: 50 mV) detailing with the response of 2 mM potassium ferrocyanide to altering direction step (a) second harmonic; (b) enlarged part from first harmonic.

5.5 Conclusions

In this chapter, an advanced hydrodynamic modulation method was applied to test the electrochemical response in the microfluidic system. Not only the infusing flow rates but also the flow direction of the solution stream was changed during measurements

The resulting current presented a big drop at the moment when the flowing stream was altered to the reverse flow direction, which is the result of thicker diffusion layer formed in the withdrawing step. Then the diffusion layer stabilized and the resulting current reached another plateau where the second limiting current can be obtained. With another alteration of the flowing direction, after the fresh solution from the syringe was infused into the microchannel, the limiting current reached the value where the first infusing step was.

With multiple changes of the flowing direction, the experimental results showed that the system is sensitive to the infusing flow rate and a Levich type response can be obtained with different infusing flow rates applied. Also, the AC components extracted from the overall signal with FTACV presented us a promising way to examine hydrodynamic modulated system with AC technique by analysing the shoulder-like shapes where the flow step took place.

 For better understanding the hydrodynamic modulated system, some further numerical work should be established for future work.

Chapter 6   Conclusions

This thesis has investigated various electrochemical mechanisms with large amplitude Fourier transformed alternating current voltammetry in microfluidic systems. The merit to utilize large amplitude FTACV is that both AC components and DC signal can be obtained at the same time. To apply large amplitude rather than small amplitude enhanced the signal-to-noise in higher harmonics, which enables more accurate analysis. A hydrodynamic modulation method was developed to enhance the response and as it can be seen from the results, the system is sensitive with the hydrodynamic parameters as well as the substrate concentrations when homogeneous reactions were studied.

Chapter 3 focused on the electrochemical performance of different reactions with large amplitude FTACV in microfluidic system. The electrochemical micro-reactors were fabricated by using microfabrication technique. Different parameters including volume flow rates and substrate concentrations were considered respectively. The results showed that peak current values in lower harmonics increased with larger flow rates, which is analogue the phenomena when DC technique was applied. While in the higher harmonics, the dependence of peak current values and flow rates became weaker which is the result of the mass transport becomes dominated by the diffusion rather than convection contribution. Also the two different homogeneous reactions were studied in the same system. The electrochemical response showed that the system is sensitive with the substrate concentrations as well in either stagnant or hydrodynamic setup, which provides an alternative for sensing research.

Chapter 4 showed how hydrodynamic modulation method could affect the system. The flow rate changed during the electrochemical detection was processing. The results showed that under hydrodynamic modulation conditions, the system showed quick response of the flow rate change. The advantage to apply hydrodynamic modulation in the analysis is that both the relationships between peak current and flow rates or substrate concentrations can be obtained simultaneously, which reveals a promising approach to get more information in a short time measurement.

Chapter 5 presented the advanced hydrodynamic modulation technique. The flow direction of analyte stream was altered during the electrochemical measurements. The dramatical drop of resulting current showed the diffusion layer on the electrode surface broke down because of the opposite flow stream. Then the new limiting current value was reached presented that the new steady state was achieved. Analogue with DC detection, the result from large amplitude FTACV showed same result which the shoulder phenomenon can be obtained.

In a conclusion, large amplitude Fourier transformed alternating current voltammetry is valuable to detect electrochemical reactions in both stagnant and hydrodynamic system. The higher harmonics in AC technique when the large amplitudes applied can be helpful to get more information which cannot be obtained from only cyclic voltammograms such as background current and double layer capacitance. Also with the hydrodynamic modulation methods applied, the relationships revealed between parameters and peak current can be obtained in a short time measurement.

To have a better understanding of the hydrodynamic modulated system, the numerical work will be carried out for the future work.

References

[1]   J. Wang, Analytical Electrochemistry, John Wiley & Sons, 2006.

[2]   G. Hanrahan, D.G. Patil, J. Wang, Electrochemical sensors for environmental monitoring: design, development and applications., J. Environ. Monit. 6 (2004) 657–664.

[3]   E. Lindner, R.E. Gyurcsányi, Quality control criteria for solid-contact, solvent polymeric membrane ion-selective electrodes, J. Solid State Electrochem. 13 (2009) 51–68.

[4]   C.R. Ispas, G. Crivat, S. Andreescu, Review: Recent Developments in Enzyme-Based Biosensors for Biomedical Analysis, Anal. Lett. 45 (2012) 168–186.

[5]   A. Wang, Y. Fang, Applications of capillary electrophoresis with electrochemical detection in pharmaceutical and biomedical analyses, in: Electrophoresis, 2000: pp. 1281–1290.

[6]   J.P. Hart, S.A. Wring, Recent developments in the design and application of screen-printed electrochemical sensors for biomedical, environmental and industrial analyses, TrAC Trends Anal. Chem. 16 (1997) 89–103.

[7]   M.J. Tierney, H.O.L. Kim, Electrochemical Gas Sensor with Extremely Fast Response Times, Anal. Chem. 65 (1993) 3435–3440.

[8]   K.R. Reddy, C. Cameselle, Overview of electrochemical remediation technologies, Electrochem. Remediat. Technol. Polluted Soils, Sediments Groundw. (2009) 1–28.

173

[9] J. Trombly, Electrochemical remediation takes to the field, Environ. Sci. Technol. 28 (1994) 289–291.

[10] J. Virkutyte, M. Sillanpää, P. Latostenmaa, Electrokinetic soil remediation - Critical overview, Sci. Total Environ. 289 (2002) 97–121.

[11] A.T. Yeung, Y.-Y. Gu, A review on techniques to enhance electrochemical remediation of contaminated soils, J. Hazard. Mater. 195 (2011) 11–29.

[12] C.A.C. Sequeira, Environmental oriented electrochemistry, Elsevier, 1994.

[13] T. Fuchigami, M. Atobe, S. Inagi, Fundamentals and applications of organic electrochemistry: synthesis, materials, devices, John Wiley & Sons, 2014.

[14] B.A. Frontana-Uribe, R.D. Little, J.G. Ibanez, A. Palma, R. Vasquez-Medrano, Organic electrosynthesis: a promising green methodology in organic chemistry, Green Chem. 12 (2010) 2099.

[15] K. Scott, Industrial Electrochemical Synthesis Processes: Recent Developments in Reactor Design, Dev. Chem. Eng. Miner. Process. 1 (1993) 71–117.

[16] S.-S. Chang, C.-L. Lee, C.R.C. Wang, Gold Nanorods: Electrochemical Synthesis and Optical Properties, J. Phys. Chem. B. 101 (1997) 6661–6664.

[17] G.R. Nasretdinova, R.R. Fazleeva, R.K. Mukhitova, I.R. Nizameev, M.K. Kadirov, A.Y. Ziganshina, V. V. Yanilkin, Electrochemical synthesis of silver nanoparticles in solution, Electrochem. Commun. 50 (2015) 69–72.

[18] G. Yuan, X. Chang, G. Zhu, Electrosynthesis and catalytic properties of silver nano/microparticles with different morphologies, Particuology. 9 (2011) 644–649.

[19] J.O. Iroh, Y. Zhu, K. Shah, K. Levine, R. Rajagopalan, T. Uyar, M. Donley, R. Mantz, J. Johnson, N.N. Voevodin, V.N. Balbyshev, A.N. Khramov, Electrochemical synthesis: A novel technique for processing multi-functional coatings, in: Prog. Org. Coatings, 2003: pp. 365–375.

174

[20] A. Martinez Joaristi, J. Juan-Alcañiz, P. Serra-Crespo, F. Kapteijn, J. Gascon, A.M. Joaristi, J. Juan-Alcaniz, P. Serra-Crespo, F. Kapteijn, J. Gascon, Electrochemical synthesis of some archetypical Zn2+, Cu2+, and Al3+ metal organic frameworks, Cryst. Growth Des. 12 (2012) 3489–3498.

[21] C. Pascal, J.L. Pascal, F. Favier, M.L.E. Moubtassim, C. Payen, Electrochemical Synthesis for the Control of γ-Fe2O3 Nanoparticle Size. Morphology, Microstructure, and Magnetic Behavior, Chem. Mater. 11 (1999) 141–147.

[22] U. Guth, W. Vonau, J. Zosel, Recent developments in electrochemical sensor application and technology—a review, Meas. Sci. Technol. 20 (2009) 042002.

[23] D. Grieshaber, R. MacKenzie, J. Vörös, E. Reimhult, Electrochemical Biosensors - Sensor Principles and Architectures, Sensors. 8 (2008) 1400–1458.

[24] J.L. Hammond, N. Formisano, P. Estrela, S. Carrara, J. Tkac, Electrochemical biosensors and nanobiosensors, Essays Biochem. 60 (2016) 69–80.

[25] A.M. Azad, S.A. Akbar, S.G. Mhaisalkar, L.D. Birkefeld, K.S. Goto, Solid-State Gas Sensors - a Review, J. Electrochem. Soc. 139 (1992) 3690–3704.

[26] T. Maruyama, S. Sasaki, Y. Saito, Potentiometric gas sensor for carbon dioxide using solid electrolytes, Solid State Ionics. 23 (1987) 107–112.

[27] D.M. Bastidas, A. Cobo, E. Otero, J.A. González, Electrochemical rehabilitation methods for reinforced concrete structures: advantages and pitfalls, Corros. Eng. Sci. Technol. 43 (2008) 248–255.

[28] E. V. Suprun, V. V. Shumyantseva, A.I. Archakov, Protein Electrochemistry: Application in Medicine. A Review, Electrochim. Acta. 140 (2014) 72–82.

[29] D.M. Radzik, S.M. Lunte, Application of liquid chromatography/electrochemistry in pharmaceutical and biochemical analysis: a critical review, Crit. Rev. Anal. Chem. 20 (1989) 317–358.

[30] L. Alting, F. Kimura, H.N. Hansen, G. Bissacco, Micro Engineering, CIRP Ann. 52 (2003) 635–657.

[31] T. Masuzawa, State of the Art of Micromachining, CIRP Ann. 49 (2000) 473–488.

[32] D.. Pham, S.. Dimov, S. Bigot, A. Ivanov, K. Popov, Micro-EDM—recent developments and research issues, J. Mater. Process. Technol. 149 (2004) 50–57.

[33] J. Chae, S.S. Park, T. Freiheit, Investigation of micro-cutting operations, Int. J. Mach. Tools Manuf. 46 (2006) 313–332.

[34] M. Heckele, W.K. Schomburg, Review on micro molding of thermoplastic polymers, J. Micromechanics Microengineering. 14 (2004).

[35] B.H. Kim, S.H. Ryu, D.K. Choi, C.N. Chu, Micro electrochemical milling, J. Micromechanics Microengineering. 15 (2005) 124–129.

[36] P.D.I. Fletcher, S.J. Haswell, E. Pombo-Villar, B.H. Warrington, P. Watts, S.Y.F. Wong, X. Zhang, Micro reactors: principles and applications in organic synthesis, Tetrahedron. 58 (2002) 4735–4757.

[37] R.M. Tiggelaar, Silicon-technology based microreactors for high-temperature heterogeneous partial oxidation reactions, 2004.

[38] J.J. Brandner, L. Bohn, T. Henning, U. Schygulla, K. Schubert, Microstructure heat exchanger applications in laboratory and industry, Heat Transf. Eng. 28 (2007) 761–771.

[39] S. Hardt, W. Ehrfeld, V. Hessel, K.M. Vanden Bussche, Strategies for size reduction of microreactors by heat transfer enhancement effects, Chem. Eng. Commun. 190 (2003) 540–559.

[40] W. Ehrfeld, V. Hessel, V. Haverkamp, Microreactors, Ullmann's Encycl. Ind. Chem. (2012) 173–198.

[41] K Schubert; W Bier; J Brandner;, Realization and testing of microstructure reactors,

micro heat exchangers and micromixers for industrial applications in chemical engineering, American Institute of Chemical Engineers, 1998.

[42]   A.-L. Dessimoz, L. Cavin, A. Renken, L. Kiwi-Minsker, Liquid–liquid two-phase flow patterns and mass transfer characteristics in rectangular glass microreactors, Chem. Eng. Sci. 63 (2008) 4035–4044.

[43]   P. Sobieszuk, J. Aubin, R. Pohorecki, Hydrodynamics and mass transfer in gas-liquid flows in microreactors, Chem. Eng. Technol. 35 (2012) 1346–1358.

[44]   K.F. Jensen, Microreaction engineering — is small better?, Chem. Eng. Sci. 56 (2001) 293–303.

[45]   A. Ghaini, M.N. Kashid, D.W. Agar, Effective interfacial area for mass transfer in the liquid–liquid slug flow capillary microreactors, Chem. Eng. Process. Process Intensif. 49 (2010) 358–366.

[46]   G. Dummann, U. Quittmann, L. Gröschel, D.W. Agar, O. Wörz, K. Morgenschweis, The capillary-microreactor: a new reactor concept for the intensification of heat and mass transfer in liquid–liquid reactions, Catal. Today. 79–80 (2003) 433–439.

[47]   D.M. Roberge, L. Ducry, N. Bieler, P. Cretton, B. Zimmermann, Microreactor technology: A revolution for the fine chemical and pharmaceutical industries?, Chem. Eng. Technol. 28 (2005) 318–323.

[48]   B.P. Mason, K.E. Price, J.L. Steinbacher, A.R. Bogdan, T.D. McQuade, Greener approaches to organic synthesis using microreactor technology, Chem. Rev. 107 (2007) 2300–2318.

[49]   R. Mazurczyk, G. El Khoury, V. Dugas, B. Hannes, E. Laurenceau, M. Cabrera, S. Krawczyk, E. Souteyrand, J.P. Cloarec, Y. Chevolot, Low-cost, fast prototyping method of fabrication of the microreactor devices in soda-lime glass, Sensors Actuators, B Chem. 128 (2008) 552–559.

[50] H. Pennemann, V. Kessel, H. Löwe, Chemical microprocess technology - From laboratory-scale to production, in: Chem. Eng. Sci., 2004: pp. 4789–4794.

[51] S.H. DeWitt, Microreactors for chemical synthesis, Curr. Opin. Chem. Biol. 3 (1999) 350–356.

[52] X. Zhang, S. Stefanick, F.J. Villani, Application of microreactor technology in process development, Org. Process Res. Dev. 8 (2004) 455–460.

[53] O. Klais, F. Westphal, W. Benaissa, D. Carson, Guidance on Safety/Health for Process Intensification including MS Design; Part II: Explosion Hazards, Chem. Eng. Technol. 32 (2009) 1966–1973.

[54] S. Bhoi, Study of microchannel reactor using cfd analysis, (2012). http://ethesis.nitrkl.ac.in/3891/.

[55] P. Watts, C. Wiles, Recent advances in synthetic micro reaction technology, Chem. Commun. (2007) 443–467.

[56] K. Schubert, J. Brandner, M. Fichtner, G. Linder, U. Schygulla, A. Wenka, Microstructure Devices for Applications in Thermal and Chemical Process Engineering, Microscale Thermophys. Eng. 5 (2001) 17–39.

[57] W. Ehrfeld, V. Hessel, C. Schulz, L. Weber, Materials of LIGA technology, Microsyst. Technol. 5 (1999) 105–112.

[58] X. Yao, Y. Zhang, L. Du, J. Liu, J. Yao, Review of the applications of microreactors, Renew. Sustain. Energy Rev. 47 (2015) 519–539.

[59] J. Bart, A.J. Kolkman, A.J.O. De Vries, K. Koch, P.J. Nieuwland, H.J.W.G. Janssen, J.P.J.M. Van Bentum, K.A.M. Ampt, F.P.J.T. Rutjes, S.S. Wijmenga, H.J.G.E. Gardeniers, A.P.M. Kentgens, A Microfluidic high-resolution NMR flow probe, J. Am. Chem. Soc. 131 (2009) 5014–5015.

[60] S.J. Haswell, R.J. Middleton, B. O'Sullivan, V. Skelton, P. Watts, P. Styring, The

application of micro reactors to synthetic chemistry, Chem. Commun. (2001) 391–398.

[61]   K. Geyer, J.D.C. Codée, P.H. Seeberger, Microreactors as tools for synthetic Chemists - The chemists' round-bottomed flask of the 21st century?, Chem. - A Eur. J. 12 (2006) 8434–8442.

[62]   T. Wirth, ed., Microreactors in Organic Chemistry and Catalysis, Wiley-VCH, 2013.

[63]   S.H. DeWitt, Micro reactors for chemical synthesis, Curr. Opin. Chem. Biol. 3 (1999) 350–356.

[64]   S.J. Haswell, P. Watts, Green chemistry: synthesis in micro reactors, Green Chem. 5 (2003) 240–249.

[65]   J.I. Yoshida, H. Kim, A. Nagaki, Green and sustainable chemical synthesis using flow microreactors, ChemSusChem. 4 (2011) 331–340.

[66]   P. Watts, S.J. Haswell, Chemical Synthesis in Microreactors, in: M.P. Hughes, K.F. Hoettges (Eds.), Microengineering Biotechnol., Humana Press, Totowa, NJ, 2010: pp. 109–120.

[67]   A.S. Bhangale, K.L. Beers, R.A. Gross, Enzyme-catalyzed polymerization of end-functionalized polymers in a microreactor, Macromolecules. 45 (2012) 7000–7008.

[68]   S.C. Terry, J.H. Herman, J.B. Angell, A gas chromatographic air analyzer fabricated on a silicon wafer, IEEE Trans. Electron Devices. 26 (1979) 1880–1886.

[69]   A. Manz, H.M. Widmers, N. Graber, Miniaturized total chemical analysis systems: A novel concept for chemical sensing, Sensors Actuators B Chem. 1 (1990) 244–248.

[70]   A. Gavriilidis, P. Angeli, E. Cao, K.K. Yeong, Y.S.S. Wan, Technology and Applications of Microengineered Reactors, Chem. Eng. Res. Des. 80 (2002) 3–30.

[71]   P.S. Dittrich, K. Tachikawa, A. Manz, Micro total analysis systems. Latest advancements and trends, Anal. Chem. 78 (2006) 3887–3908.

[72] F. Zhou, M. Lu, W. Wang, Z.-P. Bian, J.-R. Zhang, J.-J. Zhu, Electrochemical immunosensor for simultaneous detection of dual cardiac markers based on a poly (dimethylsiloxane)-gold nanoparticles composite microfluidic chip: a proof of principle, Clin. Chem. 56 (2010) 1701–1707.

[73] T. Vilkner, D. Janasek, A. Manz, Micro total analysis systems. Recent developments, Anal. Chem. 76 (2004) 3373–3386.

[74] M. Trojanowicz, Recent developments in electrochemical flow detections, a review: part I. Flow analysis and capillary electrophoresis., Anal. Chim. Acta. 653 (2009) 36–58.

[75] J. Antes, D. Boskovic, H. Krause, S. Loebbecke, N. Lutz, T. Tuercke, W. Schweikert, Analysis and improvement of strong exothermic nitrations in microreactors, Chem. Eng. Res. Des. 81 (2003) 760–765.

[76] B.C.H. Steele, A. Heinzel, Materials for fuel-cell technologies, in: Mater. Sustain. Energy A Collect. Peer-Reviewed Res. Rev. Artic. from Nat. Publ. Gr., World Scientific, 2011: pp. 224–231.

[77] V. Mehta, J.S. Cooper, Review and analysis of PEM fuel cell design and manufacturing, J. Power Sources. 114 (2003) 32–53.

[78] A. V. Pattekar, M. V. Kothare, A microreactor for hydrogen production in micro fuel cell applications, J. Microelectromechanical Syst. 13 (2004) 7–18.

[79] K. Watts, W. Gattrell, T. Wirth, A practical microreactor for electrochemistry in flow, Beilstein J. Org. Chem. 7 (2011) 1108–1114.

[80] E. L'Hostis, P.. Michel, G.. Fiaccabrino, D.. Strike, N.. de Rooij, M. Koudelka-Hep, Microreactor and electrochemical detectors fabricated using Si and EPON SU-8, Sensors Actuators B Chem. 64 (2000) 156–162.

[81] J. Křišt'ál, R. Kodým, K. Bouzek, V. Jiřičný, Electrochemical microreactor and gas-

evolving reactions, Electrochem. Commun. 10 (2008) 204–207.

[82]   A. Ziogas, H. Löwe, M. Küpper, W. Ehrfeld, Electrochemical Microreactors: A New Approach for Microreaction Technology, in: Microreact. Technol. Ind. Prospect., 2000: pp. 136–150.

[83]   H. Ernst, B. Roß, M. Knoll, Characterisation and application of the electrochemical plate microreactor in analytical chemistry, Electrochim. Acta. 47 (2002) 1795–1800.

[84]   K. Jähnisch, V. Hessel, H. Löwe, M. Baerns, Chemistry in Microstructured Reactors, Angew. Chemie - Int. Ed. 43 (2004) 406–446.

[85]   V. Mengeaud, O. Bagel, R. Ferrigno, H.H. Girault, A. Haider, A ceramic electrochemical microreactor for the methoxylation of methyl-2-furoate with direct mass spectrometry coupling, Lab Chip. 2 (2002) 39–44.

[86]   A. Rouge, B. Spoetzl, K. Gebauer, R. Schenk, A. Renken, Microchannel reactors for fast periodic operation: The catalytic dehydration of isopropanol, Chem. Eng. Sci. 56 (2001) 1419–1427.

[87]   A.C. Fisher, Electrode Dynamics, Oxford University Press, 1996.

[88]   A.J. Bard, L.R. Faulkner, Electrochemical methods—Fundamentals and applications, Wiley, 1980.

[89]   F. Zhao, R.C.T. Slade, J.R. Varcoe, Techniques for the study and development of microbial fuel cells: an electrochemical perspective, Chem. Soc. Rev. 38 (2009) 1926.

[90]   G.H. Sedahmed, Electrochemical mass transfer at a fixed bed of spheres under forced convection induced by counterelectrode gas bubbles, Can. J. Chem. Eng. 64 (1986) 75–79.

[91]   A. Manz, C.S. Effenhauser, N. Burggraf, D.J. Harrison, K. Seiler, K. Fluri, Electroosmotic pumping and electrophoretic separations for miniaturized chemical analysis systems, J. Micromechanics Microengineering. 4 (1994) 257.

http://stacks.iop.org/0960-1317/4/i=4/a=010.

[92] G. Hinds, J.M.D. Coey, M.E.G. Lyons, Influence of magnetic forces on electrochemical mass transport, Electrochem. Commun. 3 (2001) 215–218.

[93] A.S. Raja, S. Rajendran, P. Satyabama, Inhibition of Corrosion of Carbon Steel in Well Water by DL-Phenylalanine-Zn $^{2+}$ System, J. Chem. 2013 (2013) 1–8.

[94] J.-M. Savéant, Elements of molecular and biomolecular electrochemistry: an electrochemical approach to electron transfer chemistry, 2006.

[95] W. Ehrfeld, V. Hessel, H. Löwe, Microreactors - New Technology for Modern Chemistry, 2001.

[96] J.M. Saveant, E. Vianello, Potential-sweep chronoamperometry: Kinetic currents for first-order chemical reaction parallel to electron-transfer process (catalytic currents), Electrochim. Acta. 10 (1965) 905–920.

[97] P.T. Kissinger, W.R. Heineman, Cyclic voltammetry, J. Chem. Educ. 60 (1983) 702.

[98] G.C. Barker, I.L. Jenkins, Square-wave polarography, Analyst. 77 (1952) 685–696.

[99] L. Ramaley, M.S. Krause, Analytical Application of Square Wave Voltammetry, Anal. Chem. 41 (1969) 1365–1369.

[100] J.G. Osteryoung, R.A. Osteryoung, Square Wave Voltammetry, Anal. Chem. 57 (1985) 101–110.

[101] L. Ramaley, M.S. Krause, Theory of Square Wave Voltammetry, Anal. Chem. 41 (1969) 1362–1365.

[102] M.S. Krause, L. Ramaley, Analytical Application of Square Wave Voltammetry, Anal. Chem. 41 (1969). https://pubs.acs.org/doi/pdf/10.1021/ac60280a008.

[103] E. Barsoukov, J.R. Macdonald, Impedance spectroscopy: theory, experiment, and applications, John Wiley & Sons, 2018.

[104] R.G. Compton, J. Winkler, Hydrodynamic voltammetry with channel microband electrodes: Alternating current impedance measurements, J. Phys. Chem. 99 (1995) 5029–5034.

[105] W.P. Gomes, D. Vanmaekelbergh, Impedance spectroscopy at semiconductor electrodes: Review and recent developments, Electrochim. Acta. 41 (1996) 967–973.

[106] D.C. Grahame, Mathematical Thoery of the Faradaic Admittance (Pseudocapacity and Polarization Resistance), J. Electrochem. Soc. 99 (1952) 370–385.

[107] A.M. Bond, D. Elton, S.X. Guo, G.F. Kennedy, E. Mashkina, A.N. Simonov, J. Zhang, An integrated instrumental and theoretical approach to quantitative electrode kinetic studies based on large amplitude Fourier transformed a.c. voltammetry: A mini review, Electrochem. Commun. 57 (2015) 78–83.

[108] A.M. Bond, N.W. Duffy, S.-X. Guo, J. Zhang, D. Elton, Changing the look of voltammetry, Anal. Chem. (2005) 186A–195A.

[109] A. Bond, Modern polarographic methods in analytical chemistry, CRC press, 1980.

[110] C.G. Zoski, Handbook of electrochemistry, 2007.

[111] J. Zhang, A.M. Bond, Theoretical studies of large amplitude alternating current voltammetry for a reversible surface-confined electron transfer process coupled to a pseudo first-order electrocatalytic process, J. Electroanal. Chem. 600 (2007) 23–34.

[112] R.T. Boeré, A.M. Bond, S. Cronin, N.W. Duffy, P. Hazendonk, J.D. Masuda, K. Pollard, T.L. Roemmele, P. Tran, Y. Zhang, Photophysical, dynamic and redox behavior of tris(2,6-diisopropylphenyl) phosphine, New J. Chem. (2008).

[113] S. Guo, J. Zhang, D.M. Elton, A.M. Bond, Fourier transform large-amplitude alternating current cyclic voltammetry of surface-bound azurin, Anal. Chem. 76 (2004) 166–177.

[114] C.Y. Lee, J.P. Bullock, G.F. Kennedy, A.M. Bond, Effects of coupled homogeneous

chemical reactions on the response of large-amplitude AC voltammetry: Extraction of kinetic and mechanistic information by fourier transform analysis of higher harmonic data, J. Phys. Chem. A. 114 (2010) 10122–10134.

[115] S.J.M. Rosvall, M.J. Honeychurch, D.M. Elton, A.M. Bond, A practical approach to applying short time Fourier transform methods in voltammetric investigations, J. Electroanal. Chem. 515 (2001) 8–16.

[116] D.J. Gavaghan, D. Elton, K.B. Oldham, A.M. Bond, Analysis of ramped square-wave voltammetry in the frequency domain, J. Electroanal. Chem. 512 (2001) 1–15.

[117] D.J. Gavaghan, D. Elton, A.M. Bond, A comparison of sinusoidal, square wave, sawtooth, and staircase forms of transient ramped voltammetry when a reversible process is analysed in the frequency domain, J. Electroanal. Chem. 513 (2001) 73–86.

[118] D.J. Gavaghan, A.M. Bond, A complete numerical simulation of the techniques of alternating current linear sweep and cyclic voltammetry: analysis of a reversible process by conventional and fast Fourier transform methods, J. Electroanal. Chem. 480 (2000) 133–149.

[119] A.S. Baranski, Alternating current voltammetry with carbon fiber microelectrodes, J. Electrochem. Soc. 133 (1986) 93–97.

[120] W.R. Fawcett, Z. Kováčová, A.J. Motheo, C.A. Foss, Application of the ac admittance technique to double-layer studies on polycrystalline gold electrodes, J. Electroanal. Chem. 326 (1992) 91–103.

[121] S.E. Creager, T.T. Wooster, A new way of using ac voltammetry to study redox kinetics in electroactive monolayers, Anal. Chem. 70 (1998) 4257–4263.

[122] R.S. Nicholson, Some examples of the numerical solution of nonlinear integral equations, Anal. Chem. 37 (1965) 667–671.

[123] J. Zhang, S.X. Guo, A.M. Bond, Discrimination and evaluation of the effects of

uncompensated resistance and slow electrode kinetics from the higher harmonic components of a fourier transformed large-amplitude alternating current voltammogram, Anal. Chem. 79 (2007) 2276–2288.

[124] D.F. Milner, M.J. Weaver, The influence of uncompensated solution resistance on the determination of standard electrochemical rate constants by cyclic voltammetry, and some comparisons with a.c. voltammetry, Anal. Chim. Acta. 198 (1987) 245–257.

[125] B.D. Fleming, J. Zhang, A.M. Bond, S.G. Bell, L.L. Wong, Separation of electron-transfer and coupled chemical reaction components of biocatalytic processes using Fourier transform ac voltammetry, Anal. Chem. 77 (2005) 3502–3510.

[126] B. Lertanantawong, A.P. O'Mullane, J. Zhang, W. Surareungchai, M. Somasundrum, A.M. Bond, Investigation of mediated oxidation of ascorbic acid by ferrocenemethanol using large-amplitude fourier transformed ac voltammetry under quasi-reversible electron-transfer conditions at an indium tin oxide electrode, Anal. Chem. 80 (2008) 6515–6525.

[127] J.A. Alden, R.G. Compton, Hydrodynamic voltammetry with channel microband electrodes: axial diffusion effects, J. Electroanal. Chem. 404 (1996) 27–35.

[128] A. Frumkin, L. Nekrasov, B. Levich, J. Ivanov, Die anwendung der rotierenden scheibenelektrode mit einem ringe zur untersuchung von zwischenprodukten elektrochemischer reaktionen, J. Electroanal. Chem. 1 (1959) 84–90.

[129] F. Opekar, P. Beran, Rotating disk electrodes, J. Electroanal. Chem. Interfacial Electrochem. 69 (1976) 1–105.

[130] R. Navarrete, Determining the Behavior of the Rotating Disk Electrode System, (n.d.) 1–27.

[131] Z. Galus, C. Olson, H.Y. Lee, R.N. Adams, Rotating Disk Electrodes, Anal. Chem. 34 (1962) 164–166.

[132] S.M. Matthews, G.Q. Du, A.C. Fisher, Microfluidic voltammetry: Simulation of the chronoamperometric response of microband electrodes sited within microreactors, J. Solid State Electrochem. 10 (2006) 817–825.

[133] R.G. Compton, C.E. Banks, Understanding voltammetry, World Scientific, 2011.

[134] J.A. Cooper, R.G. Compton, Channel Electrodes - A Review, Electroanalysis. 10 (1998) 141–155.

[135] J. Wang, Hydrodynamic modulation voltammetry, Talanta. 28 (1981) 369–376.

[136] W.J. Blaedel, R.C. Engstrom, Investigations of the Ferricyanide-Ferrocyanide System by Pulsed Rotation Voltammetry, Anal. Chem. 50 (1978) 476–479.

[137] W.J. Blaedel, J. Wang, Characteristics of a Rotated Porous Flow-Through Electrode, Anal. Chem. 52 (1980) 1697–1700.

[138] W.J. Blaedel, J. Wang, Pulsed rotation voltammetry in a flow-through cell, Anal. Chim. Acta. 116 (1980) 315–322.

[139] W.J. Blaedel, S.L. Boyer, Submicromolar concentration measurements with tubular electrodes, Anal. Chem. 43 (1971) 1538–1540.

[140] J. V. Macpherson, Recent advances in hydrodynamic modulation voltammetry, Electroanalysis. 12 (2000) 1001–1011.

[141] S.A. Schuette, R.L. McCreery, Efficient Hydrodynamic Modulation Voltammetry with a Microcylinder Electrode, Anal. Chem. 58 (1986) 1778–1782.

[142] J. V. Macpherson, P.R. Unwin, Hydrodynamic modulation voltammetry with an oscillating microjet electrode, Anal. Chem. 71 (1999) 4642–4648.

[143] H.D. Dewald, B.A. Peterson, Ultrasonic Hydrodynamic Modulation Voltammetry, Anal. Chem. 62 (1990) 779–782.

[144] S.A. Schuette, R.L. McCreery, Hydrodynamically modulated alternating current

voltammetry, Anal. Chem. 59 (1987) 2692–2699.

[145] D.T. Schwartz, Experimental Implementation and Capabilities of Fourier Transform Hydrodynamic Modulation Voltammetry, J. Electrochem. Soc. 140 (1993) 452–458.

[146] M.J. Madou, Fundamentals of microfabrication: the science of miniaturization, CRC press, 2002.

[147] M. Verhulsel, M. Vignes, S. Descroix, L. Malaquin, D.M. Vignjevic, J.-L. Viovy, A review of microfabrication and hydrogel engineering for micro-organs on chips, Biomaterials. 35 (2014) 1816–1832.

[148] M. Abraham, W. Ehrfeld, V. Hessel, K.P. Kämper, M. Lacher, a. Picard, Microsystem technology: Between research and industrial application, Microelectron. Eng. 41–42 (1998) 47–52.

[149] D.B. Weibel, W.R. DiLuzio, G.M. Whitesides, Microfabrication meets microbiology, Nat. Rev. Microbiol. 5 (2007) 209–218.

[150] A. Pimpin, W. Srituravanich, Reviews on micro- and nanolithography techniques and their applications, Eng. J. 16 (2012) 37–55.

[151] R.F. Pease, S.Y. Chou, Lithography and other patterning techniques for future electronics, Proc. IEEE. 96 (2008) 248–270.

[152] B.D. Gates, Q. Xu, M. Stewart, D. Ryan, C.G. Willson, G.M. Whitesides, New approaches to nanofabrication: Molding, printing, and other techniques, Chem. Rev. 105 (2005) 1171–1196.

[153] S. Owa, H. Nagasaka, Immersion Lithography; its potential performance and issues, in: Opt. Microlithogr. XVI, 2003: pp. 724–734.

[154] B. Wu, A. Kumar, Extreme ultraviolet lithography: A review, J. Vac. Sci. Technol. B Microelectron. Nanom. Struct. 25 (2007) 1743.

[155] F.M. Schellenberg, Resolution enhancement technology: the past, the present, and

extensions for the future, in: Opt. Microlithogr. XVII, 2004: pp. 1–21.

[156] D.J. Ehrlich, J.Y. Tsao, Laser microfabrication: thin film processes and lithography, Elsevier, 1989.

[157] K. Sugioka, M. Meunier, A. Pique, Laser Precision Microfabrication, Sponger, 2010.

[158] H. Misawa, S. Juodkazis, Introduction, in: 3D Laser Microfabr., Wiley-Blackwell, 2006: pp. 1–4.

[159] J. Zhang, K. Sugioka, K. Midorikawa, Direct fabrication of microgratings in fused quartz by laser-induced plasma-assisted ablation with a KrF excimer laser., Opt. Lett. 23 (1998) 1486–1488.

[160] K. Tanaka, N. Yoshida, Direct microfabrication of chalcogenide glasses by light and electron-beam exposures, 1997.

[161] G. Dos Reis, F. Fenili, A. Gianfelice, G. Bongiorno, D. Marchesi, P.E. Scopelliti, A. Borgonovo, A. Podestà, M. Indrieri, E. Ranucci, P. Ferruti, C. Lenardi, P. Milani, Direct microfabrication of topographical and chemical cues for the guided growth of neural cell networks on polyamidoamine hydrogels, Macromol. Biosci. 10 (2010) 842–852.

[162] T. Katoh, N. Nishi, M. Fukagawa, H. Ueno, S. Sugiyama, Direct writing for three-dimensional microfabrication using synchrotron radiation etching, Sensors Actuators, A Phys. 89 (2001) 10–15.

[163] G. Schanz, K. Bade, Microelectroforming of Metals, Microengineering Met. Ceram. Part II Spec. Replication Tech. Autom. Prop. (n.d.) 395–420.

[164] J.A. Rogers, Rubber stamping for plastic electronics and fiber optics, MRS Bull. 26 (2001) 530–534.

[165] S. V Atre, T.J. Weaver, R.M. German, SAE TECHNICAL Injection Molding of Metals and Ceramics, (2016).

[166] R.B. Rao, K.L. Krafcik, A.M. Morales, J.A. Lewis, Microfabricated deposition nozzles for direct-write assembly of three-dimensional periodic structures, Adv. Mater. 17 (2005) 289–293.

[167] X.C. Shan, R. Maeda, Y. Murakoshi, Micro hot embossing for replication of microstructures, in: Japanese J. Appl. Physics, Part 1 Regul. Pap. Short Notes Rev. Pap., 2003: pp. 3859–3862.

[168] L. Peng, Y. Deng, P. Yi, X. Lai, Micro hot embossing of thermoplastic polymers: A review, J. Micromechanics Microengineering. 24 (2014).

[169] O. Rötting, W. Röpke, H. Becker, C. Gärtner, Polymer microfabrication technologies, Microsyst. Technol. 8 (2002) 32–36.

[170] H. Mekaru, H. Goto, M. Takahashi, Development of ultrasonic micro hot embossing technology, Microelectron. Eng. 84 (2007) 1282–1287.

[171] C.Y. Chang, S.Y. Yang, L.S. Huang, J.H. Chang, Fabrication of plastic microlens array using gas-assisted micro-hot-embossing with a silicon mold, Infrared Phys. Technol. 48 (2006) 163–173.

[172] D. V Rosato, M.G. Rosato, Injection molding handbook, Springer Science & Business Media, 2012.

[173] U.M. Attia, S. Marson, J.R. Alcock, Micro-injection moulding of polymer microfluidic devices, Microfluid. Nanofluidics. 7 (2009) 1.

[174] A.R. Agrawal, I.O. Pandelidis, M. Pecht, Injection-molding process control—A review, Polym. Eng. Sci. 27 (1987) 1345–1357.

[175] Z. Chen, L. Turng, A review of current developments in process and quality control for injection molding, Adv. Polym. Technol. 24 (2005) 165–182.

[176] B. Sha, S. Dimov, C. Griffiths, M.S. Packianather, Investigation of micro-injection moulding: Factors affecting the replication quality, J. Mater. Process. Technol. 183

(2007) 284–296.

[177] S. V Atre, T.J. Weaver, R.M. German, Injection molding of metals and ceramics, 1998.

[178] Y. Zhang, C.W. Lo, J.A. Taylor, S. Yang, Replica molding of high-aspect-ratio polymeric nanopillar arrays with high fidelity, Langmuir. 22 (2006) 8595–8601.

[179] E.W. Becker, W. Ehrfeld, P. Hagmann, A. Maner, D. Münchmeyer, Fabrication of microstructures with high aspect ratios and great structural heights by synchrotron radiation lithography, galvanoforming, and plastic moulding (LIGA process), Microelectron. Eng. 4 (1986) 35–56.

[180] P. Bley, W. Bacher, W. Menz, J. Mohr, Description of microstructures in LIGA-technology, Microelectron. Eng. 13 (1991) 509–512.

[181] X. Zhu, G. Liu, Y. Xiong, Y. Guo, Y. Tian, Fabrication of PMMA Microchip of Capillary Electrophoresis by Optimized UV-LIGA Process, J. Phys. Conf. Ser. 34 (2006) 875. http://stacks.iop.org/1742-6596/34/i=1/a=145.

[182] C.K. Malek, V. Saile, Applications of LIGA technology to precision manufacturing of high-aspect-ratio micro-components and -systems: A review, Microelectronics J. 35 (2004) 131–143.

[183] Z. Cui, R.A. Lawes, Low Cost Fabrication Of Micromechanical Systems, Microelectron. Eng. 35 (1997) 389–392.

[184] S. Bhattacharya, A. Datta, J.M. Berg, S. Gangopadhyay, Studies on surface wettability of poly(dimethyl) siloxane (PDMS) and glass under oxygen-plasma treatment and correlation with bond strength, J. Microelectromechanical Syst. 14 (2005) 590–597.

[185] B. Bilenberg, T. Nielsen, B. Clausen, A. Kristensen, PMMA to SU-8 bonding for polymer based lab-on-a-chip systems with integrated optics, J. Micromechanics Microengineering. 14 (2004) 814–818.

[186] L. Yu, F.E.H. Tay, G. Xu, B. Chen, M. Avram, C. Iliescu, Adhesive bonding with SU-

8 at wafer level for microfluidic devices, J. Phys. Conf. Ser. 34 (2006) 776–781.

[187] K.R. Williams, R.S. Muller, Etch Rates for Micromachining Processing, J. Microelectromechanical Syst. 7157 (1996) 256–269.

[188] A. Mata, A.J. Fleischman, S. Roy, Fabrication of multi-layer SU-8 microstructures, J. Micromechanics Microengineering. 16 (2006) 276–284.

[189] S. Jiguet, A. Bertsch, M. Judelewicz, H. Hofmann, P. Renaud, SU-8 nanocomposite photoresist with low stress properties for microfabrication applications, Microelectron. Eng. 83 (2006) 1966–1970.

[190] N.P.C. Stevens, A.C. Fisher, Transient voltammetry under hydrodynamic conditions, Electroanalysis. 10 (1998) 16–20.

[191] W. Zhang, H.A. Stone, J.D. Sherwood, Mass transfer at a microelectrode in channel flow, J. Phys. Chem. 100 (1996) 9462–9464.

[192] A. Gavriilidis, P. Angeli, E. Cao, K.K. Yeong, Y.S.S. Wan, Technology and Applications of Microengineered Reactors, Chem. Eng. Res. Des. 80 (2002) 3–30.

[193] P. Watts, S.J. Haswell, The application of micro reactors for organic synthesis, Chem. Soc. Rev. 34 (2005) 235.

[194] P.L. Urban, D.M. Goodall, N.C. Bruce, Enzymatic microreactors in chemical analysis and kinetic studies, Biotechnol. Adv. 24 (2006) 42–57.

[195] G. Kolb, V. Hessel, Micro-structured reactors for gas phase reactions, Chem. Eng. J. 98 (2004) 1–38.

[196] D. Schwartz, P. Stroeve, B. Higgins, Fourier transform methods in hydrodynamic modulation voltammetry, J. Electrochem. Soc. 136 (1989) 1755.

[197] S.O. Engblom, J.C. Myland, K.B. Oldham, Must ac voltammetry employ small signals?, J. Electroanal. Chem. 480 (2000) 120–132.

[198] A.P. O'Mullane, J. Zhang, A. Brajter-Toth, A.M. Bond, Higher harmonic large-amplitude fourier transformed alternating current voltammetry: Analytical attributes derived from studies of the oxidation of ferrocenemethanol and uric acid at a glassy carbon electrode, Anal. Chem. 80 (2008) 4614–4626.

[199] B. Lertanantawong, A.P. O'Mullane, W. Surareungchai, M. Somasundrum, L.D. Burke, A.M. Bond, Study of the underlying electrochemistry of polycrystalline gold electrodes in aqueous solution and electrocatalysis by large amplitude fourier transformed alternating current voltammetry, Langmuir. 24 (2008) 2856–2868.

[200] D.E. Walker, R.N. Adams, A.L. Juliard, Alternating Current Voltammetry at Solid Electrodes, Anal. Chem. 32 (1960) 1526–1528.

[201] K. Tokuda, H. Matsuda, Theory of a.c. voltammetry at a rotating disk electrode: Part I. A reversible electrode process, J. Electroanal. Chem. Interfacial Electrochem. 82 (1977) 157–171.

[202] K. Tokuda, H. Matsuda, Theory of a.c. voltammetry at a rotating disk electrode: Part II. Quasi-reversible and irreversible redox-electrode reactions, J. Electroanal. Chem. Interfacial Electrochem. 90 (1978) 149–163.

[203] S.M. Matthews, M.J.A. Shiddiky, K. Yunus, D.M. Elton, N.W. Duffy, Y. Gu, A.C. Fisher, A.M. Bond, Attributes of direct current aperiodic and alternating current harmonic components derived from large amplitude fourier transformed voltammetry under microfluidic control in a channel electrode, Anal. Chem. 84 (2012) 6686–6692.

[204] M.C. Granger, G.M. Swain, The influence of surface interactions on the reversibility of Ferri/Ferrocyanide at boron-doped diamond thin-film electrodes, J. Electrochem. Soc. 146 (1999) 4551–4558.

[205] D.H. Angell, T. Dickinson, The kinetics of the ferrous/ferric and ferro/ferricyanide reactions at platinum and gold electrodes. Part I. Kinetics at bare-metal surfaces, J. Electroanal. Chem. 35 (1972) 55–72.

192

[206] P.H. Daum, C.G. Enke, Electrochemical Kinetics of the Ferri—Ferrocyanide Couple on Platinum, Anal. Chem. 41 (1969) 653–656.

[207] J. Jordan, R.A. Javick, Electrode kinetics by hydrodynamic voltammetry-study of ferrous-ferric, ferrocyanide-ferricyanide and iodide-iodine systems, Electrochim. Acta. 6 (1962) 23–33.

[208] T. Matsue, D.H. Evans, T. Osa, N. Kobayashi, Electron-Transfer Reactions Associated with Host-Guest Complexation. Oxidation of Ferrocenecarboxylic Acid in the Presence of β-Cyclodextrin, J. Am. Chem. Soc. 107 (1985) 3411–3417.

[209] R.-R. Tian, Q.-H. Pan, J.-C. Zhan, J.-M. Li, S.-B. Wan, Q.-H. Zhang, W.-D. Huang, Comparison of Phenolic Acids and Flavan-3-ols During Wine Fermentation of Grapes with Different Harvest Times, Molecules. 14 (2009) 827–838.

[210] Y.-S. Lin, Y.-C. Chen, Laser desorption/ionization time-of-flight mass spectrometry on sol- gel-derived 2, 5-dihydroxybenzoic acid film, Anal. Chem. 74 (2002) 5793–5798.

[211] J. Yao, J.R. Scott, M.K. Young, C.L. Wilkins, Importance of matrix:analyte ratio for buffer tolerance using 2,5- dihydroxybenzoic acid as a matrix in matrix-assisted laser desorption/ionization-Fourier transform mass spectrometry and matrix- assisted laser desorption/ionization-time of flight, J Am Soc Mass Spectrom. 9 (1998) 805–13. http://www.ncbi.nlm.nih.gov/htbin-post/Entrez/query?db=m&form=6&dopt=r&uid=9692253.

[212] K. Strupat, M. Karas, F. Hillenkamp, 2,5-Dihydroxybenzoic acid: a new matrix for laser desorption-ionization mass spectrometry, Int. J. Mass Spectrom. Ion Process. 111 (1991) 89–102.

[213] M. Karas, H. Ehring, E. Nordhoff, B. Stahl, K. Strupat, F. Hillenkamp, M. Grehl, B. Krebs, Matrix-assisted laser desorptionionization mass spectrometry with additives to 2, 5-dihydroxybenzoic acid, J. Mass Spectrom. 28 (1993) 1476–1481.

[214] D. Nematollahi, S. Dehdashtian, A. Niazi, Electrochemical oxidation of some

dihydroxybenzene derivatives in the presence of indole, J. Electroanal. Chem. 616 (2008) 79–86.

[215] D. Nematollahi, M. Rafiee, Diversity in electrochemical oxidation of dihydroxybenzoic acids in the presence of acetylacetone. A green method for synthesis of new benzofuran derivatives, Green Chem. 7 (2005) 638.

[216] N. Papadopoulos, The electrochemical oxidation of 2 , 5-dihydroxybenzoic acid on a mercury electrode in aqueous solutions, Canidian J. Chem. 10 (1986) 16–19.

[217] D. Nematollahi, A. Amani, Mechanistic Study of Electrochemical Oxidation of 2,5-Dihydroxybenzoic Acid and 3,4-Dihydroxybenzaldehyde in the Presence of 3-Hydroxy-1H-phenalene-1-one, Chem. Pharm. Bull. (Tokyo). (2008).

[218] D. Nematollahi, S. Hosseinzadeh, B. Dadpou, Comproportionation and Michael addition reactions of electrochemically generated N,N,N',N'-tetramethyl-1,4-phenylenediamine dication. Synthesis of new unsymmetrical aryl sulfones containing N,N,N',N'-tetramethyl-1,4-phenylenediamine moiety, J. Electroanal. Chem. 759 (2015) 144–152.

[219] D. Nematollahi, S. Hosseinzadeh, B. Dadpou, Comproportionation and Michael addition reactions of electrochemically generated N,N,N',N'-tetramethyl-1,4-phenylenediamine dication. Synthesis of new unsymmetrical aryl sulfones containing N,N,N',N'-tetramethyl-1,4-phenylenediamine moiety, J. Electroanal. Chem. 759 (2015) 144–152.

[220] K. Yip, K.Y. Tam, K.F.C. Yiu, An efficient method of determining diffusion coefficients using eigenfunction expansions, J. Chem. Inf. Comput. Sci. 37 (1997) 367–371.

[221] M. V. Mirkin, A.J. Bard, Voltammetric Method for the Determination of Borohydride Concentration in Alkaline Aqueous Solutions, Anal. Chem. 63 (1991) 532–533.

[222] W.D. Davis, L.S. Mason, G. Stegeman, The Heats of Formation of Sodium

194

Borohydride, Lithium Borohydride and Lithium Aluminum Hydride, J. Am. Chem. Soc. 71 (1949) 2775–2781.

[223] M.B. Mathews, The reduction of cozymase by sodium borohydride, J. Biol. Chem. 176 (1948) 229–232.

[224] H.C. Brown, A.C. Boyd, Argentimetric Procedure for Borohydride Determination, Anal. Chem. 27 (1955) 156–158.

[225] J.A. Gardiner, J.W. Collat, Kinetics of the Stepwise Hydrolysis of Tetrahydroborate Ion, J. Am. Chem. Soc. 87 (1965) 1692–1700.

[226] I.E. Lichtenstein, J.S. Mras, Indirect ultraviolet spectrophotometric determination of borohydride using acetone, J. Franklin Inst. 281 (1966) 481–485.

[227] M. V. Mirkin, Borohydride Oxidation at a Gold Electrode, J. Electrochem. Soc. 139 (1992) 2212.

[228] K. Wang, J. Lu, L. Zhuang, Direct determination of diffusion coefficient for borohydride anions in alkaline solutions using chronoamperometry with spherical Au electrodes, J. Electroanal. Chem. 585 (2005) 191–196.

[229] E. Łowicka, J. Bełtowski, Hydrogen sulfide (H2S) - the third gas of interest for pharmacologists, Pharmacol. Rep. 59 (2007) 4—24. http://europepmc.org/abstract/MED/17377202.

[230] P. Kamoun, M. Belardinelli, A. Chabli, K. Lallouchi, B. Chadefaux-Vekemans, Endogenous hydrogen sulfide overproduction in Down syndrome, Am. J. Med. Genet. Part A. 116A (n.d.) 310–311.

[231] J.W. Elrod, J.W. Calvert, J. Morrison, J.E. Doeller, D.W. Kraus, L. Tao, X. Jiao, R. Scalia, L. Kiss, C. Szabo, H. Kimura, C.-W. Chow, D.J. Lefer, Hydrogen sulfide attenuates myocardial ischemia-reperfusion injury by preservation of mitochondrial function, Proc. Natl. Acad. Sci. 104 (2007) 15560 LP-15565.

http://www.pnas.org/content/104/39/15560.abstract.

[232] L. Li, M. Bhatia, Y.Z. Zhu, Y.C. Zhu, R.D. Ramnath, Z.J. Wang, F.B.M. Anuar, M. Whiteman, M. Salto-Tellez, P.K. Moore, Hydrogen sulfide is a novel mediator of lipopolysaccharide-induced inflammation in the mouse, FASEB J. 19 (2005) 1196–1198.

[233] Y. Kimura, H. Kimura, Hydrogen sulfide protects neurons from oxidative stress, FASEB J. 18 (2004) 1165–1167.

[234] N.S. Lawrence, J. Davis, R.G. Compton, Analytical strategies for the detection of sulfide: A review, Talanta. 52 (2000) 771–784.

[235] Z. Pawlak, A.S. Pawlak, Modification of iodometric determination of total and reactive sulfide in environmental samples, Talanta. 48 (1999) 347–353.

[236] J.D. Cline, Spectrophotometric determination of hydrogen sulfide in natural waters, Limnol. Oceanogr. 14 (1969) 454–458.

[237] N.S. Lawrence, R.P. Deo, J. Wang, Electrochemical determination of hydrogen sulfide at carbon nanotube modified electrodes, Anal. Chim. Acta. 517 (2004) 131–137.

[238] C.E. Banks, A.S. Yashina, G.J. Tustin, V.G.H. Lafitte, T.G.J. Jones, N.S. Lawrence, Exploring alkylated ferrocene sulfonates as electrocatalysts for sulfide detection, Electroanalysis. 19 (2007) 2518–2522.

[239] S.K. Pandey, K.H. Kim, K.T. Tang, A review of sensor-based methods for monitoring hydrogen sulfide, TrAC - Trends Anal. Chem. 32 (2012) 87–99.

[240] N.S. Lawrence, L. Jiang, T.G.J. Jones, R.G. Compton, Voltammetric characterization of a N,N′-diphenyl-p-phenylenediamine-loaded screen-printed electrode: A disposable sensor for hydrogen sulfide, Anal. Chem. 75 (2003) 2054–2059.

[241] D.G. Davis, E. Blanco, An electrochemical study of the oxidation of L-cysteine, J. Electroanal. Chem. 12 (1966) 254–260.

[242] M.A. Worosz, G.T. Cheek, Electrochemical Studies of Cysteine, Meet. Abstr. . (2016).

[243] K.R. Ward, N.S. Lawrence, R.S. Hartshorne, R.G. Compton, Cyclic voltammetry of the EC′ mechanism at hemispherical particles and their arrays: The split wave, J. Phys. Chem. C. 115 (2011) 11204–11215.

[244] L. Qu, S. Yang, G. Li, R. Yang, J. Li, L. Yu, Preparation of yttrium hexacyanoferrate/carbon nanotube/Nafion nanocomposite film-modified electrode: Application to the electrocatalytic oxidation of l-cysteine, Electrochim. Acta. 56 (2011) 2934–2940.

[245] F. de A. dos S. Silva, M.G.A. da Silva, P.R. Lima, M.R. Meneghetti, L.T. Kubota, M.O.F. Goulart, A very low potential electrochemical detection of l-cysteine based on a glassy carbon electrode modified with multi-walled carbon nanotubes/gold nanorods, Biosens. Bioelectron. 50 (2013) 202–209.

[246] P. Wang, X. Jing, W. Zhang, G. Zhu, Renewable manganous hexacyanoferrate-modified graphite organosilicate composite electrode and its electrocatalytic oxidation of L-cysteine, J. Solid State Electrochem. 5 (2001) 369–374.

[247] A. Abbaspour, A. Ghaffarinejad, Electrocatalytic oxidation of l-cysteine with a stable copper–cobalt hexacyanoferrate electrochemically modified carbon paste electrode, Electrochim. Acta. 53 (2008) 6643–6650.

[248] A. Salimi, S. Pourbeyram, Renewable sol–gel carbon ceramic electrodes modified with a Ru-complex for the amperometric detection of l-cysteine and glutathione, Talanta. 60 (2003) 205–214.

[249] A. Salimi, R. Hallaj, Catalytic oxidation of thiols at preheated glassy carbon electrode modified with abrasive immobilization of multiwall carbon nanotubes: applications to amperometric detection of thiocytosine, l-cysteine and glutathione, Talanta. 66 (2005) 967–975.

[250] H.G. Waddill, G. Gorin, Determination of Cysteine with Ferricyanide by

Amperometric Titration with Two Polarized Electrodes, Anal. Chem. 30 (1958) 1069–1071.

[251] G. Gorin, W.E. Godwin, Inhibition and catalysis in the oxidation of cysteine and other mercaptans by ferricyanide, J. Catal. 5 (1966) 279–284.

[252] J.M. Leal, B. Garcia, P.L. Domingo, Outer-sphere hexacyanoferrate(III) oxidation of organic substrates, Coord. Chem. Rev. 173 (1998) 79–131.

[253] O. Nekrassova, G.D. Allen, N.S. Lawrence, L. Jiang, T.G.J. Jones, R.G. Compton, The oxidation of cysteine by aqueous ferricyanide: A kinetic study using boron doped diamond electrode voltammetry, Electroanalysis. 14 (2002) 1464–1469.

[254] P. Song, H. Ma, L. Meng, Y. Wang, H.V. Nguyen, N.S. Lawrence, A.C. Fisher, Fourier transform large amplitude alternating current voltammetry investigations of the split wave phenomenon in electrocatalytic mechanisms, Phys. Chem. Chem. Phys. (2017).

[255] V. Valpuesta, M.A. Botella, Biosynthesis of L-ascorbic acid in plants: New pathways for an old antioxidant, Trends Plant Sci. 9 (2004) 573–577.

[256] Y. Ogiri, F. Sun, S. Hayami, A. Fujimura, K. Yamamoto, M. Yaita, S. Kojo, Very low vitamin C activity of orally administered L-dehydroascorbic acid, J. Agric. Food Chem. 50 (2002) 227–229.

[257] P.W. Washko, R.W. Welch, K.R. Dhariwal, Y. Wang, M. Levine, Ascorbic acid and dehydroascorbic acid analyses in biological samples, Anal. Biochem. 204 (1992) 1–14.

[258] G.S. Deshmukh, M.G. Bapat, Determination of ascorbic acid by potassium iodate, Fresenius' Zeitschrift Für Anal. Chemie. 145 (1955) 254–256.

[259] O.A. Zaporozhets, E.A. Krushinskaya, Determination of ascorbic acid by molecular spectroscopic techniques, J. Anal. Chem. 57 (2002) 286–297.

[260] A. Kyaw, A simple colorimetric method for ascorbic acid determination in blood

plasma, Clin Chim Acta. 86 (1978) 153–157. http://www.ncbi.nlm.nih.gov/pubmed/657538.

[261] J.H. Roe, Chemical determination of ascorbic, dehydroascorbic, and diketogulonic acids, Methods Biochem. Anal. Vol. 1. (1954) 115–139.

[262] A.M. Pisoschi, A. Pop, A.I. Serban, C. Fafaneata, Electrochemical methods for ascorbic acid determination, Electrochim. Acta. 121 (2014) 443–460.

[263] A. Malinauskas, R. Garjonyte, R. Mažeikiene, I. Jurevičiute, Electrochemical response of ascorbic acid at conducting and electrogenerated polymer modified electrodes for electroanalytical applications: A review, in: Talanta, 2004: pp. 121–129.

[264] S. Kuss, R.G. Compton, Electrocatalytic detection of ascorbic acid using N,N,N',N'-tetramethyl-para-phenylene-diamine (TMPD) mediated oxidation at unmodified gold electrodes; reaction mechanism and analytical application, Electrochim. Acta. 242 (2017) 19–24.

[265] M. Rueda, A. Aldaz, F. Sanchez-Burgos, Oxidation of L-ascorbic acid on a gold electrode, Electrochim. Acta. 23 (1978) 419–424.

[266] R.G. Compton, M.B.G. Pilkington, G.M. Stearn, Mass transport in channel electrodes. The application of the backwards implicit method to electrode reactions (EC, ECE and DISP) involving coupled homogeneous kinetics, J. Chem. Soc. Faraday Trans. 1 Phys. Chem. Condens. Phases. 84 (1988) 2155.

[267] N. V Rees, J.A. Alden, R.A.W. Dryfe, B.A. Coles, R.G. Compton, Voltammetry Under High-Mass Transport Conditions - the High-Speed Channel Electrode and Heterogeneous Kinetics, J. Phys. Chem. 99 (1995) 14813–14818.

[268] N. V. Rees, R.A.W. Dryfe, J.A. Cooper, B.A. Coles, R.G. Compton, S.G. Davies, T.D. McCarthy, Voltammetry under high mass transport conditions. A high speed channel electrode for the study of ultrafast kinetics, J. Phys. Chem. 99 (1995) 7096–7101.

[269] F. Prieto, W. Aixill, J. Alden, Voltammetry under high mass transport conditions. The high-speed channel electrode and transient measurements, J. …. 5647 (1997) 5540–5544.

[270] R.G. Compton, E. Laborda, K.R. Ward, Understanding voltammetry: simulation of electrode processes, World Scientific, 2014.

[271] R.G. Compton, P.R. Unwin, Channel and tubular electrodes, J. Electroanal. Chem. Interfacial Electrochem. (1986) 1–20.

[272] J. V. Macpherson, N. Simjee, P.R. Unwin, Hydrodynamic ultramicroelectrodes: Kinetic and analytical applications, Electrochim. Acta. 47 (2001) 29–45.

[273] J.M. Rosamilia, B. Miller, Hydrodynamic modulation applications to electroanalysis and diffusion coefficient measurement with a commercial disk rotator, Anal. Chem. 56 (1984) 2410–2413.

[274] B. Miller, S. Bruckenstein, Submicromolar Analysis with Rotating and Hydrodynamically Modulated Disk Electrodes, Anal. Chem. 46 (1974) 2026–2033.

[275] K. Tokuda, S. Bruckenstein, Sinusoidal Hydrodynamic Voltammetry at the Rotating Disk Electrode I. Theory of Electron Transfer Kinetics, J. Electrochem. Soc. 126 (1979) 431–434.

[276] S. Swathirajan, S. Bruckenstein, The anodic behavior of iodide at platinum in the presence of an iodine film under potentiostatic steady-state and hydrodynamic modulation conditions, J. Electroanal. Chem. Interfacial Electrochem. 143 (1983) 167–178.

[277] B. CHANCE, G.R. WILLIAMS, Respiratory enzymes in oxidative phosphorylation. I. Kinetics of oxygen utilization., J. Biol. Chem. 217 (1955) 383–393.

[278] W.M. Kuhtreiber, L.F. Jaffe, Detection of extracellular calcium gradients with a calcium-specific vibrating electrode, J. Cell Biol. 110 (1990) 1565–1573.

[279] J. He, V.J. Gelling, D.E. Tollman, G.P. Bierwagen, A scanning vibrating electrode study of chromated-epoxy coatings on steel and aluminum, Am. Chem. Soc. Polym. Prepr. Div. Polym. Chem. 41 (2000) 1755–1756.

[280] D.E. Williams, K. Ellis, A. Colville, S.J. Dennison, G. Laguillo, J. Larsen, Hydrodynamic modulation using vibrating electrodes: Application to electroanalysis, J. Electroanal. Chem. 432 (1997) 159–169.

[281] G. Hancock, R.G. Compton, Applications of kinetic modelling, Elsevier, 1999.

[282] J. V. Macpherson, P.R. Unwin, Hydrodynamic modulation voltammetry with a variable-height radial flow microring electrode, Anal. Chem. 71 (1999) 2939–2944.

[283] N. Simjee, P.R. Unwin, J. V. Macpherson, Hydrodynamic Modulation Voltammetry with a Dual Disk Chopped Flow-Microjet Electrode (CF-MJE), Electroanalysis. 15 (2003) 1445–1452.

[284] K.A. Gooch, A.C. Fischer, Computational electrochemistry: The simulation of voltammetry under hydrodynamic modulation control, J. Phys. Chem. B. 106 (2002) 10668–10673.

[285] C. Deslouis, B. Tribollet, Flow modulation technique and EHD impedance: a tool for electrode processes and hydrodynamic studies, Electrochim. Acta. 35 (1990) 1637–1648.

[286] C.R. Brunold, J.C.B. Hunns, M.R. Mackley, J.W. Thompson, Experimental observations on flow patterns and energy losses for oscillatory flow in ducts containing sharp edges, Chem. Eng. Sci. (1989).

[287] M.R. Mackley, X. Ni, Mixing and dispersion in a baffled tube for steady laminar and pulsatile flow, Chem. Eng. Sci. (1991).

[288] A.W. Dickens, M.R. Mackley, H.R. Williams, Experimental residence time distribution measurements for unsteady flow in baffled tubes, Chem. Eng. Sci. (1989).

[289] M.R. Mackley, G.M. Tweddle, I.D. Wyatt, Experimental heat transfer measurements for pulsatile flow in baffled tubes, Chem. Eng. Sci. (1990).

[290] M.R. Hewgill, M.R. Mackley, A.B. Pandit, S.S. Pannu, Enhancement of gas-liquid mass transfer using oscillatory flow in a baffled tube, Chem. Eng. Sci. (1993).

[291] M. Karbaschi, A. Javadi, D. Bastani, R. Miller, High frequency oscillatory flow in micro channels, Colloids Surfaces A Physicochem. Eng. Asp. (2014).

[292] A.A. Wragg, 5th European Symposium on Electrochemical Engineering, IChemE, 1999.

[293] P. Cognet, J. Berlan, G. Lacoste, P.L. Fabre, J.M. Jud, Application of metallic foams in an electrochemical pulsed flow reactor Part I: Mass transfer performance, J. Appl. Electrochem. (1995).

[294] S.L. Barker, D. Ross, M.J. Tarlov, M. Gaitan, L.E. Locascio, Control of flow direction in microfluidic devices with polyelectrolyte multilayers., Anal. Chem. 72 (2000) 5925–9.

[295] S. Liu, Y. Gu, R.B. Le Roux, S.M. Matthews, D. Bratton, K. Yunus, A.C. Fisher, W.T.S. Huck, The electrochemical detection of droplets in microfluidic devices, Lab Chip. 8 (2008) 1937.

[296] X. Fang, N. Qu, Y. Zhang, Z. Xu, D. Zhu, Effects of pulsating electrolyte flow in electrochemical machining, J. Mater. Process. Technol. 214 (2014) 36–43.

202

Appendix A Instrumentation and Signal Processing of Fourier Transformed Alternating Current Voltammetry

Fig A.1 summarises the key features in the FTACV instrumentation [108] needed to achieve a unified approach to FT voltammetry. A desktop computer can be used for instrument control, data collection and data analysis. The other necessary hardware components are widely used in commercial stereo systems. The analog-to-digital converters (ADCs) and digital-to-analog converters (DACs) are $\Delta\sum$-modulated devices. The software compensates for the time delay introduced through the ADC and DAC devices. Stereo hardware limits the upper sampling rate. The DAC can generate a DC ramp. In the overall signal, the total response is dominated by the DC component and the fundamental harmonic. A lookup-table digital signal process (DSP) and control stores a digital waveform, which is a highly accurate, 18-bit sine wave of amplitude $\pm$ 300 mV; a Fourier series of sine waves; a selected combination of sine waves; or a user-defined waveform.

The digitally generated linear DC ramp and the operator-designed AC perturbation are converted to analog signals and summed. The waveform is then fed to a conventional potentiostat, which control the three electrodes, with a rise time. When the experiment is processing, the I-E data points are collected at a constant sampling rate and stored digitally, which is accomplished by the ADC. The collected experimental data are interrogated by the software in the signal-processing section of the FT voltammetric instrumentation. An FT

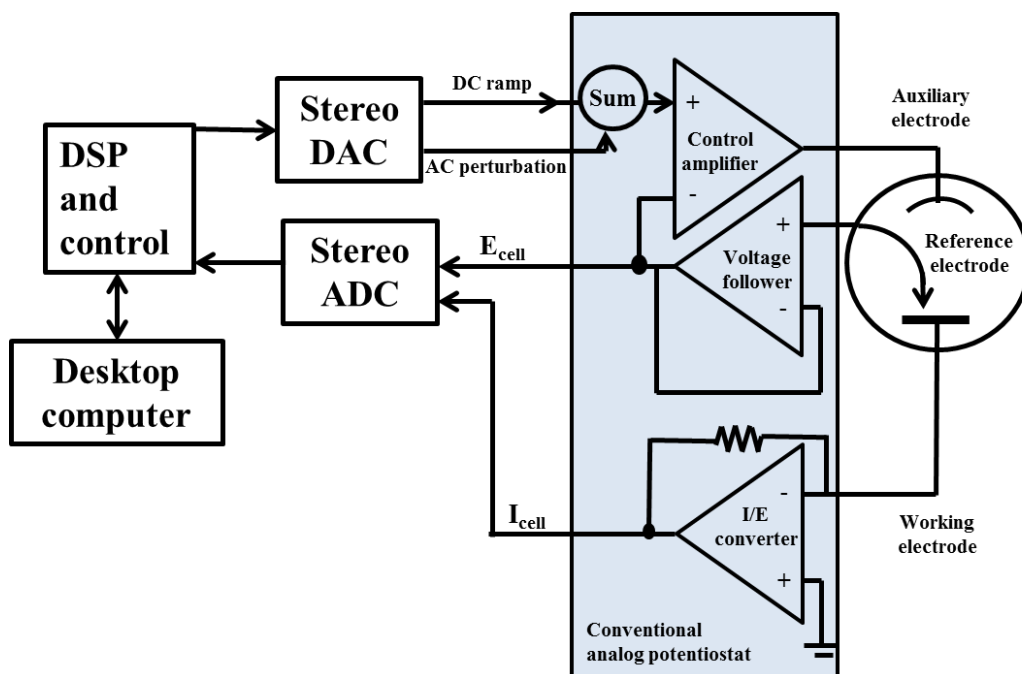algorithm initially converts the data from time-domain into power spectrum, which is frequency-domain.

Fig A.1 Schematic of FT voltammetric instrumentation

By selecting a frequency band that retains most of its energy and then zeroing the remaining portion of the power spectrum, all the components and their harmonics can be separated. Next, the inverse FT is applied to each selected component to generate DC, fundamental, second-, third- and higher-harmonic time-domain signals.